

# Exploiting path-polarization hyperentangled photons for multiqubit quantum information protocols

**Candidate:** Mario A. Ciampini, **Supervisor:** Prof. Paolo Mataloni

January 9, 2017

# Contents

<b>1</b>	<b>Principles of Classical and Quantum Information</b>	<b>8</b>
1.0.1	Defining information . . . . .	8
1.1	Classical Information Theory . . . . .	8
1.1.1	Classical Entropy . . . . .	9
1.1.2	Conditional Entropy . . . . .	10
1.1.3	Mutual Information . . . . .	11
1.2	Quantum Information Theory . . . . .	11
1.2.1	The qubit . . . . .	11
1.2.2	Multi-partite quantum systems . . . . .	13
1.2.3	Mixed States and Density Matrix . . . . .	14
1.2.4	Entanglement and Separable States . . . . .	15
1.2.5	Multipartite entanglement . . . . .	17
1.3	Distance between quantum states . . . . .	19
1.3.1	Trace Distance . . . . .	19
1.3.2	Fidelity . . . . .	20
1.3.3	Frobenius Norm . . . . .	21
1.4	Characterizing entanglement . . . . .	21
1.4.1	Concurrence . . . . .	21
1.4.2	Von Neumann Entropy . . . . .	22
1.4.3	Considerations on the entanglement quantifiers . . . . .	22
1.5	Bell Inequalities and non locality witnesses . . . . .	23
1.5.1	Derivation of the Bell inequality . . . . .	23
1.5.2	Violation of the CHSH inequality and non locality . . . . .	24
1.6	Evolution of quantum systems . . . . .	25
1.6.1	Evolution of Closed Quantum Systems and Logic Gates . . . . .	25
1.6.2	Evolution of Open Quantum Systems . . . . .	26
1.6.3	Noisy channels . . . . .	27
1.7	Measures in a quantum systems . . . . .	28
1.7.1	Observables and projective measurements . . . . .	29
1.8	Quantum correlations . . . . .	29
1.8.1	Quantum Discord . . . . .	30
<b>2</b>	<b>Quantum Information with Photons</b>	<b>33</b>
2.1	Why do we use photons? . . . . .	34
2.2	Encoding and manipulating photonic single qubits . . . . .	35
2.2.1	Polarization-encoded qubit . . . . .	35

2.2.2	Path-encoded qubit . . . . .	36
2.2.3	Hybrid photonic states . . . . .	38
2.2.4	Hyperentanglement . . . . .	39
2.3	Detection of quantum states and observables . . . . .	40
2.3.1	Measuring observables . . . . .	40
2.4	State generation via non-linear optics . . . . .	42
2.4.1	Spontaneous Parametric Down Conversion . . . . .	42
2.4.2	Correlations given by the phase-matching . . . . .	44
2.4.3	Type I phase-matching . . . . .	45
2.4.4	Type II phase-matching . . . . .	48
2.5	Integrated Photonics . . . . .	50
2.6	Quantum State Tomography . . . . .	52
2.6.1	Single-qubit state tomography . . . . .	53
2.6.2	Multi-qubits state tomography . . . . .	54
2.6.3	Maximum-Likelihood Estimation . . . . .	55
<b>3</b>	<b>Hyperentanglement</b>	<b>58</b>
3.1	Introduction . . . . .	58
3.2	The source . . . . .	60
3.3	Polarization entanglement . . . . .	61
3.4	Path Entanglement . . . . .	62
3.5	Hyperentanglement and Symmetry . . . . .	64
3.6	Hyperentanglement and Cluster state manipulation on chip . . . . .	65
3.6.1	Photon indistinguishability and entanglement witness . . . . .	68
3.6.2	Hyperentanglement measurements . . . . .	69
3.7	Discussion and perspectives . . . . .	70
<b>4</b>	<b>Cluster states and one-way quantum computation</b>	<b>72</b>
4.1	Definition of a cluster state . . . . .	72
4.2	One-Way quantum Computation . . . . .	73
4.2.1	Description of the protocol . . . . .	74
4.2.2	Universality of one-way quantum computation . . . . .	76
4.3	Experimental generation of 4-qubit linear cluster state . . . . .	77
4.4	Cluster state analysis . . . . .	80
4.4.1	The diagnostic tool . . . . .	81
4.4.2	The experimental study . . . . .	82
4.4.3	Noise modelling . . . . .	84
4.4.4	Dephasing channel . . . . .	85
4.5	Grover's algorithm . . . . .	87
4.6	Discussion and perspectives . . . . .	88
<b>5</b>	<b>Effect of noise on quantum correlations</b>	<b>90</b>
5.1	Two-qubit game - Activating Entanglement . . . . .	91
5.2	Four-qubit game . . . . .	96
5.2.1	Robustness of the 4-qubit scheme . . . . .	97
5.2.2	4 qubit game experimental implementation . . . . .	97

5.3	Discussion and perspectives . . . . .	101
<b>6</b>	<b>Quantum thermodynamics</b>	<b>103</b>
6.1	Classical Information Thermodynamics . . . . .	103
6.1.1	Maxwell's Demon . . . . .	104
6.1.2	Szilard's engine . . . . .	105
6.2	Quantum Information Thermodynamics . . . . .	106
6.2.1	Quantum Thermodynamics: The Principles . . . . .	107
6.2.2	von Neumann Entropy . . . . .	108
6.3	Using Daemons to assess quantumness . . . . .	108
6.3.1	Work Deficit . . . . .	109
6.4	Thermodynamical detection of entanglement by Maxwell's Demons . .	111
6.4.1	Work Extraction Scheme: two qubits . . . . .	111
6.4.2	Thermodynamical separability criterion . . . . .	112
6.4.3	Exorcism of Maxwell's Demon in TSC . . . . .	114
6.4.4	Protocol for tripartite systems . . . . .	115
6.5	Experimental work extraction protocol . . . . .	117
6.5.1	Two-qubit separably criterion based on thermodynamics work- extraction protocol . . . . .	117
6.5.2	Two-qubit experiment . . . . .	118
6.5.3	Three qubits experiment . . . . .	122
6.6	Discussion and perspective . . . . .	126
	<b>Bibliography</b>	<b>130</b>

## Abbreviations

<b>BBO</b>	Beta Barium Borate ( $\beta - BaB_2O_4$ )
<b>BS</b>	Beam Splitter
<b>CHSH</b>	Clauser Horne Shimony Holt
<b>FI</b>	Full Inseparability
<b>FS</b>	Full Separability
<b>GHZ</b>	Greenberger-Horne-Zeilinger
<b>HE</b>	Hyperentanglement
<b>HWP</b>	Half Wave Plate
<b>IT</b>	Information Theory
<b>LOCC</b>	Local Operation and Classical Communication
<b>LU</b>	Local Unitary

- MABK** Mermin-Ardehali-Belinskii-Klyshko
- MES** Maximally Entangled States
- MNLI** Multipartite Nonlocality Inequalities
- OWQC** One-Way Quantum Computation
- PBS** Polarizing Beam Splitter
- POVM** Positive Operator Valued Measure
- PPKTP** Periodically Poled Potassium Titanyl Phosphate
- PS** Phase Shifter
- QIT** Quantum Information Theory
- QM** Quantum Mechanics
- QWP** Quarter Wave Plate
- SPDC** Spontaneous Parametric Down Conversion
- SSS** Star Shaped States
- TSC** Thermodynamical Separability Criterion
- WWZB** Werner-Wolf-Zukowski-Brukner

# Introduction

Quantum Mechanics (QM) has probably represented the most fundamental breakthrough in Physics of the last century. It made possible to describe phenomena that are inexplicable using classical approaches, such as the black-body radiation, the photoelectric effect and numerous aspects of light-matter interaction.

Since its establishment in 1927, when the greatest scientists of that period met at the Solvay Conference in Brussels to discuss this emergent theory, QM has rapidly developed to become the most accurate description of reality, even predicting novel behaviours and features that are inexplicable and counterintuitive in the sense of our every-day experience. For example, *entanglement* of quantum system, i.e. the ability for particles to maintain correlations even when far apart in space; or the *wave function collapse*, i.e. the instantaneous modification of a quantum state after its measurement. Even Einstein himself, in his well-known article of 1935 [1] challenged these concepts with the often-misinterpreted quote: *God does not play dice with the universe*.

It turned out that Einstein was wrong. John Bell, over 20 years later, developed an experimental signature that allows to identify the non-classical behaviour of quantum system and, since then, we are witnessing a revolution in the paradigm of the QM.

Indeed, nowadays nobody challenges the counterintuitive assumptions of the theory anymore, as they are observed every day in the laboratories all around the world; instead, we are fastly moving towards discovering the *potential* and the *applications* of QM. After Feynman's famous article in 1982 [2], scientists started to explore the possibility that a quantum system having potential of processing information faster and more efficiently than what could be conceived in a classical context.

One of the most promising directions in this sense has been connecting QM to the Information Theory (IT), which was introduced by Shannon in 1948. The resulting field, Quantum Information Theory (QIT), proved that quantum resources could be surprisingly useful in order to encode, manipulate and send information more effectively compared to the classical case.

This notion has paved the way towards significant progresses over a large variety of fields in which the features of QM can be exploited in order to perform certain tasks more efficiently. Among these others, we find :

- Quantum Cryptography, where it has been demonstrated the possibility of using quantum resources to exchange a completely secure key between two parties ([3]),
- Quantum Computation, where it has been shown that quantum algorithms allowed for an increase in speed of otherwise exponentially hard classical computations, such as the factorization in prime numbers problem ([4, 5]),

- Quantum Metrology, where parameters can be estimated with a quadratic increase of precision using quantum resources compared to classical ones ([6, 7]),
- Quantum Thermodynamics in which more work can be extracted from systems that share quantum correlations ([8, 9]).

In this thesis we describe and exploit a photonic source of hyperentangled states which allows the creation of a four qubit entangled state using path and polarization of two photons; this will be the main resource for a series of experiments that are linked to the main goal of exploring the advantages that quantum correlations brings in the aforementioned tasks. In particular we will focus onto showing that the same correlations which define the *quantumness* of a state can be interpreted in two very different ways: either as something that introduces *non-locality* between qubits, or something which reduces the *information entropy* between qubits. Both interpretations allow the definition and observation of quantum advantage but, as we will show, the two views are not completely equivalent.

Our goal will be showing that quantum correlations can be seen as *currency* that can be spent to perform tasks more efficiently than in the classical case.

The outline of the thesis will be the following:

1. **Chapter 1: Principles of Classical and Quantum Information** - In this chapter we will start in defining the notion of classical information and entropy. Than we will move to the quantum realm introducing the formalism of Quantum Information, which is the main topic of the thesis. Here we present a number of tools that will be used throughout the following chapters such as the definition of distance between quantum states, measurements of entanglement and non-locality, evolution of quantum states and measurements.
2. **Chapter 2: Quantum Information with Photons** - Here we describe photonics as a possible platform for quantum information, presenting advantages and disadvantages of it. We will focus on the possibility of encoding qubits on the path and polarization of photons and we will define the concept of hyperentanglement. Than we will describe generation, manipulation and detection of photonic quantum states. A brief overview of integrated photonics will be given.
3. **Chapter 3: Hyperentanglement** - In this chapter we will discuss an hyperentangled path-polarization 2 photons - 4 qubit source. We describe in details its experimental characterization and we present a novel experiment in which we demonstrate the manipulation of hyperentanglement using an integrated device.
4. **Chapter 4: Cluster States and One Way quantum Computation** - Here we describe cluster states as resources for quantum computation and we discuss the experimental realization of a 4-qubit linear cluster state using the hyperentangled source. We will use the generated state for two tasks: the identification of the strenght of the cluster's link, and the proof-of-principle use of the cluster for implementing Grover's search algorithm.

5. **Chapter 5: Effect of noise on quantum correlations** - In this chapter we present an experiment which gives a surprising insight on the nature of quantum correlations. We demonstrate that by applying local noise onto a 2- or 4- qubit uncorrelated state, we can produce entanglement. We elaborate on the nature of entanglement robustness.
6. **Chapter 6: Quantum Thermodynamics** - In this chapter we change paradigm and we present a work-extraction protocol based on quantum correlation. Here we discuss Maxwell's Demon and Landauer's principle and we extend it to a quantum scenario. We demonstrate both theoretically and experimentally that entanglement can be used to extract more work compared to using classical resources. Finally we present a three qubit protocol in which we use work-extraction as an entanglement quantifier. We compare this perspective to that of a Bell-like inequalities violation approach.

# Chapter 1

## Principles of Classical and Quantum Information

In this chapter we introduce all the theoretical tools and definitions that will be used in this thesis. Aim of this chapter is to provide an introductory basis to understand the main aspects of this thesis and it is not conceived to represent a complete and detailed reference on these topics, which are thoroughly discussed in Refs. [3, 10, 11].

### 1.0.1 Defining information

When thinking about the term ‘information’, there are a lot of concepts that come to mind, most of which pretty intuitive indeed. One can think about the *bit*, which is the basic unit of information and is a whatsoever system which can take value ‘0’ or ‘1’; we can think about a *message*, which is part of information to be shared, or sent between two parties; one can think about *computers*, which are the means to process and transform information; or about *cryptology*, which is the way to encode information so that only a few number of designated parties can access to it. The list could continue, however nothing here gives the proper definition of what ‘information’ is. This is because information is the very substrate of our reality, and *everything* which constitutes it can be seen as in essence as information. In this thesis some of these aspects will be presented following the point of view of a quantum world.

## 1.1 Classical Information Theory

Classical information theory is built on the concept of *bit*, which is a logic unit that can take two values. Conventionally we indicate these two values as ‘0’ and ‘1’ but any other set of two symbols can be adopted to represent it [12]. Any physical representation of a two-level system can be adopted to encode a bit: for example we can consider the flip of a coin. We define ‘head’ to be a logical 0, ‘tail’ to be a logical 1. Starting from here we can start talking about information when two parties are involved: we introduce *Albus* and *Bellatrix*; the first is the sender of a message, the latter is the receiver. A message is simply a string of bits which is shared among Albus and Bellatrix.

### 1.1.1 Classical Entropy

Suppose now that Albus has to toss a coin and describe the outcome to Bellatrix. We assume that Albus has an *a priori* knowledge of the statistical behaviour of the coin; we can identify the following problems:

1. How much does Albus know about the state of the coin after he tossed it?
2. How does he describe the state of the coin? That is, what does he respond to Bellatrix?

In a classical world the answers are straightforward: let us consider the following three cases:

- We suppose Albus can look at the coin after tossing it, or that he knows the coin is completely unfair and always gives the same result. In both cases he knows with absolute certainty the final state of the coin, so the answers to questions 1) and 2) are: he exactly knows the state and he can describe it simply stating if it is head or tail.
- We consider now the opposite case where he is not allowed to observe the result and he knows that the coin is perfectly fair. He is now completely ignorant about the state of the coin and can only tell Bellatrix that there is a 50% chance that it is head and a 50% chance that it is tail.
- Finally, we consider the case where he knows the coin is unbalanced: let's suppose for example it gives head with 0.7 probability and tail with 0.3 probability. Although he is not able to know exactly the state of the coin again, he can make a more precise guess on the state of the coin than the previous case, as now Albus knows that it is more likely to be head than tail. To describe the state he says that there is a 70% chance that it is head and 30% chance that it is tail.

In general the coin will have a probability distribution for the outcomes  $\{p_{head}, p_{tail}\}$ , with  $p_{head} + p_{tail} = 1$ . Formally the answers to 1) and 2) are generally addressed in the following manner:

- Our knowledge on the state of the system depends only on the probability distribution  $\{p_0, p_1\}$ , with  $p_1 = 1 - p_0$ . If the outcome probability is completely random, that is  $p_0 = p_1 = 1/2$ , we are totally ignorant on the expected result. On the contrary, the more the distribution is unbalanced the less ignorant we are. In the extremal case in which  $p_0 = 1$  and  $p_1 = 0$  (or viceversa), we have a complete knowledge of the state (because we know for sure what the outcome will be) and our ignorance is zero. We can define as a good quantifier of our ignorance for a two-level system, given the distribution  $\{p, 1 - p\}$ , the Binary Shannon Entropy, defined as

$$H(p) = -p \log_2(p) - (1 - p) \log_2(1 - p). \quad (1.1)$$

As we expect, Fig.1.1 shows that this quantity has his maximum in  $p = 1/2$ , e.g. when the distribution is totally random, and decreases to zero when  $p$  goes to

0 or to 1, corresponding to a totally unbalanced distribution. This means that the more entropy a system has, the more is difficult to predict its outcome. We can see an analogy here with the thermodynamic entropy, which represents the statistical disorder of a system. We can say in some sorts that the concepts of *ignorance* and *disorder* are related. This relation will be discussed in detail in Chap. 6.

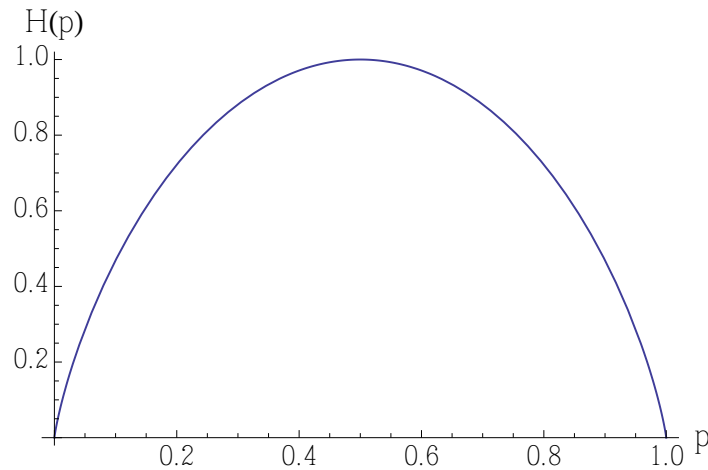


Figure 1.1: Shannon binary entropy for the distribution  $\{p, 1 - p\}$ . It is symmetric on  $p$ . The maximum value of  $H(p) = 1$  is achieved for  $p = 1/2$ .  $H(p)$  decreases to 0 when  $p$  goes to 0 or 1.

- In analogy with the quantum formalism that will be discussed in section 1.2, we can define “classical pure states” the cases where  $p = 0$  or  $p = 1$ , corresponding to the cases when we have full knowledge of the state. Otherwise we will talk about “classical mixed states”. We have seen that, in order to describe the two-level system to Bellatrix, Albus has to communicate her the distribution  $\{p, 1 - p\}$  for a general mixed state, but if the state is pure it reduces in telling her 0 or 1.

Sometimes we are interested in the *relation* between different events. Suppose, for example, that we know for sure that Albus, who lives in Rome, is used to go running whenever it isn’t raining. Then he tells Bellatrix, who lives in Milan, that yesterday he went out running. Of course Bellatrix can deduce that *yesterday didn’t rain in Rome*. Now suppose that Bellatrix knows that Albus runs *every day*. Of course in this case she cannot deduce anything about the weather in Rome, because *running* and *the weather* are not related in any way. We define the concept of mutual information to formalize this problem.

### 1.1.2 Conditional Entropy

Suppose we have a discrete probability space  $(\Omega, \Sigma, \mathbb{R})$ ; we introduce two different *events*, described by two discrete random variables  $X : \Omega \rightarrow \mathbb{R}$  and  $Y : \Omega \rightarrow \mathbb{R}$ , such that  $Im(X) = \{X(x) | x \in \Omega\}$  and  $Im(Y) = \{Y(y) | y \in \Omega\}$ .

In IT, the conditional entropy quantifies the amount of information needed to describe the outcome of variable  $Y$  given that the value of  $X$  is known through a prior probability distribution  $p(x)$  (which is called *marginal distribution*). The entropy of  $Y$  given  $X$  results is written as  $H(Y|X)$  and can be thought as the weighted sum of  $H(Y|X = x)$  for each possible outcome of  $x$  using  $p(x)$  as weight. It takes the form:

$$\begin{aligned} H(Y|X) &= \sum_{x \in \text{Im}(X)} p(x) H(Y|X = x) \\ &= \sum_{x \in \text{Im}(X), y \in \text{Im}(Y)} p(x, y) \log \frac{p(x)}{p(x, y)}. \end{aligned} \quad (1.2)$$

Here  $p(x, y) = p(X = x, Y = y) = p(y|x) \cdot p(x)$  represents the *joint probability* of  $X$  and  $Y$ . We note that if  $H(Y|X) = 0$ , then the value of  $Y$  is completely determined by the value of  $X$ , and conversely if  $H(Y|X) = H(Y)$ , then  $Y$  and  $X$  are independent random variables, as  $X$  plays no role in the characterization of  $Y$ .

### 1.1.3 Mutual Information

Mutual information is a quantity which represents how much information  $X$  and  $Y$  share: if one measures one of the two events, how much this reduces the uncertainty about the other? If the two events are independent, then knowing  $X$  does not give any information about  $Y$  and vice versa, so their mutual information is zero. On the other hand, if  $X$  is a deterministic function of  $Y$  and  $Y$  is a deterministic function of  $X$  then all information conveyed by  $X$  is shared with  $Y$ , and as such knowing one means knowing the other and viceversa. We define the mutual information between  $X$  and  $Y$  as:

$$I(X, Y) = \sum p(x, y) \log \frac{p(x, y)}{p(x)p(y)} \quad (1.3)$$

This can conveniently be expressed in terms of entropy as:

$$\begin{aligned} I(X, Y) &= H(X) - H(X|Y), \\ &= H(X) + H(Y) - H(X, Y). \end{aligned} \quad (1.4)$$

## 1.2 Quantum Information Theory

While the bit is the fundamental concept of classical computation and classical information, quantum computation and quantum information are built upon the concept of *the quantum bit*, or *qubit*. In this section we introduce the properties of single and multiple qubits, comparing their properties to those of classical bits. Exactly as we have done for classical information theory, everything we introduce here is device-independent, meaning that we are talking about abstract entities which do not depend on the specific physical realization of the system to work.

### 1.2.1 The qubit

A quantum system in a pure state is completely described by a normalized vector  $|\psi\rangle$ , called “wavefunction”, living in a  $N$  dimensional Hilbert space  $\mathcal{H}$ .  $N$  defines the

dimension of the system. If we consider only 2-dimensional quantum systems, we can define the “qubit” (quantum bit) which is the quantum equivalent of the classical bit.

We can consider an arbitrary 2-vector orthonormal basis of  $\mathcal{H}$  and name the two vectors  $|0\rangle$  and  $|1\rangle$ , in analogy with the states 0 and 1 of the classical bits. In the  $\{|0\rangle, |1\rangle\}$  basis, called *computational basis*, any possible state of the system can be written in the form:

$$|\psi\rangle = \alpha|0\rangle + \beta|1\rangle = \begin{pmatrix} \alpha \\ \beta \end{pmatrix}, \quad (1.5)$$

with  $\alpha^2 + \beta^2 = 1$ . According to the measurement principle of Quantum Mechanics [], if  $|\psi\rangle$  is the state of a system and if  $|\phi\rangle$  represents a second state, the probability of finding the first system in the second state when observing it, is given by  $p(|\psi\rangle, |\phi\rangle) = |\langle\psi|\phi\rangle|^2$ . For this reason,  $\alpha^2$  and  $\beta^2$  represent the probability of finding the qubit described in Eq. 1.5 respectively in state  $|0\rangle$  or  $|1\rangle$ .

The qubit can also be represented by means of polar coordinates over a three-dimensional sphere by introducing variables  $\theta$  and  $\phi$  as:

$$|\psi\rangle = \cos\left(\frac{\theta}{2}\right)|0\rangle + e^{i\phi}\sin\left(\frac{\theta}{2}\right)|1\rangle = \begin{pmatrix} \cos(\frac{\theta}{2}) \\ e^{i\theta}\sin(\frac{\theta}{2}) \end{pmatrix} \quad (1.6)$$

The angles define a point on a sphere of radius 1, which is called *Bloch sphere*, represented in Fig.1.2. A transformation which brings a qubit to another point of the sphere’s surface is called “unitary”.

Any state can then be represented by any of the points on the surface of the sphere via a unitary transformation.

We define a set of orthogonal states which will conventionally constitutes the vertices of the sphere along axes x,y,z.

$$\begin{aligned} |+\rangle &= \frac{1}{\sqrt{2}}(|0\rangle + |1\rangle) = \frac{1}{\sqrt{2}} \begin{pmatrix} 1 \\ 1 \end{pmatrix}, & |-\rangle &= \frac{1}{\sqrt{2}}(|0\rangle - |1\rangle) = \frac{1}{\sqrt{2}} \begin{pmatrix} 1 \\ -1 \end{pmatrix}, \\ |L\rangle &= \frac{1}{\sqrt{2}}(|0\rangle + i|1\rangle) = \frac{1}{\sqrt{2}} \begin{pmatrix} 1 \\ i \end{pmatrix}, & |R\rangle &= \frac{1}{\sqrt{2}}(|0\rangle - i|1\rangle) = \frac{1}{\sqrt{2}} \begin{pmatrix} 1 \\ -i \end{pmatrix}, \end{aligned} \quad (1.7)$$

Conventionally we define  $\{|0\rangle, |1\rangle\}$  as the *computational basis*,  $\{|+\rangle, |-\rangle\}$  as the *diagonal basis* and  $\{|R\rangle, |L\rangle\}$  as the *circular basis*. Each couple is a complete set of linearly independent vectors.

Suppose now to have a qubit initially in the state  $|\psi\rangle$ , and decide to observe whether it is in another non-orthogonal state  $|\phi\rangle$ . This kind of observations are called *projective measurements* and are described by the operator  $\Pi_{|\phi\rangle} = |\phi\rangle\langle\phi|$ . As stated before, we have a non-zero probability  $|\langle\psi|\phi\rangle|^2$  to measure the system in  $|\phi\rangle$ . When we perform the measurement, the system changes in:

$$\frac{\Pi_{|\phi\rangle}|\psi\rangle}{\sqrt{|\langle\psi|\Pi_{|\phi\rangle}|\psi\rangle|^2}} = |\phi\rangle. \quad (1.8)$$

This points out an interesting property of quantum systems: performing a measurement on the system we change the state of the system itself. For classical systems this could not be achieved: if we measure a bit, for example in 0, then we are sure that

also the initial state was 0.

Moreover, the state changes instantaneously from  $|\psi\rangle$  to  $|\phi\rangle$  as soon as the measurement is performed. This instantaneous update of the state is called *collapse of the wave-function* [13].

We introduce the first link between quantum and classical information by observing that the result of a measurement onto a qubit can be represented by a bit: 0 if the state of the qubit collapses in  $|0\rangle$ , 1 if the state of the qubit collapses in  $|1\rangle$ . This means that a measurement onto a qubit produces exactly one bit of classical information.

Thus the difference between Quantum and Classical information cannot lie on the characteristics of the measurement results, as we inherently destroy the quantumness of the state when we measure it; indeed suppose we have  $N$  copies of identical qubits, and that we perform the same measurement onto them all. Depending on  $\alpha$  and  $\beta$  we will obtain different results for each measurement even if the qubit was the same (unless either  $\alpha$  or  $\beta$  are 0). This represents a profound difference between the nature itself of bits and qubits: if we make measurements onto multiple copies of a bit, we will always obtain the same result. The phenomenon of having a quantum state in somehow both state at the same time is called Quantum Superposition [3].

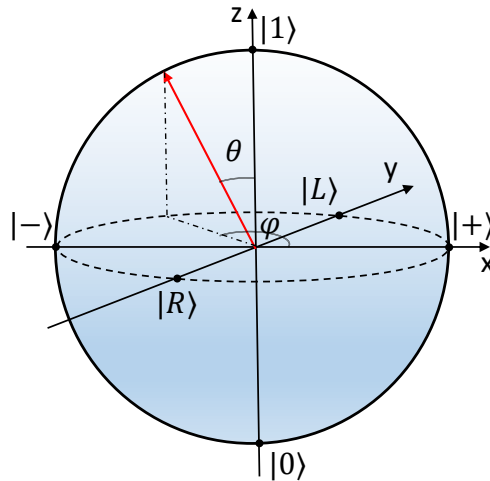


Figure 1.2: Bloch representation of a qubit, by the angles  $\theta$  and  $\varphi$ .

## 1.2.2 Multi-partite quantum systems

The pure state of an ensemble of  $M$  dimensional quantum subsystem is fully described by a normalized vector  $|\psi\rangle_{1,\dots,M}$  in an Hilbert space  $\mathcal{H}$  given by the *tensor product* of all the Hilbert spaces of the single subsystems  $\mathcal{H}_i$ :

$$\mathcal{H} = \mathcal{H}_1 \otimes \mathcal{H}_2 \otimes \dots \otimes \mathcal{H}_M.$$

If each subsystem is  $N$ -dimensional, the dimension of the total system  $\mathcal{H}$  is  $N^M$ . Mixed states are also described by the density matrix formalism. We may outline another difference between classical and quantum systems: for a classical ensemble of systems we used the cartesian product, here we use the tensor product.

If we are interested in describing only a subset of systems, we proceed analogously

to the classical case: we “trace out” the remaining subsystems. For example, for a bipartite system composed of A and B, the density matrix for the subsystem A alone is given by:

$$\rho_A = \text{Tr}_B(\rho_{AB}),$$

where  $\rho_{AB}$  is the density matrix of the total bipartite system, and  $\text{Tr}_B$  is the *partial trace* over system B, defined as  $\text{Tr}_B(\rho_{AB}) = \sum_i \langle \phi_i | \rho_{AB} | \phi_i \rangle_B$  with  $\{|\phi_i\rangle_B\}$  an orthonormal basis of the Hilbert space  $\mathcal{H}_B$ . Note that  $\text{Tr}_B$  is independent from the chosen basis  $\{|\phi_i\rangle_B\}$ , so we can use the one that suits us better.

### 1.2.3 Mixed States and Density Matrix

If the wavefunction of a state is exactly known, the state is said to be *pure* and can be represented as a vector on the surface of the Bloch sphere. However, exactly as in the classical case, we could have non-perfect knowledge of the quantum state: for example, we could have a system which is in state  $|\psi_1\rangle$  with probability  $p_1$  and in state  $|\psi_2\rangle$  with probability  $p_2$ . In this case the state cannot be effectively represented as a linear superposition of base vectors, and it is called a *quantum mixed state*. The only way to represent mathematically a mixed state is via the density matrix formalism. The *completely mixed* state, is the state represented by a null vector in the center of the Bloch sphere.

The density matrix formalism provides a very interesting way to describe quantum systems whose state is not completely known. If a quantum system is in a pure state  $|\psi\rangle$ , the corresponding density matrix is:

$$\rho = |\psi\rangle\langle\psi| \quad (1.9)$$

The density matrix of a pure state satisfies the property  $\rho^2 = \rho$ .

However it is possible to generalize the definition to mixed states by considering an *ensemble of pure states* defining a set of possible quantum states of a system, indexed by  $i$  and defined as  $\{p_i, |\psi_i\rangle\}$ . The corresponding density matrix can be represented as:

$$\rho = \sum_i p_i |\psi_i\rangle\langle\psi_i| \quad (1.10)$$

where  $0 < p_i \leq 1$  and  $\sum_i p_i = 1$ . In this situation  $\rho^2 \neq \rho$ .

The density operator  $\rho$ , which is represented by the density matrix, has the following properties:

- (Trace condition)  $\text{Tr}(\rho) = 1$ ;
- (Positivity condition)  $\rho$  is a positive operator;
- (Hermiticity)  $\rho = \rho^\dagger$ .

These properties lead to some interesting and useful features of the density matrix. A pure state for example will be described by a density matrix whose diagonalized form

possesses only one non-zero eigenvalue. Furthermore it can be shown that  $\text{Tr}(\rho^2) \leq 1$ , saturated only if and only if  $\rho$  is a pure state.

The expected value of a given operator  $\hat{A}$  by using the density operator:

$$\langle A \rangle = \text{Tr}(\rho A) = \sum_i \langle \psi_i | A | \psi_i \rangle \quad (1.11)$$

The density operator can be used to describe subsystems of a composite quantum system. Suppose having two physical system A and B, whose state is described by a density matrix  $\rho_{AB}$ : the *reduced density operator* for system A is defined by:

$$\rho_A = \text{Tr}_B(\rho_{AB}) \quad (1.12)$$

where  $\text{Tr}_B$  is the *partial trace* over system B. Operationally the partial trace is defined as:

$$\text{Tr}_B(|a_1\rangle\langle a_2| \otimes |b_1\rangle\langle b_2|) = |a_1\rangle\langle a_2| \text{Tr}(|b_1\rangle\langle b_2|) \quad (1.13)$$

where  $|a_1\rangle$  and  $|a_2\rangle$  are two vectors in the state space of A and the other two in the state space of B.

### 1.2.4 Entanglement and Separable States

Entanglement was first described by Einstein, Podolsky and Rosen [1] and Schrodinger [14] as a strange phenomenon of quantum mechanics that could allow very unintuitive behaviour of quantum systems. After a long debate between Einstein and Bohr on the completeness of quantum mechanics, Bell recognized that entanglement leads to experimentally testable deviations of quantum mechanics from classical physics [15]. Only with the advent of quantum information and computation theory, entanglement was finally recognized as a fundamental resource enabling tasks like quantum teleportation [16] [17] [18] or quantum cryptography (for example Ekert91 Protocol) [19]. The rapidly increasing interest in quantum information processing has motivated the detailed study of entanglement in multipartite system [20]. While the two-qubit entanglement is well understood, the multi-qubit entanglement is not a trivial extension of the bipartite case. In this section, the basic notions of entanglement will be explained.

#### Bipartite entanglement of pure states

Considering two systems, A and B, of two different Hilbert spaces  $H_A$  and  $H_B$  with dimensions  $d_A$  and  $d_B$ , it is possible to write the most generical pure bipartite state as:

$$|\psi\rangle = \sum_{i,j=1}^{d_A,d_B} c_{ij} |a_i\rangle \otimes |b_j\rangle \quad (1.14)$$

in the Hilbert space  $H_A \otimes H_B$ , with a complex  $d_A \times d_B$  matrix  $C = (c_{ij})$ .

**Definition 1 (Entanglement for pure states)** A pure state  $|\psi\rangle \in H$  is called separable if there exists  $|\phi_A\rangle \in H_A$  and  $|\phi_B\rangle \in H_B$  such that:

$$|\psi\rangle = |\phi_A\rangle \otimes |\phi_B\rangle \quad (1.15)$$

holds. Otherwise the state  $|\psi\rangle$  is called entangled.

**Definition 2 (Entanglement for mixed states)** Let  $\rho$  be a density matrix for a composite system.  $\rho$  is a product state if there exist  $\rho^A, \rho^B$  such that:

$$\rho = \rho^A \otimes \rho^B. \quad (1.16)$$

The state is called separable, if there exists a set of convex weights  $p_i$  and of product states  $\rho_i^A \otimes \rho_i^B$  such that:

$$\rho = \sum_i p_i \rho_i^A \otimes \rho_i^B \quad (1.17)$$

holds. Otherwise the state is called entangled.

Physically, the definition of product states means that the state is uncorrelated. A product state such that in Eq.(1.15) or Eq.(1.17) can be obtained by a Local Operation and Classical Communication (LOCC) procedure: Albus and Bellatrix can share a random number generator that produces the outcomes  $i$  with probabilities  $p_i$ . For each of the outcomes, they can agree to produce the state  $\rho_i^A \otimes \rho_i^B$  locally. If a state is entangled, the correlation could not originate from a LOCC procedure: in this sense entangled states are a typical feature of quantum mechanics.

There are several criteria that imply separability or entanglement of a state such as the positive partial transpose separability criterion, the entanglement witnesses criterion, the reduction criterion, the range criterion, the matrix realignment criterion and the linear contraction criterion and probably much more [3]. It is above the aim of this thesis to present every criterion in detail, but just the *presence* of such a number of different criteria for assessing entanglement should suffice to understand that the entanglement of a quantum state is something difficult to grasp thoroughly, and thing only get worse when the dimension of the Hilbert state gets larger.

### Maximally Two-Qubit Entangled State and Distillation

The Hilbert Space  $H_{AB}$  could be described using a basis made of  $d$  entangled or separable states. In the case of  $d = 4$ , it is possible to define the Bell States:

$$|\phi^+\rangle = \frac{1}{\sqrt{2}} (|0\rangle|0\rangle + |1\rangle|1\rangle)_{AB} \quad (1.18)$$

$$|\phi^-\rangle = \frac{1}{\sqrt{2}} (|0\rangle|0\rangle - |1\rangle|1\rangle)_{AB} \quad (1.19)$$

$$|\psi^+\rangle = \frac{1}{\sqrt{2}} (|0\rangle|1\rangle + |1\rangle|0\rangle)_{AB} \quad (1.20)$$

$$|\psi^-\rangle = \frac{1}{\sqrt{2}} (|0\rangle|1\rangle - |1\rangle|0\rangle)_{AB} \quad (1.21)$$

These states represent an entangled basis for a two-qubit systems. In this situation the Bell States represent the Maximally Entangled States (MES) for the Hilbert Space  $H_{AB}$  [21]. This states are fundamental for many tasks in quantum information theory.

### 1.2.5 Multipartite entanglement

When moving to higher dimensions the problem of assessing entanglment becomes much more complex. Indeed in the case of an Hilbert Space  $H_{A_1 \dots A_n} = H_{A_1} \otimes \dots \otimes H_{A_n}$ , there are many types of quantum states and the definition of entanglement becomes vague. The natural extension of bipartite non-separability becomes  $\rho_{AB} = \sum_{i=1}^k p_i \rho_{A_1}^i \otimes \dots \otimes \rho_{A_n}^i$ , which basically means that whatever bipartition one may take from the multipartite state, it will always be in a mixed state form, this condition is called *full separability*, but of course it doesn't represent the complete set of possible multipartite entangled states. In this thesis we will consider system of no more than four qubits but for simplicity's sake, we will present the whole zoology of *tripartite entangled states*.

#### Entanglement of three qubits

Acin et al. [20] and Sabin et al. [22] introduced a classification of mixed three-qubit states which comprises of:

- Full Separability (FS),
- Biseparability,
- Full Inseparability (FI).

This definition holds for both pure and non-pure states. Conventionally these classes are identified by the number of entangled reduced two-qubit states. Reduced biseparable and FI states are Local Unitary (LU) invariants: LOCC procedure cannot produce entanglement and therefore all the invertible local operation (unitary ones in particular) must leave these classes of entanglement invariant.

A state in any of these subtypes cannot be transformed in another subtype by a LU transformation.

The classification of the different three-qubit quantum states is equally valid for pure and non-pure quantum states: there are quantum subtypes existing only for non-pure quantum states.

- Type 0-0: FS three-qubit quantum states which present (*no entanglement*);
- Type 1: biseparable quantum states wich possess bipartite entanglement;
  - $1^1-0$ : These are biseparable quantum states with no reduced entanglement: meaning that two of the three qubit are entangled when the total three-qubit quantum state is considered, but when one takes the partial trace over the third qubit, the reduced two-particle state is separable. This subtype exists only for non-pure three-qubit systems. An example is:

$$\rho = \frac{1}{2}|1\rangle\langle 1|_A \otimes |\psi_+\rangle\langle \psi_+|_{BC} + \frac{1}{2}|0\rangle\langle 0|_A \otimes |\psi_-\rangle\langle \psi_-|_{BC} \quad (1.22)$$

where  $|\psi_{\pm}\rangle$  are Bell States. Tracing out qubit A:

$$\text{Tr}_A(\rho) = \rho^{(BC)} = \frac{1}{2}|\psi_+\rangle\langle\psi_+|_{BC} + \frac{1}{2}|\psi_-\rangle\langle\psi_-|_{BC} \quad (1.23)$$

that is a separable state;

- 1<sup>1</sup>-1: These are biseparable quantum states with entanglement remaining when the separable qubit is traced over. All pure biseparable states belong to this category. An example of pure state could be:

$$|\psi\rangle = |\varphi\rangle_A \otimes |\phi\rangle_{BC} \quad (1.24)$$

with  $|\phi\rangle_{BC}$  entangled. This state gives a reduced state:  $\rho^{(BC)} = |\phi\rangle\langle\phi|_{BC}$ .

- 1<sup>2</sup>: this subtype contains generalized biseparable states with bipartite entanglement in two pair of qubits. A simple example of a state  $\rho \in (1^2)$  subtype is:

$$\rho = p_{1A}(\rho_1^A \otimes \rho_1^{BC}) + p_{1B}(\rho_1^B \otimes \rho_1^{AC}) + p_{2A}(\rho_2^A \otimes \rho_2^{BC}) + p_{2B}(\rho_2^B \otimes \rho_2^{AC}) \quad (1.25)$$

with the normalization condition of the probabilities:  $\sum_{iJ} p_{iJ} = 1$  and at least one  $\rho_i^{XY}$  entangled for each  $XY$ ;

- Subtype 1<sup>3</sup>: this subtype contains generalized biseparable states in the three pairs of qubit, for example:

$$\rho = p_A(\rho^A \otimes \rho^{BC}) + p_B(\rho^B \otimes \rho^{AC}) + p_C(\rho^C \otimes \rho^{AB}) \quad (1.26)$$

with the normalization condition of the probabilities:  $\sum_J p_J = 1$  and the three  $\rho_i^{XY}$  entangled;

- Type 2: FI states. Both mixed and pure state can belong to this category;
  - 2-0: This type of entanglement is *fragile* because it disappears with an operation of partial tracing over the tripartite quantum system. The three-qubit pure Greenberger-Horne-Zeilinger (GHZ) state belong here:

$$|GHZ\rangle = \frac{1}{\sqrt{2}}(|000\rangle + |111\rangle) \quad (1.27)$$

Tracing out qubit A we obtain  $\rho^{(BC)} = \text{Tr}_A(\rho_{GHZ})$ :

$$\rho^{(BC)} = \text{Tr}_A(\rho_{GHZ}) = \begin{pmatrix} \frac{1}{2} & 0 & 0 & 0 \\ 0 & 0 & 0 & 0 \\ 0 & 0 & 0 & 0 \\ 0 & 0 & 0 & \frac{1}{2} \end{pmatrix}$$

which is separable.

- 2-1: When tracing out qubits, one couple of qubits preserve entanglement, the other two are separable;
- 2-2: two reduced entanglements are non-zero. In the case of pure states  $\rho \in (2-2)$ ,  $\rho$  is called a Star Shaped States (SSS) [23];
- 2-3: three reduced entanglements are non-zero. These particular states are called W-states [24]. This type of entanglement is *robust* because it survives after a partial trace operation. The pure W state of three-qubit is:

$$|W\rangle = \frac{1}{\sqrt{3}} (|001\rangle + |010\rangle + |100\rangle) \quad (1.28)$$

If we trace out qubit A  $\rho^{(BC)} = Tr_A(\rho_W)$ :

$$\rho^{(BC)} = Tr_A(\rho_W) = \begin{pmatrix} \frac{1}{3} & 0 & 0 & 0 \\ 0 & \frac{1}{3} & \frac{1}{3} & 0 \\ 0 & \frac{1}{3} & \frac{1}{3} & 0 \\ 0 & 0 & 0 & 0 \end{pmatrix}$$

The presence of off-diagonal elements shows the presence of (bipartite) entanglement even after the trace operation. The symmetry of the W state allows this operation to be performed on every qubit with the same results.

Vectors belonging to GHZ- and W- types cannot be transformed into each other by local operation and classical communication (LOCC) [20].

Here we showed that the passage from two qubit states (which could be ‘entangled’ or ‘separable’ and nothin else) to three qubit states (which have at least 8 different categories) leads to an outstanding increase in the categorization of entangled states and properties. The generalization to a n-dimensional multipartite state is a non trivial task and definitely one of the open problems in quantum information theory.

## 1.3 Distance between quantum states

Until now we have introduced tools which identify characteristics of quantum states, now we present the methods which quantify how quantum states are *similar* one to each other.

### 1.3.1 Trace Distance

**Definition 3 (Trace Distance)** *The Trace Distance between two quantum states  $\rho$  and  $\sigma$  is*

$$D(\rho, \sigma) = \frac{1}{2} Tr|\rho - \sigma| \quad (1.29)$$

In particular, if  $\rho$  and  $\sigma$  commute, then we can consider the (same) basis in which the two matrixes are diagonal:

$$\rho = \sum_i r_i |i\rangle\langle i| ; \quad \sigma = \sum_i s_i |i\rangle\langle i| \quad (1.30)$$

for some orthonormal basis  $|i\rangle$ . Thus:

$$D(\rho, \sigma) = \frac{1}{2} \left| \sum_i (r_i - s_i) |i\rangle\langle i| \right| = D(r_i, s_i) \quad (1.31)$$

It is possible to demonstrate that the trace distance between two qubits represented as vectors on the Bloch sphere can be expressed as half the Euclidean distance between the two vectors. This justifies the consideration that any unitary rotation on the Bloch sphere leaves the trace distance invariant:

$$D(U\rho U^\dagger, U\sigma U^\dagger) = D(\rho, \sigma) \quad (1.32)$$

### 1.3.2 Fidelity

**Definition 4 (Fidelity)** *The fidelity of two quantum states  $\rho$  and  $\sigma$  is:*

$$F(\rho, \sigma) = \text{Tr} \sqrt{\rho^{\frac{1}{2}} \sigma \rho^{\frac{1}{2}}} \quad (1.33)$$

When  $\rho$  and  $\sigma$  commute the Fidelity can be expressed as:

$$F(\rho, \sigma) = \text{Tr} \sqrt{\sum_i r_i s_i |i\rangle\langle i|} = \text{Tr} \left( \sum_i \sqrt{r_i s_i} |i\rangle\langle i| \right) = \sum_i \sqrt{r_i s_i} = F(r_i, s_i) \quad (1.34)$$

When  $\rho$  and  $\sigma$  commute, the quantum fidelity correspond to the classical fidelity between the eigenvalues of  $\rho$  and  $\sigma$ . The Fidelity generalized formula (1.33) could be simplified in the case of the distance between a pure state and a density matrix:

$$F(|\psi\rangle, \rho) = \text{Tr} \sqrt{\langle \psi | \rho | \psi \rangle | \psi \rangle \langle \psi |} = \sqrt{\langle \psi | \rho | \psi \rangle} \quad (1.35)$$

In the case of the two pure states:

$$F(|\psi\rangle, |\phi\rangle) = |\langle \psi | \phi \rangle|^2 \quad (1.36)$$

F can assume values from 0 (orthogonal state) to 1 (same state). In the case of the Fidelity there is no parallelism with an euclidean distance over the Bloch sphere.

### 1.3.3 Frobenius Norm

The *Frobenius Norm* (or *Hilbert-Schmidt Norm*) is a very useful mathematical tool to determine the distance between two different matrices: as in the case of *trace distance* and *fidelity*, the Frobenius norm could be used to determine how far are two density matrix operators; given  $\rho$  and  $\rho'$ , it is possible to compute ( $A = \rho - \rho'$ ) and calculate the Frobenius Matrix Norm on A:

$$\|A\|_F^2 = \sum_{i,j} |a_{ij}|^2 \quad (1.37)$$

It is very useful to utilize the Frobenius Matrix Norm in minimization problems: given a matrix depending on some parameters, it is possible to find them in order to minimize the distance between two different matrices.

## 1.4 Characterizing entanglement

Now we have a definition of entanglement, and a way to compare the distance between arbitrary quantum states. However we still need tools enabling us to *measure* the amount of entanglement that is in a quantum state. Of course, checking if the state can be written as a tensor product of pure states becomes not only computationally hard (as it implies the diagonalization of  $2^N \times 2^N$  matrixes where N is the dimension of the system), but also doesn't take into account the inevitable presence of experimental imperfections in any physical implementation.

To characterize entanglement we then need some function of the state able to quantify the degree of entanglement in an algorithmic fashion. Finding and studying these quantities has been a very active field in the last decades. The task is relatively simple for bipartite states [25], but for systems with more than two qubits an operative entanglement quantifier is known just for very specific cases [26–28]. Here we report some examples of the most used entanglement quantifiers for bipartite systems and that will be used throughout the following chapters:

### 1.4.1 Concurrence

One of the most used metrics for pure bipartite states is the *concurrence* [29]. For a mixed state  $\rho$  it can be operatively defined as:

$$C \equiv \max(0, \lambda_1 - \lambda_2 - \lambda_3 - \lambda_4), \quad (1.38)$$

where which  $\lambda_1, \dots, \lambda_4$  are the eigenvalues of the matrix

$$\Lambda = \rho(\sigma_y \otimes \sigma_y)\rho^*(\sigma_y \otimes \sigma_y) \quad (1.39)$$

in decreasing order. For a pure state  $|\psi\rangle = \alpha|00\rangle + \beta|01\rangle + \gamma|10\rangle + \delta|11\rangle$  the concurrence can be simply rewritten as the quantity  $C = 2|\alpha\delta - \beta\gamma|$ .

The concurrence has the following properties:

1.  $0 \leq C \leq 1$  for any state  $\rho$ ,

2.  $C = 0$  if and only if the state is separable,
3.  $C = 1$  if and only if the state is maximally entangled.

Therefore, the concurrence tells us how close a state is to be separable or maximally entangled.

### 1.4.2 Von Neumann Entropy

The von Neumann entropy is defined as  $S(\rho) = -\text{Tr}(\rho \log \rho)$ . This is a generalization of the Shannon entropy to quantum systems. It is easy to notice that this quantity is equivalent to the Shannon entropy of the eigenvalues of  $\rho$ , so if  $\{\lambda_i\}$  are the eigenvalues of  $\rho$  the definition can be re-expressed  $S(\rho) = -\sum_i \lambda_i \log \lambda_i = H(\{\lambda_i\})$ . As a consequence,  $S = 0$  if and only if the state is pure, while for a completely mixed system the entropy reaches its maximum value  $S = \log N$ , where  $N$  is the dimension of the Hilbert space.

The entropy of the reduced density matrix is a good measure of entanglement [8]:  $\mathcal{C} = S(\rho_A) = -\text{Tr}(\rho_A \log \rho_A)$ , where  $\rho_A = \text{Tr}_B(\rho)$ . It can be proven that this quantity is the same independently of which subsystem we trace over first.

For example, if the state is maximally entangled, by definition the reduced state is completely mixed and  $\mathcal{C}$  has its maximum value  $\mathcal{C} = \log N$ . On the other hand, if we have a pure separable state, the reduced state is also pure and  $\mathcal{C} = 0$ .

### 1.4.3 Considerations on the entanglement quantifiers

Note that entanglement is a global property of a quantum state and cannot be fully evaluated by accessing only a part of it. Therefore entanglement quantifiers are not direct observables, i.e. they can not be determined by only one measure.

For example, to calculate the concurrence we first have to measure the state of the system in order to determine  $\Lambda$  in eq.(1.39) and its eigenvalues. The determination of the state is performed via a *quantum state tomography* [30], which requires a number of measures scaling exponentially with the size of the system. Therefore, calculating an entanglement quantifier is considered a demanding task experimentally. Quantum state tomography will be presented in chapter 2.6.

On the other hand, we could just be interested in knowing whether our state is entangled or separable, and not be bothered in exactly quantifying the degree of the entanglement. In these cases other quantities, called *entanglement witnesses*, can be used, which only certify the presence of entanglement in our state without quantifying it.

The entanglement witnesses are much less demanding experimentally and are therefore the more efficient way to check if a system is entangled or not. They will be discussed in more detail in the following.

Recently an efficient way to extract the concurrence from a system was theoretically proposed [31, 32] and experimentally realized [33].

## 1.5 Bell Inequalities and non locality witnesses

In this section we introduce Bell's Inequalities, which are one of the most important discoveries in Quantum Information Theory. In 1935, Einstein, Podolsky and Rosemberg published a famous paper [1] in which they tried to prove that Quantum Mechanics as formulated by Bohr and Schroedinger couldn't be a complete theory. Their *gedankenexperiment*, which became famous as the EPR paradox consisted in predicting paradoxical results when considering measures taken over a pair of entangled particles. The authors claimed that given a specific experiment which uses entangled particles, there are cases in which the outcome of a measurement is known before the measurement takes place. But if something is known with certain, than it becomes an 'element of reality', which, according to the authors, must be *local*, in the sense that each belongs to a certain point in spacetime. Each element may only be influenced by events which are located in the backward light cone of its point in spacetime (i.e., the past). These claims are founded on assumptions about nature that constitute what is now known as local realism.

As in Quantum Mechanics the element of reality changes according to another measurement (random) result, the authors concluded that the theory wasn't complete, meaning *there was still something missing* in order for the theory to give a complete description of reality.

The paradox was solved thirty years later by John Bell in 1964 [34]. Bell formulated a quantitative expression that allowed direct observation of the consequences of EPR's predictions: we can suppose having a bipartite system and performing measurements on both parties, we can assume that the results of the measurements existed *locally* before the measurement and we can assume realism. Then it is possible to formulate an inequality on a particular set of measurements that assumes a different bound depending if the theory behind Quantum Mechanics is incomplete or not.

### 1.5.1 Derivation of the Bell inequality

An incomplete theory means that it is possible to postulate that there exist an hidden variable  $\lambda$  such that a deterministic result  $O(\lambda)$  is obtained from the measurement of a physical observable  $O$ . The introduction of  $\lambda$  potentially restores local realism of QM. Using a probability distribution  $p(\lambda)$  it is possible to obtain the expected value of  $O$ :

$$\langle O \rangle = \int O(\lambda)p(\lambda)d\lambda \quad (1.40)$$

Here  $p(\lambda)$  is the probability function of the hidden variable. We define  $A(a, \lambda)$  and  $B(b, \lambda)$  the measurements which are causally disconnected of a dichotomic variable which can assume either +1 or -1 value, and we assume that the locality principle holds. The measurements are then independent as they are not connected in any way. The main value of the correlations between their outcomes is:

$$C(a, b) = \int A(a, \lambda)B(b, \lambda)p(\lambda)d\lambda \quad (1.41)$$

At the same time:

$$C(a, b') = \int A(a, \lambda)B(b', \lambda)p(\lambda)d\lambda \quad (1.42)$$

We repeat the procedure in order to calculate  $C(a', b)$  and  $C(a', b')$  and then we use the *triangular inequality*:

$$|C(a, b) - C(a, b') + C(a', b) + C(a', b')| \leq \int d\lambda p(\lambda) [ |B(b, \lambda) - B(b', \lambda)| + |B(b, \lambda) + B(b', \lambda)| ] \quad (1.43)$$

Now, as the results are dichotomic we obtain a numerical bound:

$$|C(a, b) - C(a, b') + C(a', b) + C(a', b')| \leq 2 \quad (1.44)$$

Eq. (1.44) is best known as the Clauser Horne Shimony Holt (CHSH) inequality [35] [36]. This inequality is satisfied if the starting assumptions hold true. In this case, if there exist an hidden variable inside QM. Let's see what happens if we link CHSH-Bell inequality to a quantum state measurement: taking, for example, the observables  $A_1 = -\sigma_x$ ,  $A_2 = -\sigma_y$ ,  $B_1 = (\sigma_x + \sigma_y)/\sqrt{2}$  and finally  $B_2 = (\sigma_x - \sigma_y)/\sqrt{2}$ , the quantum state with the highest violation of CHSH-Bell inequality is the singlet Bell state is:  $|\psi\rangle = \frac{1}{\sqrt{2}}(|01\rangle - |10\rangle)$ . It can be shown that quantum mechanics does not allow for violation higher than  $2\sqrt{2}$ : this value is called the *Tsirelson Bound* [37].

## 1.5.2 Violation of the CHSH inequality and non locality

The violation of the CHSH inequalities was demonstrated experimentally by Aspect et al. in 1981 [38]. This finally closed a 50 year long debate and 'local realism' was finally put apart. Indeed the violation of a CHSH-Bell inequality corresponds to *non-locality*: the results of the measurements realized on a given system could not be explained via a local hidden variables model.

A violation of the inequality, in quantum mechanics, implies that a given state is entangled.

A very straightforward demonstration of this:

Considering the form of a density operator for a separable state  $\rho = \sum_k p_k \rho_k^A \otimes \rho_k^B$  and the mathematical expression of the expected value of  $\langle A_i B_j \rangle = Tr(\rho A_i B_j)$ , we can write:

$$\langle A_i B_j \rangle = \sum_k p_k \mathbb{A}_k(A_i) \mathbb{B}_k(B_j) \quad (1.45)$$

where  $\mathbb{A}_k(A_i) = Tr(A_i \rho_k^A)$  and  $\mathbb{B}_k(B_j) = Tr(B_j \rho_k^B)$ . Violating Bell's inequalities means we can't recover the form in Eq. (1.45), thus the state is *entangled*.

It is very interesting to note that non-locality implies entanglement but the viceversa doesn't hold true: there exist entangled states that do not violate any Bell-like inequality. For this reason, we can say that the quantum feature given by non-locality, which is assessed by violation of Bell's inequalities is the *strongest* among all the quantum correlation, as it implies all the others [39].

## 1.6 Evolution of quantum systems

### 1.6.1 Evolution of Closed Quantum Systems and Logic Gates

The evolution of a closed quantum system  $|\psi\rangle$  is given by the well-known Schrödinger's equation

$$i\hbar \frac{d|\psi\rangle}{dt} = H|\psi\rangle, \quad (1.46)$$

where  $H$  is the hamiltonian of the system. A closed system means that it does not interact with an external one: all the dynamics of the system is completely described by the system's Hamiltonian  $H$ . It can be rewritten for a mixed state as the Von Neumann's equation:

$$i\hbar \frac{\partial \rho}{\partial t} = -[\rho, H]. \quad (1.47)$$

Equations (1.46) and (1.47) are equivalent to:  $|\psi\rangle_t = U(t)|\psi\rangle$ ,  $\rho_t = U(t)\rho_0U^\dagger(t)$ , where  $U(t)$  is a general unitary operator ( $UU^\dagger = \mathbb{I}$ ) which, for a time-independent hamiltonian, is in the form  $U(t) = \exp(-iHt/\hbar)$ . We can distinguish two different sets of unitary transformation, that constitute the building stones of any quantum operation: single and multiple qubit logic gates.

#### Single qubit logic gates

In classical information the only non-trivial operation on a single bit is the NOT gate, which switches the value of the bit. When considering qubits, however, any unitary 2x2 matrix can be used as single qubit logic gate.

The most common single qubit gates are the Pauli matrices  $\sigma_x$ ,  $\sigma_y$  and  $\sigma_z$  (sometimes we may also indicate them simply with  $X$ ,  $Y$  and  $Z$ ), the Hadamard gate

$$H = \frac{1}{\sqrt{2}}(Z + X) = \frac{1}{\sqrt{2}} \begin{pmatrix} 1 & 1 \\ 1 & -1 \end{pmatrix}, \quad (1.48)$$

and the phase shift operation

$$U_\phi = \begin{pmatrix} 1 & 0 \\ 0 & e^{i\phi} \end{pmatrix}. \quad (1.49)$$

A generic rotation of an angle  $\theta$  around an axis  $\hat{n}$  is given by the operator  $U = e^{i\frac{\theta}{2}\hat{n}\cdot\vec{\sigma}}$ . If we have a multipartite system with Hilbert space  $\mathcal{H} = \mathcal{H}_1 \otimes \mathcal{H}_2 \otimes \dots \otimes \mathcal{H}_N$  and operate single qubit gates separately on each subsystem, the total operation is obviously given by the unitary

$$U = U^{(1)} \otimes U^{(2)} \otimes \dots \otimes U^{(N)}. \quad (1.50)$$

It is easy to notice from eq. (1.50) that if we apply  $U$  to a separable state, it remains separable, and entangled states remain entangled as well. This means that operating single qubit gates on the subsystems of a multi-partite state, we can not generate nor destroy entanglement. In other words, via single qubit gates there are not interactions between the subsystems.

## Two qubit logic gates

In order to generate interactions, and hence manipulate entanglement, we need to operate gates that cannot be written in the form of eq.(1.50), i.e. that cannot be written as single qubit gates acting separately.

The representation of a two-qubit gate operator is a 4x4 unitary matrix. The most general two-qubit gate is the C-U gate and its operator is written in the form  $C-U = |0\rangle\langle 0|_c \otimes \mathbb{I}_t + |1\rangle\langle 1|_c \otimes U_t$ . This gate acts on a *target* qubit applying the single qubit gate U to it, depending on the state of a *control* qubit. Examples of notable gates are:

- The *C-PHASE* gate ( $U_t = U_\phi$ ):

$$C-PHASE = \begin{pmatrix} 1 & 0 & 0 & 0 \\ 0 & 1 & 0 & 0 \\ 0 & 0 & 1 & 0 \\ 0 & 0 & 0 & e^{i\phi} \end{pmatrix} \quad (1.51)$$

- The *C-NOT* gate (which has  $U_t = X$ ):

$$C-NOT = \begin{pmatrix} 1 & 0 & 0 & 0 \\ 0 & 1 & 0 & 0 \\ 0 & 0 & 0 & 1 \\ 0 & 0 & 1 & 0 \end{pmatrix} \quad (1.52)$$

In particular the action of the *C-NOT* gate can be easily written as  $C-NOT |x\rangle_c |y\rangle_t = |x\rangle_c |x \oplus y\rangle_t$

In order to show that this kind of gates generate entanglement, let us consider an initial state  $|+\rangle |0\rangle = (|0\rangle + |1\rangle) |0\rangle / \sqrt{2}$ , which is clearly separable. If we perform a *C-NOT* gate on this state we obtain  $C-NOT |+\rangle |0\rangle = (|00\rangle + |11\rangle) / \sqrt{2} = |\Phi^+\rangle$ , that is a Bell state. We have hence generated a maximally entangled state starting from a product state.

It has been demonstrated [11] that any non trivial two-qubit logic gate, e.g. the *C-NOT* gate, and the single qubit Hadamard gate form a universal set of quantum gates. Which means that any quantum operation on an ensemble of any number of qubits can be performed with a sequence of only *C-NOT* and Hadamard gates.

## 1.6.2 Evolution of Open Quantum Systems

### Kraus Representation

We now want to generalize and study the possible evolutions for systems which are not closed. In these cases the dynamics of the system may not be described by a Hamiltonian, thus in general we can have an evolution which is not unitary but given by a map  $\rho \mapsto \xi(\rho) = \rho'$ .

Let us assume that our system  $S$  is in contact with an external bath  $B$ . The overall system  $S + B$  is closed and undergoes the usual unitary evolution. We assume the

initial state as represented by the separable density matrix  $\rho = \rho_S \otimes |0\rangle\langle 0|_B$ <sup>1</sup>. The evolution of the total system is then of the form  $\rho' = U_{SB}(\rho_S \otimes |0\rangle\langle 0|_B)U_{SB}^\dagger$ . If we are only interested in the evolution of the system  $S$  we can at this point perform a partial trace on  $B$ :  $\rho'_S = Tr_B(\rho') = \sum_k \langle k|_B U_{SB}(\rho_S \otimes |0\rangle\langle 0|_B)U_{SB}^\dagger |k\rangle_B = \sum_k M_k \rho_S M_k^\dagger$ , where  $\{|k\rangle_B\}$  is an orthonormal basis for  $\mathcal{H}_B$ , and  $M_k = \langle k|_B U_{SB} |0\rangle_B$  are operators which act only on the system  $S$  and satisfy  $\sum_k M_k^\dagger M_k = \mathbb{I}^2$ . The map  $\xi$  of the evolution of the open system  $S$  is then given by  $\rho \mapsto \xi(\rho) = \sum_k M_k \rho M_k^\dagger$ . The properties of such a map are:

1. **Linearity:**  $\xi(\rho_1 + \rho_2) = \xi(\rho_1) + \xi(\rho_2)$  being  $M_k$  linear operators.
2. **Trace preserving:**  $Tr(\rho') = \sum_k Tr(M_k \rho M_k^\dagger) = \sum_k Tr(\rho M_k^\dagger M_k) = Tr(\rho \sum_k M_k^\dagger M_k) = Tr(\rho)$ .
3. **Hermiticity preserving:**  $(\rho')^\dagger = (\sum_k M_k \rho M_k^\dagger)^\dagger = \sum_k M_k \rho M_k^\dagger = \rho'$ .
4. **Positivity:**  $\langle \varphi | \rho' | \varphi \rangle = \sum_k \langle \varphi | M_k \rho M_k^\dagger | \varphi \rangle = \sum_k \langle \varphi' | \rho | \varphi' \rangle \geq 0$ .

We have obtained these properties in the case of system+bath, but they are expected to be satisfied by any physical evolution: 1) is valid for the linearity of quantum mechanics, and 2), 3) and 4) must be valid as we want the process to transform any physical state  $\rho$  into a state  $\rho'$  which is still physical. That is,  $\rho'$  has to satisfy the properties of a density matrix. In addition, if we want to characterize all the possible physical processes we have to consider that if we have a bipartite system and we apply the map  $\xi \otimes \mathbb{I}$ , we would still like to obtain a density matrix on the composite system. Unfortunately, if the map is simply positive, this is not the case as the positivity of the second subsystem is not assured. Thus we require a new condition:

- 4'. **Complete positivity:**  $\xi_1 \otimes \mathbb{I}_2$  is positive for any extension  $\mathcal{H}_2$  of  $\mathcal{H}_1$ .

So far we have seen the properties of a map in the form  $\xi\rho = \sum_k M_k \rho M_k^\dagger$ , with  $\sum_k M_k^\dagger M_k = \mathbb{I}$ , which can be regarded as a representation of a physical process. The *Kraus Theorem* assures that not only a map of that form represents a physical process, but that every physical transformation, which satisfies 1-3 and 4', can be represented in the form  $\rho \mapsto \xi(\rho) = \sum_k M_k \rho M_k^\dagger$  with  $\sum_k M_k^\dagger M_k = \mathbb{I}$ . This is called the *Kraus representation* of a physical transformation, and the operators  $M_k$  are called the *Kraus operators*.

### 1.6.3 Noisy channels

Any process allows a Kraus representation, but the representation is not unique: we have a freedom in the choice of the Kraus operators  $M_k$ . Indeed it can be demonstrated

<sup>1</sup>We can always assume the bath in a pure state, namely  $|0\rangle_B$ , otherwise we could just consider the bath as part of a larger system which is in a pure state and recall this system as our new bath.

<sup>2</sup> $\sum_k M_k^\dagger M_k = \sum_k \langle 0| U_{SB}^\dagger |k\rangle \langle k| U_{SB} |0\rangle = \langle 0| U_{SB}^\dagger U_{SB} |0\rangle = \langle 0| \mathbb{I}_{SB} |0\rangle = \mathbb{I}_S$

[11] that if we have two sets of Kraus operators  $\{E_1, \dots, E_N\}$  and  $\{F_1, \dots, F_N\}$ <sup>3</sup>, if and only if there exist complex numbers  $u_{ij}$ , such that  $E_i = \sum_j u_{ij} F_j$ , then the two representations give exactly the same physical process.

This freedom in choosing of the Kraus operators turns out to be very useful in many applications, such as, for example, in quantum error-correction protocols [11].

### Amplitude damping channels

Let us now consider an important example of open quantum system evolution using the Kraus representation: the *amplitude damping channel*. It is a schematic model of energy dissipation-effect due to loss of energy from a quantum system. For example, it describes the noise given by the decay of an excited state of a (two-level) atom due to spontaneous emission of a photon into the environment. Let us outline the process behind this phenomenon:

the evolution is described by a unitary transformation acting on the quantum system (A) and environment (E) according to  $|0\rangle_A |0\rangle_E \rightarrow |0\rangle_A |0\rangle_E$   $|1\rangle_A |0\rangle_E \rightarrow \sqrt{1-p} |1\rangle_A |0\rangle_E + \sqrt{p} |0\rangle_A |1\rangle_E$ . Here  $p$  represents the probability that an excited state in  $|1\rangle$  spontaneously decays in  $|0\rangle$ . By evaluating the partial trace over the environment, we find the Kraus operators

$$M_0 = \begin{pmatrix} 1 & 0 \\ 0 & \sqrt{1-p} \end{pmatrix}, \quad M_1 = \begin{pmatrix} 0 & \sqrt{p} \\ 0 & 0 \end{pmatrix}. \quad (1.53)$$

$M_0$  and  $M_1$  are the Kraus representation of the amplitude damping channel. The operator  $M_1$  induces a “quantum jump”, the decay from  $|1\rangle_A$  to  $|0\rangle_A$ , and  $M_0$  describes how the state evolves if there is no spontaneous decay.

### Depolarizing channels

Another important example of quantum noise is the *depolarizing channel*.

Consider a qubit that with probability  $p$  is replaced by the completely mixed state  $\mathbb{I}/2$  and with probability  $1-p$  it is left untouched.

The state transformation after this noise is given by the map:

$$\rho \rightarrow p \frac{\mathbb{I}}{2} + (1-p)\rho. \quad (1.54)$$

This map represents every process where a white noise occurs. For example, it can be used to describe imperfections in an interferometer due to non-ideal beams superposition and defects in the experimental apparatus.

## 1.7 Measures in a quantum systems

The last process that we need to use in order to obtain useful (classical) information from a quantum system is *measure* it. Indeed the properties of the state which are

<sup>3</sup>By appending zero operators to the shorter list of elements we may ensure that the two sets of operators have the same number of elements.

accessible to a measurement process are called ‘observables’. In this section we will formalize the nature of the quantum observables and how can they be measured.

### 1.7.1 Observables and projective measurements

An observable is a linear Hermitian operator on the Hilbert space of the system. Let  $A$  be an observable with eigenvalues  $a_k$  and relative eigenvectors  $|k\rangle$ .  $A$  can be expressed as  $A = \sum_k a_k |k\rangle \langle k| = \sum_k a_k \Pi_k$ , where  $\Pi_k = |k\rangle \langle k|$  are the projective operators on the eigenvectors  $k$ . If the system is in the state  $|\psi\rangle = \sum_k 1^N a_k |k\rangle$ , the probability of obtaining  $a_k$  as the outcome of the measurement is  $p(a_k) = |\langle k | \psi \rangle|^2 = \langle \psi | \Pi_k | \psi \rangle$ . In general for a system in a mixed state  $\rho$  we have  $p(a_k) = \langle k | \rho | k \rangle = \text{Tr}(\Pi_k \rho)$ .

Immediately after a measurement giving us the result  $a_k$ , the state of the system instantaneously collapses on the  $|k\rangle$  eigenstate. This process is called *wave function collapse* and it’s one of the most distinctive features of a quantum state.

In other words, the state instantaneously becomes

$$|\psi'\rangle = \frac{\Pi_k |\psi\rangle}{\sqrt{\langle \psi | \Pi_k | \psi \rangle}}. \quad (1.55)$$

Once the state has collapsed to a given eigenvector, any number of successive measurements over it will give the same result with certainty.

In conclusion, the measurement of an observable proceeds as it follows: we project the state of the system to the eigenstates of the observable, and, if the system is found in the eigenstate  $|k\rangle$ , the result of the measurement is the relative eigenvalue  $a_k$  and the system is in the new state  $|\psi'\rangle = |k\rangle$ .

This type of process is called *Projective measurement*, and is the most typical quantum measurement, although it is not the most general [40].

Analogously to how we passed from the evolution of closed systems to the evolution of open systems, we could consider the case where together with our system  $S$  we have an external ancillary system  $A$ , initially in a given state  $|a\rangle$ , that we are able to entangle with  $S$ . If we control the interaction and perform a projective measurement on the joint system  $S + A$ , tracing out  $A$  we have obtained information on  $S$ , i.e. we have achieved a measure. This type of measurement, called Positive Operator Valued Measure (POVM), is the more general measure we could perform, but is obviously more difficult to be implemented experimentally.

For a POVM the final state, resulted from the wave function collapse, is in general a mixed state, while for the projective measurement it is always a pure state [40].

## 1.8 Quantum correlations

We close this first chapter with a brief discussion on the correlations of quantum systems. In particular, we are interested in the following question: what are the properties that determine classical or quantum behaviour of a system? That is, when

can a system be regarded as genuinely quantum? Separable quantum states might have correlations that cannot be captured by a probability distribution defined over the states of an equivalent classical system. In other words, entanglement is a special kind of quantum correlation, however not the only one. We will introduce a quantity which makes possible to quantify all quantum correlations, including entanglement: the *Quantum Discord*.

### 1.8.1 Quantum Discord

The main measure of correlations between two systems  $A$  and  $B$  is the mutual information [8], which is defined as

$$\mathcal{I}(A : B) = S(A) + S(B) - S(A, B). \quad (1.56)$$

Here  $S(A, B)$ ,  $S(A)$  and  $S(B)$  are the Von Neumann entropies of the bipartite system  $AB$  and of the single subsystems  $A$  and  $B$ , respectively, and are given by

$$\begin{aligned} S(A, B) &= -\text{Tr}(\rho_{AB} \log \rho_{AB}), \\ S(A) &= -\text{Tr}(\rho_A \log \rho_A), \\ S(B) &= -\text{Tr}(\rho_B \log \rho_B), \end{aligned}$$

with  $\rho_A = \text{Tr}_B(\rho_{AB})$  and  $\rho_B = \text{Tr}_A(\rho_{AB})$  the two reduced density matrices of the subsystems.

Bayes's Theorem gives the conditional probability for a classical distribution  $p(a|b) = p(a, b)/p(b)$ , and the conditional Shannon entropy:

$$H(A|B) = -\sum_{a,b} p(a|b) \log(p(a|b)) = H(A, B) - H(B), \quad (1.57)$$

Then, using eq. 1.56, Bayes's rule leads to an equivalent expression for mutual information,

$$\mathcal{I}_C(A : B) = H(A) - H(A|B). \quad (1.58)$$

Now note that Bayes's Theorem applies only if we consider that the probabilities distribution of the two systems doesn't affect each other i.e. they are independent. In Quantum Mechanics this is of course not the case, and therefore for the Von Neumann entropy of a quantum system Eq.1.57 no longer applies.

For generalizing the classical conditional entropy to the quantum case we can recognize that classically  $H(A|B)$  quantifies the ignorance about the system  $A$  that remains if we make measurements to determine  $B$ . When  $B$  is a quantum system, the amount of information we can extract about it depends on the choice of measurement. If we restrict to projective measurements described by a complete set of orthogonal projectors on system  $B$ ,  $\{\Pi_j^{(B)}\}$ , corresponding to outcomes  $j$ , then the state of  $A$  after a measurement is given by

$$\rho_{A|j} = \frac{\text{Tr}_B \left( \Pi_j^{(B)} \rho_{AB} \Pi_j^{(B)} \right)}{p_j},$$

where  $p_j = \text{Tr}_{AB}(\rho_{AB}\Pi_j^{(B)})$ , is the probability of measuring the outcome  $j$ . A quantum analogue of the conditional entropy can then be defined as the average of the von Neumann entropies of the matrices  $\rho_{A|j}$ :

$$\bar{S}_{\Pi_j^{(B)}}(A|B) = \sum_j p_j S(\rho_{A|j}).$$

In addition, the concavity of the von Neumann entropy implies [41]:

$$S(A) \geq \bar{S}_{\Pi_j^{(B)}}(A|B). \quad (1.59)$$

That means that the equivalent of the mutual information in a quantum world becomes:

$$\mathcal{J}_{\{\Pi_j^{(B)}\}}(A : B) = S(A) - \bar{S}_{\Pi_j^{(B)}}(A|B) \geq 0, \quad (1.60)$$

which is analogous to the classical version (1.58).

Now,  $\mathcal{J}_{\{\Pi_j^{(B)}\}}$  depends on the choice of  $\Pi_j^{(B)}$  i.e. of the measurement choice. In order to quantify the entire set of classical correlations in  $\rho_{AB}$  we have to maximize  $\mathcal{J}_{\{\Pi_j^{(B)}\}}$  over all possible sets of projective operators. We then define

$$\mathcal{J}(A : B) = S(A) - \bar{S}(A|B), \quad (1.61)$$

with  $\bar{S}(A|B) = \min_{\{\Pi_j\}} \sum_j p_j S(\rho_{S|j})$ .

Mutual information quantifies the whole class of correlations that are in  $\rho_{AB}$  (quantum and classical), and  $\mathcal{J}(A : B)$  quantifies only the purely classical correlations. Therefore, their difference

$$\mathcal{D}(A, B) = \mathcal{I}(A : B) - \mathcal{J}(A : B) \quad (1.62)$$

is a measurement of the non-classical correlations of  $\rho_{AB}$ .  $\mathcal{D}(A : B)$  is called *quantum discord*. A nonzero value of  $\mathcal{D}(A : B)$  indicates the presence of non-classical correlations [41, 42].

This gives us a powerful tool which encompasses the whole range on non classical correlation, and entanglement, of course becomes just a particular case of discord.

For example, the two-qubit Werner state:  $\rho_W = \mathbb{I}(1-p)/4 + p|\psi\rangle\langle\psi|$  is entangled only for  $p > \frac{1}{3}$  (as it can be easily demonstrated using an entanglement witness like the concurrence), while it presents non-zero discord for any  $p > 0$ .

Furtermore, when the state  $\rho_{AB}$  is pure,  $S(A, B)$  and  $\bar{S}(A, B)$  are zero, and the discord is equal to  $S(B)$ , which is a measure of entanglement for bipartite pure states. In other words, for pure states all non-classical correlations characterized by quantum discord can be identified as entanglement, but for mixed states it is not the case.

The concept of discord was introduced in 2001 independently by Olliver and Zurek [41], and Henderson and Vedral [42]. It was later demonstrated that several fundamental features of quantum systems originally accounted to entanglement, as the

computational speed-up [43, 44], enhancement in metrology [45] and security [46], are also present for separable states with nonzero discord. These discoveries have recently focused the attention of the scientific community in characterizing the quantum discord. In the last few years important results were obtained [47–50].

# Chapter 2

## Quantum Information with Photons

So far we have analysed some basic concepts of the quantum information theory. An important physical aspect is the implementation of these ideas in an experiment. This is largely an open problem: it is still not clear if there is a physical system which allows us to simultaneously encode, process and readout quantum information in an efficient way. The required properties are:

1. Ability to efficiently generate qubits.
2. Ability to initialize the state of the qubits, for example in  $|0\rangle$  or in a maximally entangled state. The state of the initialization depends on the particular experiment.
3. Low noise level, in order to preserve and control the state of the qubits during the process.
4. Ability to perform single-qubit gates.
5. Ability to perform two-qubit gates (e.g. the CNOT gate) in order to generate entanglement.
6. Ability to efficiently perform measurements and readout the results.

It's easy to notice that it is very difficult for a physical system to possess requirements 3 and 5 altogether. Indeed, for a system to have low noise means that it must interact very weakly with the environment, as any interaction would change the state, affecting the computation. On the other hand, to perform two-qubit gates two subsystem have to interact strongly one with each other.

Any physical system we use to process quantum information (e.g. solid state qubits, trapped ions, photons, super-conductive qubits) is typically good in satisfying some of these properties and bad for some of the others. Because of these reasons, it is still an open question how to find a physical “hardware” allowing the experimental realization of general complex quantum operations. Many progresses have been made in this field recently[51–54], but it is still not clear which physical system is the best candidate for

processing quantum information, although each of them possess both strengths and weaknesses.

## 2.1 Why do we use photons?

In this chapter we report some methods for implementing quantum information protocols through optics. Photons are indeed good candidates for encoding qubits. First of all, they have approximately no interaction with the environment, and hence are very low noise systems. Photons may essentially be regarded as zero-temperature systems: they have approximately infinite coherence. This property allows the transmission of qubits over long distances. For example, single photon states transmission between an observer on the Earth and another on a satellite is feasible with the present technology [55].

Photons are thus especially suitable for quantum communication protocols. They are also very easy to manipulate singularly via simple optical elements, as we will see, thus allowing easy single-qubit gates implementation. Moreover, optical elements (e.g. beam-splitters, wave-plates) operate on single photons in the exact same way they operate on classical light. Indeed, differences between quantum and classical behaviour arise only as a result of the different nature of the states, while the operations performed are the same in both cases. In other words, the quantumness of a process depends only on the quantumness of the state, although the operation performed by an optical element does not depend on the nature of the input state.

This means that a quantum optical apparatus is really easy to calibrate: we simply have to mount and describe the apparatus using classical light<sup>1</sup>. Once all the apparatus is calibrated, the quantum behaviour is obtained sending quantum states encoded in single photons instead of classical light, and the experiment can be finally performed in the quantum regime. Regarding the efficiency of the readout, recently the development of superconducting nanowire single-photon detectors has increased the measurement efficiency up to 95% [56], and the performances of this type of detectors are expected to improve further.

Photons are thus very good in satisfying requirements 2, 3 and 4, and recently they are also rather good for 6.

On the other hand, the main big issue using photons is performing two-qubit gates, due to the absence of photon-photon interaction, which is a consequence of 3. A method for implementing two-qubit gates could be to mediate an interaction between two photons using a non-linearity induced by one of the two photons by the Kerr effect. Unfortunately, the non-linearity induced by the intensity of a single photon is so low that in order to obtain a CNOT gate we would require approximately  $10^9$  meters of non-linear material. This obviously makes this protocol very unlikely to be experimentally feasible.

---

<sup>1</sup>The classical light we use to calibrate the apparatus must have the same frequency of the photons, in order to have a response from the optical elements which is as similar as possible.

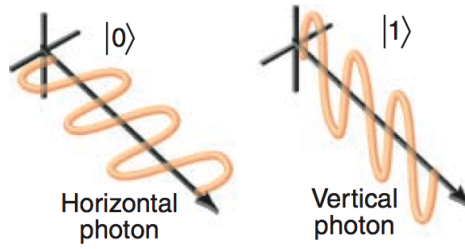


Figure 2.1: Qubit encoded in polarization. A horizontal polarized photon represents a logical “0” ( $|0\rangle \equiv |H\rangle$ ) and a vertical polarized photon represents a logical “1” ( $|1\rangle \equiv |V\rangle$ ).

Two-qubit gates can be implemented optically via a probabilistic scheme [57] using the Hong-Hou-Mandel effect [58], or deterministically via hybrid states or one-way quantum computation, as we will see in detail in section 2.2.3 and 4.2.

In addition, with the present technology, single-photon sources are highly inefficient. For example, the most used sources are based on Spontaneous Parametric Down Conversion (SPDC), which, being a non-linear process, has an efficiency of  $\approx 1\%$ . Recently some progresses have been made in this field [59–62], but the sources inefficiency still remains a huge obstacle for the scalability of optical schemes.

In conclusion, despite presenting some serious issues in terms of scalability, photonic architectures are considered among the best candidates for quantum information processing and many of the fundamental and most important experiments on quantum information have been performed via quantum optics [17, 38]. In this chapter we will describe how qubits can be encoded, processed and measured using photons.

## 2.2 Encoding and manipulating photonic single qubits

Photons enable encoding in many degrees of freedom, for example, polarization, path, angular momentum, time-bin or frequency. Here we will focus on the first two types of encoding.

### 2.2.1 Polarization-encoded qubit

Figure 2.1 shows how a qubit can be encoded in the polarization of a single photon. A horizontal polarized photon represents a quantum system in the logical state “0”, while a vertical polarized photon represents a logical “1”. We hence have the identification  $|0\rangle \equiv |H\rangle$  and  $|1\rangle \equiv |V\rangle$ . Diagonal and anti-diagonal polarized photons are then respectively in the state  $|+\rangle = (|H\rangle + |V\rangle)/\sqrt{2}$  and  $|-\rangle = (|H\rangle - |V\rangle)/\sqrt{2}$ , while for left and right circular polarized photons we have  $|L\rangle = (|H\rangle + i|V\rangle)/\sqrt{2}$  and  $|R\rangle = (|H\rangle - i|V\rangle)/\sqrt{2}$ .

Manipulation of single polarization qubits can be implemented using a birefringent wave plate, which, if the optical axis is along the vertical direction, introduces a phase

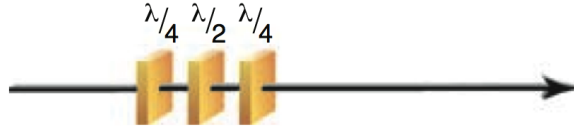


Figure 2.2: An arbitrary unitary transformation on a polarization qubit requires a  $\lambda/4$ - $\lambda/2$ - $\lambda/4$  sequence of wave-plates.

shift  $\varphi$  between  $|H\rangle$  and  $|V\rangle$ . The unitary matrix of a wave-plate with vertical axis, expressed in the computational basis, is then

$$M_{\varphi} = \begin{pmatrix} 1 & 0 \\ 0 & e^{i\varphi} \end{pmatrix}.$$

For  $\varphi = \pi$  we call the device *half wave-plate* (HWP), while for  $\varphi = \pi/2$  we have a *quarter wave-plate* (QWP). If the optical axis is rotated by an angle  $\theta$  from the vertical, the two different wave-plates give the transformations

$$M_{\text{HWP}}(\theta) = \frac{1}{\sqrt{2}} \begin{pmatrix} \cos(2\theta) & -\sin(2\theta) \\ -\sin(2\theta) & -\cos(2\theta) \end{pmatrix}$$

$$M_{\text{QWP}}(\theta) = \frac{1}{\sqrt{2}} \begin{pmatrix} i - \cos(2\theta) & \sin(2\theta) \\ \sin(2\theta) & i + \cos(2\theta) \end{pmatrix}.$$

It can be demonstrated [53] that an arbitrary single qubit unitary transformation can be achieved by a sequence of three wave-plates in the order  $\lambda/4$ - $\lambda/2$ - $\lambda/4$ , as shown in fig.2.2

For example, an Hadamard gate is obtained using a HWP rotated by  $\theta = \pi/8$ :

$$H = \frac{1}{\sqrt{2}} \begin{pmatrix} 1 & 1 \\ 1 & -1 \end{pmatrix} = M_{\text{HWP}}\left(\frac{\pi}{8}\right),$$

while for the Pauli gates we have:

$$Z \equiv \sigma_z = \begin{pmatrix} 1 & 0 \\ 0 & -1 \end{pmatrix} = M_{\text{HWP}}(0),$$

$$X \equiv \sigma_x = \begin{pmatrix} 0 & 1 \\ 1 & 0 \end{pmatrix} = M_{\text{HWP}}\left(\frac{\pi}{4}\right),$$

$$Y \equiv \sigma_y = \begin{pmatrix} 0 & -i \\ i & 0 \end{pmatrix} = M_{\text{HWP}}\left(\frac{\pi}{4}\right) \cdot M_{\text{QWP}}(0).$$

### 2.2.2 Path-encoded qubit

We can also encode the qubit in the path taken by the photon. This technique is alternatively called momentum-encoding. Consider for example that a photon may emerge from two sides of a beam-splitter (BS). We can say that the photon state is  $|\ell\rangle$

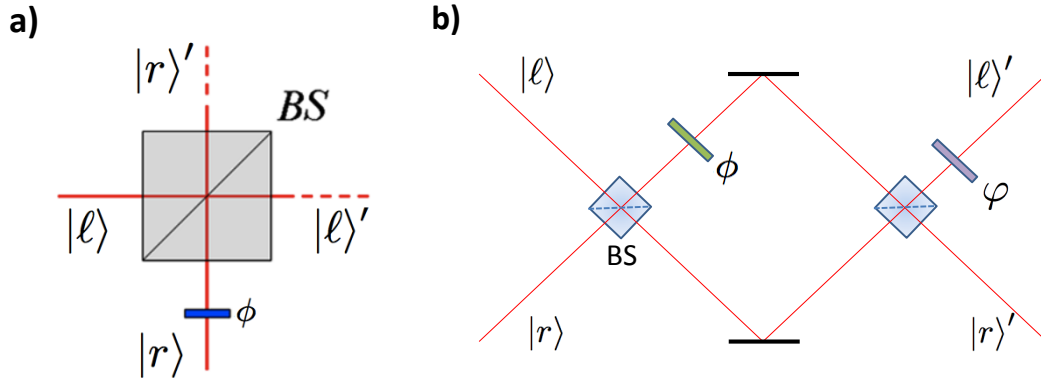


Figure 2.3: State manipulation for path-encoded qubit. **a)** A glass plate and a beam splitter implement the transformation  $|\ell'\rangle = \frac{1}{\sqrt{2}}(|\ell\rangle + e^{i\phi}|r\rangle)$ ,  $|r'\rangle = \frac{1}{\sqrt{2}}(|\ell\rangle - e^{i\phi}|r\rangle)$ . **b)** An arbitrary unitary transformation can be achieved via a Max-Zender interferometer and two phase shifters.

if it exits from the left side of the BS, while it is  $|r\rangle$  if it exits from the right side. We label these two states as the logic values  $|0\rangle \equiv |\ell\rangle$  and  $|1\rangle \equiv |r\rangle$ . Note that an arbitrary photon state  $\alpha|\ell\rangle + \beta|r\rangle$  represents a photon being both in the left path and the right path simultaneously. This means that, as the photon is in a superposition of  $|\ell\rangle$  and  $|r\rangle$ , it no longer behaves like a particle but more like a wave, i.e. it goes through both paths simultaneously. This outlines the well-known wave-particle duality of a quantum particle [63].

Inserting a phase shifter (for example a tilting glass plate) on the right path we can perform the transformation

$$U_\phi = \begin{pmatrix} 1 & 0 \\ 0 & e^{i\phi} \end{pmatrix}.$$

Note that for  $\phi = \pi$  it gives the  $Z$  Pauli gate. If the modes  $|\ell\rangle$  and  $|r\rangle$  are sent as inputs into a 50:50 beam-splitter, and we label  $|\ell'\rangle$  and  $|r'\rangle$  the two output modes, than the BS acts as an Hadamard gate:

$$\begin{cases} |\ell'\rangle = \frac{1}{\sqrt{2}}(|\ell\rangle + |r\rangle), \\ |r'\rangle = \frac{1}{\sqrt{2}}(|\ell\rangle - |r\rangle). \end{cases}$$

Inserting a phase shifter on the  $|r\rangle$  mode before the BS, as shown in fig.2.3a, we have the transformation

$$\begin{cases} |\ell'\rangle = \frac{1}{\sqrt{2}}(|\ell\rangle + e^{i\phi}|r\rangle), \\ |r'\rangle = \frac{1}{\sqrt{2}}(|\ell\rangle - e^{i\phi}|r\rangle). \end{cases} \quad (2.1)$$

As we will see in section 2.3, this type of manipulation is useful for measuring the Pauli operators for path-encoded qubits. An arbitrary unitary operation on a path qubit can be achieved using a Mach-Zehnder (MZ) interferometer and two phase shifters. The optical implementation of this scheme is depicted in fig.2.3b. If  $\phi$  is the phase given by the glass plate inside the MZ, and  $\varphi$  the one given by the phase shifter in the output mode, the transformation is given by

$$U = \begin{pmatrix} e^{i\varphi} \sin \phi & e^{i\varphi} \cos \phi \\ \cos \phi & -\sin \phi \end{pmatrix}.$$

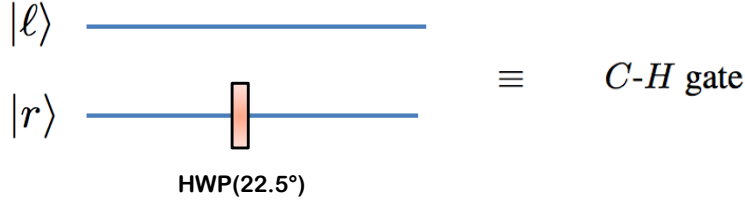


Figure 2.4: Experimental scheme for a controlled-Hadamard gate. If the photon passes in  $|\ell\rangle$  its polarization is left untouched, while if it passes in  $|r\rangle$  a HWP at  $\pi/8$  performs an Hadamard gate on the polarization.

This scheme can be generalized to factorize any  $N \times N$  unitary matrix into a sequence of two-dimensional BSs and phase shifters, using  $N$  input and output modes [64].

### 2.2.3 Hybrid photonic states

We have seen that photons allow us to encode qubits in polarization and path. We can also decide to use both degrees of freedom to simultaneously encode the information. In this way each photon carries two qubits, and we can have  $N$ -photons  $2N$ -qubits states. We call these states *hybrid photonic states*. If we have one photon  $A$  with qubits encoded in path and polarization, its separable pure states are of the form

$$|\pi\rangle_A \otimes |k\rangle_A,$$

where  $|\pi\rangle_A$  and  $|k\rangle_A$  label the polarization encoded and the path (momentum) encoded qubit, respectively. Note that, while in the case of only one degree of freedom the state of the single photon lives in a 2-dimensional Hilbert space, in this case it is 4-dimensional. In general, if we encode qubits in  $N$  degrees of freedom, the Hilbert space of the photon increases exponentially as  $2^N$ . Using more degrees of freedom then allows us to enlarge the Hilbert space exponentially, without increasing the required number of photons. This is an important resource for photonic architectures. Indeed, as we have discussed, increasing the photon number is a very inefficient task due to the non-linear nature of the sources. On the other hand, high-dimensional Hilbert spaces are required for quantum computation [11]. Therefore, hybrid states represent a valid approach to perform tasks of increasing complexity using photonic schemes.

Moreover, in hybrid states two-qubit logic gates can be implemented. We have seen that entangling gates for a two-photon two-qubit states is not allowed because of the absence of photon-photon interaction. However, if the two qubits are encoded in the same photon, no interaction is needed and controlled gates become feasible. For example, in fig.2.4 we report a simple scheme for implementing a controlled-Hadamard gate, with the path acting as the control qubit and the polarization acting as the target. If the photon passes in  $|\ell\rangle$  then polarization is left untouched, while if it passes in  $|r\rangle$  then an HWP rotated by  $\pi/8$  acts on the polarization qubit as an Hadamard gate. By definition of controlled gates, it is clear that this set-up implements a  $C-H$  gate.

Using a sequence of wave-plates we could perform any unitary transformation  $U$  on the lower mode, thus this scheme can also implement an arbitrary  $C-U$  gate. As we have seen in section 1.6.1, combining a non-trivial controlled gate with single-qubit gates we can achieve any two-qubit unitary transformation, thus the previous scheme can be generalized using only beam-splitters and phase shifters to obtain an arbitrary  $4 \times 4$  matrix.

## 2.2.4 Hyperentanglement

We now introduce a special class of hybrid states: the *hyperentangled states*. Suppose we have two photons, namely  $A$  and  $B$ , and we use both path and polarization to encode two qubits per photon. A hyperentangled state of the system is a state of the form

$$|\Pi\rangle_{AB} \otimes |\mathcal{K}\rangle_{AB},$$

where  $|\Pi\rangle$  is an entangled state of the two polarization qubits, and  $|\mathcal{K}\rangle_{AB}$  is an entangled state of the two path qubits. Examples of hyperentangled state are

$$\begin{aligned} |\Xi^{\pm\pm}\rangle &= |\Psi_{\pi}^{\pm}\rangle \otimes |\psi_k^{\pm}\rangle \\ &= \frac{1}{\sqrt{2}} \left( |H\rangle_A |V\rangle_B \pm |V\rangle_A |H\rangle_B \right) \otimes \frac{1}{\sqrt{2}} \left( |\ell\rangle_A |r\rangle_B \pm |r\rangle_A |\ell\rangle_B \right), \end{aligned}$$

where  $|\Psi_{\pi}^{\pm}\rangle$  and  $|\psi_k^{\pm}\rangle$  are the Bell states respectively for the polarization and the path qubits<sup>2</sup>. Note that the symmetry of the state  $|\Xi^{\theta\phi}\rangle$  depends on the values of  $\theta$  and  $\phi$ : for  $(\theta, \phi) = (+, +)$  and  $(-, -)$  the total state is symmetric for an exchange of  $A$  and  $B$ , while for  $(+, -)$  and  $(-, +)$  it is antisymmetric.

In general, a hyperentangled state is an entangled, as it cannot be separated into a product of four states, but can be factorized in two parts, each one corresponding to one photonic degree of freedom. In other words, there is entanglement between the qubits encoded in the same degree of freedom, but there are no correlations between the polarization qubits and the path qubits. If for instance we measure the polarization of one photon, then the polarization of the other one is automatically determined. On the other hand, we still have no information on the paths of the two photons, as the two degrees of freedom are separated. This means that a projective measurement does not induce the collapsing of the state of the system in a pure separable state. As a consequence, an hyperentangled state, although being entangled, is not a maximally entangled state, as defined in section 1.4. We can alternatively say that a hyperentangled state does not present *genuine multipartite entanglement*.

---

<sup>2</sup>In general we will use upper cases for polarization states and observables, and lower cases for the path.

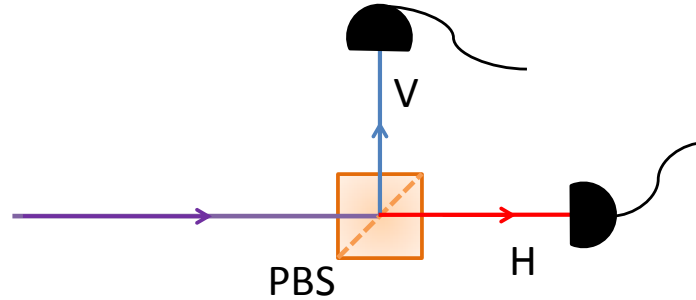


Figure 2.5: Experimental scheme of a projective measurement in the computational basis for a polarization-encoded qubit.

## 2.3 Detection of quantum states and observables

### 2.3.1 Measuring observables

Let us now analyse the process of performing measurements on single photon states. The basic element of a measurement is a *single photon detector*, which is simply a device making a “click” when a photon is detected. Standard single-photon detectors are *avalanche photodiodes*, with a typical quantum efficiency, i.e. the probability of detecting a photon when it arrives, of  $\approx 75\%$ . Using superconducting nanowires the efficiency can increase up to  $\approx 95\%$  [56].

Let us now consider projective measurements in the computational basis  $\{|0\rangle, |1\rangle\}$ , that means  $\{|H\rangle, |V\rangle\}$  for polarization qubits and  $\{|\ell\rangle, |r\rangle\}$  for path qubits. This measurement is trivially obtained for path-encoded qubits setting two detectors on the two modes: if the detector in  $\ell$  clicks then the projector operator  $|\ell\rangle\langle\ell|$  is applied, while if the one in  $r$  clicks then it is  $|r\rangle\langle r|$ . Note that in principle there is also a third option: none of the two detectors clicks. This case is a consequence of the non-ideal efficiency of the detectors, and it is simply discarded. Not considering the unmeasured cases is called “post-selection”. For a polarization-encoded qubit the projective measurement in the computational basis is performed using a polarizing beam-splitter (PBS), which is a device transmitting only H polarized photons and reflects all V polarized photons. The PBS hence maps the photon polarization state in its path, following  $|H\rangle \rightarrow |\ell\rangle$  and  $|V\rangle \rightarrow |r\rangle$ , where now  $|\ell\rangle$  and  $|r\rangle$  are respectively the transmitted and the reflected output modes of the PBS. The projective measurement in the  $\{|H\rangle, |V\rangle\}$  can then be achieved by a PBS followed projective measurement in the path basis  $\{|\ell\rangle, |r\rangle\}$ , as fig.2.5 shows. If the detector in  $|\ell\rangle$  clicks then the projector is  $|H\rangle\langle H|$ , if the one in  $|r\rangle$  clicks then it is  $|V\rangle\langle V|$ .

These kind of measurements can be performed both on path and polarization contextually (i.e. simultaneously). We simply have to insert a polarization measurement apparatus on each of the two modes of the photon. We will have four detectors, two

	Polarization	Path
$U_z$	$\theta_{HWP} = 0^\circ, \theta_{QWP} = 0^\circ$	No BS
$U_x$	$\theta_{HWP} = 22.5^\circ, \theta_{QWP} = 45^\circ$	BS, $\phi = 0$
$U_y$	$\theta_{HWP} = 22.5^\circ, \theta_{QWP} = 0^\circ$	BS, $\phi = \pi$

Table 2.1: Parameters for Pauli matrices measurements for path- and polarization-encoded qubits.

for each path. The detector that clicks determines both the path and the polarization simultaneously.

We have seen in section 1.7.1 that, in order to measure an observable  $A$  with eigenvalues  $\{a_i\}$  and relative eigenvectors  $\{|a_i\rangle\}$ , we have to perform a projective measurement on the  $\{|a_i\rangle\}$  basis, assigning to each measure the corresponding eigenvalue. For a single qubit the observable is a  $2 \times 2$  matrix, with eigenvectors  $\{|a_1\rangle, |a_2\rangle\}$ . Consider now an operation  $U_A$  which maps the two eigenvectors of  $A$  to the computational basis:

$$\begin{cases} |a_1\rangle \rightarrow |0\rangle, \\ |a_2\rangle \rightarrow |1\rangle. \end{cases} \quad (2.2)$$

Applying  $U_A$  and then a projective measurement on the computational basis is equivalent to perform a projective measurement on the basis  $\{|a_1\rangle, |a_2\rangle\}$ . Indeed, we now simply associate the eigenvalues  $\{a_1, a_2\}$  to  $\{|0\rangle, |1\rangle\}$  instead of  $\{|a_1\rangle, |a_2\rangle\}$ , but the observable measurement is the same. The aspect that differs is the state in which the system collapses.

Therefore, to measure an arbitrary observable  $A$  we need to perform projective measurement on the computational basis in the same manner we have seen before, but this time they have to follow the  $U_A$  operation. The  $U_A$  is a single-qubit transformation, and can be achieved using the schemes presented in the previous section. Note that, as the eigenvector basis  $\{|a_1\rangle, |a_2\rangle\}$  of an observable  $A$  is not unique, also the transformation  $U_A$  is not unique. This gives us some freedom on the choice of  $U_A$  for the measurement. In general, if an operator  $U_A$  allows the measurement of  $A$ , i.e. performs a transformation of the form of eq.(2.2), then another operator  $U'_A$  also allows the measurement of  $A$  if and only if  $[U_A, U'_A] = 0$  [11]. For example, in measuring an arbitrary observable  $A$  for a polarization qubit, the freedom on the choice allows us to perform  $U_A$  using only two wave-plates (a QWP and a HWP) instead of three.

Within an experiment we are typically interested in measuring the Pauli matrices. The  $\sigma_z$  matrix is already diagonal in the logical basis, so it only requires projective measurements on  $\{|H\rangle, |V\rangle\}$  or  $\{|\ell\rangle, |r\rangle\}$ . For measuring  $\sigma_x$  and  $\sigma_y$  on a path-encoded qubit the transformation we need is exactly the one reported in eq.(2.1) for  $\phi = 0$  and  $\phi = \pi$ , respectively. Thus, we only need a BS and a glass plate giving a phase  $\phi$ . For a polarization encoded qubits we need to rotate the QWP and the HWP to angle  $\theta_{QWP}$  and  $\theta_{HWP}$  in order to obtain a correct  $U_i$  ( $i = x, y, z$ ). The parameters for measuring the Pauli matrices are summarized in tab.2.1 and the experimental set-ups are shown in fig.2.6.

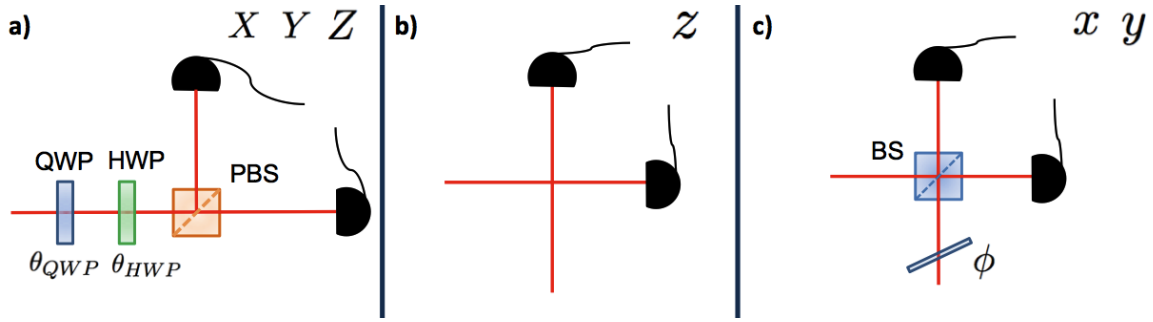


Figure 2.6: Experimental apparatus for measuring the expectation value of Pauli matrices. **a)** For polarization-encoded qubits the measurement of the matrices  $X, Y$  and  $Z$  requires a QWP and a HWP followed by a PBS. **b), c)** For path-encoded qubits measuring  $z$  does not require any optical element, while for  $x$  and  $y$  we need a phase shifter and a BS. The parameters for any measurement are reported in tab.2.1.

## 2.4 State generation via non-linear optics

We now focus on the generation of entangled multi-qubit states, which are a requirement for complex quantum information and quantum computation protocols. For generating photonic states we take advantage of non-linear processes, where the reaction of a medium to an external electromagnetic field, characterized by the polarization function  $\vec{P}$ , depends non-linearly on the strength of the field. Thus, the dependence of the  $i$ -th component of the polarization can be written as

$$P_i(t) = \epsilon_0 \chi_{ij}^{(1)} E_j(t) + \epsilon_0 \chi_{ijk}^{(2)} E_j(t) E_k(t) + o(E^3),$$

where the coefficients  $\chi_{ij}^{(1)}$  and  $\chi_{ijk}^{(2)}$  are the components of the *electric susceptibility* tensors of the first and second order, respectively.  $\epsilon_0$  is the vacuum permeability. The presence of a non-zero  $\chi^{(2)}$  enables second order processes, such as Sum Frequency Generation, Difference Frequency Generation and Spontaneous Parametric Down Conversion [Boyd, 65]. The latter is the process we use to generate photonic entangled states.

### 2.4.1 Spontaneous Parametric Down Conversion

The *Spontaneous Parametric Down Conversion* (SPDC), or Parametric Fluorescence, is a non-linear process where an electromagnetic field, called *pump* (p), with frequency  $\omega_p$  and wave vector  $\vec{k}_p$ , interacts non-linearly with a birefringent crystal. This interaction simultaneously generates two strong-correlated fields, namely *signal* (s) and *idler* (i), with lower frequencies  $\omega_s$  and  $\omega_p$  and wave vectors  $\vec{k}_s$  and  $\vec{k}_i$ .

As initially the only field propagating inside the field is the pump, this process represents the spontaneous amplifications of vacuum fluctuations of the electromagnetic field. As vacuum states are not present in the classical electromagnetic theory, this effect is purely quantum [10, 65].

The state of a pair of photons generated through SPDC can be explicitly calculated using first-order perturbation theory using a semi-classical approximation. The interaction Hamiltonian of the fields inside the crystal can be written as [65]:

$$H(t) = \epsilon_0 \int_V d\vec{r} E_p(\vec{r}, t) E_s^{(-)}(\vec{r}, t) E_i^{(-)}(\vec{r}, t) \chi^{(2)} + h.c. .$$

The integral is over the volume  $V$  where the interaction is present. The second-order susceptibility  $\chi^{(2)}$  is supposed to be a scalar for simplicity.  $E_p$  is the input pump field and  $E_s^{(-)}$  and  $E_i^{(-)}$  are the emitted signal and idler fields.

The pump is typically an intense laser field, and can thus be treated classically. Assuming its polarization to be linear, we have

$$E_p(\vec{r}, t) = \vec{E}_p e^{i(\vec{k}_p \cdot \vec{r} - \omega_p t)}.$$

The emitted fields  $E_s^{(-)}$  and  $E_i^{(-)}$  are instead single photons, and therefore must be described using the formalism of quantum mechanics. The operator associated to the field of a single photon, with frequency  $\omega$  and momentum  $\vec{k}$ , is given by [65]

$$E^{(-)}(\vec{r}, t) = i \int d\vec{k} \sqrt{\frac{\hbar\omega}{2\epsilon_0 n^2(k)V}} a_{\vec{k}}^\dagger e^{i(\vec{k} \cdot \vec{r} - \omega t)},$$

where  $a_{\vec{k}}^\dagger$  is the creation operator of the mode  $\vec{k}$ , and  $n^2(k)$  is the refraction index of the medium at wave length  $\lambda = 2\pi/k$ .

Neglecting the dependence on  $\vec{k}$  for slow varying functions, such as  $n^2$ , we can rewrite the interaction Hamiltonian as

$$H(t) = C \int d\vec{r} \int d\vec{k}_p \int d\vec{k}_s \int d\vec{k}_i e^{i(\vec{k}_p - \vec{k}_s - \vec{k}_i) \cdot \vec{r}} e^{-i(\omega_p - \omega_s - \omega_i)t} a_{\vec{k}_s}^\dagger a_{\vec{k}_i}^\dagger,$$

with  $C$  a constant.

As the process is spontaneous, the initial state of the output modes is the vacuum. The final output state can be then written as

$$|\psi\rangle = U(t) |0\rangle,$$

where  $|0\rangle$  is the vacuum state and  $U(t)$  is the time evolution operator, given by

$$U(t) = \exp \left[ -\frac{i}{\hbar} \int_{-\infty}^{+\infty} dt H(t) \right].$$

Since the effect is a second-order process, the coupling between the fields is weak, and therefore the interaction Hamiltonian  $H(t)$  is small. We can then follow a perturbative approach to the evolution of the state, approximating  $U(t)$  as

$$U(t) \approx \mathbb{I} - \frac{i}{\hbar} \int_{-\infty}^{+\infty} dt H(t).$$

The output state of the fluorescence is then:

$$\vec{\psi} = |0\rangle + \alpha \int d\vec{k}_s d\vec{k}_i \delta(\vec{k}_p - \vec{k}_s - \vec{k}_i) \delta(\omega_p - \omega_s - \omega_i) a_{\vec{k}_s}^\dagger a_{\vec{k}_i}^\dagger |0\rangle \quad (2.3)$$

where  $\alpha$  is a constant, with  $|\alpha| \ll 1$ .

The term  $a_{\vec{k}_s}^\dagger a_{\vec{k}_i}^\dagger |0\rangle$  shows that the output is a two-photons state. However, as  $\alpha$  is

small, the process is very unlikely to happen. This means that generating pairs of photon via SPDC has a very low efficiency: typically, only one pair of photons is emitted per  $10^{12}$  incoming pump photons.

Higher order terms of the perturbative expansion of  $U(t)$  gives rise to states with more and more photons. For example in the second order term we have a four-photons output state. However, the efficiency of these processes decreases exponentially with the perturbative order, thus the cases with more than two photons are usually neglected. Eq.(2.3) also shows that the frequencies  $\omega_s$  and  $\omega_i$  of the two emitted photons, and their wave vectors  $\vec{k}_s$  and  $\vec{k}_i$ , must satisfy the energy and momentum conservation laws

$$\omega_p = \omega_s + \omega_i \quad (2.4)$$

$$\vec{k}_p = \vec{k}_s + \vec{k}_i. \quad (2.5)$$

These relations are called *Phase-Matching*, and imply correlations between the two output photons which will give rise to entanglement.

### 2.4.2 Correlations given by the phase-matching

We are now interested in studying the phase-matching conditions given by eq.(2.4) and eq.(2.5). Let us define  $\theta_s$  ( $\theta_i$ ) as the angle between the propagating directions of the pump and the signal (idler), thus between  $\vec{k}_p$  and  $\vec{k}_s$  ( $\vec{k}_i$ ), as shown in fig.2.7. Eq.(2.5) can be separated for the components parallel and orthogonal to  $\vec{k}_p$ , and rewritten as

$$k_p = k_s \cos \theta_s + k_i \cos \theta_i \quad (2.6)$$

$$k_s \sin \theta_s - k_i \sin \theta_i = 0. \quad (2.7)$$

If the three fields are collinear, that is  $\theta_s = 0$  and  $\theta_i = 0$ , then the second equation is trivially satisfied, while the first one gives  $k_p = k_s + k_i$ . Using the dispersion law  $k = n(\omega)\omega/c$ , with  $n(\omega)$  the refraction index of the medium and  $c$  the speed of light in free space, the phase-matching relations for this case can be rewritten in the form

$$\omega_p = \omega_s + \omega_i \quad (2.8)$$

$$n(\omega_p)\omega_p = n(\omega_s)\omega_s + n(\omega_i)\omega_i. \quad (2.9)$$

As the first equation implies that  $\omega_p > \omega_s, \omega_i$ , the second one gives us  $n(\omega_p) < n(\omega_i), n(\omega_s)$ . These conditions cannot be satisfied in a medium with normal dispersion, where the refraction index increases monotonically with the frequency.

However, a non-linear medium is typically also birefringent, and this fact can be exploited in order to satisfy the phase matching conditions [10]. Let us consider the case of a uniaxial crystal and a field propagating in it, along a direction  $\hat{q}$  with an angle  $\varphi$  to the optical axis of the medium. The polarization components of the field which lays in the plane containing  $\hat{q}$  and the optical axis, called *ordinary* component, will be affected by a refraction index  $n_0(\lambda)$ , which depends on the wavelength of the field  $\lambda$ .

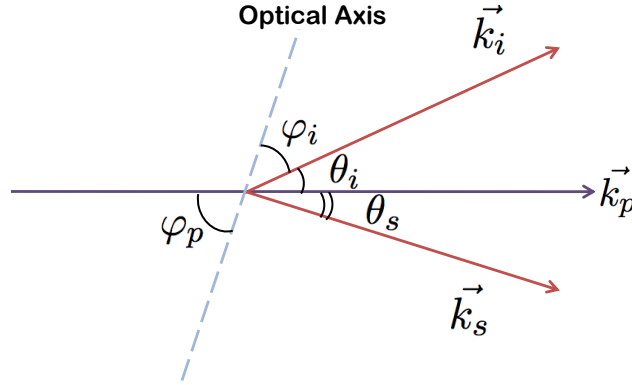


Figure 2.7: Wave vectors of the pump, signal and idler fields inside a non linear crystal.  $\theta_s$  ( $\theta_i$ ) is defined as the angle between the directions of the pump and the signal (idler).  $\varphi_p$  and  $\varphi_i$  are the angles between the optical axis and  $\hat{k}_p$  and  $\hat{k}_i$ , respectively. For type I phase matching, where the geometry is planar as in this picture, we have the relation  $\varphi_p = \varphi_i + \theta_i$ .

The polarization component orthogonal to the plane, called *extraordinary*, will instead travel with a refraction index  $n_e(\varphi, \lambda)$  given by

$$\frac{1}{n_e^2(\varphi, \lambda)} = \frac{\sin^2(\varphi)}{n_e^2} + \frac{\cos^2(\varphi)}{n_o^2}, \quad (2.10)$$

where  $n_e = n_e(\varphi = \pi/2)$ .

In order to satisfy eq.(2.8) and eq.(2.9) we have seen that the refraction index for the pump, which has the highest frequency, must be the lower than those of the signal and the idler. Hence, if our crystal is negative uniaxial, that is  $n_e < n_o$ , the pump field must have extraordinary polarization. For the signal and idler photons we have two possibilities: they both have the same polarization, or their polarizations are different. The first case is defined as *Type I phase-matching*, while the second as *Type II phase-matching*. For a negative uniaxial crystal we can then write the phase-matching relations, eq.(2.4) and eq. (2.5), in the following form:

$$\begin{aligned} \text{Type I:} & \quad \begin{cases} \omega_p = \omega_s + \omega_i, \\ \vec{k}_p^e = \vec{k}_s^o + \vec{k}_i^o. \end{cases} \\ \text{Type II:} & \quad \begin{cases} \omega_p = \omega_s + \omega_i, \\ \vec{k}_p^e = \vec{k}_s^{o,e} + \vec{k}_i^{e,o}. \end{cases} \end{aligned}$$

Here  $o$  and  $e$  indicate the ordinary and extraordinary polarizations of the fields. Analogous relations can be obtained for a positive uniaxial crystal, where we simply have to exchange the  $o$  and  $e$  indices.

### 2.4.3 Type I phase-matching

The equation that has to be satisfied for type I phase-matching is  $\vec{k}_p^e = \vec{k}_s^o + \vec{k}_i^o$ . As the signal and the idler photon are both ordinary, this equation is symmetrical under

rotations around the axis  $\hat{k}_p$  identified by the pump field. We can thus describe this case using a planar geometry. We define  $\varphi_p$  and  $\varphi_i$  as the angles between the optical axis of the crystal and respectively the pump and the idler directions, as shown in fig.2.7. We have the relation:

$$\varphi_p = \varphi_i + \theta_i. \quad (2.11)$$

The modulus of the wave vectors are given by

$$\begin{aligned} k_s(\lambda_s) &= \frac{2\pi n_o(\lambda_s)}{\lambda_s}, \\ k_i(\lambda_i) &= \frac{2\pi n_o(\lambda_i)}{\lambda_i}, \\ k_p(\lambda_p, \varphi_p) &= \frac{2\pi n_e(\lambda_p, \varphi_p)}{\lambda_p}. \end{aligned}$$

Inserting these relations in the phase-matching conditions (2.6) and (2.7) we can obtain formulas for the directions  $\theta_s$  and  $\theta_i$  of the output photons:

$$\frac{n_e(\lambda_p, \varphi_p)}{\lambda_p} = \frac{n_o(\lambda_s)}{\lambda_s} \cos \theta_s + \frac{n_o(\lambda_i)}{\lambda_i} \sqrt{1 - \left( \frac{\lambda_i n_o(\lambda_s)}{\lambda_s n_o(\lambda_i)} \right)^2 \sin^2 \theta_s}, \quad (2.12)$$

$$\frac{n_e(\lambda_p, \varphi_p)}{\lambda_p} = \frac{n_o(\lambda_i)}{\lambda_i} \cos \theta_i + \frac{n_o(\lambda_s)}{\lambda_s} \sqrt{1 - \left( \frac{\lambda_s n_o(\lambda_i)}{\lambda_i n_o(\lambda_s)} \right)^2 \sin^2 \theta_i}. \quad (2.13)$$

Thus, given the angle  $\varphi_p$  between the pump field and the optical axis, and the three wave lengths ( $\lambda_p$ ,  $\lambda_s$  and  $\lambda_i$ ), inverting eq.(2.12) and eq.(2.13) we can obtain  $\theta_s$  and  $\theta_i$ , respectively. This means that we can calculate the directions of the signal and idler photons that emerge from the crystal. In light of the rotational symmetry around  $\hat{k}_p$ , the directions  $\hat{k}_s$  and  $\hat{k}_i$  of the signal and idler photons lay along two coaxial cones with opening angles  $\theta_s$  and  $\theta_i$ , respectively, as shown in fig.2.8a. As a consequence of the momentum conservation (eq.(2.7)) the two output photons must emerge in diametrically opposite directions.

In the degenerate case, with  $\omega_s = \omega_i = \omega_p/2$ , we have  $\theta_i = \theta_s$ , meaning that the two cones coincide, hence, as shown in fig.2.8b, we have a single degenerate cone with axis along  $\hat{k}_p$ . If we select two pairs of diametrically opposite points on this cone, for example using an holed mask (fig.2.8c), there is no way to know in which pair of modes the photons will chose to emerge. In fact, the two photons coherently pass through both the pairs of holes simultaneously. Moreover, the two photons are generated at the same time and have same frequency, which means that they are completely undistinguishable in time and frequency. Then, if we say that a photon is in the state  $|\ell\rangle$  ( $|r\rangle$ ) if it emerges from one of the two left (right) holes, the state of the two photons is

$$|\mathcal{K}\rangle = \frac{1}{\sqrt{2}}(|r\rangle_A |\ell\rangle_B + |\ell\rangle_A |r\rangle_B),$$

where with  $A$  we label the photon emerging from one of the two upper holes, and with  $B$  the one emerging in the lower holes. We can arbitrarily chose  $|\ell\rangle$  as the logic state

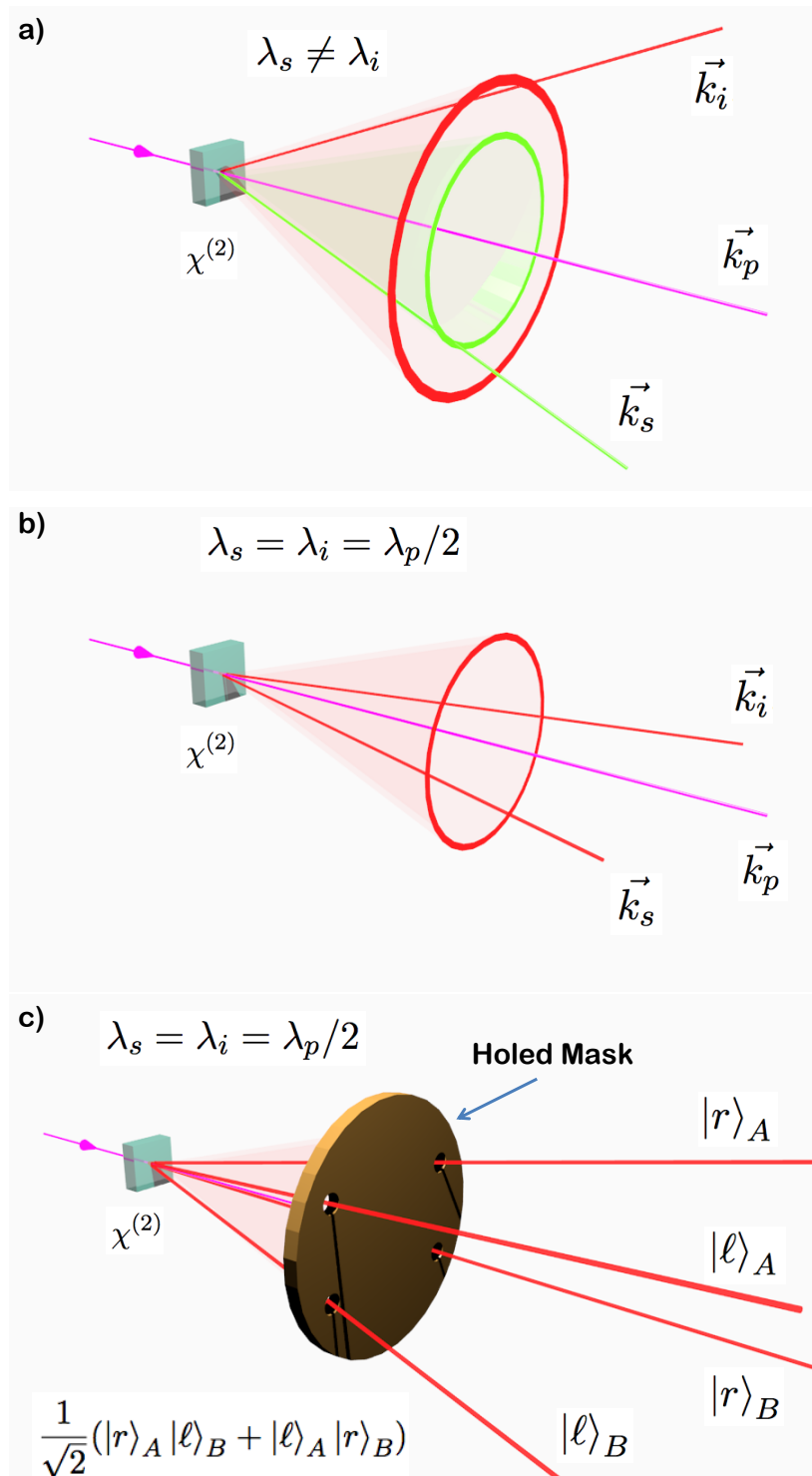


Figure 2.8: Emitted fluorescence from the SPDC process in type I phase-matching conditions. **a)** The signal and idler photons emerge in two coaxial cones with opening angles  $\theta_s$  and  $\theta_i$ . To conserve the momentum, the directions of the output photons must be diametrical opposite. **b)** If the two emitted photons have the same frequency the two cones coincide. The idler and signal photons are now indistinguishable. **c)** Selecting four modes via a holed mask, the pair of emitted photons emerges coherently in both of the two pairs of diametrical opposite spatial modes. The output system is then in the two-qubit path-encoded entangled Bell state  $|\psi_{\mathbf{k}}^+\rangle$ .

$|0\rangle$ , and  $|r\rangle$  as  $|1\rangle$ . The generated state is then the two-qubit path-encoded entangled Bell state  $|\psi_{\mathbf{k}}^+\rangle$ .

However, the two photons both have ordinary polarizations, hence the polarization state generated using type I phase-matching is

$$|\Pi\rangle = |o\rangle_A |o\rangle_B$$

which is not entangled.

In chapter 3 we will see an experimental method to generate, via type I phase-matching, also entanglement in the polarizations. In this way we will obtain a photonic system entangled in both the polarization and path degrees of freedom, i.e. a hyperentangled state [66, 67].

#### 2.4.4 Type II phase-matching

Proceeding analogously to the type I case, we have

$$\begin{aligned} k_s(\lambda_s) &= \frac{2\pi n_o(\lambda_s)}{\lambda_s}, \\ k_i(\lambda_i, \varphi_i) &= \frac{2\pi n_e(\lambda_i, \varphi_i)}{\lambda_i}, \\ k_p(\lambda_p, \varphi_p) &= \frac{2\pi n_e(\lambda_p, \varphi_p)}{\lambda_p}. \end{aligned}$$

Substituting in eq.(2.6) and eq.(2.7) we obtain the two desired equations for  $\theta_s$  and  $\theta_i$ :

$$\begin{aligned} \frac{n_e(\lambda_p, \phi_p)}{\lambda_p} &= \frac{n_o(\lambda_s)}{\lambda_s} \cos \theta_s + \sqrt{\left(\frac{n_e(\lambda_i, \varphi_i)}{\lambda_i}\right)^2 + \left(\frac{n_o(\lambda_s)}{\lambda_s}\right)^2 \sin^2 \theta_s^2}, \\ \frac{n_e(\lambda_p, \phi_p)}{\lambda_p} &= \frac{n_e(\lambda_i, \varphi_i)}{\lambda_i} \cos \theta_i + \sqrt{\left(\frac{n_o(\lambda_s)}{\lambda_s}\right)^2 + \left(\frac{n_e(\lambda_i, \varphi_i)}{\lambda_i}\right)^2 \sin^2 \theta_i^2}. \end{aligned}$$

As depicted in fig.2.9a, the two photons are generated along two cones which are not coaxial, both having the vertex on the point inside the crystal in which the fluorescence is generated. One cone contains the photons with ordinary polarization and the other photons with extraordinary polarization.

In the degenerate case (fig.2.9b) the cones have the same opening angles, and may or may not intersect in two points, depending on the value of  $\varphi_p$ . Adjusting the angle  $\varphi_p$  (i.e.the direction of the pump) and selecting the modes passing through the intersecting points, as shown in fig.2.9c, we achieve the indistinguishability of the two photons. The generated polarization state is the entangled Bell state

$$|\Psi_{\pi}^-\rangle = \frac{1}{\sqrt{2}}(|o\rangle_1 |e\rangle_2 - |e\rangle_1 |o\rangle_2).$$

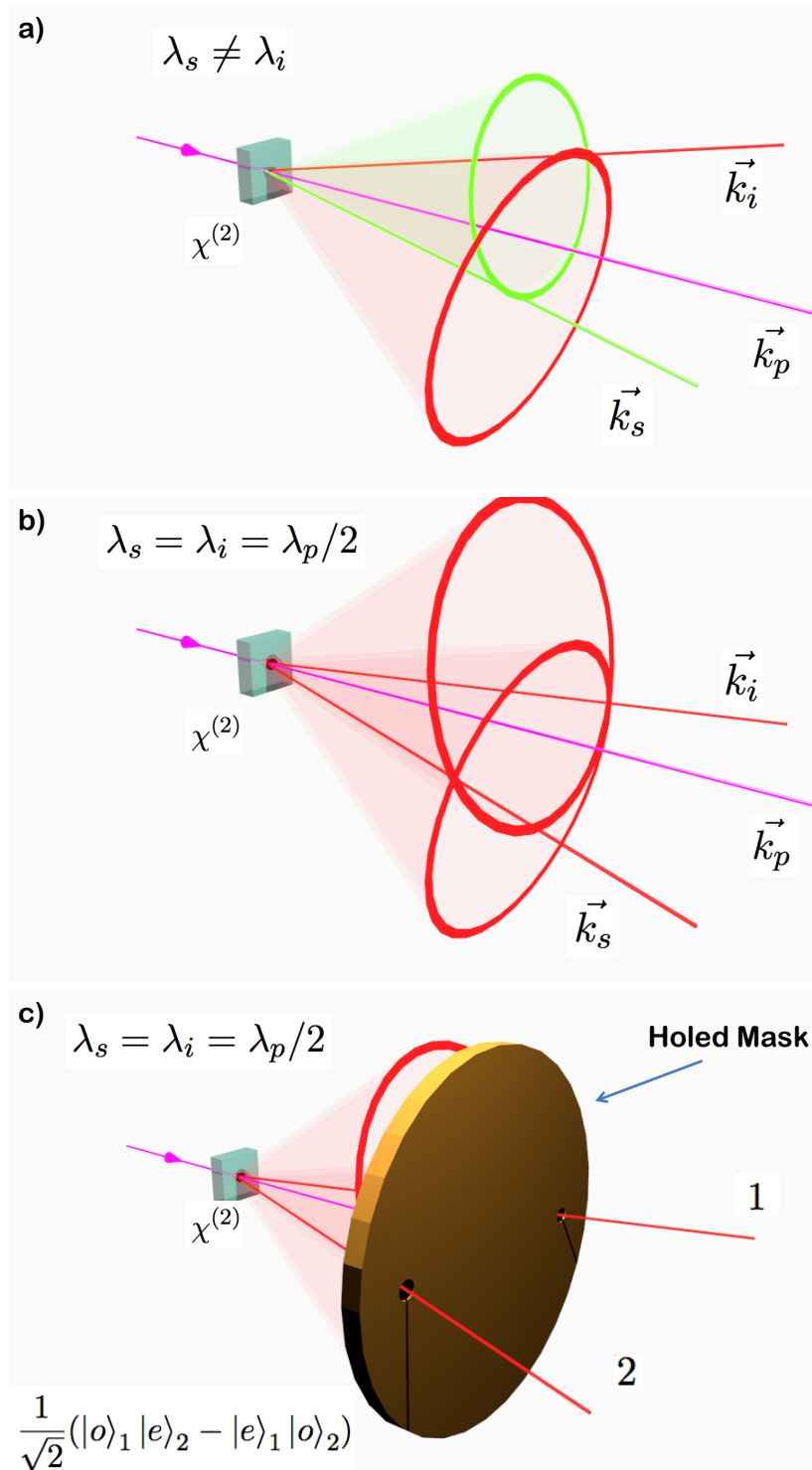


Figure 2.9: Emitted fluorescence from the SPDC process in type II phase-matching conditions. **a)** The signal and idler photons emerge in two non coaxial cones with opening angles  $\theta_s$  and  $\theta_i$ , having vertices in the point where the photons are emitted. **b)** In the degenerate case the two cones may intersect themselves in two points. **c)** Selecting the modes at the intersection between the two cones we assure the spatial indistinguishability of the two photons. The output system is hence in the two-qubit polarization-encoded entangled Bell state  $|\psi_{\pi}^{-}\rangle$ .

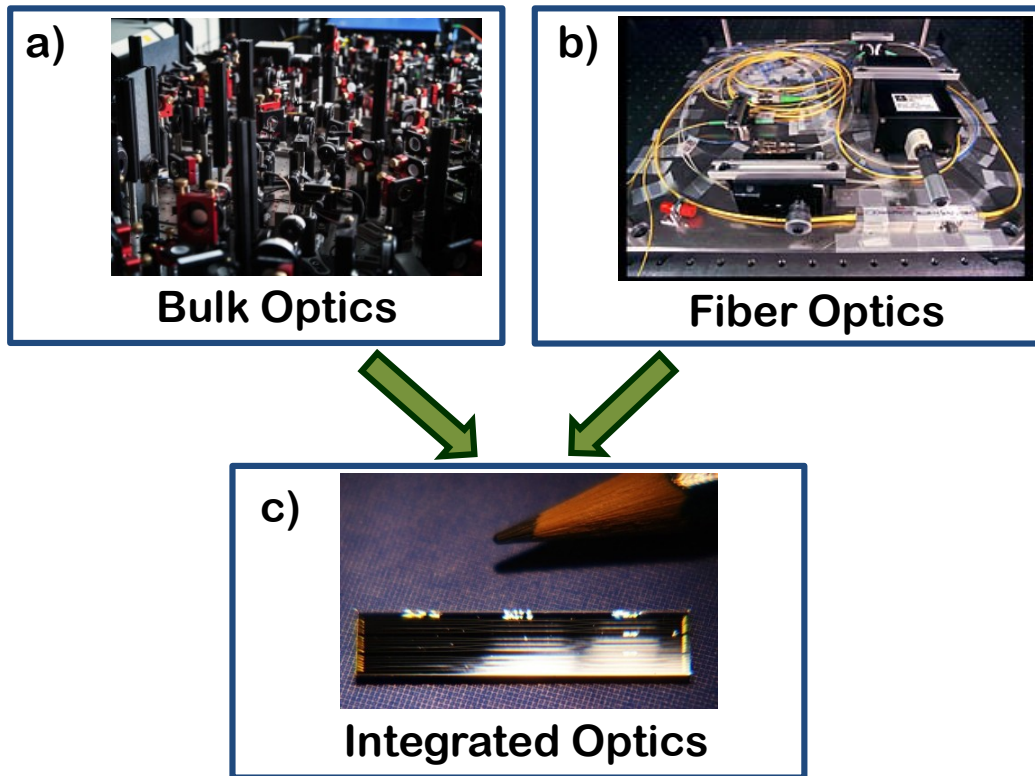


Figure 2.10: Differences in the miniaturization of optical schemes for three different techniques. While bulk optics **a)** and fiber optics **b)** approaches to quantum information protocols result in complex experimental architectures, which often imply lack of stability and scalability, integrated photonics **c)** allows to implement elaborated optical schemes on small scale chips.

In type II phase-matching we have to select the two particular modes where the cones intersect, and therefore the paths of the two emerging photons cannot be entangled.

The first source for generating pairs of entangled photons using SPDC with type II phase-matching was realized in 1995 [68]. Since then, many advances in terms of efficiency and purity of states were achieved for this type of SPDC sources, due mainly to the development of non-linear material as Beta Barium Borate ( $\beta\text{-BaB}_2\text{O}_4$ ) (BBO) crystals and Periodically Poled Potassium Titanyl Phosphate (PPKTP) [69, 70].

## 2.5 Integrated Photonics

We conclude the chapter with a brief review of the *integrated technology* applications in quantum optics. In the last few years this topic has represented a major breakthrough in the field of photonics.

Quantum computation harnesses the properties of quantum systems to deliver significant improvements in information processing. In 2001 Knill, Laflamme and Milburn demonstrated that scalable quantum computing is possible using only single-photon sources, detectors, and linear optical circuits [51]. Since then, many experimental

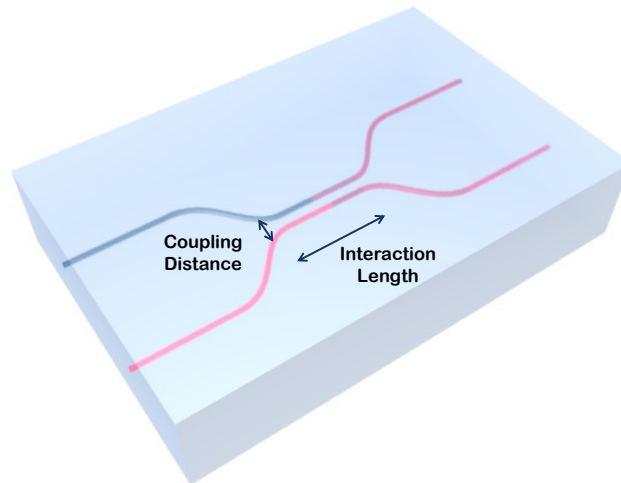


Figure 2.11: Scheme of an integrated directional coupler. If the distance between two waveguides is reduced to few micrometers, the photons may pass from one guide to the other. Adjusting the coupling distance and the interaction length we can determine the transmittivity and the reflectivity of the device in the fabrication process.

demonstrations of simple quantum algorithms [54, 57, 71] and simple error-correcting codes [72] were performed. However, these demonstrations have relied on large-scale optical elements (such as beam-splitters and mirrors) mounted in room-sized optical tables, with photons propagating through air. As a consequence, even simple applications of quantum information protocols require a complex optical architecture: most of the bulk optics experiments look like the disordered configuration shown in fig.2.10a. As one can immediately see, these approaches do not offer the miniaturisation and scalability that are essential for the realization of a quantum computer.

A first step forward could be obtained using optical fibers instead of free-air propagation. In this approach we avoid to use a large number of mirrors for a precise control of the beam direction. Optical elements, such as beam-splitters and phase-shifters, can be integrated directly on the fiber, thus allowing the manipulation of the states without the need of passing in free-space. Yet, this improvement does not ensure proper scalability and stability for optical schemes. In fact, we are only passing from the “forest of mirrors” of fig.2.10a to the “spaghetti” configuration shown in fig.2.10b.

The most promising approach for the miniaturization and stability of optical architectures is represented by integrated optics. This technology allows to fabricate practical, standardized, low cost, interconnectable, and reconfigurable optical schemes in a small-scale chip, as shown in fig.2.10c [73].

In a standard integrated chip micrometric-scale waveguides are fabricated on a semiconductor substrate using the lithographic techniques, already developed for electronic technologies. The precision in the positioning of the guides is high: typically tens of nanometers. Optical elements can be fabricated directly on-chip. The basic element of an integrated optical scheme is the *directional coupler*, shown in fig.2.11, which acts as a beam-splitter. The functioning of a directional coupler is the following. Suppose a photon is propagating in a waveguide  $\ell$ . When another waveguide  $r$  is brought close

to  $\ell$ , the photon has a non-zero probability to pass from the guide  $\ell$  to  $r$  because of the *quantum tunneling effect*<sup>3</sup>. As the probability decreases exponentially with the distance, the two waveguides must be very close in order to achieve a good coupling (typically  $\approx 10\mu\text{m}$ , depending on the wave-length of the photons). Adjusting the distance between the guides and the interaction length (i.e. the length of the interval in which the two wave-guides are brought closer) we can obtain a precise control of the coupling ratio of the beam-splitter, which is the analogous of the transmission and reflection coefficient. We can as well integrate a phase-shifter using thermal heaters: changing the temperature of a region we can modify the length of a waveguide, thus inserting a controllable phase.

Using the integrated optical elements we described above, interference visibilities of over 99.6% were achieved, demonstrating a great precision and stability [54]. Moreover, single-photon sources and single-photon detectors have already been demonstrated to be implementable directly on an integrated device, showing that it is possible to generate, manipulate and detect quantum states entirely on-chip [61, 62, 74–77].

On the other hand, the natural birefringence of such semiconductor waveguides usually becomes more complicated using polarisation encoding, since it does not preserve the states. Recently, an alternative approach has been developed for the fabrication of integrated devices, called *femtosecond laser writing*, which allows to integrate optical schemes on non-birefringent materials. Therefore, this technique enables the encoding in both path and polarization. The fabrication of a femtosecond laser written device, and an experimental implementation, will be described in detail in chapter 3.

In any application of quantum information and quantum computation a key point is the state preparation and the ability to perform quantum operations on the system. It is hence important the implementation of a protocol which allows the experimenter to completely characterize the state of a system and the operation performed in a quantum process. The former is called *Quantum State Tomography* (QST), the latter *Quantum Process Tomography* (QPT).

## 2.6 Quantum State Tomography

The quantum state tomography is an experimental procedure which allows to estimate the state of a given system [30]. The difference between a measurement on the system and a QST is the following: performing a measurement we obtain the exact state of the system only after the measure, while with a QST we are interested to characterize the system before the measurement, that is, before it collapses. QST requires the experimenter to be able to produce a large number  $\mathcal{N}$  of identical copies of the system. Indeed, it can be demonstrated [11] that the average fidelity between the state obtained using the QST protocol  $\rho_{QST}$  and the real state of the system  $\rho$  is

$$F(\rho, \rho_{QST}) = 1 - \left(1 - \frac{1}{M}\right) \frac{1}{\sqrt{\mathcal{N}}},$$

---

<sup>3</sup>In the case of an intense laser beam, instead of a single photon, propagating inside the integrated device, the coupling between the two waveguides is due to the *evanescent wave*.

where  $M$  is the Hilbert space dimension of the system. This quantity is close to one only if  $\mathcal{N}$  is large, which means that we need a large number of identical copies of the system to correctly characterize its state. In an optical environment we can typically produce thousands of identical photonic states per second, and therefore high precision tomographies are usually easily performed in less than an hour. For other kinds of implementations, e.g. trapped ions, it takes more time to produce a large number of copies of the same system, hence QSTs are typically more demanding.

### 2.6.1 Single-qubit state tomography

We start from the simplest case where our system is composed of a single qubit. The tomographic reconstruction of the density matrix is analogous to the procedure, used in classical optics, for determining the polarization state of a field via Stoke's parameters [78]. Using the properties of Pauli matrices  $\sigma_i \sigma_j = \delta_{ij} \mathbb{I}$ , for  $i, j = x, y, z$ , we can rewrite eq.(1.10) as

$$\begin{aligned} \rho &= \frac{\text{Tr}(\rho)\mathbb{I} + \text{Tr}(X\rho)X + \text{Tr}(Y\rho)Y + \text{Tr}(Z\rho)Z}{2} \\ &= \frac{\mathbb{I} + \langle X \rangle X + \langle Y \rangle Y + \langle Z \rangle Z}{2}. \end{aligned} \quad (2.14)$$

The spectral decompositions of the Pauli matrices are

$$\begin{aligned} Z &= |0\rangle\langle 0| - |1\rangle\langle 1| = |L\rangle\langle R| + |R\rangle\langle L| \\ X &= |+\rangle\langle +| - |-\rangle\langle -| = i|L\rangle\langle R| - i|R\rangle\langle L| \\ Y &= |L\rangle\langle L| - |R\rangle\langle R| \end{aligned}$$

where  $|\pm\rangle = (|0\rangle \pm |1\rangle)/\sqrt{2}$  and  $|L(R)\rangle = (|0\rangle \pm i|1\rangle)/\sqrt{2}$ . We now define the Stoke's parameters as the expected values of the Pauli operators, multiplied by the number of copies  $\mathcal{N}$ :

$$\begin{aligned} \mathcal{S}_0 &= \mathcal{N} = \mathcal{N}\langle \mathbb{I} \rangle, \\ \mathcal{S}_1 &= \mathcal{N}\langle X \rangle, \\ \mathcal{S}_2 &= \mathcal{N}\langle Y \rangle, \\ \mathcal{S}_3 &= \mathcal{N}\langle Z \rangle. \end{aligned}$$

Substituting in eq.(2.14) we obtain the density matrix in terms of the Stokes parameters:

$$\rho = \frac{1}{2} \sum_{i=0}^3 \frac{\mathcal{S}_i}{\mathcal{S}_0} \sigma_i. \quad (2.15)$$

Thus, in order to reconstruct the density matrix of our state we have to measure the Stoke's parameters. Consider the quantities

$$\begin{aligned} n_0 &= \frac{\mathcal{N}}{2} (\langle 0|\rho|0\rangle + \langle 1|\rho|1\rangle) = \frac{\mathcal{N}}{2} (\langle L|\rho|L\rangle + \langle R|\rho|R\rangle), \\ n_1 &= \mathcal{N} \langle +|\rho|+\rangle = \frac{\mathcal{N}}{2} (\langle R|\rho|R\rangle + \langle L|\rho|L\rangle - i\langle L|\rho|R\rangle + i\langle R|\rho|L\rangle), \end{aligned}$$

$$n_2 = \mathcal{N} \langle R | \rho | R \rangle,$$

$$n_3 = \mathcal{N} \langle 0 | \rho | 0 \rangle = \frac{\mathcal{N}}{2} (\langle R | \rho | R \rangle + \langle R | \rho | L \rangle + \langle L | \rho | R \rangle + \langle L | \rho | L \rangle).$$

It can be easily seen that the Stoke's parameters can be rewritten as [11]:

$$\begin{aligned} \mathcal{S}_0 &= 2n_0 \\ \mathcal{S}_1 &= 2(n_1 - n_0), \\ \mathcal{S}_2 &= 2(n_2 - n_0), \\ \mathcal{S}_3 &= 2(n_3 - n_0). \end{aligned}$$

Then, to determine the Stoke's parameters, and hence the  $\rho$  we have to measure the average values of the four operators  $\mu_0 = |0\rangle\langle 0| + |1\rangle\langle 1|$ ,  $\mu_1 = |+\rangle\langle +|$ ,  $\mu_2 = |R\rangle\langle R|$  and  $\mu_3 = |0\rangle\langle 0|$ , where the average is taken on all the identical copies of the system. This will give us the  $n_i$  and then the  $\mathcal{S}_i$ .

Note that the choice of the operators  $\mu_i$ , which allow the measurement of the Stoke's parameters, is not unique. For example, we could have chosen directly the Pauli matrices. In general, we can choose the set of four operators which suits the experiment best.

## 2.6.2 Multi-qubits state tomography

We can now extend the protocol to a  $n$ -qubits system. This generalization is straightforward. As the matrices of the form  $\sigma_{i_1} \otimes \sigma_{i_2} \otimes \dots \otimes \sigma_{i_n}$ , with  $i_k = 0, 1, 2, 3$ , form a basis of a  $2^n$ -dimensional Hilbert space, we can write a generic state  $\rho$  as

$$\rho = \frac{1}{2^n} \sum_{i_1, \dots, i_n=0}^3 r_{i_1, \dots, i_n} \sigma_{i_1} \otimes \dots \otimes \sigma_{i_n}, \quad (2.16)$$

with  $r_{i_1, \dots, i_n} = \langle \sigma_{i_1} \otimes \dots \otimes \sigma_{i_n} \rangle$ . The Stoke's parameters are defined analogously to the one qubit case:

$$\mathcal{S}_{i_1, \dots, i_n} = \mathcal{N} \langle \sigma_{i_1} \otimes \dots \otimes \sigma_{i_n} \rangle,$$

thus we can rewrite eq.(2.16) as

$$\rho = \frac{1}{2^n} \sum_{i_1, \dots, i_n=0}^3 \frac{\mathcal{S}_{i_1, \dots, i_n}}{\mathcal{S}_{0, \dots, 0}} \sigma_{i_1} \otimes \dots \otimes \sigma_{i_n}.$$

The Stoke's parameters can be determined by the  $4^n$  projective measurements

$$\mu_{i_1} \otimes \mu_{i_2} \otimes \dots \otimes \mu_{i_n} \quad \text{with } i_k = 0, 1, 2, 3 \text{ and } k = 1, 2, \dots, n.$$

Analogously to the 1-qubit case, we define the expected value of these operators  $n_{i_1, \dots, i_n} = \mathcal{N} \langle \mu_{i_1} \otimes \dots \otimes \mu_{i_n} \rangle$ . For a 2-qubits system we require 16 projective measurements. In tab.2.2 it is reported an example of set of measurement for a two-qubit QST. This is the set that was used for the quantum state tomographies performed in the experimental setup that will be used as the main platform for this thesis from Chap.3 onwards. As the number of projective operators increases exponentially with the size of the system, QST is considered a demanding experimental protocol. For example, the first state tomography for a 4-qubit state was only achieved in 2005 [79].

# Measure	Projection on qubit 1	Projection on qubit 2
1	$ 0\rangle\langle 0 $	$ 0\rangle\langle 0 $
2	$ 0\rangle\langle 0 $	$ 1\rangle\langle 1 $
3	$ 1\rangle\langle 1 $	$ 1\rangle\langle 1 $
4	$ 1\rangle\langle 1 $	$ 0\rangle\langle 0 $
5	$ R\rangle\langle R $	$ 0\rangle\langle 0 $
6	$ R\rangle\langle R $	$ 1\rangle\langle 1 $
7	$ +\rangle\langle + $	$ 1\rangle\langle 1 $
8	$ +\rangle\langle + $	$ 0\rangle\langle 0 $
9	$ +\rangle\langle + $	$ R\rangle\langle R $
10	$ +\rangle\langle + $	$ +\rangle\langle + $
11	$ R\rangle\langle R $	$ +\rangle\langle + $
12	$ 0\rangle\langle 0 $	$ +\rangle\langle + $
13	$ 1\rangle\langle 1 $	$ +\rangle\langle + $
14	$ 1\rangle\langle 1 $	$ L\rangle\langle L $
15	$ 0\rangle\langle 0 $	$ L\rangle\langle L $
16	$ R\rangle\langle R $	$ L\rangle\langle L $

Table 2.2: Example of a set of 16 projective measurements  $\mu_{i_1} \otimes \mu_{i_2}$  for 2-qubit state tomography. This set of operators was used for the QSTs performed in the experiment presented in chapter ??.

### 2.6.3 Maximum-Likelihood Estimation

We have described a protocol to characterize the state  $\rho$  of a quantum system. As we have seen in section 1.2.3, the matrix  $\rho$  must satisfy the properties of hermiticity, unitary trace and positivity. However, experimental inaccuracies and statistical fluctuations, which are always present in a real experiment, may cause a reconstructed matrix  $\rho_{QST}$  that violates some of these properties, and therefore is not physical. To avoid this problem we may employ a technique called *maximum-likelihood estimation* of density matrices [30]. We describe here this method for a two-qubit state tomography. The approach is the following:

1. Give the general form of an explicitly physical density matrix, i.e., the most general matrix that satisfies the three important properties of Hermiticity, unitary trace and positivity. This matrix will be a function of 16 real variables, that we will call  $\{t_1, t_2, \dots, t_{16}\}$ . We will denote the matrix as  $\rho_p(t_1, t_2, \dots, t_{16})$
2. Introduce a *likelihood function*, which quantifies how good the density matrix  $\rho_p(t_1, t_2, \dots, t_{16})$  approximates the experimental data. This likelihood function is a function of the 16 real parameters  $t_i$  and of the 16 experimental data  $n_{i_1, i_2} \equiv n_j$ , with  $j = 1, \dots, 16$ . We will denote this function as  $\mathcal{L}(t_1, \dots, t_{16}; n_1, \dots, n_{16})$ .
3. Using standard numerical optimization techniques, find the optimum set of variables  $t_i$ , which we will call  $\{t_1^{opt}, \dots, t_{16}^{opt}\}$ , for which the function  $\mathcal{L}(t_1, \dots, t_{16}; n_1, \dots, n_{16})$  has its maximum value. The best estimate for the density matrix is then  $\rho = \rho_p(t_1^{opt}, \dots, t_{16}^{opt})$ .

We start noticing that the positivity condition ( $\langle \phi | \mathcal{G} | \phi \rangle \geq 0$  for every  $|\phi\rangle$ ) is satisfied for every matrix of the form  $\mathcal{G} = T^\dagger T$ . Indeed  $\langle \phi | T^\dagger T | \phi \rangle = \langle \phi' | \phi' \rangle \geq 0$ , where

we have taken  $|\phi'\rangle = T|\phi\rangle$ . Moreover, such a  $\mathcal{G}$  is trivially Hermitian. To ensure normalization, one can simply divide by the trace. Therefore, the matrix  $g$ , given by the formula

$$g = \frac{T^\dagger T}{\text{Tr}(T^\dagger T)},$$

has all of the three mathematical properties that we require for density matrices. It is convenient to choose a tridiagonal form for  $T$ , with real diagonal elements. The matrix  $T$  is then written in the following form

$$T(t) = \begin{pmatrix} t_1 & 0 & 0 & 0 \\ t_5 + it_6 & t_2 & 0 & 0 \\ t_{11} + it_{12} & t_7 + it_8 & t_3 & 0 \\ t_{15} + it_{16} & t_{13} + it_{14} & t_9 + it_{10} & t_4 \end{pmatrix},$$

where we have explicit dependence on the 16 real parameters  $\{t_1, \dots, t_{16}\}$ . Thus the explicitly “physical” density matrix  $\rho_p$  is given by the formula

$$\rho_p(t) = \frac{T^\dagger(t)T(t)}{\text{Tr}(T^\dagger(t)T(t))}.$$

The measurement data consist of a set of 16 values  $n_i$  with expected value given by  $\bar{n}_i = \mathcal{N} \text{Tr}(\rho \mu_i)$ , with  $i = 1, \dots, 16$ . The  $\mu_i$  are the 16 projective operators we have chosen for the QST. Let us assume the noise on the measurements of the  $n_i$ s has a Gaussian probability distribution. Thus the probability of obtaining a set of 16 measures  $\{n_1, \dots, n_{16}\}$  is

$$P(n_1, \dots, n_{16}) = \frac{1}{N_{norm}} \prod_{i=1}^{16} \exp \left[ -\frac{(n_i - \bar{n}_i)^2}{2\sigma_i} \right],$$

where  $\sigma_i$  is the standard deviation for the  $i$ -th measurement, which can be typically approximated by  $\sqrt{\bar{n}_i}$ .  $N_{norm}$  is a normalization constant. For our physical density matrix  $\rho_p$ , the measure expected for the  $i$ -th operator is

$$\hat{n}_i(t_1, \dots, t_{16}) = \text{Tr}(\rho_p(t_1, \dots, t_{16})\mu_i).$$

Thus the likelihood that the matrix  $\rho_p(t_1, \dots, t_{16})$  could produce the measured data is:

$$P(n_1, \dots, n_{16}) = \frac{1}{N_{norm}} \prod_{i=1}^{16} \exp \left[ -\frac{[\text{Tr}(\rho_p(t_1, \dots, t_{16})\mu_i) - n_i]^2}{2 \text{Tr}(\rho_p(t_1, \dots, t_{16})\mu_i)} \right].$$

We can neglect the dependence of the normalization constant on  $t_1, \dots, t_{16}$ , and under this assumption the formula remarkably simplifies: rather than find the maximum value of  $P(n_1, \dots, n_{16})$ , we can find the maximum of its logarithm. Using the properties of the logarithm, and multiplying by -1 the equation (which implies we now have to find the minimum instead of the maximum), the optimization problem reduces to finding the minimum of the following “likelihood” function:

$$\mathcal{L}(t_1, \dots, t_{16}) = \sum_{i=1}^{16} \frac{[\text{Tr}(\rho_p(t_1, \dots, t_{16})\mu_i) - n_i]^2}{2 \text{Tr}(\rho_p(t_1, \dots, t_{16})\mu_i)}. \quad (2.17)$$

This problem can be solved using standard numerical optimization routines. Once we obtain the values  $(t_1^{opt}, \dots, t_{16}^{opt})$  that minimize eq.(2.17), we can finally calculate  $\rho_p(t_1^{opt}, \dots, t_{16}^{opt})$ , which is the physical matrix that best approximates our measures. In other words,  $\rho_p(t_1^{opt}, \dots, t_{16}^{opt})$  is the best physical guess we can make on the real state of the system  $\rho$ .

# Chapter 3

## Hyperentanglement

In the previous chapter we have discussed about advantages and disadvantages of using photons as quantum information carriers. We highlighted two major drawbacks of photons: the exponentially increasing complexity of experimental setups using a large number of particles and the difficulty of realizing two-photon interactions and thus constructing two qubits gates which, as said, are essential for the creation of a universal quantum computer. In this chapter we analyze in detail the concept of Hyperentanglement and its experimental realization. Hyperentanglement is a way to increase the number of qubits while keeping constant the number of photons. Using different DOFs of photons, Hyperentanglement can find useful applications for up to 8-10 qubits [80].

### 3.1 Introduction

Hyperentanglement or, in general, the possibility of encoding more qubits in different DOFs of the same particle is a useful tool for quantum computation. The realization of multiqubit states can be achieved with relevant advantages in terms of generation rate and state fidelity, compared with multiphoton states. Indeed, by increasing the number of qubits encoded in different DOFs of the same particle, the overall detection efficiency, and hence the repetition rate of detection is constant, since it scales with the power of the number of photons  $N$ . Furthermore, an entangled state built on a larger number of particles is in principle more affected by decoherence because of the increased difficulty of making photons indistinguishable. It is worth to remember that increasing the number  $n$  of involved DOFs implies an exponential requirement of resources. For instance,  $2n$  modes must be exploited to encode  $n$  qubits into a photon. However, working with a limited number of DOFs (such as  $n = 2, 3, 4$ ) offers still more advantages than working with a corresponding number of photons, because of the higher repetition rate and state generation and detection efficiency.

Note that using different DOFs is not sufficient to create an hyperentangled state, which has maximal entanglement for each DOF. In a HE state, the amount of entanglement between the two particles grows with the number of independent DOFs added to the state.

Different experiments were performed with multiDOF states; we refer here to two

important examples. In the first case a ten-qubit entangled state was engineered by entangling the path and the polarization of five photons initially prepared into a Greenberger, Horne, Zeilinger (GHZ) polarization state [80]. In addition, it has been shown that a multiDOF approach was essential in increasing the efficiency of quantum teleportation and dense coding experiments [81];

Integrated photonics allowed substantial advances within the realm of quantum information [82], disclosing new perspectives towards quantum communication [83], quantum computation [71], and the quantum simulation of physical phenomena [2, 84, 85]. The miniaturization of integrated photonic devices represents a necessary step towards the implementation of state-of-the-art quantum information protocols, which require cascading a high number of elements with excellent stability, impossible to achieve with standard bulk optical setup. The generation of a large number of photons, in particular in an integrated environment is still an outstanding task; therefore, encoding a larger number of qubits onto a single photon becomes an appealing feature.

A Hyperentanglement (HE) quantum state consists in a quantum system in which qubits are encoded in multiple degrees of freedom (DOFs) of the same particles and a maximally entangled state is achieved for each of the DOFs, such that the overall HE state can be written as:

$$|H\rangle = \bigotimes_{i=1}^n |ME\rangle_i \quad (3.1)$$

Here, ME is a general multidimensional maximally entangled quantum state,  $i$  labels the DOF and  $\otimes$  is the standard outer product. In this thesis only bipartite states will be considered so that the HE resource can be rewritten as

$$|H\rangle = \bigotimes_{i=1}^n |Bell\rangle_i \quad (3.2)$$

where  $|Bell\rangle_i$  denotes a two qubit Bell state, which is maximally entangled.

In a photonic system qubit can be encoded in several DOFs of the particles, such as their polarization, orbital angular momentum (OAM), path, energy-time, photonic number and frequency [86–88]. Here a path-polarization two photon HE source will be described which was invented and realized in 2005 by Barbieri and colleagues [67].

As we have seen in Chap. 2, polarization of photons is a convenient tool in quantum information processing as it is relatively *easy* to generate entanglement using non linear-optical processes such as SPDC (see Sec. 2) and to manipulate it by using waveplates which are standard tools in linear optics.

Encoding qubits in path means that interferometers can be used to effectively control and manipulate the qubits: in this case Beam Splitter (BS)s and Phase Shifter (PS)s are the standard tools used for controlling qubits. In addition this configuration allows to easily create interaction between different kind of DOFs: a Polarizing Beam Splitter (PBS) for example allows the mapping of the polarization DOF into the path DOF and viceversa. In the following Sections we will address in detail all the aspects of a path-polarization hyperentanglement experiment by examining the source and the experimental setup needed to analyze and manipulate it. Integrated photonics will then be used to demonstrate the feasibility of manipulating hyperentanglement in a chip.

### 3.2 The source

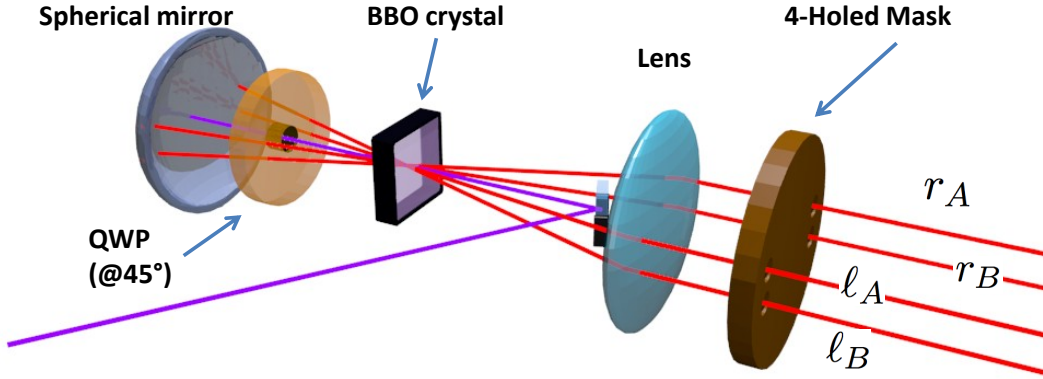


Figure 3.1: Schematic representation of the HE source

The path-polarization hyperentanglement source that we refer to in this thesis was first introduced in [67] and is represented in Fig. 3.1. An UV laser (GENESIS, Coherent Inc., Santa Clara, USA) of 100mW of power, wavelength  $\lambda_i=355\text{nm}$ , continuous wave operation,  $<10\text{GHz}$  bandwidth, vertically polarized, is used as a pump of a BBO type I non linear crystal, of width 1.5mm. As detailed in sec. 2, the BBO produces by means of a SPDC process a couple of horizontally polarized (HH) photons of wavelength  $\lambda_o=710\text{nm}$ , emitted over a cone defined by the phasematching of the crystal.

Photon polarization is rotated by a Quarter Wave Plate (QWP) tuned for  $\lambda_i$  (which operates as an Half Wave Plate (HWP) for  $\lambda_o$ ) to a vertical polarization (VV) and they are then reflected by a spherical mirror ( $M_S$ ). The pump which doesn't interact with the BBO in the first passage, is reflected back by  $M_S$ , and left untouched by the QWP, which has an hole in its center. The pump then is injected through the BBO from the opposite direction and again generates a couple of correlated horizontally polarized photons over the same symmetric Phase Matching cone.

The two cones are collimated by a lens ( $f=15\text{cm}$ ) which focus is centered in the middle of the BBO crystal. This transforms the conical emission into a cylindrical one, whose transverse section identifies the entanglement ring. Finally a brass mask with four symmetric holes, properly located in the entanglement ring, selects two pair of symmetric modes of the cones.

Here the entanglement in polarization is generated by the coherent superposition of the two (HH and VV) cones. The high coherence time of the pump photons guarantees a complete indistinguishability of SPDC degenerate cones. The spherical mirror can be adjusted through the longitudinal axes perpendicular to the BBO crystal to change the phase relation between the two cones, thus producing effectively the state:

$$|\Phi\rangle_p = \frac{1}{\sqrt{2}}(|HH\rangle + e^{i\phi}|VV\rangle). \quad (3.3)$$

Path entanglement is generated through the brass mask and it is ultimately caused by the geometry and simmetry of the radiation emitted by the source itself. Indeed

when the photons are generated through SPDC, they are produced isotropically over a cone, with the two photons being diametrically opposite respect the center of the cone itself.

In other words that means that every time a pair is generated by the BBO we can't know what is the angle respect to the axis of the crystal with which the photons will be generated, but we know that if a photon has been generated at a certain angle, its twin will be diametrically opposite to it.

When we apply the brass mask, we are selecting of all the possible angles in which the cones are generated, only two of them: the one we label "right" ( $|r\rangle$ ) and the one we label "left" ( $|\ell\rangle$ ). If now we call the first photon "A" and the second photon "B" just to distinguish the two particles, we will have that if photon A passes through "right", photon B will be in "left" and viceversa. Again the pairs of modes are undistinguishable so that the state after the mask can be written as:

$$|\Psi\rangle_\pi = \frac{1}{\sqrt{2}}(|\ell_A r_B\rangle + e^{i\theta}|r_A \ell_B\rangle). \quad (3.4)$$

Here  $\theta$  is the phase relation between the two pairs of paths and can be adjusted by changing the optical path of a pair respect to the other, for example adding and rotating a thin glass plate. Eq. 3.4 represents an entangled state in the path dof. Note that in principle one could increase the dimension of the Hilbert space of the path dof by simply adding more holes in the mask: this approach which has been demonstrated in the case of 6 qubits [89], is theoretically viable but experimentally very hard to perform. Indeed it is non-scalable as requires an exponentially growing number of modes increasing the dimension of the qudits.

In the following we will discuss the realization of an experimental scheme to assess and analyze the presence of entanglement in both DOFs in our system. We start by considering each dof singularly. We follow the experimental procedure given in Ref. [67] for a complete description of the analysis process.

### 3.3 Polarization entanglement

When qubits are encoded in the polarization degree of freedom, the most convenient way to measure their density matrix is through a tomographic reconstruction process already described in Sec. 2.6.2. For this purpose, a set of a QWP, HWP and a PBS are placed over the photonic modes. Single photon coincidence measurements are carried out through two single photon avalanche photodiodes, counting in coincidence in a time window of  $<5\text{ns}$ .

Coincidence counting allows to discriminate random photons by those generated simultaneously by the source. Indistinguishability between photons is obtained by filtering the bandwidth with an interference filter. For our purposes we used a 710nm centered, 6nm bandwidth filter. QWP and HWP are used in order to perform 36 measurement of polarization over three different basis. There is actual redundancy in the amount of information collected by this number of measurement which is used to ensure statistical stability of the density matrix reconstructing protocol. Measurement

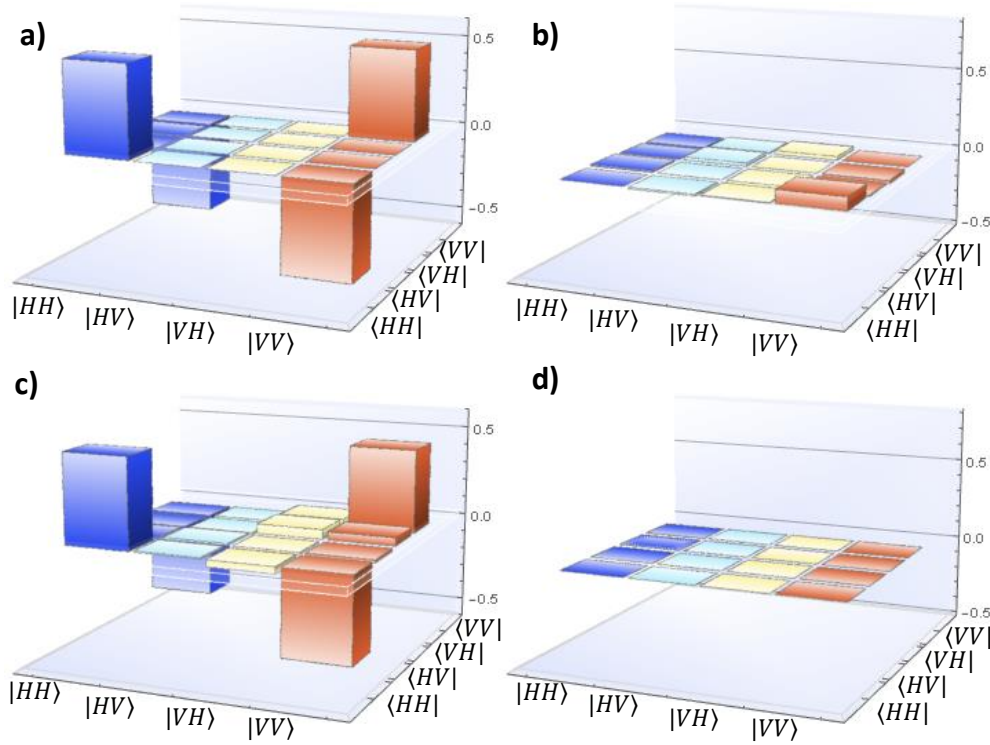


Figure 3.2: Tomographic reconstruction of polarization density matrix generated by an HE source. Phase was selected in order to generate a  $|\psi^-\rangle$  state. **a)**  $Re(\rho_{exp})$ , **b)**  $Re(\rho_{theo})$ , **c)**  $Im(\rho_{exp})$ , **d)**  $Im(\rho_{theo})$ . Fidelity to the theoretical state is  $0.92 \pm 0.01\%$ , Concurrence is  $C = 0.888 \pm 0.003$ , Purity of the state is  $P = 0.887 \pm 0.003$ .

is conducted in the computational basis ( $|H\rangle, |V\rangle$ ), in the diagonal basis ( $|+\rangle, |-\rangle$ ) and in the circular basis ( $|L\rangle, |R\rangle$ ).

In Fig. 3.2 typical tomography results are shown as a 3D-barplot. Once the density matrix has been extracted, we calculate some state descriptors (described in Sec. 1.3) to prove the goodness of the state. In particular we calculate the Fidelity to the theoretical expected state, the purity (which indicates the amount of decoherence which the experimental state is subject to), and the Concurrence, which is an entanglement quantifier.

The values for these parameters are very sensible to the alignment of the source and the condition in which the photons are detected, and prove that the source must be carefully calibrated to achieve good state quality.

### 3.4 Path Entanglement

Detection of path entanglement is trickier as it requires the mixing of different paths in order to change the basis of measurements.

A photon travelling along two different directions can be represented by  $|\phi\rangle = \alpha|r\rangle + \beta|\ell\rangle$  with  $\alpha, \beta$  complex numbers so that the normalization condition holds. The density matrix of such state could be determined by measuring the presence of the photon in the following basis:

- the computational basis ( $|\ell\rangle, |r\rangle$ ),

- the diagonal basis  $(|+\rangle = \frac{1}{\sqrt{2}}(|\ell\rangle + |r\rangle), |-\rangle = \frac{1}{\sqrt{2}}(|\ell\rangle - |r\rangle))$
- the circular basis  $(|\odot\rangle = \frac{1}{\sqrt{2}}(|\ell\rangle + i|r\rangle), |\ominus\rangle = \frac{1}{\sqrt{2}}(|\ell\rangle - i|r\rangle))$ .

A beam splitter, along with a phase shifter, is used to obtain the change of basis transformation. The beam splitter is an optical elements which performs the following operation:

$$\begin{aligned} |\ell\rangle &\rightarrow \frac{1}{\sqrt{2}}(|\ell\rangle + |r\rangle), \\ |r\rangle &\rightarrow \frac{1}{\sqrt{2}}(|\ell\rangle - |r\rangle), \end{aligned} \quad (3.5)$$

The phase shifter is an optical elements which performs the following operation:

$$\begin{aligned} |\ell'\rangle &\rightarrow |\ell\rangle, \\ |r'\rangle &\rightarrow e^{i\varphi}|r\rangle, \end{aligned} \quad (3.6)$$

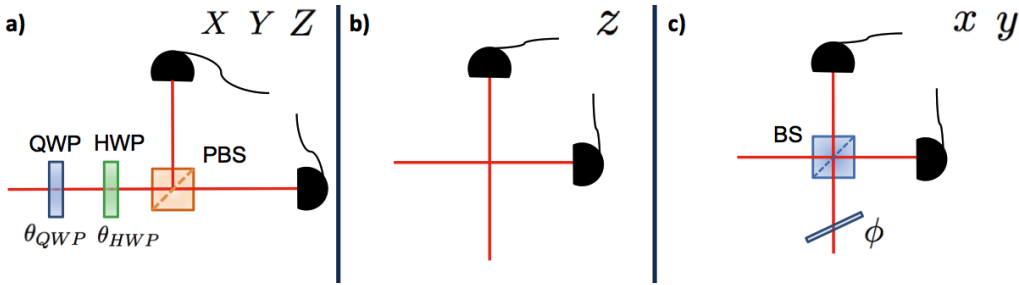


Figure 3.3: Schematic representation of the measurement setup for HE. **a)** a tomographic setup permits the projection of the polarization state via the three pauli operators X,Y,Z. **b)** to perform Z projection on a path encoded state nothing excepts the photon counters are needed. **c)** a BS and phase shifter is needed in the path mode to perform X, Y operations.

In Fig. 3.3 we show a scheme of how the measurement works for the path dof; there we show that in order to change the measurement basis a beam splitter (BS) is needed. Here we have the four input modes, labeled as  $|\ell\rangle_{AB}$ ,  $|r\rangle_{AB}$ ; a measurement in the computational basis means placing detectors over the four modes, without doing any operations on them. In this case we expect to obtain a maximum of coincidence counts when detectors are placed on modes  $|\ell r\rangle_{AB}$  or  $|r\ell\rangle_{AB}$  due to the form of the state in Eq. (3.4).

Note that a single photon detector represents a projection of a path qubit over the mode in which the detector is placed. For example, a detector which is placed in path  $|\ell\rangle$  performs the operation  $|\ell\rangle\langle\ell|$ .

Now, if we put the BS so that photon A (B) goes into BS A (B), then we notice considering Eq. 3.5 that if the input state is in the coherent superposition of the form:  $\frac{1}{\sqrt{2}}(|r\ell\rangle + |\ell r\rangle)$  (and thus it's entangled), then we expect a maximum in the coincidence counts for either detectors  $|\ell r\rangle_{AB}$  and  $|r\ell\rangle_{AB}$  (and a minimum for  $|\ell\ell\rangle_{AB}$  or  $|rr\rangle_{AB}$ ) or viceversa, depending on the value of the phase  $\varphi$ . The same is true when considering the transformation on the circular basis which can be obtained by selecting phase  $\varphi = \pm\pi/2$ .

If we inject as input state a mixed state, such as  $\rho_{mix} = \frac{1}{\sqrt{2}}(|\ell r\rangle\langle\ell r| + |r\ell\rangle\langle r\ell|)$  we obtain, when changing basis, a balanced output over all the possible exits, so changing the phase wouldn't produce any results. Following this, we can demonstrate

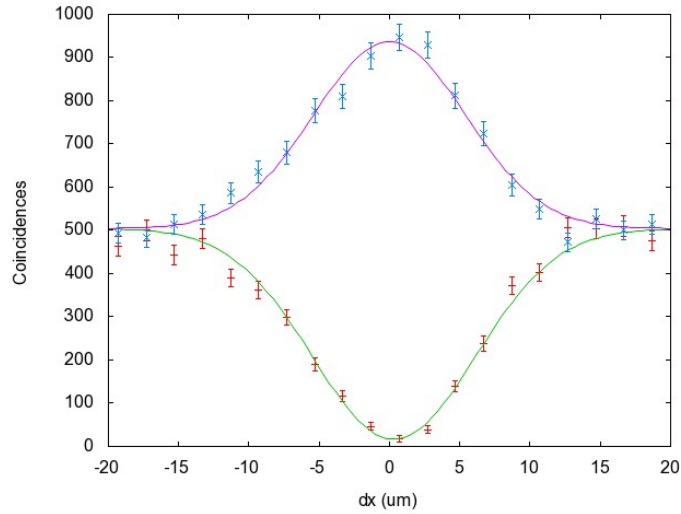


Figure 3.4: Path entanglement experimental signature. Coincidences are taken in a 30s time window. Experimental error bars take into account Poissonian statistic of the photon counts. Red points are for  $\varphi = 0$ , blue points are for  $\varphi = \pi$ . Green and violet line represent respective gaussian fit of experimental data. Visibility for peak is  $V_{peak} = 0.84 \pm 0.03$ , visibility for dip is  $V_{dip} = 0.925 \pm 0.004$ .

the presence of coherent superposition by observing the change in the coincidence counts between two detectors, say lr, when changing  $\varphi$ . In Fig. 3.4 we show a proof of entanglement in path by the observation of the peak-dip of the coincidence counts as a function of  $\Delta x$  in a test calibration of the source.

Here  $\Delta x$  represents the difference in optical path between the two pairs of modes - indeed the interference effect in changing the basis will manifest only if the two pairs are perfectly indistinguishable. In the figure, it is shown that by changing  $\varphi$  from 0 to  $\pi$  one can observe the transition between a peak and a dip in coincidences. The visibility of the peak is  $V_{peak} = 0.84 \pm 0.03$  and the visibility of the dip is  $V_{dip} = 0.925 \pm 0.004$ .

### 3.5 Hyperentanglement and Symmetry

In the previous sections we have analyzed the methods for measuring entanglement in polarization and in path. However the presence of hyperentanglement must still be proved, as the simultaneous presence of entanglement in path and in polarization is not sufficient to prove that the state generated is indeed that of Eq. 3.4.

The reconstruction of the density matrix for a 4 qubit state becomes rapidly demanding in terms of number of measurements required ( $6^4 = 1296$ ) so that a more affordable way of proving the presence of hyperentanglement must be found.

Indeed one efficient way of observing hyperentanglement is by making wave-function symmetry considerations.

We now consider a general hyperentangled state which is tensor product between two  $|\psi^\pm\rangle$  Bell's functions, with  $|\psi^+\rangle$  symmetric to the swap of the two qubits, and  $|\psi^-\rangle$  antisymmetric to the swap of the two qubits. We know photons are bosons and we expect their wavefunction to be symmetric. However when considering a composite system such as that of the HE state we can effectively change the overall symmetry of the state by acting on the phase of the two DOFs individually. This means that we

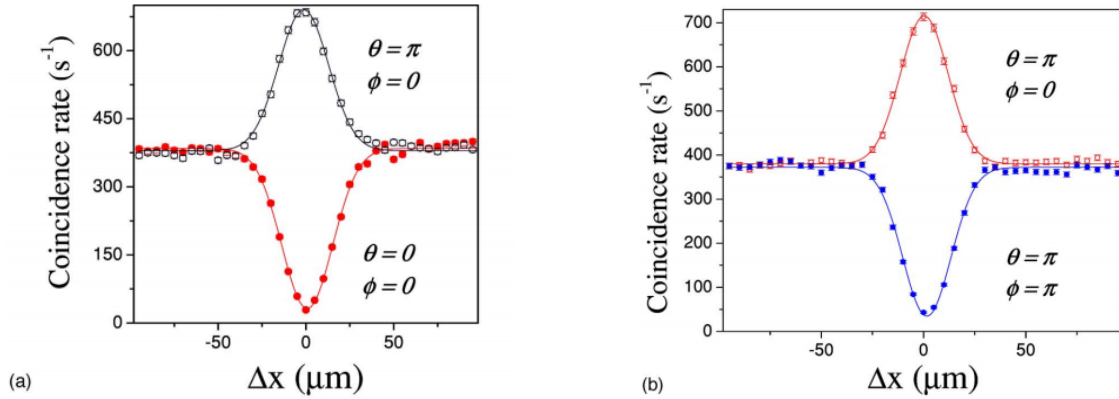


Figure 3.5: Experimental signature of HE from Ref. [67]. Coincidences as a function of optical path difference for HE state, changing the values of  $\theta$  (phase of path dof) and  $\varphi$  (phase of polarization dof). Peaks represent an antisymmetric (fermion-like) behaviour, dips represent a symmetric (boson-like) behaviour.

can force photons to behave like fermions (antisymmetric wavefunction) or bosons (symmetric wavefunction) depending on the values of the phases  $\varphi, \theta$ . In this way we are effectively making the two DOFs interact with each other. Furthermore, if the overall wave function wasn't hyperentangled (in other terms: if the product tensor wasn't a coherent operation) there would have been no way to make the two DOFs interact as they would have been completely independent, thus being unable to change the overall symmetry of the state.

Because of this reason, Fig. 3.5, which is taken from [67], is an experimental signature of the presence of hyperentanglement in the system. The peak and dips, similar to those of Fig. 3.4 can now be changed not only by moving the phase shift  $\varphi$ , which is linked to the path dof, but also by changing  $\vartheta$ , which is linked to the polarization dof. This is a complete proof of hyperentanglement of the system, and of the quality of the source.

### 3.6 Hyperentanglement and Cluster state manipulation on chip

Here we discuss the main experiment of this thesis which has been conducted in 2014/2015 [90]. In this experiment we aim to demonstrate the possibility of encoding and reveal the presence of hyperentanglement and multipartite correlations by means of an integrated photonic device. As shown in Sec. 2.5, femtosecond laser writing is a promising technology to create integrated photonic device, especially due to the very low birefringence of the substrate. This devices allow in principle the preservation and manipulation of polarization and path of photons (as shown in [91]).

In this experiment we demonstrated the simultaneous control of both degrees of freedom by effectively controlling for the first time two DOFs by using a photonic integrated device. In Fig. 3.6 we show the experimental scheme: in the inset the chip can be seen in more detail. The chip consists of two waveguide balanced beam splitters ( $BS_A$  and  $BS_B$ ), yielding polarization insensitive behaviour[92], fabricated by

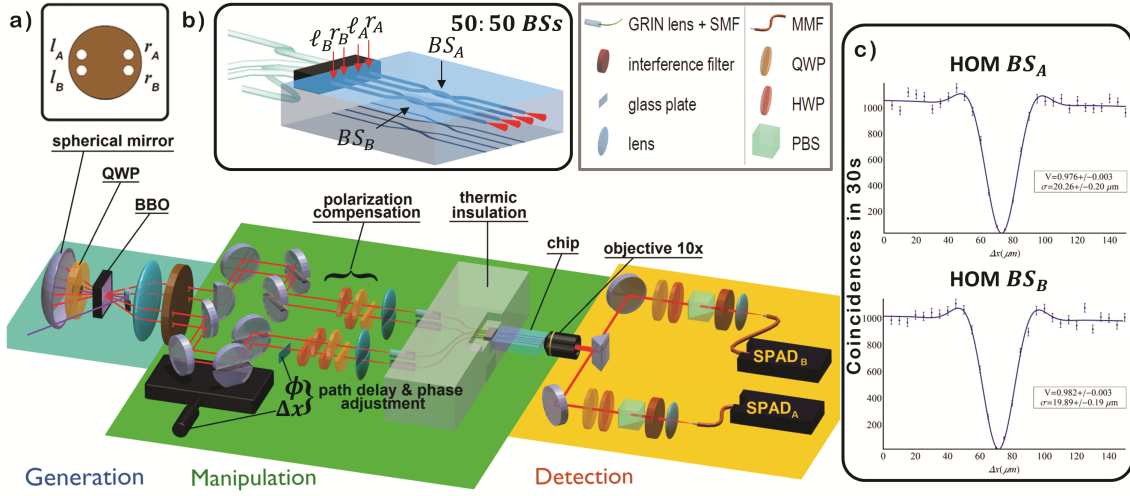


Figure 3.6: The state  $|\Omega\rangle$  is generated by the hyperentangled source in blue area. The 4-hole screen in **a**) selects the spatial modes  $l_A, l_B, r_A, r_B$ . In the green area the four modes are independently addressed using half mirrors, half wave plates and half lenses so to compensate their polarization and to couple them into the fiber array. A translation stage is used to control path indistinguishability between left and right modes, a glass plate in mode  $l_B$  is used to control the path phase. The chip is connected to the fiber array using a NanoMax 6-axis stage. In the orange area measurements are performed: two of the outputs of the chip are addressed into multi-mode fibers connected to SPADs in coincidence mode. Polarization analysis is performed using QWP, HWP and PBS. **b**) Schematic representation of the integrated device. **c**) Hong-Ou-Mandel dip of  $BS_A$  and  $BS_B$ .

femtosecond laser waveguide writing[93] using the second harmonic ( $\lambda=515$  nm) of a Yb:KYW cavity-dumped laser oscillator (300 fs pulse duration, 1 MHz repetition rate). Femtosecond laser pulses are focused by a 0.6 NA microscope objective into the volume of the glass substrate (EAGLE 2000, Corning), where nonlinear energy absorption creates a permanent and localized refractive index increase. Waveguides are produced by smoothly translating the sample under the laser beam, using Aerotech FiberGLIDE 3D air-bearing stages. Under proper irradiation conditions (100 nJ pulse energy and  $10 \text{ mm s}^{-1}$  translation speed) single-mode waveguides at 710 nm are produced, at  $170 \mu$  depth below the glass surface, characterized by a mode diameter of  $\sim 8 \mu m$ , propagation loss of  $1.5 \text{ dB cm}^{-1}$  and coupling loss to single mode fibers  $< 1 \text{ dB}$  per facet. Integrated beam splitters are realized following a particular three-dimensional directional-coupler design[92] that ensures insensitivity to the polarization. To achieve a balanced splitting ratio the waveguides, initially  $127 \mu m$  far, are brought closer (with a bending radius of 90 mm) down to  $10 \mu m$  distance for an interaction length of 1.8 mm. Overall chip length is 34 mm.

The experiment is conceptually the same as explained in the previous sections, but now the path manipulation is performed through the chip. The main experimental realization is being able to control simultaneously and independently the four modes that are generated by the source in order to inject them into the chip.

For this reason we engineered a custom-made device which contains the chip and a fiber array which is coupled to it. The chip can move in all the six degrees of spatial freedom by using a NanoMax micrometric translational stage and a three-axis tilter. The fiber array is fixed and allocated into a small aluminium case (Fig. 3.7) which can be thermally insulated and covered. Thermal insulation is obtained by filling the case with plastic material. The input side of the four fibers are coupled to a custom

made GRIN (GRadient INdexed) lenses, which are cylindrical glass tubes which have a gradient in their index of refraction so that light can be forced to be coupled to the fiber. The GRIN lenses are placed and fixed into four mechanical arms which can be tilted in order to facilitate the coupling of light.

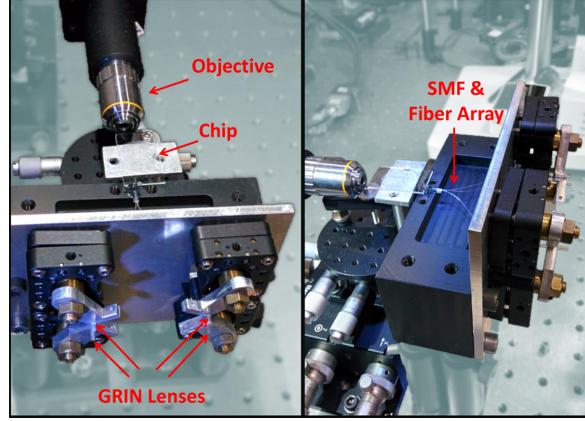


Figure 3.7: Detail of the support for the fiber array and the chip. In the figure the GRIN lenses are highlighted.

The four output modes of the source are coupled independently on their respective GRIN lenses. This is performed by using an optical setup which consists of a set of half-mirrors, half-lenses, each of which could be moved independently from the others. In order to maintain photon spatial indistinguishability, a translation stage is included on the left modes. This micrometric stage can be moved to obtain the condition of same optical path for right and left modes. Polarization compensation is performed on the four modes by adding into each of them a set of three (half) wave plates (QWP, HWP, QWP).

After the chip, the four modes are collimated through a 10x objective (NA=1.5) and then split by means of a 90 degree-angle prism. The two external modes are then sent into a tomographic apparatus consisting of a QWP, HWP and PBS, and then coupled into a multimode fiber which is connected to a single photon detector (APDs). Bandwidth indistinguishability between photons is achieved by means of interferometric filters ( $\lambda_0 = 710\text{nm}$ ,  $\Delta\lambda = 6\text{nm}$ ) which are placed right before the multimode fiber.

Detectors are connected to a digital counter which allows the visualization of both single clicks and coincidence clicks between the two detectors. Coincidences are set to be counted in a time gate of approx. 9ns between the click in the first detector and the second.

The two BSs have been tested beforehand with an Hong-Ou-Mandel experiment which results are shown in Fig. 3.6c: Hong-Ou-Mandel (HOM) dips are obtained when the two photons are injected within  $BS_A$  and  $BS_B$ , respectively. We obtained the following visibilities:  $\mathcal{V}_A = (0.976 \pm 0.003)$  for  $BS_A$  and  $\mathcal{V}_B = (0.982 \pm 0.003)$  for  $BS_B$ , thus showing the correct operation of the two systems. After removing  $N_{acc} = 12$  accidental coincidences every 30 sec, we obtain  $\mathcal{V}_{A-net} = (0.985 \pm 0.003)$  and  $\mathcal{V}_{B-net} = (0.991 \pm 0.003)$ .

Coupling efficiencies are reported in Tab. 3.1

Input mode:	Fiber Array	Chip	Collection	Tot
$\ell_A$	59%	42%	87%	22%
$r_A$	65%	41%	87%	23%
$\ell_B$	48%	32%	87%	13%
$r_B$	51%	40%	87%	18%

Table 3.1: Measured coupling efficiencies for the four input modes of the fiber array, the integrated device and of the detectors' multimode fibers

### 3.6.1 Photon indistinguishability and entanglement witness

The main conceptual delicacy of the above experiment is that photon must retain their undistinguishability in all their degrees of freedom at least until they get to interfere inside the chip. For this reason a number of careful adjustments have to be made. First of all the photons, which are entangled in polarization are subject to a unitary transformation caused by the fibers of the fiber array. The overall quality of the resource degrades in this case, consequently a suitable compensation to this effect is performed through the polarization compensation setup shown in Fig. 3.6. The effect of the fiber array depends on the current tilting and stretching of the fibers and thus can vary greatly depending on the current configuration of the scheme and even by the temperature of the room.

In Ref. [94] it is shown that a set of cascading QWP, HWP, QWP can be used in order to compensate for any unitary operation on the quantum state of a qubit.

As shown in Fig. 1, we used a QWP (quarter wave plate) and a HWP (half wave plate) to compensate them in the H-V basis, while the phases between  $H_i$  and  $V_i$  ( $i = A, B$ ) were adjusted tilting on the vertical axis a HWP at  $0^\circ$  in the mode  $\ell_B$  and using the spherical mirror of the source. We firstly compensated the polarization so that modes  $\ell_A$  and  $r_A$  behave such that  $H \rightarrow H$  and  $V \rightarrow V$  while modes  $\ell_B$  and  $r_B$  behave such that  $H \rightarrow V$  and  $V \rightarrow H$ . Measured fidelity for state  $|r_A \ell_B\rangle \otimes \frac{1}{\sqrt{2}}(|H_A V_B\rangle + |V_A H_B\rangle) = |r_A \ell_B\rangle \otimes |\psi^+\rangle$  is  $F = 0.91 \pm 0.09$  (see Fig. 3.8b), thus showing that the integrated devices preserve the polarization entanglement.

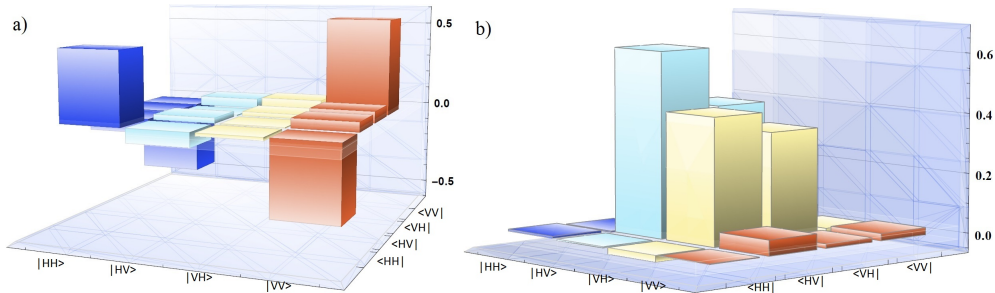


Figure 3.8: **a)** Two photon tomography of state  $|r_A \ell_B\rangle \otimes |\phi^-\rangle$  performed before the integrated device, (Concurrence= $0.85 \pm 0.08$ , Fidelity= $0.90 \pm 0.10$ , **b)** Two photon tomography of state  $|r_A \ell_B\rangle \otimes |\psi^+\rangle$  performed after polarization compensation and the integrated device (Concurrence= $0.83 \pm 0.08$ , Fidelity= $0.91 \pm 0.09$ ).

Indistinguishability in the path degree of freedom is trickier: photon *pairs* must enter the BS exactly at the same time in order to have an interference effect. This must be true even considering the path they make inside the fibers. As explained before,

the translation stage is used over mode  $\ell$  to obtain the zero optical delay between the paths, but at difference from the bulk setup, now phase stability cannot be assumed.

Indeed a temperature gradient between the fibers would dilate different fibers by a different quantity, thus creating a phase instability on the state. In order to prevent this from happening we isolated thermally the fibers by covering them in an alluminium box full of plastic material, and then covering the whole apparatus in which chip and fibers are allocated with a especially made poliester box.

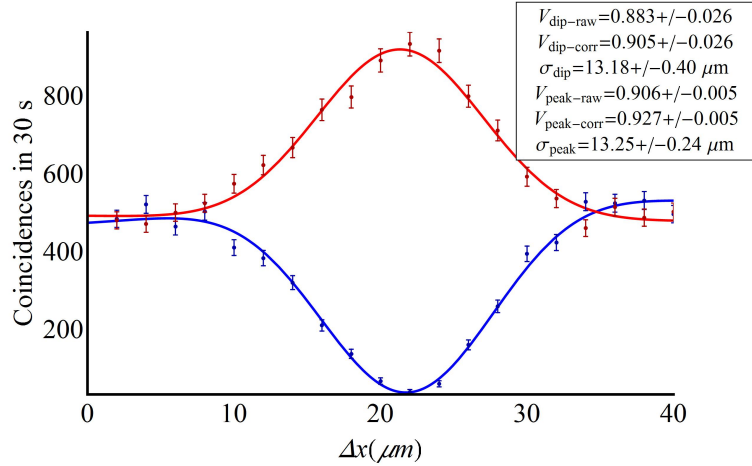


Figure 3.9: Interference pattern between modes  $|\ell_A r_B\rangle$  and  $|r_A \ell_B\rangle$ . Peak is for  $\phi = \pi$ , dip is for  $\phi = 0$ . Experimental data is fitted with gaussian curves.

The presence of path entanglement has been shown by observing interference effects using only one polarization of the light emitted from the source. On this purpose the state  $|H_A H_B\rangle \otimes (|r_A \ell_B\rangle + e^{i\phi} |\ell_A r_B\rangle)$  was injected in the integrated device. We observed interference effects between the two couples of modes measuring the visibility of the peak (for  $\phi = 0$ ) and the dip (for  $\phi = \pi$ ) in the condition of path indistinguishability. We changed  $\phi$  by tilting a glass plate inserted in mode  $\ell_B$  and we obtained path indistinguishability varying the length of paths  $\ell_B$  and  $\ell_A$  using a micrometric translation stage. In Fig. 3.9 we report as an example the peak and dip as coincidences as function of the delay  $\Delta x$ . We obtained  $V_{\text{peak}} = 0.892 \pm 0.007$  and  $V_{\text{dip}} = 0.915 \pm 0.008$  after a fit with a gaussian curve. We used 10nm gaussian filters centered in  $\lambda = 710\text{nm}$ , the FWHM of the fitted curves have  $\sigma = 13.2 \pm 0.02 \mu\text{m}$ .

### 3.6.2 Hyperentanglement measurements

Here we show definite proof of the preservation of path and polarization dof into an integrated device, using the same methods in the previous section. We proceeded to compensate the polarization of our state by applying the transformation  $|H\rangle_B \rightarrow |V\rangle_B$ ,  $|V\rangle_B \rightarrow |H\rangle_B$ , so that the polarization state becomes  $|\Psi^{pm}\rangle$ , which is symmetric or antisymmetric depending on the phase of the state. Again we measure the coincidences between two output modes of the chip, one from  $BS_A$ , one from  $BS_B$  in the condition of path indistinguishability.

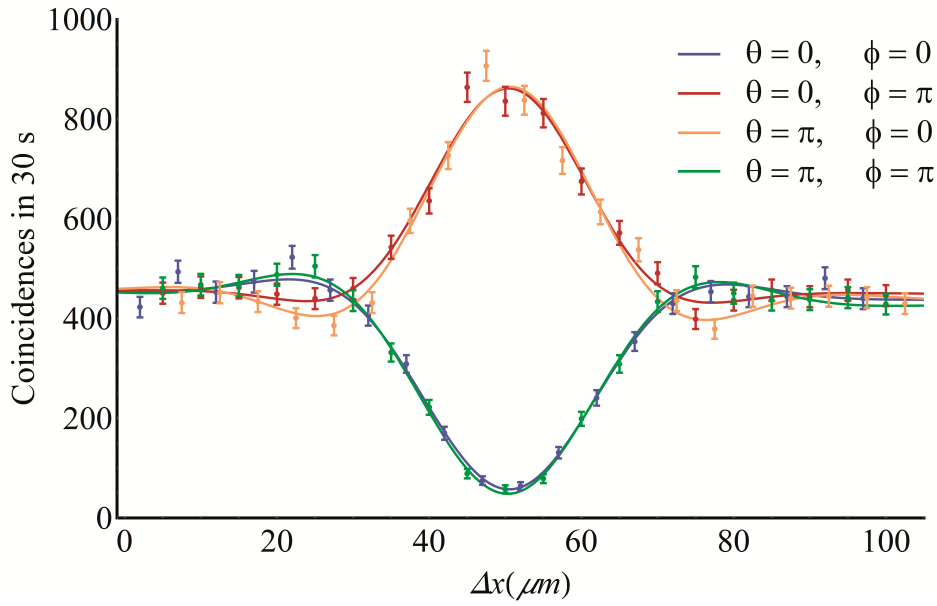


Figure 3.10: **Hyperentangled state interference.** Interference pattern between modes  $|\ell_{A^T B}\rangle$  and  $|r_{A \ell_B}\rangle$  varying both  $\theta$  and  $\phi$ . Peaks and dips derive from the symmetry of the entire HE wave function. Experimental data of each curve are fitted with the convolution of a gaussian with a sinc function; error bars derive from the Poissonian statistical distribution of counts. Errors on the peak/dip visibilities are estimated by using a Monte Carlo statistical analysis on experimental data.

The overall symmetry of the state determines the behaviour of the two photons: if the wavefunction of the HE state is symmetric they emerge from the same output port of the beam-splitters, corresponding to a coincidence dip, while the expected result in the case of an antisymmetric wavefunction is a coincidence peak. This behaviour can be analysed by recovering the dips and peaks of path entanglement varying both  $\phi$  and  $\theta$  so that a dip can be obtained with  $(\phi, \theta) = (0, 0), (\pi, \pi)$  and a peak with  $(\phi, \theta) = (0, \pi), (\pi, 0)$ . Results are shown in Fig. 3.10, which represents the main result of this experiment. The average peak/dip visibilities are  $\mathcal{V}_{peak} = 0.93 \pm 0.20$  and  $\mathcal{V}_{dip} = 0.860 \pm 0.005$ . These results are comparable with those of Ref. [67] and prove the achievement of path-polarization hyperentanglement on chip with good fidelity.

### 3.7 Discussion and perspectives

During this work, the author contributed to the design and realization of the experimental setup, including the chip and fiber array support and the mounts for the half mirrors. He was the main performer the experiment and analyzed the data. The demonstration of hyperentanglement preservation and partial manipulation into an integrated device is just the stepping stone for a new take on integrated quantum experiments. There is a number of interesting paths that can be explored starting from this results; here we consider some of them.

- First of all, recent works have shown the possibility of manipulating the polarization inside a femtosecond-laser written chip [91]. This is a natural progression for our work, since it would allow to control both DOFs directly inside the integrated device. Note that there are no conceptual obstacles in the realization of such a

device, so that its realization is just a matter of engineering a phase-polarization tunable chip.

- Apart from than providing a mere increase in the qubit density stored in the particles DOFs, are particularly useful in generating cluster states, as it will be explained in the next Chapter. On Chip manipulation on chip of such states opens up the possibility of performing one-way quantum computation on chip with photons, which is a promising benchmark for a number of quantum algorithms such as Grover's. We will analyze cluster state generation, manipulation, analysis and one-way quantum computation in greater detail in the following chapters.
- In this experiment the chip is used as a mean for changing from the computational to the diagonal basis, so that the presence of path entanglement could be measured. However now path entanglement can be used as a resource, meaning that the two beam splitters aren't strictly necessary. The chip itself could be substituted by a more complex version of it, which could be used to perform operations in both path and polarization which would not be possible (or practical) with a bulk setup.

# Chapter 4

## Cluster states and one-way quantum computation

In this chapter we extend the theory behind the hyperentanglement scheme to generate cluster states. We will describe these states and their relevance for quantum information protocol through the principles of one-way quantum computation. Then we will discuss a method for assessing internal correlations of cluster states by means of multipartite non locality Bell-like equations, and finally we will exploit a 4-qubit linear cluster state in order to demonstrate a simple Grover's search algorithm.

### 4.1 Definition of a cluster state

Cluster states are a particular family of composite quantum states composed by qubits sharing correlations among them. They can be represented as graphs in which each node is associated to one qubit and each vertex, or link, corresponds to a quantum correlation among two qubits. For this reason the zoology of a multiqubit cluster state is vast and the global and local properties of each cluster strongly depend on the interconnection existing among the qubits. A N-dimensional cluster state can be easily generated by initializing each of its N qubits in  $|+\rangle = \frac{1}{\sqrt{2}}(|0\rangle + |1\rangle)$ . A link between qubits i,j is created by applying a C-Phase(i,j) operation which entangles the two qubits, so that the general form of a cluster state becomes:

$$|C_N\rangle = \prod_{\{i,j\}} \text{C-Phase}(i,j) |+\rangle_1 |+\rangle_2 \cdots |+\rangle_N. \quad (4.1)$$

Here  $\{i, j\}$  stands for the couples of qubits which share a link in the cluster state. For example we shall create a two qubit cluster state by considering the following system:

$$\begin{aligned} \text{C-Phase}(1,2) |+\rangle_1 |+\rangle_2 &= |00\rangle_{12} + |01\rangle_{12} + |10\rangle_{12} - |11\rangle_{12} \\ &= |0\rangle_1 (|0\rangle_2 + |1\rangle_2) + |1\rangle_1 (|0\rangle_2 - |1\rangle_2) \\ &= |0\rangle_1 |+\rangle_2 + |1\rangle_1 |-\rangle_2 \end{aligned} \quad (4.2)$$

Now we apply an Hadamard operation (see Eq.1.48) to qubit 2, retrieving  $\frac{1}{\sqrt{2}}(|00\rangle_{12} + |11\rangle_{12})$  which is the formal expression of the Bell state  $\Psi^+$ . This demonstrates that a 2-qubit cluster state is equivalent to the maximally entangled two qubit

Bell states, and, regarding this dimension, no more connections can be added would change the properties of the system. We are stating that the whole zooology of entangled state for a multipartite system, which we briefly discussed in Sec. 1.2.5 can be fully understood using the cluster state formalism. Indeed representing a three-qubit state as a graph allows the graphic representation of the whole spectrum of categories which we described in the previous chapters.

Cluster state are interesting from two different perspectives:

- They represent a family of structured quantum states connected by multipartite correlations and as such they can be used as models for simulating complex quantum systems,
- They can be exploited as resources for quantum computation following the One-Way Quantum Computation (OWQC) scheme.

For now we address the attention on the second point of the list by describing the principles of the OWQC.

## 4.2 One-Way quantum Computation

Standard quantum computation, based on unitary quantum logic gates, is, on one hand, a powerful application of the laws of quantum physics, allowing far more efficient factorization [4] or database searches [5] compared to classical computation. On the other hand, complex algorithms require a great ability in controlling the state of the system and the interactions which allow multi-qubit gates. As we have already discussed in the previous chapters, satisfying both these requirements is experimentally very demanding, and, according to the present technology, only very simple algorithms are feasible in laboratory [54, 71, 95]. In 2001 Raussendorf and Briegel proposed an alternative approach to quantum computation, called One-Way Quantum Computation (OWQC) [52], which has important implications, not only in the fundamental understanding of the role of entanglement and measurements in the quantum computation, but also in the experimental feasibility of quantum algorithms.

Indeed, this type of computation exploits the particular properties of the correlations in a cluster state, and uses measurements on a subset of the cluster qubits to perform arbitrary gates on another subset. The only resources needed for OWQC are therefore the initial cluster state and one-qubit measurements, while no two-qubit gate is required. As a consequence, this “measurement based” computation is often well-suited for optical schemes, where states with a certain degree of complexity can be generated with good fidelity, and measurements are easily implementable. Furthermore, OWQC is universal, i.e. it allows any possible algorithm if a suitable cluster state is used, and deterministic, although requires a classical “feed-forward” process which depends on the outcomes of the measurements. The feed-forward can be avoided implying a probabilistic computation.

In order to describe the computational scheme, we need to distinguish between the *physical qubits* (for example, the polarization state of photons or ions) which make up the cluster state and on which actual measurements are carried out, and encoded qubits, on which the computation is actually taking place.

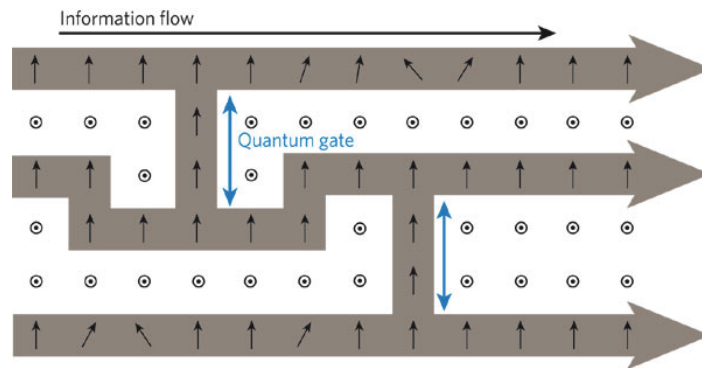


Figure 4.1: Scheme of a one-way quantum computation protocol. The encoded qubits are initially in the state  $|+\rangle$  and are written on the physical qubits on the left end of each row of the cluster. The information flows from left to right as measurements are performed on the physical qubits, implementing single-qubit transformation on the encoded qubits. Vertical links between rows represent two-qubit gates.

The one-way quantum computer does not perform quantum logic on individual qubits of the cluster state. In other words, no individual physical qubit carries any information about an input state of the computation. Instead, each encoded qubit is written on the cluster state non-locally; that is, the information is carried by the correlations between the physical qubits. The cluster can then be regarded as a “substrate” on which the encoded qubits are “written”. As the quantum computation proceeds, the encoded input qubits are processed in the “imprinted” circuit, whose output is finally transferred onto physical readout qubits from which the information can be extracted. By imprinted circuit we mean a logical circuit representing the performed computation algorithm. This circuit is determined by the particular form of the cluster state and the choice of the measurement sequence.

While in standard computation measurements are used only to extract information from the final state, in OWQC they have an active role in information processing. However, performing measurements, i.e. non-unitary transformations, we are inevitably changing the connections between the physical qubits of the cluster, which cannot be used again for another computation. This kind of processing is therefore non-reversible (and hence called “one-way”). Interestingly, even if the entanglement between the physical qubits in general decreases during the computation as a result of the measurement sequence, the entanglement between encoded qubits may increase [52].

### 4.2.1 Description of the protocol

Let us see in more detail how OWQC works. We will not demonstrate each step, but just describe how an arbitrary algorithm can be performed. A scheme of a OWQC protocol is depicted in Fig.4.1. A cluster can be seen as a network of Physical Qubits

(PQ). Each row (or “wire”) of this network is associated to an Encoded Qubit (EQ), on which we want to carry on the computation. Quantum information is propagated horizontally through the cluster (we arbitrarily choose the flow to go from left to right) while physical qubits on vertical connections are used to realize two-bit quantum gates. The EQs are then initially written on the physical qubits on the left end of each row, and are in the initial state  $|+\rangle_E$  (note that the state of an EQ is different from the state of the PQ it is written on). We can measure the  $j$ -th PQ on a basis  $\mathcal{B}_j(\alpha_j) = \{|+\alpha_j\rangle, |-\alpha_j\rangle\}$ , where  $|\pm\alpha\rangle = (|0\rangle_j + e^{\pm i\alpha} |1\rangle_j)/\sqrt{2}$ . We associate the measurement value  $s = 0$  if the PQ is measured in the state  $|+\alpha\rangle$ , while  $s = 1$  if it is found in  $|-\alpha\rangle$ .

In Ref.[52] the authors demonstrated that, as a consequence of the particular correlations of the cluster state, measuring the PQ (on which the EQ is written) in the base  $\mathcal{B}(\alpha)$  is equivalent to transferring the information to the PQ on the right and applying the following single-qubit operation:

$$\mathcal{O}(\alpha, s) = X^s H R_z(\alpha), \quad (4.3)$$

where  $H$  is the Hadamard gate,  $R_z(\alpha) = \exp^{-i\alpha Z/2}$  represents a single-qubit rotation around the  $z$  axis of the Bloch sphere, and  $X = \sigma_x$  and  $Z = \sigma_z$  are the Pauli operators. This transformation depends on both the measurement choice  $\alpha$ , which can be controlled by the experimenter, and the measurement outcome  $s$ , which is instead probabilistic and cannot be pre-determined. To perform a deterministic computation we then require a classical feed-forward protocol, where the choice of the measurement basis on the  $j$ -th PQ depends on the outcomes of all the previous measurements performed on the PQs of the cluster. In this way the Pauli errors occurring when we obtain an outcome  $s = 1$  can be deterministically corrected. However, for large size cluster states this procedure could not be easy to implement experimentally. Sometimes it is more suitable to adopt a probabilistic computation, avoiding the feed-forward operations. This can be achieved by post-selecting only the cases where each measurement gives the outcome  $s = 0$ , that is, when no Pauli errors occurred in the whole computation. The operation performed by each measurement simplifies in

$$\mathcal{O}(\alpha) = H R_z(\alpha). \quad (4.4)$$

For simplicity, we will consider only this probabilistic post-selected computation in the following discussions.

Summarizing, each time we measure a PQ the EQ is transferred to the PQ on its right, and a single-qubit operation of the form (4.4) is performed to the EQ. The transformation can be adjusted by the choice of the parameter  $\alpha$  in the measurement process. A vertical link between two rows of the cluster, as shown in Fig.4.1, represents a C-Z operation between the two EQs associated to the rows. Once the measurement sequence is completed, the EQ will be written on the PQ on the right end of each row. After the measurements, all the entanglement on each row of the cluster is destroyed, thus the state of the EQs now coincides with the state of the last unmeasured PQs, which can thus be used to extract the information obtained by the information processing.

## 4.2.2 Universality of one-way quantum computation

Here we want to demonstrate that the One-Way Quantum Computation approach is universal. That is, any quantum algorithm can be performed via OWQC. For simplicity we will demonstrate it for probabilistic quantum computation, post-selecting the cases where no Pauli errors occur. However, we have to bear in mind that, using the feed-forward protocol, we can extend the demonstration for a generic deterministic algorithm. The demonstration goes by showing three properties of OWQC. i) We first show that an arbitrary state of an encoded qubit can be propagated through a wire (i.e. through a linear cluster). While this first property does not have any implication in terms of universality, it allows us to separate the total cluster in different parts, each performing a subroutine of the total algorithm. In fact, this feature shows that the output of a subroutine can be sent as input on another subroutine using a linear cluster, thus simplifying the scheme. We will then proceed demonstrating ii) that any single-qubit operation can be performed on the encoded qubits and iii) that a non-trivial two-qubit gate between the encoded qubits is implementable. Recalling from section 1.6.1 that one-qubit gates and a non-trivial two-qubit operation are the only resources required for a universal computation, properties ii) and iii) will conclude the demonstration.

1. **Information propagation in a wire of qubits.** Let us consider a wire of an *odd* number  $N$  of physical qubits, such that the initial state of the encoded qubit, written in the first physical qubit, is  $|\psi\rangle_{E,in}$ . If for the first  $N - 1$  physical qubits we perform measurements in the same basis  $\mathcal{B}(0)$ , i.e. in the diagonal basis  $\{|+\rangle, |-\rangle\}$ , the encoded qubit will be teleported to the  $N$ -th qubit, and its state will be given by

$$\begin{aligned}
 |\psi\rangle_{E,out} &= \underbrace{HR_z(0)HR_z(0)\dots HR_z(0)HR_z(0)}_{N-1 \text{ times}} |\psi\rangle_{E,in} \\
 &= \underbrace{HTHT\dots HTHT}_{N-1 \text{ times}} |\psi\rangle_{E,in} \\
 &= H^{N-1} |\psi\rangle_{E,in} \\
 &= (H^2)^{(N-1)/2} |\psi\rangle_{E,in} \\
 &= |\psi\rangle_{E,in},
 \end{aligned}$$

where we have used that  $H^2 = \mathcal{I}$  and that, being  $N$  odd,  $N - 1$  is even. Therefore, the state of the encoded qubit is propagated from one end of the wire to the other, remaining unaltered.

2. **An arbitrary single-qubit unitary can be achieved in a wire.** Let us consider a chain of four physical qubits. We want to show that an arbitrary unitary operation  $\bar{U}$  on the encoded qubit can be performed using this four-qubit wire. Measuring the first three qubits in the basis  $\mathcal{B}(\alpha)$ ,  $\mathcal{B}(\beta)$  and  $\mathcal{B}(\gamma)$  we can implement the transformation

$$\begin{aligned}
 T(\alpha, \beta, \gamma) &= HR_z(\gamma)HR_z(\beta)HR_z(\alpha) \\
 &= HR_z(\gamma)R_x(\beta)R_z(\alpha).
 \end{aligned} \tag{4.5}$$

Using the Euler representation [11, 52], an arbitrary unitary  $U$  can be decomposed in rotations as

$$U(\alpha, \beta, \gamma) = R_z(\gamma)R_x(\beta)R_z(\alpha).$$

Substituting in eq.(4.5) we have

$$T(\alpha, \beta, \gamma) = HU(\alpha, \beta, \gamma). \quad (4.6)$$

We can in particular adjust the measurements parameters  $\alpha$ ,  $\beta$  and  $\gamma$  such that  $U(\bar{\alpha}, \bar{\beta}, \bar{\gamma}) = H\bar{U}$ , obtaining

$$\begin{aligned} T(\bar{\alpha}, \bar{\beta}, \bar{\gamma}) &= H^2\bar{U} \\ &= \bar{U}. \end{aligned}$$

A four-qubit chain is then sufficient for implementing any unitary transformation.

3. **A non-trivial two qubit gate is implementable.** We have seen that a link between two rows gives a  $C$ - $Z$  gate between the two associated encoded qubits. Therefore, this property of OWQC is immediately satisfied.

The demonstration of the universal character of OWQC is then completed.

We remark that this universal scheme does not make use of active multi-qubit gates, in contrast to standard quantum computation. Instead, only uses the correlations which are already intrinsically present in the computational substrate formed by the cluster state. This is a powerful aspect of OWQC, and a great advantage with respect to the standard approach. However, one could argue that in generating the cluster state itself we have to use multi-qubit gates, so that the advantage is only illusory. This is not always the case: the process of generating a state is, in general, different from the manipulation. In fact, in the generation of a state we can make use of interactions which might not be employed for the implementation of gates. For example, in Chap. 2 we have argued that a two-qubit photonic gate is not implementable using the non-linearity of a medium. However, in the next section we will report how easy is it to generate a cluster state by starting from an hyperentangled source.

The cluster states and the implementation of OWQC have been introduced in 2001 by Raussendorf and Briegel. The first experimental realization of a four-qubit cluster state, and simple OWQC algorithms, was reported in 2005 by the Zeilinger's group in Vienna [79], soon followed by other groups [96–98]. A six-photon six-qubit cluster realization was reported in 2007 [99], while a two-photon six-qubit cluster state in 2008 [100]. The largest cluster state up to now is a eight-photon eight-qubit cluster, recorded in 2012 [101].

### 4.3 Experimental generation of 4-qubit linear cluster state

In this thesis work we are interested in 4-qubit cluster states that are produced using the hyperentangled source described in Fig. 3.1. As one may expect, the full range of

possible cluster categories becomes too complex to be elencated here, and as such we will discuss in detail the simplest (and yet most useful) one: the 4-qubit linear cluster state. It has been shown that a linear 4-qubit state can be used in order to obtain any unitary and as such it represents the building block for realizing OWQC protocols. First of all, we give the explicit definition of a 4-qubit linear cluster state: following the definition in Eq. 4.1, we obtain:

$$|C_4\rangle_{lin} = \text{C-Phase}_{12} \cdot \text{C-Phase}_{23} \cdot \text{C-Phase}_{34} |+\rangle_1 |+\rangle_2 |+\rangle_3 |+\rangle_4 \quad (4.7)$$

$$= \text{C-Phase}_{12} \cdot \text{C-Phase}_{23} \cdot \text{C-Phase}_{34} (|0\rangle_1 + |1\rangle_1)(|0\rangle_2 + |1\rangle_2)(|0\rangle_3 + |1\rangle_3)(|0\rangle_4 + |1\rangle_4), \quad (4.8)$$

We introduce a notation in which we can represent a cluster state as a  $2^N$  dimensional vector, N being the number of qubits. Each vector element represents the coefficient of the ket of the cluster state corresponding to its binary representation. For example considering the previous 2 qubit example, the normalized vector of state 4.2 is  $1/2(1, 1, 1, -1)$ , which, after the Hadamard operation on qubit 2, becomes the much simpler expression  $\frac{1}{\sqrt{2}}(1, 0, 0, 1)$ . In this notation we have that the four qubit linear cluster state can be written (up to local unitary transformations) as:

$$|C_4\rangle_{lin} = \frac{1}{4}(1, 1, 1, -1, 1, 1, 1, -1, 1, -1, 1, 1, -1, 1, -1, 1) \quad (4.9)$$

which becomes after two Hadamard operations on qubit 2 and 3:

$$|C_4\rangle_{lin} = \frac{1}{2}(1, 0, 0, 1, 0, 0, 0, 0, 0, 0, 0, 0, 1, 0, 0, -1) \quad (4.10)$$

which takes the simple form:

$$|C_4\rangle_{lin} = \frac{1}{2}(|0000\rangle + |0011\rangle + |1100\rangle - |1111\rangle). \quad (4.11)$$

Now we want to show that it is very easy using our HE source to generate state  $|C_4\rangle_{lin}$ . Indeed let's consider HE state, which can be represented graphically as in Fig. 4.2a: if we consider the ordering of the qubits so that polarization of photon A(B) is qubit 1 (2), and the path of photon A(B) is qubit 4 (3), we obtain the following, by expanding the state:

$$|HE\rangle = \frac{1}{2}(|HH\ell r\rangle_{AB} + |HHr\ell\rangle_{AB} + |VV\ell r\rangle_{AB} + |VVr\ell\rangle_{AB}) \quad (4.12)$$

$$= \frac{1}{2}(|0001\rangle_{AB} + |0010\rangle_{AB} + |1101\rangle_{AB} + |1110\rangle_{AB}) \quad (4.13)$$

We note that this state is equivalent to Eq. 4.11 up to a bit-flip operation on qubit 4 and a  $\pi$  phase on the last term which produces a minus sign. In order to change that sign we perform a C-Phase operation between qubit 2 and 3, respectively the polarization and the path of photon B. By putting a simple HWP at 0 degrees over mode r, we actively perform the following operation:  $|\ell H\rangle, |\ell V\rangle, |r H\rangle \rightarrow |\ell H\rangle, |\ell V\rangle, |r H\rangle$  and  $|r V\rangle \rightarrow -|r V\rangle$  which effectively changes the sign of the correct term. So after

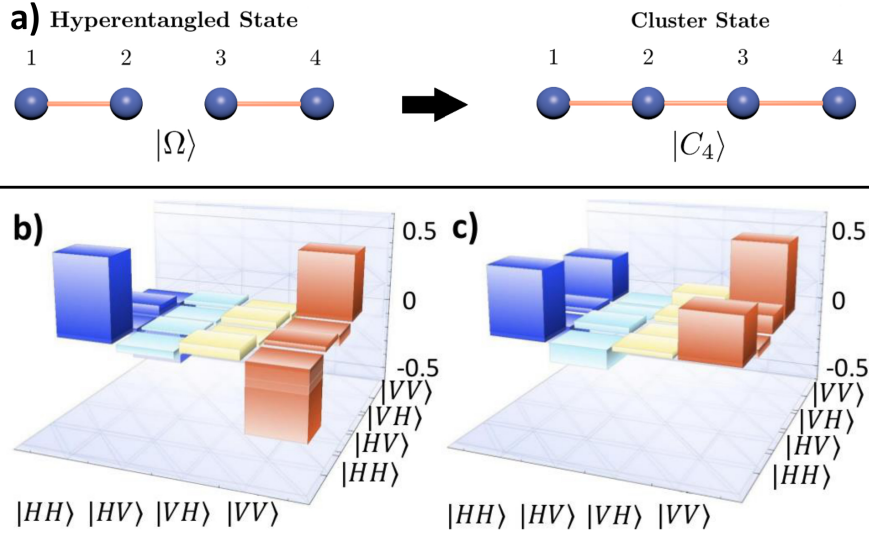


Figure 4.2: **Cluster state.** **a)** Graphical representation of four qubits hyperentangled and cluster states. **b)** Real part of the two qubits polarization tomography of pair  $|\ell_A r_B\rangle$  of the cluster state, which is compensated to be a  $|\Phi^-\rangle$  state. **c)** Real part of the two qubits polarization tomography of pair  $|r_A \ell_B\rangle$  of the cluster state, compensated to be a  $|\Phi^+\rangle$  state. Imaginary parts of the two tomographies are negligible.

the transformation, we are able to transform the HE state to a 4-qubits linear cluster state as shown again in Fig. 4.2a. Now, retrieving the explicit expression of the HE state by reintroducing the phases dependence we obtain:

$$|Cl_4\rangle_{lin} = |\ell r\rangle_{AB} (|HH\rangle_{AB} + e^{i\phi} |VV\rangle_{AB}) + e^{i\theta} |r\ell\rangle_{AB} (|HH\rangle_{AB} - e^{i\phi} |VV\rangle_{AB}) \quad (4.14)$$

$$= |\ell r\rangle_{AB} |\Phi^\pm\rangle \pm |r\ell\rangle_{AB} |\Phi^\mp\rangle_{AB}, \quad (4.15)$$

where in Eq. 4.17 we have considered the special cases for  $\theta, \phi = 0, \pi$ . Thus that a simple way to experimentally evaluate the correct engineering of the linear cluster state in our HE setup is to perform a tomography of respectively modes  $|\ell_A r_B\rangle$  and  $|r_A \ell_B\rangle$ ; in the first case we expect the tomography to obtain a polarization two-qubits state which is similar to a  $|\Phi^\pm\rangle$  and in the second case the same state with opposite phase.

The quantum state tomographies corresponding to the two mode pairs are reported in Fig. 4.2b-c and correspond to the following parameters:

$$\begin{aligned} F_{\Phi^-} &= 0.91 \pm 0.10, & C_{\Phi^-} &= 0.88 \pm 0.08, \\ F_{\Phi^+} &= 0.83 \pm 0.11, & C_{\Phi^+} &= 0.91 \pm 0.08. \end{aligned}$$

Here  $F$  is the fidelity and  $C$  is the concurrence of the experimental state, while errors are calculated from a Monte Carlo analysis of the experimental data. The obtained results are comparable with those of the tomographies of the hyperentanglement source reported in the previous Chapter, thus proving that the cluster state is correctly generated.

The stabilizer formalism, explained in Ref.[102] can be adopted to measure a gen-

$Z_A Z_B$	$+0.940 \pm 0.028$
$X_A X_B z_A$	$-0.860 \pm 0.030$
$X_A X_B z_B$	$+0.860 \pm 0.030$
$z_A z_B$	$-0.990 \pm 0.007$
$Z_A x_A x_B$	$+0.8092 \pm 0.036$
$Z_B x_A x_B$	$+0.8081 \pm 0.035$

Table 4.1: Measured outcomes of the stabilizer used for calculating the genuine multipartite entanglement witness  $\mathcal{W}$ .

uine multipartite entanglement witness:

$$\mathcal{W} = \frac{1}{2}(4\mathbb{I} - Z_A Z_B - Z_A x_A x_B + X_A z_A X_B + z_A z_B - x_A Z_B x_B - X_A X_B z_B), \quad (4.16)$$

where upper case  $X, Z$  define the Pauli operators for the polarization of the state, lower case  $x, z$  define the Pauli operators for the momentum. The state is entangled when  $-1 \leq \mathcal{W} < 0$  and particularly it is purely entangled for  $\mathcal{W} = -1$ . The polarization dependent stabilizers are measured by rotating the analysis waveplates. The two beamsplitters perform the transformation in the path of each photon  $|d\rangle_i = (|\ell\rangle_i + |r\rangle_i)/\sqrt{2} \rightarrow |\ell'\rangle_i$  and  $|a\rangle_i = (|\ell\rangle_i - |r\rangle_i)/\sqrt{2} \rightarrow |r'\rangle_i$ , where  $|d\rangle_i \leftrightarrow |a\rangle_i$  is achieved by changing the phase  $\phi_i$ , i.e. tilting the correspondent glass plate on mode  $r_i$ . This manipulation allows us to measure the momentum-dependent stabilizers involving  $x_i$ . We report in Tab. 4.1 the measured outcomes for the stabilizers. The overall value of  $\mathcal{W} = -0.634 \pm 0.036$  demonstrates that the state presents genuine multipartite entanglement, and we can derive a lower bound following again Ref.[102] for the fidelity of the created cluster state  $F_{|C_4\rangle} \geq \frac{1}{2}(1 - \mathcal{W}) = 0.817 \pm 0.018$ . This result is comparable with that of Ref. [96] which characterized a cluster state generated from the same source, but without exploiting the chip.

## 4.4 Cluster state analysis

Here we characterize the cluster state generated by the setup shown in the previous chapter. Our goal is to understand what is the *strength* of the links between the qubits of our state so that we can check if there is a failure somewhere in the generation process. In order to do this, we present a new scheme based on the verification of especially tailored- multipartite general Bell inequalities which are used to test the presence of four- three and bi-partite non locality inside our cluster state.

We build our strategy on the information about the structure of quantum correlations provided by the assessment of Multipartite Nonlocality Inequalities (MNLI)s. The rationale behind our approach is that, by post-processing the data provided by MNLI, useful information on both two-qubit entangling operations and single-qubit preparation stages can be gathered, even in those cases where an assessment based on the direct quantification of entanglement would be problematic, such as in the presence of multipartite mixed resources.

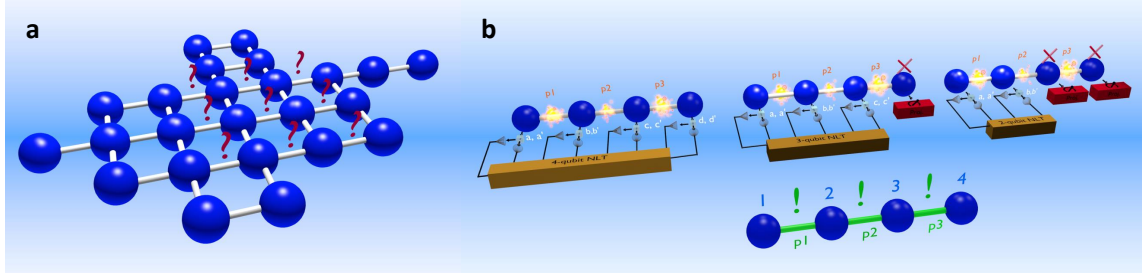


Figure 4.3: Schematic representation of the protocol, in which given a large network of correlated qubits we aim to assess the strength of the correlations of a linear cluster by verifying the violation of custom made multipartite Bell-like inequalities.

In particular, we show that quantitative bounds to the quality of individual nodes and bonds of the assessed network can be established through our method. We demonstrate the effectiveness of the proposed approach by addressing experimentally a two-photon, four-qubit cluster state and using, as a quantitative instrument, the inequality proposed by Werner and Wolf [103] and, independently, Żukowski and Brukner [104], which we dub Werner-Wolf-Zukowski-Brukner (WWZB).

The proposed tool incorporates a sufficient degree of flexibility to be insightful without the complications entailed by a test for genuine multipartite nonlocality. A violation of this inequality quantifies through our simple model the strength of the links between the qubits of an addressed experimental resource. Moreover it enables a more powerful diagnosis than the simple assessment of two-qubit nonlocality tests, as it is able to address *generalized bipartitions*, thus attacking directly the implications of the sharing of quantum correlations above and beyond any study on two-qubit quantum correlations.

We show that our diagnostic tool is informative enough to bound the amount of local noise acting on individual qubits of the network. When combined with pre-available knowledge on the features of a given network to be tested, our tool allows for the localisation of the source of single-qubit noise.

#### 4.4.1 The diagnostic tool

The situation we address is illustrated in Fig. 4.3 **a**. We consider a network of generally interconnected qubits, whose quality we would like to characterise. The connections among the network elements could be embodied by either physical interaction channels or general quantum correlated ones, such as in the situation that is explicitly illustrated here.

While we assume to have full knowledge of the shape of the network (i.e. we assume knowledge of the adjacency matrix of the network), we do not know *how well* the nodes are actually connected. In this sense, the problem of assessing the quality of the state is reduced to that of assigning a quality measure to each link.

##### The WWZB parameter

Consider  $N$  agents, each endowed with the possibility to choose between two dichotomic observables  $\{\hat{A}_j(\mathbf{n}_1), \hat{A}_j(\mathbf{n}_2)\}$  ( $j = 1 \dots N$ ), where  $\mathbf{n}_k$  are local vectors in

the single-qubit Bloch sphere, and which have been rescaled so that they can only take values  $\pm 1$ .

For local realistic theories, the correlation function for the choice of local observables is thus  $E(\{k_j\}) = \langle \otimes_{j=1}^N \hat{A}_j(\mathbf{n}_{k_j}) \rangle$  ( $k_j = 1, 2$ ). By choosing a suitable function  $S(\{s_j\})$  that can take, again, only values  $\pm 1$  and depends on the indices  $s_j \in \{-1, 1\}$ , one can derive the following family of  $4^N$  Bell inequalities [104]

$$\left| \sum_{\{s_j\}=\pm 1} S(\{s_j\}) \sum_{\{k_j\}=1,2} \left( \prod_{j=1}^N s_j^{k_j-1} \right) E(\{k_j\}) \right| \leq 2^N, \quad (4.17)$$

whose right-hand side holds for local realistic theories. Eq. (4.17) contains interesting instances of Bell inequalities for  $N$  particles, being trivially identical to the CHSH version of Bell's inequality for  $N = 2$  [35]. It is possible to show that the fulfilment of Eq. (4.17) implies the possibility to construct local realistic models for the correlation function  $E(\{k_j\})$ , thus establishing such a family of inequalities as necessary and sufficient conditions for the local realistic description of the correlation function of an  $N$ -partite system [104].

In what follows, we make the choice of  $S(\{s_j\}) = \sqrt{2} \cos[\pi/4(\sum_j s_j - N - 1)]$ , which allows us to recover the Mermin-Ardehali-Belinskii-Klyshko (MABK) inequality [105–107]. Eq. (4.17) embodies the main tool for the diagnostic study that is at the core of this work. In order to assess the features of our proposal, we specialise our study to the case of a linear cluster state, as illustrated in Fig. 4.3 **b**. As it will be made evident, such an example is significant and motivated, as it addresses a network of correlated information carriers correlated in a genuinely multipartite fashion.

#### 4.4.2 The experimental study

The experimental demonstration of the effectiveness of our proposal makes use of the resource embodied by a two-photon four-qubit cluster state engineered by means of the hyperentangled platform shown in Fig. 4.4.

A strategy for obtaining an appropriate metric is suggested by the standard procedure for building arbitrary clusters: first each qubit is initialised in the superposition of its logical states  $|+\rangle = (|0\rangle + |1\rangle)/\sqrt{2}$ ; next, a controlled-Phase (C-Phase) gate is applied to each pair of nodes that need being linked.

The quality of the link can then be traced back to the quality of the C-Phase gate that has been used. We have formalised the connection between the results of WWZB nonlocality tests on a cluster and a measurement of the fidelity of the underlying gates. The tests are conducted on the whole cluster, as well as subsections in which qubits are excluded by means of a measurement.

By this connection, we obtain a number assessing the quality of each link from the experimental values of WWZB inequalities. It is important to stress that the diagnostic strategy proposed here addresses the quality of a given resource, not the actual implementation strategy chosen to accomplish this task. Therefore, our methodology can be applied *tout court* to any other resource, regardless of its implementation.

Further, in some architectures, entangling operations are implemented with high fidelity, while the state of the nodes can be corrupted by noise processes, peculiar

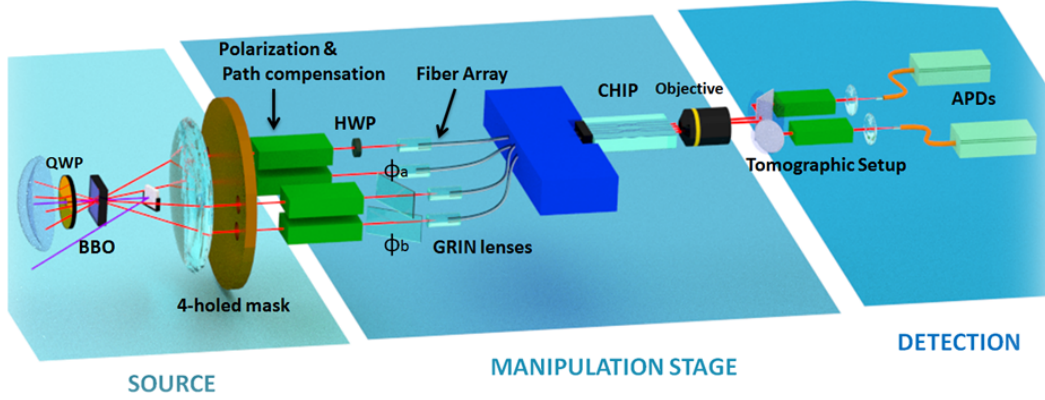


Figure 4.4: The experimental setup consists of the path-polarization hyperentangled source that generates the state  $|\Xi\rangle = \frac{1}{2}(|HH\rangle_{AB} + |VV\rangle_{AB}) \otimes (|lr\rangle_{AB} + |rl\rangle_{AB})$ ; A half waveplate (HWP) is put on the  $l_a$  mode in order to generate a linear cluster state by performing a C-Phase operation between polarisation and path of the same photon. The chip hosts two beam-splitters that are used, in a combination with the phase retarders  $\phi_A$  and  $\phi_B$  to change the basis of the path qubits; polarisation analysis is performed by a standard tomographic setup. Results are obtained by measuring coincidence counts over two of the four output modes using single photon detectors. The typical counting rate through the chip was 50 coincidences/s.

to the physical system. For instance, dissipation mechanisms (including amplitude damping), should be taken into account in atomic or atom-like systems. In photonics, the loss of quantum entanglement can be usually described in terms of pure dephasing. We have investigated the possibility of pursuing our approach in the presence of perfect gates and noisy qubits.

We illustrate our method in a photonic implementation, in which we realise a four-qubit linear cluster states by two-photon hyperentanglement [90, 96], adopting the setup shown in Fig. 4.4. This can produce a linear cluster in the form:

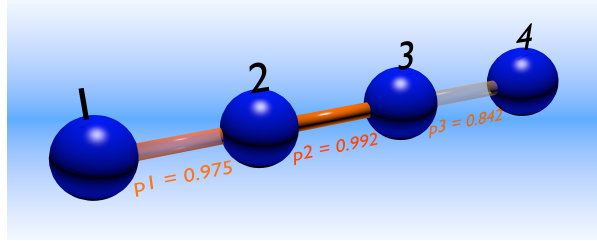
$$|C_4\rangle = \frac{1}{2}(|H_a H_b r_a l_b\rangle + |V_a V_b r_a l_b\rangle + |H_a H_b l_a r_b\rangle - |V_a V_b l_a r_b\rangle), \quad (4.18)$$

where  $H_x$  ( $V_x$ ) denotes the horizontal (vertical) polarisation of the photon  $x = a, b$ , while  $r_x$  ( $l_x$ ) denotes a photon taking the right (left) path. We have performed a measurement of the four-party WWZB correlators: we have observed an experimental value of  $18.53 \pm 0.23$ , which has to be compared with the local realistic limit  $2^4 = 16$ , and with the quantum expectation  $16\sqrt{2} \simeq 22.63$ .

The clear deviation of the actual value from the ideal prediction flags the presence of reduced correlations within the cluster network. For the complete analysis, we have then measured WWZB correlators for different sub-partitions of the cluster, obtained by excluding the unwanted qubits by a suitable measurement; our results are reported in ???. Our task is then to account for the observed violations of all the WWZB inequalities for all the eleven possible four-, three- and two-qubit groupings by comparing the actual results with those of a theoretical specular resource corrupted by noise. The amount of noise that reproduces the values obtained will be a measure of the quality of the cluster realised in the laboratory.

qubit group	$WWZB_{max}$	$WWZB_{exp}$
$1 - 2 - 4 \equiv (\pi_A, \pi_B, k_B)$	11.31	$9.32 \pm 0.19$
$1 - 2 - 3 \equiv (\pi_A, \pi_B, k_A)$	11.31	$9.25 \pm 0.19$
$1 - 3 - 4 \equiv (\pi_A, k_A, k_B)$	13.66	$11.71 \pm 0.17$
$2 - 3 - 4 \equiv (\pi_B, k_A, k_B)$	13.66	$11.08 \pm 0.13$
$1 - 4 \equiv (\pi_A - k_B)$	5.66	$4.55 \pm 0.13$
$1 - 3 \equiv (\pi_A - k_A)$	5.66	$4.62 \pm 0.13$
$2 - 3 \equiv (\pi_B - k_A)$	5.66	$4.33 \pm 0.15$
$2 - 4 \equiv (\pi_B - k_B)$	5.66	$4.69 \pm 0.17$
$1 - 2 \equiv (\pi_A - \pi_B)$	5.66	$4.97 \pm 0.14$
$3 - 4 \equiv (k_A - k_B)$	5.66	$4.50 \pm 0.14$

Table 4.2: Summary of the observed violations of the WWZB inequality for different qubit grouping within the cluster.


 Figure 4.5: Link strength for a 4-qubit linear cluster state, using faulty-gates, each succeeding with probability  $p_i$ . The problem of assessing the quality of the state is reduced to that of assigning a quality measure to each link.  $p_i$  can assume values ranging from 0 to 1:  $p_i = 0$  implies full failure of the C-Phase operation in the building process of the cluster state, while  $p_i = 1$  implies its full success.

### 4.4.3 Noise modelling

Our four-qubit cluster state can be obtained by applying a chain of three C-Phase gates to an initial  $|++++\rangle_{1234}$  state of four separable qubits; we first model the nonideal behaviour of the gates by allowing for a failure probability  $1-p$ ; the operation of the gate will then be described by a Kraus map of the form:

$M(\hat{\rho}) = p(\hat{U}_{cp}\hat{\rho}\hat{U}_{cp}^\dagger) + (1-p)\hat{\rho}$ , where  $\hat{U}$  is the C-Phase operation. We then apply three maps on the initial state, realising the chain:  $\hat{\rho}_{fin}(p_1, p_2, p_3) = M_{34}(M_{23}(M_{12}(\hat{\rho}_{in})))$ . In this way, we can express the linear cluster state as a function of the probabilities that describe the C-Phase entangling gates; in turn, this gives expressions for the eleven WWZB parameters as a function of  $(p_1, p_2, p_3)$ . We can then find the values  $(p_1^*, p_2^*, p_3^*)$  that best describe the actual violations, by minimising the distance of the predictions to the observations:  $(p_1^*, p_2^*, p_3^*) = \text{argmin} \sum_{i=1}^{11} |WWZB_i(p_1, p_2, p_3) - WWZB_i^{exp}|$ , where the summation index runs over the 11 subgroupings.

The analysis gives the results  $p_1^* = 0.975 \pm 0.024$ ,  $p_2^* = 0.992 \pm 0.010$ ,  $p_3^* = 0.842 \pm 0.022$  (see Fig. 4.5). These values give the indication that the weakest link between the qubits is the one connecting the two path qubits, stemming from a reduced quality of the corresponding entangled resource. This observation is supported by direct experimental inspection, and it is likely due to unavoidable spatial phase instabilities present in our experimental scheme.

It could be argued that in quantum photonics systems, failures of real-world gates

are seldom described by our modelling; a commonplace imperfection is rather the loss of coherence, as described by single-qubit dephasing channels in the form  $\varepsilon(\hat{\rho})=p\hat{\rho} + (1-p)\hat{\sigma}_z\hat{\rho}\hat{\sigma}_z$  ( $\hat{\sigma}_z$  is the third Pauli matrix).

We can repeat our analysis by adopting such a different noise model, and consider four dephasing channels acting on the cluster qubits, each with its own probability  $p_1, p_2, p_3$ , and  $p_4$ , along with perfect C-Phase gates. Direct inspection reveals that the predicted WWZB correlators only depend on the products  $p_1p_2$  and  $p_3p_4$ . This is expected since, in this specific case, a dephasing channel on the first qubit can be replaced with an equivalent one acting on the second, obtaining the same theoretical expressions, and likewise for the fourth and third.

The values we obtained are:  $p_1^*p_2^* = 0.913 \pm 0.051$ , and  $p_3^*p_4^* = 0.892 \pm 0.060$ . These can be somehow interpreted as an effective strength of the nodes 2 and 3 - rather than of the links - and these values too support the previous diagnosis that path entanglement is primarily responsible for the imperfections in the whole cluster state.

If  $p_1 = p_2 = p_3 = 1$  they act as ideal entangling gates, generating perfect “strong” links, which means an ideal linear cluster state; if  $p_1 = p_2 = p_3 = 0$  they act as identity operators generating no cluster state. Having now the expression of  $\hat{\rho}_{\Gamma_4}(p_1, p_2, p_3)$ , we can calculate again all the eleven WWZB parameters as a function of  $(p_1, p_2, p_3)$ . In this way we can obtain a sistem of eleven equations. Now we can find the values of  $p_1, p_2, p_3$  that reproduce the WWZBs obtained. The strategy is to find  $(p_1^*, p_2^*, p_3^*)$  that minimize the sum of the absolute difference between each of the WWZBs expressed above and the corresponding WWZB experimentally obtained:

having imposed as constraints that each of the WWZB parameters is Gaussian distributed assuming its error as standard deviation. These results show that the links building the cluster are strong, as expected from the violation of all the inequalities above. In particular it must be highlighted that the strongest link is the 2-3 one, whose  $p_2$  is the closest to 1. It can be easily explained by the fact that this entangling gate is created by the action of a simple HWP at zero degrees, that can scarcely fail as a c-phase, while the third link is much more fragile as it could be affected by phase instabilities of the mirror inside the Hyperentangled state source.

In order to be confident about the minimization process above, we can carry out a simple test: we generate an arbitrarily damaged resource by fixing  $p_1, p_2, p_3$ ; then we calculate the WWZB parameters and repeat the procedure of minimization as to find  $(p_1^*, p_2^*, p_3^*)$ . If this process gives back the same  $p_1, p_2, p_3$  established initially, then the former is reliable. This rapid test works for the kind of expressions derived in case of noisy gate.

#### 4.4.4 Dephasing channel

An analogous method of evaluating the quality of the cluster resource is comparing it with a resource damaged by a dephasing channel acting on each component of the system. This is an alternative perspective that focalizes on the resource from the point of view of the single qubits quality rather than the quality of a two qubit link.

In our case the overall Kraus map, acting on each of the components of cluster state, is the Kronecker product of four dephasing channels:

$$\varepsilon_{tot}(\hat{\rho}_{cluster}) = \varepsilon_1(p_1) \otimes \varepsilon_2(p_2) \otimes \varepsilon_3(p_3) \otimes \varepsilon_4(p_4),$$

where  $\varepsilon_i(p_i)$  represents the  $i^{th}$  dephasing channel acting on the  $i^{th}$  qubit. Proceeding in an analogous way as in the case of noisy gate, we can determine the degree of dephasing characterizing our resource.  $p_1 = p_2 = p_3 = p_4 = 1$  implies that the cluster state is solid against any loss of correlations due to dephasing channels. Again we can calculate all the eleven WWZB parameters, now functions of  $(p_1, p_2, p_3, p_4)$ , using exactly the same procedure described in the previous section.

Now we can find the values of  $p_1, p_2, p_3, p_4$  that reproduce the WWZBs obtained. The strategy is exactly the same as in the previous case: finding  $(p_1^*, p_2^*, p_3^*, p_4^*)$  that minimize the sum of the absolute difference between each of the WWZBs expressed above and the corresponding WWZB experimentally obtained:

By doing this we find:

$$p_1^* = 0.954 \pm 0.038 \quad p_2^* = 0.957 \pm 0.038 \quad p_3^* = 0.949 \pm 0.045 \quad p_4^* = 0.940 \pm 0.045.$$

having imposed as constraints that each of the WWZB parameters is Gaussian distributed assuming its error as standard deviation.

In order to be confident about the minimization process mentioned above we develop do the same test as in the case of noisy gate: we generate an arbitrarily damaged resource by fixing  $p_1, p_2, p_3, p_4$ ; then we calculate the WWZB parameters and repeat the procedure of minimization as to find  $(p_1^*, p_2^*, p_3^*, p_4^*)$ . If this process gives back the same  $p_1, p_2, p_3, p_4$  established initially, then the method is reliable. This rapid check does not work in case of dephasing channel. This is due to the kind of analytic expressions derived, which are affected by the symmetries of the channel combined with the ones of the state.

As this problem is due to symmetries, we unbalance the initial state, keeping the topology of the specific linear cluster, and recalculate the WWZBs to see whether we can find expressions where the parameters occur singularly. It is possible to demonstrate that this unbalance has no effects on the unseparability of the couples  $p_1, p_2$  and  $p_3, p_4$ , but only on the factors that multiply them. We can deduce that it can be a problem due to the simultaneous symmetries of the specific linear state and the channel considered.

Furthermore with minimal inspection of the physics governing the generation of our cluster, we can obtain a more refined model. As a first example, we can observe that, while the initial polarisation and path entangled states are directly produced by our source, the final cluster is obtained by implementing a C-Phase gate between polarisation and path degrees of freedom of the same photon.

As seen in Fig. 4.4 the cluster state  $|C_4\rangle$  is experimentally engineered by introducing a half-waveplate at zero degrees over mode  $\ell_A$ . This represents a C-Phase operation between the target polarization qubit and the control path qubit of photon A.

We can use the depolarisation to describe the corruption of the gate between qubits 1-2 ( $p_1$ ) and 3-4 ( $p_3$ ), and use the probabilistic model  $M(\hat{\rho})$  ( $p_2$ ) in order to describe the gate between qubits 2-3. This analysis gives the values  $p_1^* = 0.909 \pm 0.019$ , and

$p_3^* = 0.901 \pm 0.017$  for the action of the dephasing, and  $p_2^* = 0.980 \pm 0.012$ , once again in qualitative agreement with simpler models. This approach can be extended by including further depolarisation (captured by a probability  $p_g$ ) acting identically on every qubit as a result of traversing the chip; in this case we get:  $p_1^* = 0.986 \pm 0.025$ ,  $p_2^* = 0.996 \pm 0.007$ ,  $p_3^* = 0.967 \pm 0.043$ , and  $p_g^* = 0.866 \pm 0.056$ .

The aforementioned results show that we have experimentally assessed a diagnostic method able to probe the quality of bonds and links in a complex network of correlated particles. The methodology that we propose, makes no assumptions on the form of the noise affecting the connection of the cluster state and it is generalizable to larger networks. In particular we obtained experimental proof of the good quality of our cluster state, in the sense that it is linked by strong correlations. The last step in our analysis of correlations in cluster states is performing a quantum algorithm with it.

## 4.5 Grover's algorithm

Last thing we need to prove is that our cluster state, generated by our HE source and partially manipulated inside an integrated device can be used for actual quantum information protocols. We chose to perform the Grover's search algorithm [5] which in its 4-qubits variant consists in using two qubits to select what item to tag in a database of four, consisting of the last two qubits.

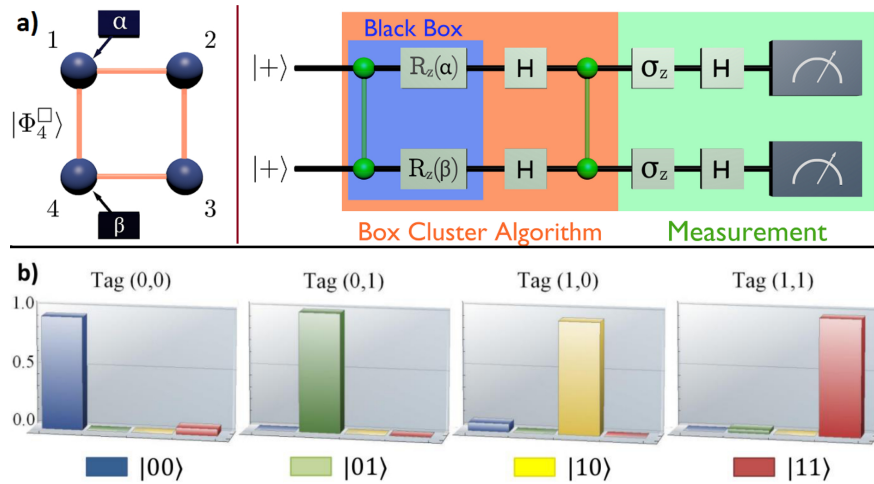


Figure 4.6: **Grover's algorithm scheme.** **a)** Quantum circuit for Grover's algorithm. The black box tags the item through the measurements of qubits 1 and 4. The information is then encoded and processed in qubits 2 and 3 of the cluster state  $|\Phi_4^{\square}\rangle$ . The single qubit operations are implemented by the choice of the measurement basis. **b)** Outcome probability for different tagged items for the probabilistic Grover's algorithm. The average success rate of the algorithm is  $s = 0.960 \pm 0.007$ .

This is, to the best of our knowledge, the first achievement of a one-way quantum computation basic operation based on multiple DOFs through integrated photonics. The quantum circuit is represented in Fig. 4.6a. It consists of two qubits initially prepared in the state  $|+\rangle_1|+\rangle_2$ , a black box tagging one item of the database and an operation which allows us to identify the tagged item in the readout. The algorithm can be implemented [52, 108] using the four qubit box cluster state  $|\Phi_4^{\square}\rangle$  defined in Refs. [79, 98]. An approach based on a linear optic implementation of the Grover's algorithm

using multiple DOFs was originally proposed by Kwiat et al.[109]. Following Fig. 4.6a, the black box tags the item by choosing the bases  $\alpha$  and  $\beta$  for the measurements on qubits 1 and 4. The information is processed and read on qubits 2 and 3. Labelling the physical qubits in the order  $(1, 2, 3, 4) = (k_B, \pi_A, k_A, \pi_B)$ , with  $k(\pi)$  standing for the path (polarization) qubits, the cluster state  $|C_4\rangle$  is equivalent to  $|\Phi_4^\square\rangle$  up to the single qubit unitaries

$$\mathcal{U} = \sigma_x H \otimes H \otimes \sigma_z H \otimes H. \quad (4.19)$$

$\mathcal{U}$  can be implemented by simply rotating the measurement basis, as  $\mathcal{U}$  is a single qubit transformation. First, we performed a probabilistic computation where we post-selected the cases with no errors occurring in the one-way computation model[97, 98]. The results are reported in Fig. 4.6b in which we show that the average success rate in identifying the correct item in the database is  $s = 0.960 \pm 0.007$  at an average protocol rate of 17 Hz. This result is probabilistic and depends on the postselection of the measurement outcomes. We may then apply a feed-forward protocol in which the outcomes are relabelled depending on the results of the measurements performed by the black box [79, 98]. In this case the computation is deterministic with a success rate of  $s = 0.964 \pm 0.003$  and protocol rate of 68 Hz. This procedure of passive feed-forward corresponds to corrections made in the post-selection process by relabelling the outputs.

## 4.6 Discussion and perspectives

In this Chapter we have discussed generation, manipulation, analysis and use of cluster state for quantum computation. We presented a novel method to assess the strength of their internal correlation which is completely general and scalable: in a future perspective it can be used in larger networks of entangled qubits in order to identify weak links due to the presence of noise or to a generation problem.

The author contributed to this work by designing the experiment starting from the setup described in Chap. 3. He was also the main conductor of the experiment itself. He contributed to the analysis of the data.

In addition, the One-Way Quantum Computation (OWQC) approach, which has been discussed in this Chapter gives an interesting insight on the nature of quantum correlations: indeed it represent a change of point of view in the normal quantum computation process; while the universal quantum computation scheme comprises of gates generating entanglement between qubits and then smartly uses them to achieve the correct calculation, in the OWQC approach the correlations are present in the state *before* the beginning of the algorithm and only single qubit gates and local measurements are used in order to perform the calculations.

What is important here is that what *drives* the quantum advantage which is given by Quantum Computing is the *presence* of quantum correlations - such as entanglement, either *before* or *during* the protocol. Our analysis scheme shows that *the more* this state is correlated (in our case that means in the sense of non-locality), *the more* it is suitable to perform quantum tasks.

One direction from here can be to find a protocol that doesn't depend on the geometry of the cluster state itself, such as a black-box system which takes any cluster

of a certain dimension, and reconstruct its graph state by giving a strength value for each link.

# Chapter 5

## Effect of noise on quantum correlations

In the previous chapters we discussed the importance of correlations in a quantum state and how they can be exploited to perform quantum computation algorithm. In this chapter we present a surprising experiment which gives a different insight on the nature of classical and quantum correlations.

This experiment consists in a scheme in which local noise is used to activate entanglement which was not present in the state beforehand and it shows how the real meaning of non-locality has its heart in the properties of non unital operation. We will present this scheme as a game in which a player can use only limited resource to create entanglement in a quantum system, while the other player tries to perform operations that would destroy the generated entanglement. We will use this game to analyze the ‘robustness’ of quantum correlations under local measurements. This chapter follows Ref. [110].

As it should be clear at this point entanglement is a precious resource of the quantum world, yet it is very much fragile. One of the most powerful adversary of entanglement is the presence of noise, in the form of decoherence or dissipation. In this chapter we introduce a surprising scenario where, given an input state and a fixed number of gates, no entanglement can be produced unless one switches on a local non-unital noise source (such as dissipation).

Entanglement is zero without noise, and it grows concordingly to the amount of noise. In addition we will show that as long as the dimension of the Hilbert space is two, an adversary can always manage to prevent the production of entanglement by applying a suitable local rotation. Increasing the dimension of the system, i.e. to four qubits the creation of entanglement can be made robust against any possible unitary action of the adversary.

This experiment highlights the counterintuitive connections between quantum correlations and environment, and gives a perspective on the fact that the interpretation of entanglement is far from being definite or completely understood. In this sense the intuition of entanglement given in this chapter is different from that of being the fundamental resource in the creation of cluster states and will be also different in the

next chapter when we will introduce extractable work. What these notions of entanglement have in common is that they can be used as resources for quantum protocols outperforming classical ones.

Generation of quantum correlations by local noise was theoretically investigated in [111–113], and experimentally demonstrated with trapped ions [114], while entanglement activation from quantum correlations was theoretically proposed in [115], and experimentally demonstrated in [116]. In the scheme that we propose here these two effects are combined, and as a quite surprising result we are able to generate entanglement in a robust way, starting from classically correlated states and switching on just a local noisy device.

## 5.1 Two-qubit game - Activating Entanglement

Here we define the entanglement generation scheme as a game (see Fig. 5.1a): suppose we are given two qubits in a product state, where a qubit is in the maximally mixed state  $\rho_A = \frac{\mathbb{I}}{2}$  and an ancilla is in the state  $\rho_C = |0\rangle\langle 0|$ . We are also given a CNOT gate with  $A$  ( $C$ ) the control (target) qubit and we are allowed to perform any possible local unitary operation on  $A$  and  $C$ . The goal of the game is to create entanglement in the total state  $\rho_{out}$  of qubits  $A$  and  $C$ . Is this achievable by using only these resources? It turns out that, with only these resources at disposal, there is no way to create entanglement in the bipartite system considered here.

We will now change slightly the rules of the game and consider in addition a local noisy device, as reported in Fig. 5.1a. The noisy device acts only on qubit  $A$  and can be switched on linearly at will. While we would not expect any creation of entanglement by this operation, which is local and noisy, counterintuitively, it turns out that if this extra resource is non-unital (i.e. if it does not preserve the identity) it allows to produce an entangled output state  $\rho_{out}$ .

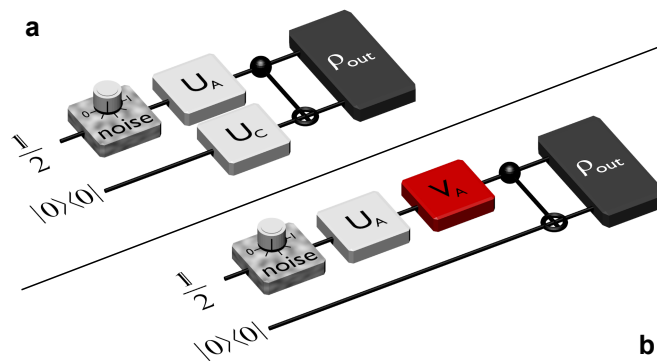


Figure 5.1: **The game.** **a)** Two-qubit scheme aimed at generating entanglement in the output state by starting from the initial state  $\frac{\mathbb{I}}{2} \otimes |0\rangle\langle 0|$ , and using local unitaries  $U_A$  and  $U_C$  and a CNOT gate. The additional device represents a local noisy element that can be switched on by turning the knob. **b)** The same game in presence of an adversary player using a local unitary  $V_A$  to try and prevent the generation of entanglement.

Let us consider the simplified scenario where we have qubit  $A$  in a generic input state  $\rho$  (instead of  $\frac{\mathbb{I}}{2}$ ) and qubit  $C$  in state  $|0\rangle$ , and we act on them with a CNOT gate in the computational basis. This situation is described in Fig. 5.1a, where  $\rho$  is

the resulting state of qubit  $A$  after the application of the noisy device and the unitary  $U_A$ , while  $U_C = \mathbb{I}$ . Within this framework,  $\rho_{out}$  is entangled if and only if the input state  $\rho$  has non-vanishing off-diagonal terms, i.e.  $\rho_{01} \neq 0$ . This follows from using the entanglement measure “negativity”  $N$  [24], defined as

$$N(\rho_{AC}) = \sum_i |\lambda_i^-|, \quad (5.1)$$

where  $\lambda_i^-$  are the negative eigenvalues of the matrix resulting from the partial transposition of  $\rho_{AC}$ . It is straightforward to show that the negativity of  $\rho_{out}$  is connected to the off-diagonal terms of  $\rho$  via the formula

$$N(\rho_{out}) = |\rho_{01}|. \quad (5.2)$$

Hence, the higher the off-diagonal terms of the input state  $\rho$ , the more entangled is the bipartite output state  $\rho_{out}$ . On the other hand, if  $\rho$  is diagonal in the computation basis, that is  $\rho = p|0\rangle\langle 0| + (1-p)|1\rangle\langle 1|$ , the output state turns out to be at most classically correlated, i.e.  $\rho_{out} = p|00\rangle\langle 00| + (1-p)|11\rangle\langle 11|$ .

The above analysis shows why, within the scheme of Fig. 5.1a, we are able to create entanglement by using a non-unital channel while we cannot otherwise: since the state  $\frac{\mathbb{I}}{2}$  is invariant under any unitary transformation  $U_A$ , it is not possible to produce nonvanishing off-diagonal terms in  $\rho_A$  by unitary operations. If, however, a non-unital channel  $\Lambda$  is present, it transforms by definition the identity to a different state, i.e.  $\Lambda[\frac{\mathbb{I}}{2}] = \sigma$ , where  $\sigma \neq \frac{\mathbb{I}}{2}$ . Therefore, by applying a suitable local unitary  $U_A$  on  $\sigma$  it is possible to generate nonvanishing off-diagonal terms.

This intuition is no more than trivial but gives a good perspective in the role of correlations: in a sense noise is detrimental to the state when it acts on the diagonal terms of the density matrix, however if the state is rotated through a unitary operation, we can manage the noise to act to non-diagonal terms of it, thus creating quantum correlations.

Let us now introduce in the game an adversary player (Eve) whose aim is to prevent the generation of entanglement in  $\rho_{out}$  by performing a unitary operation on qubit  $A$  after the state preparation and before the action of the CNOT gate. This adversary can be interested in such achievement as we have seen that entangled is useful for a variety of tasks, such as quantum computation. Eve, as a malevolent party, could want to block the formation of a particular link in a cluster state so that a OWQC protocol would fail - in other terms it is *interesting* to show the robustness of the entanglement creation scheme.

We can thus imagine that a unitary  $V_A$  is in Eve’s hands, as depicted in Fig. 5.1b. In this configuration, Eve can always win, provided that she knows the quantum state after the action of  $U_A$ .

In fact, any single-qubit state can be made diagonal in the computational basis by applying a suitable rotation.

The two-qubit protocol considered here is therefore not *robust* against local rotations: the generation of entanglement at the end can always be prevented by a suitable local rotation performed by an adversary before the action of the CNOT gate.

The two-qubit game was implemented by the circuitual scheme depicted in Fig. 5.2a using a photonic implementation. Here the input state  $\rho^d = p|0\rangle\langle 0| + (1-p)|1\rangle\langle 1|$  is

diagonal in the computational basis,  $H$  is the Hadamard gate, and  $\Lambda_\eta$  is the amplitude damping channel defined by its action  $\Lambda_\eta(\rho) = \sum_{i=1}^2 A_i^\dagger \rho A_i$ , with the Kraus operators  $A_1 = |0\rangle\langle 0| + \sqrt{1-\eta}|1\rangle\langle 1|$ ,  $A_2 = \sqrt{\eta}|0\rangle\langle 1|$  with  $\eta \in [0, 1]$ . Here  $\eta$  represents the noise parameter,  $\eta = 0$  ( $\eta = 1$ ) corresponding to the no-noise (maximum noise) case.

Starting from a diagonal state  $\rho^d$ , the block of gates  $H\Lambda_\eta H$  always produces off-diagonal terms whenever  $0 < \eta \leq 1$ . Therefore, according to Eq. (5.2), the output state  $\rho_{out}$  will be entangled for these values of  $\eta$ . Furthermore the negativity of  $\rho_{out}$  is given by

$$N(\rho_{out}) = \frac{\eta}{2}, \quad (5.3)$$

Thus, in the configuration of Fig. 5.2a, the final entanglement depends only on the damping parameter  $\eta$  and not on the parameter  $p$  which appears in  $\rho^d$ . Notice from Eq. (5.3) that, counterintuitively, the amount of entanglement grows with the amount of noise.

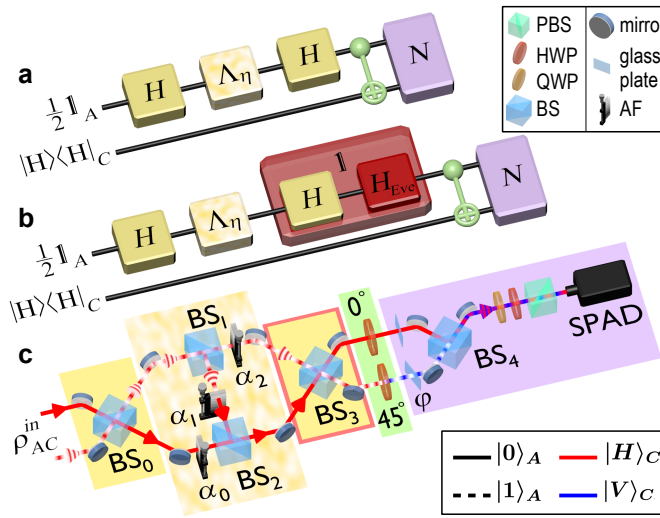


Figure 5.2: **The two-qubit game: experimental set-up.** a) Quantum circuit of the experimental set-up.  $N$  corresponds to the measurement of the negativity in the final state. Qubits  $A$  and  $C$  are respectively encoded in the path and polarization degrees of freedom of a single photon. b) Quantum circuit of the experimental set-up, when Eve attacks with the Hadamard gate  $H$  (see main text). c) Optical implementation of the set-up. BS: balanced beam-splitter, AF: tunable attenuation filter with transmission  $\alpha$ ,  $\varphi$ : phase adjusted by a thin glass plate, H(Q)WP: half-(quarter-)wave plate, PBS: polarizing beam-splitter, SPAD: single photon avalanche photodiode. Photon counting measurements are performed in coincidence with a trigger photon (not shown in the figure). BS<sub>3</sub> is removed from the set-up when we simulate Eve's attack.

We experimentally implemented this game with the optical set-up shown in Fig. 5.2c. Qubits  $A$  and  $C$  were encoded respectively in the path and in the polarization degrees of freedom (DOFs) of a single photon generated by the non-linear source of photon pairs described in the previous chapters. The input state was prepared with the path qubit in the state  $\rho_A^d = \frac{1}{2}|0\rangle\langle 0| + \frac{1}{2}|1\rangle\langle 1|$ , and the polarization qubit was in the state  $|H\rangle\langle H|_C$ ,  $H$  ( $V$ ) designating the horizontal (vertical) polarization, corresponding to the state 0 (1) of the computational basis. Both Hadamard gates  $H$  were realized with balanced beam-splitters (BSs). The amplitude damping channel  $\Lambda_\eta$  was achieved by a combination of two balanced BSs and three attenuation filters whose transmission coefficients could be adjusted separately to obtain any value of  $\eta \in [0, 1]$

The CNOT gate, controlled by the path qubit with the polarization qubit as target, was implemented by inserting a half-wave plate (HWP) at  $45^\circ$  in the path mode corresponding to  $|1\rangle_A$ . Note that a HWP at  $0^\circ$  was also inserted in the other path mode so as to maintain the same optical length for both modes. The entanglement in the final state of  $AC$  was estimated by a standard tomographic reconstruction measurement of the two-qubit state (see Sec. 2.6.2) from which we recovered the negativity  $N$ .

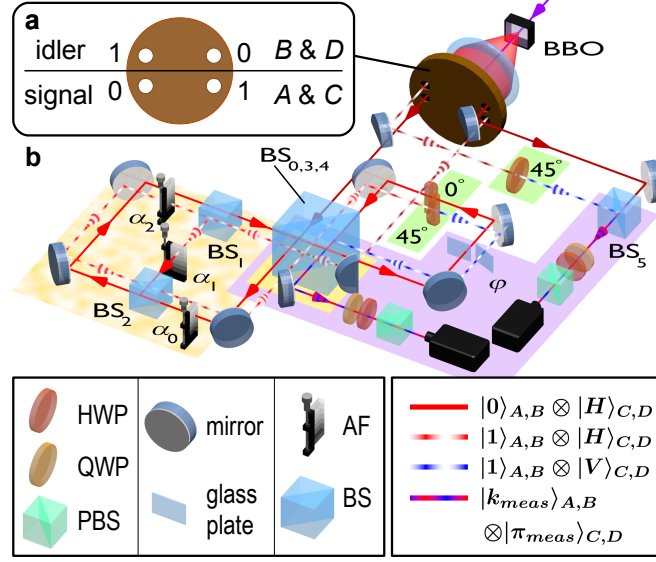


Figure 5.3: **Actual experimental set-up.** **a)** Emission modes of the SPDC source. Qubit  $A$  ( $B$ ) is encoded in the polarization of the signal (idler) photon, Qubit  $C$  ( $D$ ) is encoded in the path of the signal (idler) photon. **b)** Actual experimental set-up for the four-qubit protocol (for the two-qubit experiment, the same apparatus is used but the CNOT on the idler photon is removed so that this photon serves only as trigger).  $|k_{meas}\rangle \otimes |\pi_{meas}\rangle$ : path-polarization state of the photon selected by the projective measurement set-up (see magenta box in Fig. 5.3c and 5.6). The central beam-splitter is used three times and plays successively the role of  $BS_0$ ,  $BS_3$  and  $BS_4$  (see Fig. 3c and 5b of the main text).

The experimental implementation of the amplitude-damping channel consists of a combination of two beam-splitters ( $BS_1$  and  $BS_2$ ) and three attenuation filters (see the blurred yellow gate in the figures) allowing to transfer, in a tunable way, a portion of mode  $|1\rangle$  onto mode  $|0\rangle$  of the path qubit  $A$ , encoded in the signal photon. Here we explain the relationship between the noise parameter  $\eta$  and the intensity transmission coefficients  $\alpha_0$ ,  $\alpha_1$  and  $\alpha_2$  of the attenuation filters.

Let us consider a generic input state (with  $\beta, |\gamma| \in [0, 1]$ )

$$\rho = (1 - \beta) |0\rangle \langle 0| + \beta |1\rangle \langle 1| + \gamma |0\rangle \langle 1| + \gamma^* |1\rangle \langle 0|.$$

The channel  $\Lambda_\eta$  (defined by the Kraus operators  $\{|0\rangle \langle 0| + \sqrt{1 - \eta} |1\rangle \langle 1|, \sqrt{\eta} |0\rangle \langle 1|\}$ ) transforms it into the state

$$\begin{aligned} \rho' = & (1 - (1 - \eta)\beta) |0\rangle \langle 0| + (1 - \eta)\beta |1\rangle \langle 1| \\ & + \sqrt{1 - \eta}\gamma |0\rangle \langle 1| + \sqrt{1 - \eta}\gamma^* |1\rangle \langle 0|. \end{aligned}$$

If we input the same state  $\rho$  in the set-up of the blurred yellow gate in Fig. 3c or 5b

of the main text, we obtain the final state

$$\rho'' = \xi[(1 - \beta)T\alpha_0 + \beta R^2\alpha_1] |0\rangle \langle 0| + \xi\beta T\alpha_2 |1\rangle \langle 1| \\ + \xi\gamma T\sqrt{\alpha_0\alpha_2} |0\rangle \langle 1| + \xi\gamma^* T\sqrt{\alpha_0\alpha_2} |1\rangle \langle 0|,$$

where  $T = 57.5\%$  ( $R = 42.5\%$ ) is the measured intensity transmission (reflection) coefficient of the beam-splitters and  $\xi = ((1 - \beta)T\alpha_0 + \beta R^2\alpha_1 + \beta T\alpha_2)^{-1}$  is a normalization factor. Term by term identification between  $\rho'$  and  $\rho''$  gives:

$$1 - (1 - \eta)\beta = \xi((1 - \beta)T\alpha_0 + \beta R^2\alpha_1), \\ (1 - \eta)\beta = \xi\beta T\alpha_2, \\ \sqrt{1 - \eta}\gamma = \xi\gamma T\sqrt{\alpha_0\alpha_2}.$$

From these equations, by choosing  $\alpha_0 = \frac{R^2}{T} = 31\%$ , we obtain  $\alpha_1 = \eta$  and  $\alpha_2 = \alpha_0(1 - \eta) = \frac{R^2}{T}(1 - \eta)$ . For each setting of  $\eta$ , the attenuators transmission coefficients are tuned to these values by adjusting their vertical position with respect to the beam (see Fig. 5.3 b).

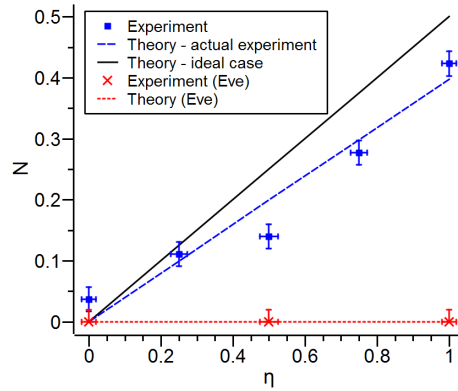


Figure 5.4: **The two-qubit game: experimental results.** Negativity  $N(\rho_{out})$  as a function of the noise parameter  $\eta$  for the two-qubit set-up. The dotted lines correspond to theoretical calculations taking into account the actual experimental apparatus. Error bars are calculated from photon counting statistics.

In Fig. 5.4 we report the measured negativity  $N$  of the final 2-qubit state obtained for different values of  $\eta$  (blue squares), together with its theoretical value given by Eq. (5.3) (dark line). The dashed blue line corresponds to the expected theoretical value when we take into account the experimental imperfections of our set-up. The good agreement between the measured and theoretical behaviors demonstrate the soundness of this protocol.

We also checked experimentally that Eve is able to prevent the creation of entanglement in the final 2-qubit state for any amount of noise. Her best strategy is to perform another Hadamard gate ( $V_A = H_{Eve}$ ) to cancel the action of the second Hadamard within the block  $H\Lambda_\eta H$  (see Fig. 5.2b). Indeed, in this way, even though the noise is non-unital, the density matrix of qubit  $A$  remains diagonal (in the computational basis) and no entanglement is then generated. To simulate Eve's attack experimentally we removed the beam-splitter  $BS_3$  from our set-up (see Fig. 5.2c). As expected, the negativity measured in this case is always vanishing, as can be seen in Fig. 5.4 (red crosses).

## 5.2 Four-qubit game

Let us now generalize the game to the case of four qubits. We start with a two-qubit state  $\rho_{AB}$ , which exhibits at most classical correlations in the computational basis, and two ancilla qubits  $C$  and  $D$ , both initialized in the state  $|0\rangle\langle 0|$ . We are then allowed to apply two CNOT gates that operate on qubits  $AC$  and  $BD$  (this situation corresponds to the scheme shown in Fig. 5.5 when the noisy device is switched off).

We again introduce on qubit  $A$  a local noisy channel given by the same block of gates  $H\Lambda_\eta H$  as previously, shown in Fig. 5.5 where the knob tunes the value of the noise parameter  $\eta$ . We can show that by adding only this extra resource, which is noisy and local, entanglement is switched on at the output of the circuit in the bipartition  $AB|CD$  starting from states which are at most classically correlated. Similarly to the two-qubit case, the scheme of Fig. 5.5 generates only separable states as long as the noisy device is switched off, while entanglement is generated for any nonvanishing value of  $\eta$  as soon as the knob is turned on, and it increases with  $\eta$ . Here and in the following, when we say that  $\rho_{out}$  is entangled we will always refer to the splitting  $AB|CD$ .

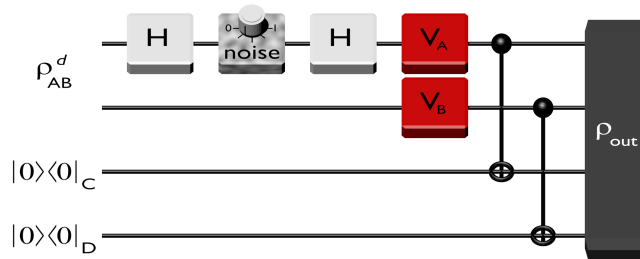


Figure 5.5: **The game with four qubits.** Here  $\rho_{AB}^d$  represents a bipartite state diagonal in the computational basis, while  $H\Lambda_\eta H$  is the same block of gates defined in the two-qubit scenario, the local noise element here being the amplitude-damping channel  $\Lambda_\eta$ . We are interested in switching on entanglement of  $\rho_{out}$  with respect to the cut  $AB|CD$  by just exploiting local noise.

To underline the differences between the two- and four-qubit schemes and in particular to show the robustness of the latter, we refer to a more general scenario where we have a generic input state  $\rho_{AB}$  for the first two qubits (thus, not necessarily diagonal in the computational basis) and we analyze the properties of the input state that guarantee entanglement at the output state  $\rho_{out}$  in the splitting  $AB|CD$ . Following the set-up in Fig. 5.5 with a general two-qubit input state  $\rho_{AB}$  and no noise (i.e.  $\eta = 0$ ), we have that  $\rho_{out}$  is entangled iff the input state  $\rho_{AB}$  has nonvanishing off-diagonal terms. This result can be proven by noticing that the negativity of  $\rho_{out}$  is connected to the off-diagonal terms of  $\rho_{AB}$  via the formula [117]

$$N(\rho_{out}) = \sum_{i < j} |\rho_{ij}|. \quad (5.4)$$

Moreover,  $\rho_{out}$  is separable whenever  $\rho_{AB}$  is diagonal in the computational product basis. Hence, within this set-up, the negativity can be regarded as a faithful entanglement measure. This result explains the role that local noise plays here: it introduces off-diagonal elements in the input state, making the final state  $\rho_{out}$  entangled.

As before, we introduce an adversary (Eve) whose goal is to prevent the realization of an entangled output state. In this 4-qubit scheme, we still suppose that she can use only two local unitaries  $V_A$  and  $V_B$  just before the CNOT gates. As shown in Ref. [115], Eve's action is always successful if and only if  $\rho_{AB}$  is at most classically correlated. Thus, if we want to create an entangled output state  $\rho_{out}$  with certainty in the presence of an adversary a successful strategy is to prepare an input state  $\rho_{AB}$  which has quantum correlations, i.e. correlations that are not strictly classical.

Contrary to the simplified two-qubit protocol, the four-qubit protocol turns out to be robust against local unitaries performed by an adversary. This can be proven in the following way:

### 5.2.1 Robustness of the 4-qubit scheme

Let us denote the state after the action of the block  $H\Lambda_\eta H$  on  $A$  by  $\rho'_{AB}$ , i.e.  $\rho'_{AB} = (H\Lambda_\eta H)_A[\rho_{AB}^D]$ . We want first to prove that, whenever the input state  $\rho_{AB}^d$  is not factorised (namely when  $p \neq 0, 1$  and  $r \neq q$  in Eq. (5.7)), the state  $\rho'_{AB}$  is a quantum correlated state, namely its eigenvectors do not provide a factorised bi-orthogonal basis. By writing the input state  $\rho_{AB}^d$  as in Eq. (5.7), we can rewrite  $\rho'_{AB}$  as

$$\rho'_{AB} = p\rho'_A(q) \otimes |0\rangle\langle 0| + (1-p)\rho'_A(r) \otimes |1\rangle\langle 1|, \quad (5.5)$$

where  $\rho'_A(x) = \frac{1}{2}(\mathbb{I} + \eta\sigma_x + (2x-1)\sqrt{1-\eta}\sigma_z)$ . After excluding the trivial cases of  $p = 0, 1$ , the state (5.5) is diagonalised in a factorised bi-orthogonal basis iff  $\rho'_A(q)$  and  $\rho'_A(r)$  can be simultaneously diagonalized. This happens iff they commute, that is iff  $[\rho'_A(q), \rho'_A(r)] = 0$ . By inserting the general form of  $\rho'_A(x)$ , we can easily see that the commutativity relation above reduces to

$$2i\eta\sqrt{1-\eta}(q-r)\sigma_y = 0, \quad (5.6)$$

which holds only when either  $q = r$  or  $\eta = 0, 1$ . By neglecting the noiseless case with  $\eta = 0$ , where  $\rho'_{AB}$  is the classically correlated state (5.7), and the case with  $\eta = 1$ , which gives  $\rho'_{AB} = |0\rangle\langle 0| \otimes [p|0\rangle\langle 0| + (1-p)|1\rangle\langle 1|]$ , we can see that for initial states  $\rho_{AB}$  that are classically correlated ( $q \neq r$ ) the state  $\rho'_{AB}$  is always quantum correlated. According to Ref. [117], the presence of quantum correlations in  $\rho'_{AB}$  guarantees that if the state  $\rho'_{AB}$  is the input to the sequence of CNOT gates, then the entanglement production is robust against local unitaries on  $A$  and  $B$ .

Therefore, we can conclude that whenever the input state  $\rho_{AB}$  is at least classically correlated the entanglement generation process is guaranteed to be robust.

### 5.2.2 4 qubit game experimental implementation

We implemented experimentally the four-qubit scheme shown in Fig. 5.6a. There, by  $\rho_{AB}^d$  we denote an input state diagonal in the computational basis of the 2 qubits. Such a state can be generally written as

$$\rho_{AB}^d = p\sigma_A^d \otimes |0\rangle\langle 0| + (1-p)\tau_A^d \otimes |1\rangle\langle 1|, \quad (5.7)$$

with  $\sigma_A^d = q|0\rangle\langle 0| + (1 - q)|1\rangle\langle 1|$  and  $\tau_A^d = r|0\rangle\langle 0| + (1 - r)|1\rangle\langle 1|$ . Notice that the above state is at most classically correlated (since it is diagonal in a factorized basis) and it is factorized (thus it does not contain even classical correlations) if and only if either  $p = 0, 1$  or  $q = r$ .

It can be easily checked by direct calculation that the output state  $\rho_{out}$  is entangled in the splitting  $AB|CD$  whenever  $0 < \eta \leq 1$ .

The following cases can happen in the concerned scenario: in the absence of noise, namely for  $\eta = 0$ , there is no entanglement at the output of the protocol. For  $\eta > 0$  entanglement can always be generated at the output and the negativity of entanglement of  $\rho_{out}$  is always

$$N(\rho_{out}) = \frac{\eta}{2}, \quad (5.8)$$

independently of the values of  $p, q, r$  in  $\rho_{AB}^d$ . If the input state  $\rho_{AB}^d$  is factorized, i.e. it does not contain any type of correlations, or  $\eta = 1$ , the protocol is not robust against local unitaries performed by Eve. If  $\rho_{AB}^d$  is not factorized (i.e. it contains classical correlations) and  $0 < \eta < 1$  the entanglement production provided by the protocol is robust against local unitaries on  $A$  and  $B$ . It is thus worth stressing that the presence of initial classical correlations guarantees the robustness of the protocol against local unitaries.

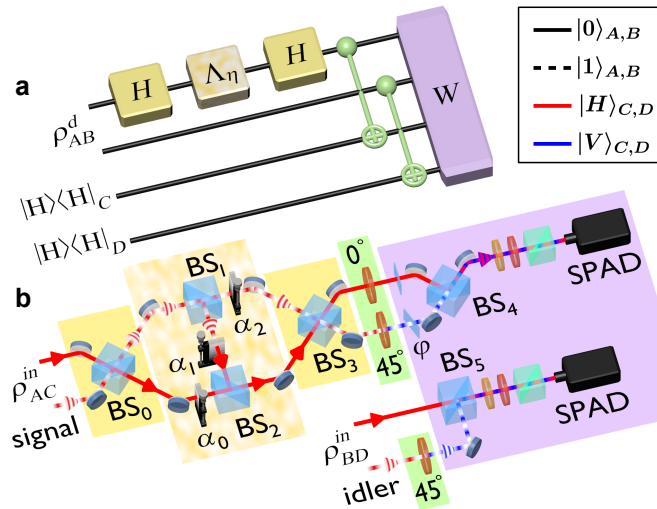


Figure 5.6: **The four-qubit game: experimental set-up.** a) Quantum circuit of the experimental set-up.  $W$  corresponds to the measure of the witness  $W$  in the final state. A non-linear source generates a pair of photons that we call the signal and idler photons. Qubits  $A$  ( $B$ ) and  $C$  ( $D$ ) are respectively encoded in the path and polarization degrees of freedom of a the signal (idler) photon. b) Optical implementation of the set-up.

Experimentally, we implemented the optical set-up shown in Fig. 5.6b. It is based on the previous two-qubit set-up, where we add two extra qubits  $B$  and  $D$ . Qubit  $A$  ( $B$ ) is encoded in the path DOF of the signal (idler) photon, while qubit  $C$  and  $D$  is encoded in the polarization DOF of the signal (idler) photon. The path qubits are prepared in the state  $\rho_{AB}^d = p|00\rangle\langle 00| + (1 - p)|11\rangle\langle 11|$ , with  $p \simeq 0.5$ , and the polarization qubits are both in the state  $|H\rangle\langle H|_{C,D}$ . All the gates were implemented as in the previous two-qubit set-up. The additional CNOT gate between qubits  $B$  and  $D$  is implemented by inserting a half-wave plate (HWP) at  $45^\circ$  in the path mode corresponding to  $|1\rangle_B$ .

The actual experimental implementation of the four qubit setup is shown in Fig. 5.3 b. It consists in a folded version of the set-up, built on two combined Sagnac interferometers, which both guarantees an intrinsic phase stability for the path qubits and requires less optical elements.

For the signal photon, the central beam-splitter plays successively the role of both Hadamard gates ( $BS_0$  and  $BS_3$  in Fig. 3c and 5b of the main text) and of the path qubit measurement beam-splitter  $BS_4$ . Between the Hadamard gates, the photon passes through a first Sagnac loop interferometer, in which the amplitude-damping channel is implemented. Then the CNOT gate between qubits  $A$  and  $C$  is realized by a half-wave plate at  $45^\circ$  on mode  $|1\rangle_A$  and a half-wave plate at  $0^\circ$  on mode  $|0\rangle_A$ . The path qubit is then projected onto the measured state  $|k_{meas}\rangle_A$  by the phase plate  $\varphi$  and the third passage through the central beam-splitter. Finally, after this second Sagnac loop, the polarization qubit is projected on the measured state  $|\pi_{meas}\rangle_C$  by a quarter- and a half-wave plate and a polarizing beam-splitter. The photon is finally detected on a single-photon avalanche photodiode (SPAD) after spatial filtering with a pinhole and spectral filtering with an interference filter (710 nm central wavelength and 10 nm bandwidth).

On the idler photon, we implement the CNOT gate between qubits  $B$  and  $D$  with a half-wave plate at  $45^\circ$ . Both qubits are then projectively measured with the same type of measurement apparatus used for the signal photon. The same set-up is used for the two-qubit protocol, however in that case the gate  $\text{CNOT}_{BD}$  is removed and the idler photon plays only the role of a trigger photon.

We checked for entanglement in the splitting  $AB|CD$  by using an entanglement witness.

By following the scheme depicted in Fig. 5.6 a, if we choose as input the state

$$\rho_{in} = [p|00\rangle\langle 00| + (1-p)|11\rangle\langle 11|]_{AB} \otimes |00\rangle\langle 00|_{CD}, \quad (5.9)$$

the output state turns out to be block-diagonal and explicitly given by

$$\rho_{out} = p\rho_{AC}^+ \otimes |00\rangle\langle 00|_{BD} + (1-p)\rho_{AC}^- \otimes |11\rangle\langle 11|_{BD}. \quad (5.10)$$

Here we have defined

$$\rho^\pm = \frac{1}{2} \begin{pmatrix} 1 \pm \sqrt{\bar{\eta}} & 0 & 0 & \eta \\ 0 & 0 & 0 & 0 \\ 0 & 0 & 0 & 0 \\ \eta & 0 & 0 & 1 \mp \sqrt{\bar{\eta}} \end{pmatrix}, \quad (5.11)$$

and  $\bar{\eta} = 1 - \eta$  for convenience. In order to construct a witness operator that detects the entanglement of  $\rho_{out}$  with respect to the splitting  $AB|CD$ , we apply the partial transposition  $T_{AB}$  with respect to  $AB$ , and study the negative eigenvalues of  $\rho_{out}^{T_{AB}}$ . From simple algebra it turns out that, whenever  $\eta \neq 0$ , the only two negative eigenvalues are  $\lambda_1^- = -p\frac{\eta}{2}$  and  $\lambda_2^- = -(1-p)\frac{\eta}{2}$ . This proves that  $N(\rho_{out}) = \frac{\eta}{2}$ , independently of  $p$ . Furthermore, the corresponding eigenvectors are given by

$$\begin{aligned} |\lambda_1^-\rangle &= |\Psi^-\rangle_{AC} \otimes |00\rangle_{BD}, \\ |\lambda_2^-\rangle &= |\Psi^-\rangle_{AC} \otimes |11\rangle_{BD}, \end{aligned}$$

with  $|\Psi^-\rangle = \frac{1}{\sqrt{2}}(|01\rangle - |10\rangle)$ . Therefore, an entanglement witness operator can be defined as

$$W = (|\lambda_1^-\rangle\langle\lambda_1^-| + |\lambda_2^-\rangle\langle\lambda_2^-|)^{TAB}, \quad (5.12)$$

which, if decomposed in terms of local operators, reads

$$W = \frac{1}{8} (\mathbb{I} \otimes \mathbb{I} - \sigma_x \otimes \sigma_x + \sigma_y \otimes \sigma_y - \sigma_z \otimes \sigma_z)_{AC} \otimes (\mathbb{I} \otimes \mathbb{I} + \sigma_z \otimes \sigma_z)_{BD}, \quad (5.13)$$

Notice that the experimental detection of  $W$  requires only the three measurement settings  $\{\sigma_z\sigma_x\sigma_z\sigma_x, \sigma_z\sigma_y\sigma_z\sigma_y, \sigma_z\sigma_z\sigma_z\sigma_z\}$  (in lexicographic order  $ABCD$ ).

This witness certifies the presence of bipartite entanglement in the final state of  $ABCD$  whenever  $\langle W \rangle < 0$ .

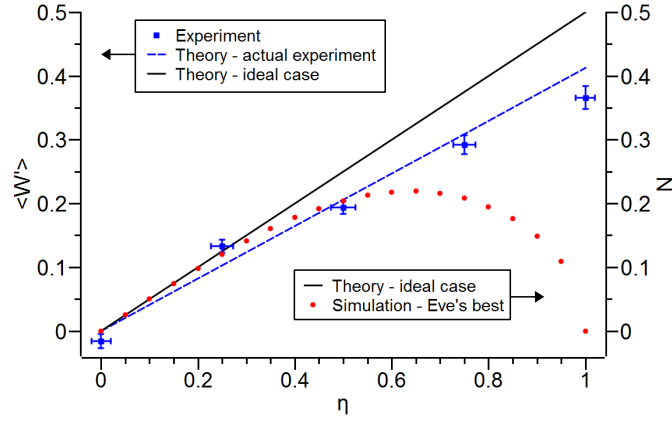


Figure 5.7: **The four-qubit game: experimental results.** Expectation value  $\langle W' \rangle = -\langle W \rangle$  of the entanglement witness applied to  $\rho_{out}$  as a function of the noise parameter  $\eta$  for the four-qubit set-up. The dashed line corresponds to a theoretical calculation that takes into account the actual experimental apparatus. The red dots instead represent Eve's best strategy and report a numerical optimization of the minimal amount of entanglement (quantified by the negativity) that can be generated after the application of local rotations on qubits  $A$  and  $B$  by Eve.

In Fig. 5.7 we show the measured expectation value  $\langle W' \rangle = -\langle W \rangle$  of the witness as a function of the noise parameter  $\eta$  (blue squares). This quantity provides a lower bound for the negativity of  $\rho_{out}$ , namely  $N(\rho_{out}) \geq \langle W' \rangle$ . The blue dashed line corresponds to the theoretical evolution computed by taking into account the experimental imperfections and the actual measured value of  $p$  in the input state.

To fairly compare our measurement results with the theory, we have to take into account some imperfections of the experimental apparatus.

The main point we have to consider is the finite interference visibility  $V_i$ , ( $i = 1, 2$ ) achieved in both Sagnac loops, due to an imperfect spatial and temporal coherence of modes  $|0\rangle$  and  $|1\rangle$  of the path qubit encoded in the signal photon. We modelled this effect by two dephasing channels acting respectively between the amplitude-damping channel and the second Hadamard gate ( $D_1$ ), and between the CNOT gate and the measurement ( $D_2$ ):

$$D_i[\rho] = \frac{1 + V_i}{2} \rho + \frac{1 - V_i}{2} \sigma_z \rho \sigma_z, \quad (i = 1, 2).$$

The measured values that were used to compute the dashed line in the plots are respectively  $V_2 = 80\%$  for Fig. 3 of the main text (blue dashed line),  $V_1 = 75\%$  and  $V_2 = 83\%$  for Fig. 6 of the main text (blue dashed line). Note that for the two-qubit scheme the entanglement generated is independent of the interference visibility in the first Sagnac loop.

We have also taken into account two other experimental parameters that have an influence on the amount of entanglement generated, although to a smaller extent than for the mentioned dephasing processes. The first one is relevant only for the four-qubit scheme and is given by the measured value of  $p$  in the input state (see Eq. 5 of the main text). We used the measured values  $p = 0.515$  for Fig. 6 of the main text (blue dashed line). The second parameter is the deviation of the beam-splitter from the ideal Hadamard operation. Indeed, for the "balanced" beam-splitter in our set-up we measured an intensity transmission coefficient  $T_H = 55.8\%$  ( $T_V = 40.7\%$ ) and reflection coefficient  $R_H = 44.2\%$  ( $R_V = 59.3\%$ ) for the horizontal (vertical) polarization. For the calculation of the dashed lines in both plots (Fig. 3 and 6 of the main text), we thus replaced the Hadamard operator  $H = \frac{1}{\sqrt{2}}(\sigma_x + \sigma_z)$  by the experimental beam-splitter operator

$$H_{exp} = \begin{pmatrix} \sqrt{T_H} & \sqrt{R_H} \\ \sqrt{R_H} & -\sqrt{T_H} \end{pmatrix}.$$

Our results are in agreement with Eq. (5.8): while there is no entanglement when local noise is absent ( $\eta = 0$ ), it is generated as the noise increases.

The experimental demonstration of the robustness of the protocol would require the actual measurement of a non-vanishing entanglement measure for every possible unitary operations that Eve can apply on qubits  $A$  and  $B$ . As this is not practically feasible in our set-up, instead we numerically computed the minimal amount of entanglement that is generated by the protocol when Eve adopts the local rotations on qubits  $A$  and  $B$  that best reduce this entanglement. This result (see red dot in Fig. 5.7) is obtained, for each value of  $\eta$ , by a numerical minimisation of the negativity over all possible unitaries  $V_A$  and  $V_B$ . Notice that when the noise level is low, i.e.  $\eta$  is close to zero, Eve's best attack cannot reduce much the amount of entanglement we can switch on. Only in the extreme cases  $\eta = 0, 1$  she can totally prevent the creation of an entangled output state.

### 5.3 Discussion and perspectives

The work illustrated in this Chapter proves experimentally that quantum entanglement can be counterintuitively switched on by the help of a local noisy device. The amount of entanglement is also shown to grow by increasing the amount of noise introduced on purpose in the set-up. In this work, the author contributed by performing the experiment and analysing the data.

Our experiments have implemented some subtle features of the quantum world: while, obviously, no local action can produce correlations, a local quantum channel can turn classical correlations into quantum correlations. We have realised a local

amplitude damping channel that performs this task, while preserving separability of the state.

In a second step, the quantum correlations were then activated into entanglement [117], by using non-local gates. We emphasize that without the noisy channel no entanglement could have been produced. The underlying dimension of the Hilbert space played a crucial role in terms of robustness of the protocol.

Furthermore it proves an important point: quantum correlations arise and are destroyed in very surprising manners. In this case what allowed the state to become *useful* in a quantum sense was the introduction of a non unitary operation which converted classical into quantum correlations. These results can be used as benchmark for increasing the efficiency of noisy quantum channels. Given that noise, or external malevolent manipulation of the resources are inherently present in any real implementation of quantum communication protocols, our work shows that proper transformations on the channel can help minimize this interference by transforming it into useful entanglement.

Another interesting perspective from here would be asking: *what is the cost of the non unitary operation?*

We know that unitary LOCC operations on a quantum state doesn't change its entanglement. However here we demonstrated that a non unitary operation (such as noise) does. But a correlated state can be exploited in order to perform tasks more efficiently than classical states so that means that noise *added* something to the state. Can we express the difference between the two states in terms of *work*?

In the following chapter we will try to do as such.

# Chapter 6

## Quantum thermodynamics

In the previous chapters we discussed the properties of cluster state, assessing their internal correlations and using them as resources for quantum information protocols. Then we demonstrated via an interesting experiment that quantum correlations are in fact more elusive than what previously thought, as even noise, in particular conditions can generate entanglement. In this chapter we will make a step forward by interpreting the internal correlations of cluster state using a thermodynamic point of view. We will present a criteria based on informational work and we will use it to assess which kind of correlation is present into a three qubit cluster state.

### 6.1 Classical Information Thermodynamics

Thermodynamics is a fundamental theory that is frequently said to be the only *classic* theory to have escaped from the onslaught of quantum mechanics. Both classical electrodynamics and classical Newtonian physics have been modified to accommodate the principles of quantum physics while *it seems* that thermodynamics remained completely unchanged. Nevertheless the robustness of thermodynamics is an *half-truth*. From a first point of view it is true that the classical formulation of thermodynamics allowed to derive the black body formula from which quantum physics developed; on the other hand, it is not true that thermodynamics remained unchanged: the thermodynamical notions of entropy, heat, work and energy have been mapped in a new quantum language. *Landauer's erasure principle* showed that an intrinsic relation between thermodynamics and information theory exists. In this context, for example, the notion of entropy has been completely transformed because in the case of a setting in which the information held by an observer can be *quantum-mechanical* it is possible to show that the conditional entropy can become negative [118]: this is a very paradoxical result. Anyway while it has been possible to realize a mapping between the energy of a system and the Hamiltonian of the same system, *work* does not seem to allow an operator description when translated in quantum physics. These array of problems contribute to explain why there exist many approaches to quantum thermodynamics [119]. The realization of a connection between quantum thermodynamics and quantum information theory has a very important value for two principle reasons: i) thermodynamics needs to be utilized in the nanoscopic world where the laws

of classical physics cannot be used; ii) thermodynamics appears intuitive and natural while quantum mechanics does not; showing that all those quantum quirks like the superposition principle, non-locality and entanglement could be encapsulated in the thermodynamical context might help to understand, accept and maybe demystify quantum physics.

Here we show the connection between thermodynamics and entanglement by presenting the thermodynamical detection of bipartite and tripartite entanglement by Maxwell's Demon. This leads to presenting an experiment of a work extraction scheme which allows the detection of quantum correlations in a tripartite quantum state.

### 6.1.1 Maxwell's Demon

Maxwell's Daemon paradox was introduced in 1871 to discuss the 'limits of the second law of thermodynamics'. Maxwell proposed a *gedankenexperiment* in which the second law of thermodynamics was seemingly violated. For reference, the Second Law states:

*It is impossible to devise an engine which, working in a thermodynamical cycle, shall produce no effect other than the extraction of heat from a reservoir and the performance of an equal amount of mechanical work.*

Another formulation of the second law of thermodynamics could be given in terms of entropy: *in any cyclic process the total entropy of the physical systems involved in the process will either increase or remain the same.*

The starting point of the paradox [120] is having a box in which a great number of particles are in thermodynamical equilibrium at temperature  $T$ . In the middle of the box there is a barrier which separates the left and right part. If we close the barrier at any moment, the two parts of the box will have the same temperature  $T$ , as in any moment the *mean* velocities of the particles in the left or right side is identical.

Now we suppose to have a Daemon, a tiny, powerful entity which can open or close very rapidly the barrier in the middle and can in some way measure the velocity of the single particles. This Daemon will operate the barrier so that it will let pass all the particles faster than a given velocity on the left side of the box, while maintaining all the others in the right part of the box. After the procedure, it is clear to see that we will have a different temperature for the two parts of the box. We can define entropy as

$$S = k_B \ln(\Omega) \quad (6.1)$$

where  $k_B$  is the Boltzmann constant, and  $\Omega$  is the number of different possible states of the microscopic system. After the Daemon operation the particles are more *ordered* (the faster particles on the left, the slower on the right). This means that  $\Omega$  decreased and so the Daemon reduced the entropy of the system. We can also assume that if the Daemon continues this process dividing again the box in smaller parts, he can, repeating the process, decrease arbitrarily the entropy of the system.

The very interesting problem here is that, speaking in thermodynamical terms, the Daemon *isn't* performing any work in the system, he is just opening and closing very

rapidly a barrier. Indeed the Daemon is just using its knowledge on the system to change its state. This is in apparent open contrast with the Second thermodynamic Principle, as our knowledge of the system becomes higher and higher at no apparent work expense.

For many years the debate was ‘where is the trick?’ or in other terms, who or what is performing the work on the system that is necessary to compensate for the loss of entropy in the system and thus validate the Second Principle again? At first it was widely believed that the solution of the paradox lied on the energy cost that the Daemon had to spend to perform measurements on the velocity of the particles, but Landauer and Bennet managed to prove that it was possible to obtain that information at no energy cost. The answer to the paradox was found by Landauer in 1961 [121]:

**Theorem 1** *Each time a single bit of information is erased the amount of energy dissipated into the environment is at least  $k_B T \ln 2$ , where  $k_B$  is the Boltzmann constant and  $T$  the temperature of the surrounding environment. Equivalently, we may say that the entropy of the environment increases by at least  $k_B \ln 2$ .*

The revolution here is stating that the energy cost is associated to the *erasure* of a bit from the memory of the Daemon which is then dissipated into the environment. That means that we are linking a pure thermodynamic quantity which is work, to information or our knowledge of a system. This led Landauer to formulate the formula *information is physical*, which, in the opinion of the author of this thesis, is the most profound and fascinating discovery of the last century.

There is a convenient example to understand Landauer’s principle and it has been formulated by Szilard in 1929 [122].

### 6.1.2 Szilard’s engine

A classical (non-quantum) analysis of Maxwell’s Demon was presented by Leo Szilard formulating an idealized heat engine with one-molecule gas [122]. The final result of Szilard’s work was epoch making considering that it realized the deep connection between information and physics [121, 123]. The process employed by Szilard’s engine is schematically depicted in Fig.6.1:

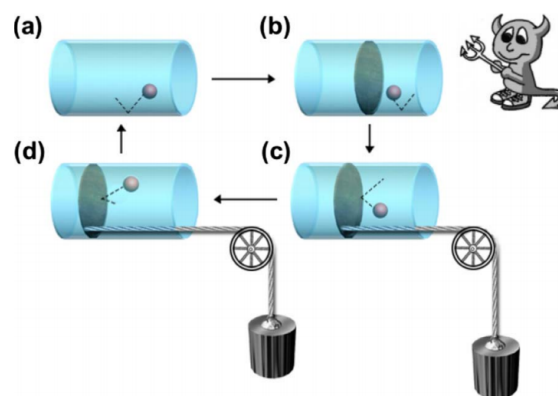


Figure 6.1: Schematic diagram of Szilard’s heat engine

In Fig.6.1, we see a representation of Szilard engine: a single molecule is placed in a box, of volume  $V$  (see a). In (b) a Daemon inserts a partition in the middle of the box in order to determine if the particle is in the left or in the right side of the box. He encodes this information by identifying the particle position with a bit: 0 if the particole is in the left, 1 if it is in the right. The Daemon records this information *in his memory*. In step (c) the Daemon uses the information obtained to replace the partition with a piston and couples it to a load. In the last step (d) the one-molecule gas is put in contact with the reservoir and does work to lift the load. Note that after the transformation, the particle positon has returned to its original state (that means that the daemon doesn't know anymore if in a given time the particle is in 0 or in 1). However, the information about the previous particle position is still stored in the Daemon's memory, so we still cannot consider this process to be completely cyclic (and thus in contrast with the Second Principle) at this point.

As the gas is expanded isothermically, the amount of extracted work could be easily calculated; considering that the displacement of the piston is  $dx$ , the extracted amount of extracted work is given by:

$$\delta L = F dx = p A dx = p dV \quad (6.2)$$

Since the gas contained in the Szilard's engine is made of a single molecule, concepts such as pressure and force must be understood in a time-averaged sense. Using the equation of state for ideal gases,

$$pV = Nk_B T \quad (6.3)$$

with  $N=1$ , it is possible to compute the amount of extracted work as follows:

$$W = \int_{\frac{V}{2}}^V p dV' = \int_{\frac{V}{2}}^V \frac{k_B T}{V'} dV' = k_B T \ln 2 \quad (6.4)$$

This  $k_B T \ln 2$  factor that appears in the theory of the Szilard's engine is conventionally called *1 bit* and represents the amount of energy which is still stored inside the Daemon's mind. Consequently, in order to complete the cycle this bit of information needs to be erased to return the Demon's mind to its initial state. This principle is called *Landauer's erasure principle* [121]. By using the previous calculation, this erasure has an energy cost:

$$W_{erasure} = -k_B T \ln 2 \quad (6.5)$$

## 6.2 Quantum Information Thermodynamics

After a brief overview about the link between thermodynamics and information theory, we want to extend the previous concepts to the quantum world. We aim to link quantum information, and its counterintuitive phenomena to its thermodynamic counterpart.

### 6.2.1 Quantum Thermodynamics: The Principles

It is possible to define a quantum system  $\rho$  evolving through an Hamiltonian  $H(t)$  its average internal energy with the expectation value  $\text{Tr}[\rho^{(t)}H^{(t)}]$  [124], with  $t \in [0, \tau]$ . The variation of internal energy after a transformation from time 0 to time  $t$  can be defined as:

$$\Delta U = \text{Tr}[\rho^{(\tau)}H^{(\tau)}] - \text{Tr}[\rho^{(0)}H^{(0)}] \quad (6.6)$$

We can describe the previous expression by identifying the equivalent quantities of *work* and *heat*, where we intend work as a somewhat ‘controllable’ energy which can be used in a thermodynamic process, while we intend heat as wasteful energy. Since the time-variation of  $H$  is controllable, as usually the evolution process is something we can decide, its energy change could be identified as work while the contribution due to the reconfiguration of the system state caused by Hamiltonian change could be identified with heat. For these reasons we define:

$$\langle Q \rangle = \int_0^\tau \text{Tr}[\dot{\rho}^{(t)}H^{(t)}]dt \quad \langle W \rangle = \int_0^\tau \text{Tr}[\rho^{(t)}\dot{H}^{(t)}]dt \quad (6.7)$$

The formulation of the *First Law of Thermodynamics* can be rewritten using this quantities: *the sum of average heat and work done on the system is equal to its internal average energy change*

$$\langle Q \rangle + \langle W \rangle = \int_0^\tau \frac{d}{dt} \text{Tr}[\rho^{(t)}H^{(t)}] = \text{Tr}[\rho^{(\tau)}H^{(\tau)}] - \text{Tr}[\rho^{(0)}H^{(0)}] = \Delta U \quad (6.8)$$

While the internal energy is a state function in thermodynamics, in the previous expressions work and heat are dependent processes that describe how the system evolves in time from the initial to the final states: the last two physical quantities infinitesimal changes, described by  $\delta$  indicate that heat and work are in general *not* total differentials and do not correspond to observables in direct contrast with the differential quantity  $dU$ . By using  $\langle \delta Q \rangle$ , it is possible to define another state function called *thermodynamic entropy*  $S_{th}$  that is very helpful to define *reversibility* and *irreversibility* in quantum thermodynamic process:

$$\Delta S_{th} = \int_{rev} \frac{\langle \delta Q \rangle}{T} \quad (6.9)$$

where  $\langle \delta Q \rangle$  is the heat absorbed by the system along the process and  $T$  is the temperature at which the heat is being exchanged between the system and the bath. The Clausius thermodynamical inequality states that:

$$\oint \frac{\langle \delta Q \rangle}{T} = \int_A^B \frac{\langle \delta Q \rangle}{T} + \int_B^A \frac{\langle \delta Q \rangle}{T} \leq 0 \quad (6.10)$$

In the case of a reversible transformation between B and A and a generical transformation between A and B, the following holds:

$$S(B) - S(A) \geq \int_A^B \frac{\langle \delta Q \rangle}{T} \quad (6.11)$$

This result could be interpreted as another formulation of the Second Law of Thermodynamics: *in a generical transformation, the entropy sum of a closed system and its components cannot decrease.*

The definition of the ensemble entropy for a system being in a microstate  $i$ , energy  $E_i$  and with a given probability of being in that microstate  $p_i = \frac{e^{-\beta E_i}}{Z}$  is [125]:

$$S = -k_B \sum_i p_i \ln p_i \quad (6.12)$$

The (6.12) formula, with the mathematical rearrangement  $\kappa = \frac{k_b}{\log_2 e} = 9.57 \times 10^{-24} J/K^{-1} \text{bit}^{-1}$ , is called the *Shannon entropy*. Now recall that we already defined the Shannon entropy in a very different context, in Sec. 1.1.1, when we introduced that quantity from the classical information theory point of view. Here we found, following a thermodynamic reasoning the same expression which now constitutes a generalization of classical thermodynamic entropy. The equivalence between the two formulations of the Shannon entropies, in the context of a 2d Hilbert space (the qubit) will be explicated in the following sections.

## 6.2.2 von Neumann Entropy

The Shannon entropy measures the amount of uncertainty about  $X$  before the same value is known via a classical probability distribution. Quantum states, however, are described with density operators replacing probability distributions. The generalization of Shannon entropy to quantum states is called *von Neumann entropy* and it is defined as [3]:

$$S(\rho) = -\text{Tr}[\rho \log_2 \rho] \quad (6.13)$$

Knowing  $\text{Eigen}(\rho) = \{\lambda_1, \dots, \lambda_n\}$  for a density operator  $\rho$  in an  $n$ -dimensional Hilbert space, (6.13) can be re-expressed in this form:

$$S(\rho) = -\sum_{i=1}^n \lambda_i \log_2 \lambda_i \quad (6.14)$$

Von Neumann entropy is non-negative and can be zero only if  $\rho$  state is pure.

## 6.3 Using Daemons to assess quantumness

Separability criteria, as we have seen several times up to this point, are in general expressed in terms of an operator or a function such as in the case of entanglement witnesses or the correlation function in Bell's inequality. Despite the simplicity of defining the problem of finding if a state is separable or entangled, it is very hard to construct and to find an efficient separability criterion that discriminates entangled

states. The hardness of the problem is related to the convexity of the separable subspace formed by all the separable states: this makes impossible for any operator or function to be linear with respect to the matrix elements of a density operator. In other words, if we want to assess with certainty if a state is entangled, we in general need to reconstruct its density matrix, which, as we have seen in Sec. 2.6.2, is an experimentally hard task [126]. As entanglement can be regarded as a valuable resource in quantum information processing and computation, its quantification becomes a problem of great interest and importance.

In this section we will introduce the Work Deficit. The final goal is to achieve a thermodynamical separability criterion: Vedral's inequalities for bipartite and tripartite entangled systems will be presented as a new thermodynamical witness criteria.

### 6.3.1 Work Deficit

Landauer principle confirms the equality between information and work: to demonstrate the equality, with no loss of generality, it has been used the Szilard's engine showing that it is a general information-storage apparatus. It is possible to determine how much work can be extracted from a single heat bath if the information is distributed between two different and separate parties, Alice and Bob. Their engines will be certainly more efficient when information is localized and the connection between the efficiency of their engines and the localization of information could shed light to the connection between quantum nonlocality and thermodynamics.

We introduce here the *work deficit*  $\Delta$  [127]. Let's consider two parties, Albus and Bellatrix which share a bipartite quantum state. They interact with the state by performing local operations and classical communication (LOCC) and can communicate using a classical channel with each other. The amount of potential work that *cannot* be extracted by two separated parties is defined by  $\Delta$ :

**Definition 5 (Work Deficit  $\Delta$ )** *Work deficit  $\Delta$  is the difference between the amount of work that can be extracted from a state under LOCC versus the amount that can be extracted by a party who holds the entire state.*

For pure states,  $\Delta$  is equal to the amount of distillable entanglement  $E_D$  of a given state. It can be used to quantify the quantum correlations in a state jointly held by two parties. It is possible to show another interesting deep connection between information and thermodynamical work: thermodynamically is it not possible to extract work from an unknown state using a Szilard's engine but work can be extracted if classical correlations exist between two different unknown states; suppose, for example, that two classical bits are in an unknown state but we know that both are in the same. Performing a CNOT operation on the bits, the control bit will be remained in an unknown state but the target one is certainly in the 0 state and 1 bit of work can be extracted from it.

In general, given a n-bit classical random variable  $X$  with Shannon entropy  $H(X)$  by using the first law of thermodynamics the amount of work  $W_C$  that can be extracted is:

$$W_C = n - H(X) \quad (6.15)$$

To show how this results are mapped in the quantum case, having  $n$  qubits in a state  $\rho$  and von Neumann entropy  $S(\rho)$ , it is possible to extract:

$$W_t = n - S(\rho) \quad (6.16)$$

that corresponds to the amount of work extractable in total ( $W_t$ ) by a party who has access to the entire quantum state  $\rho$ . As in the classical situation, all correlation could be used to extract work from the state. Suppose Alice and Bob want to extract work from a common quantum state  $\rho$  having two quantum engines which can be used locally: under LOCC they try to extract the largest amount of work  $W_l$  possible. In this situation the work deficit is defined as:

$$\Delta = W_t - W_l \quad (6.17)$$

A very simple and intriguing classical example could be considering a classical correlated quantum state as:

$$\rho_{AB} = \frac{1}{2} (|00\rangle\langle 00| + |11\rangle\langle 11|) = \begin{pmatrix} \frac{1}{2} & 0 & 0 & 0 \\ 0 & 0 & 0 & 0 \\ 0 & 0 & 0 & 0 \\ 0 & 0 & 0 & \frac{1}{2} \end{pmatrix}$$

In this case  $\Delta = 0$ . Here we demonstrate why:

Alice and Bob have an unknown state that could be either  $|0\rangle$  or  $|1\rangle$ . We represent this state as  $|?\rangle$ ;

1. Alice prepares an ancilla in  $|0\rangle$ . She then performs a CNOT quantum operation using  $|?\rangle$  as control and the ancilla as target:  $\text{CNOT}(|?\rangle_C |0\rangle_T) = |?\rangle_C |?\rangle_T$ ;
2. Now that means that Alice's ancilla is in the same as her original qubit. Alice sends one of her qubits to Bob.
3. Bob performs a CNOT operation using his  $|?\rangle$  qubit as target and Alice's qubit as control. As a result he will obtain a  $|0\rangle$  with certainty. This allows Bob to extract one bit of work through a Szilard engine.
4. Bob control qubit, which remained unmodified, is sent backward to erase the information stored in Alice memory after her CNOT application. At the end, Alice state will be in a new unknown state  $|?\rangle$ , completing the thermodynamic cycle.

The same protocol can be used in the case of maximally entangled state (MES), for exmple a Bell state like  $|\psi^+\rangle$ . In this case  $\Delta = 1$ . Unlike the previous case, decoherence effect will play the role of an irreversible transformation so that entanglement is destroyed. On the other hand, someone with access to the entire state could extract 2 bits of work since the state is pure and has zero entropy.

These two examples suggest that the strength of correlation can be reflected in the deficit but the deficit might not necessarily correspond to the amount of entanglement. Horodecki *et al.* [128, 129] interpreted the quantum work deficit as the amount of quantumness of correlations but not as the amount of entanglement. It has been shown in [127] that the work deficit is bounded from below as

$$\Delta \geq \max\{S(\rho^A), S(\rho^B)\} - S(\rho) \quad (6.18)$$

where  $\rho_A$  and  $\rho_B$  are defined as the reduced density operators. The upper bound can be achieved when the state is pure and it turns out to be equal to the entanglement measure for pure states.

## 6.4 Thermodynamical detection of entanglement by Maxwell's Demons

It is now well established that quantum systems can be more correlated than classical ones. One of the central problems in quantum thermodynamics and information theory is to understand how these excess correlations could be used to do something useful. For example there are many indications from the field of quantum computation that entanglement could increase the computational speed up but, until today, there is not a precise and reproducible link between the two. It is possible to show that there is a very deep and important connection between entanglement and quantum thermodynamics: *a work-extracting scenario could discriminate between classical and quantum correlations.* While Horodecki *et al.* and Zurek play with quantum correlations by defining work deficit [127] and quantum discord [130], Maruyama *et al.* [9] and Viguie *et al.* [131] clarified the differences between classical and quantum correlations writing a Bell-like inequality based on locally observable thermodynamic quantities, respectively for the bipartite and tripartite state. The thermodynamic inequality is satisfied by all classically correlated states but can be violated by entangled states. Until today, this is the deepest connection between the separability of a quantum state and thermodynamics.

### 6.4.1 Work Extraction Scheme: two qubits

Following Ref. [9], consider a two-dimensional classical system as a *one-molecule gas* which can be in the left or the right hand side of a chamber:  $k_B T \log_2$  of work can be extracted from the system supposing to know the exact position of the classical molecule, as we have seen in Sec. 6.1.2. Having only partial information about the position of the molecule, the extracted work could be represented as  $k_B T \log_2(1 - H(X))$  where  $H(X)$  is the Shannon entropy and  $X$  is a variable describing the molecule position. The same situation could be presented in the quantum case provided that the nature of the projection operators employed to obtain the information. Considering a bipartite correlated system, retained by Alice and Bob and a set of identical prepared copies of the system for which Alice chooses  $A_\theta = \{P_\theta, P_\theta^\perp\}$  and Bob chooses  $B_{\theta'} = \{P_{\theta'}, P_{\theta'}^\perp\}$  as bases for their measurement and the two angles  $\theta$  and  $\theta'$  corresponding

to the two measurement angles. Now Alice can communicate classically either the operator she used for the measurement or the result itself by using an ancilla. At the same time, Bob could extract  $(1 - H(A_\theta|B_{\theta'}))$  bits of work *per pair* on his side.

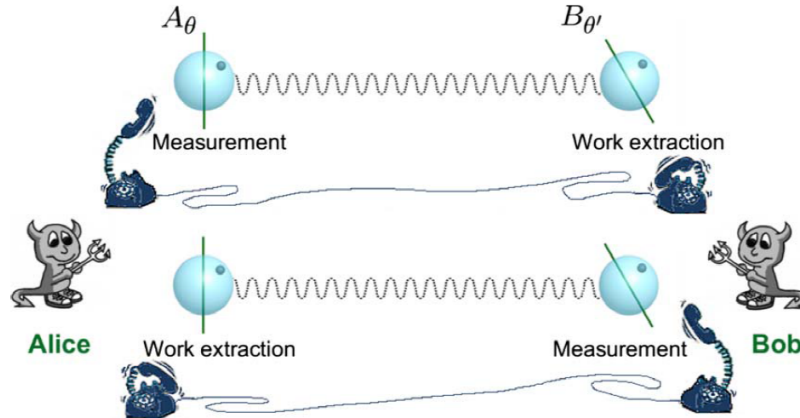


Figure 6.2: Schematic representation of the protocol to extract work from entangled states. The two pairs represent an ensemble of entangled quantum states for which Alice and Bob use the operators  $A_\theta$  and  $B_{\theta'}$ , respectively to perform measurement. In the first case, Alice measures her state and sends her result to Bob by use of a communication channel and Bob performs the extraction of work. For the second case, Alice and Bob exchange their roles.

When the bipartite state they share is maximally entangled,  $H(A_\theta|B_\theta) = 0$ . This means that in this case more work can be extracted from entangled states pairs than from classically correlated states.

### 6.4.2 Thermodynamical separability criterion

In this section the thermodynamical separability criterion will be presented as a new Bell-like approach to detect entanglement. The main point here is considering the whole set or rotation of measurement operators over a great circle of the Bloch sphere as shown in Fig. 6.3. The sum of the whole amount of work that can be extracted by considering this circle is a good indicator of the quantum correlations that are present inside the state.

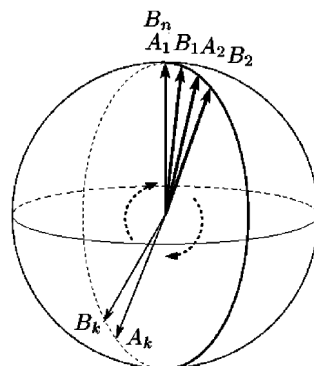


Figure 6.3: The great circle that maximize the work extraction is shown. Bases  $A_1, B_1, \dots, B_n$  are chosen to cover the great circle on the Bloch-Poincaré sphere: from a theoretical point of view, it is possible to consider the situation in which  $n \rightarrow \infty$ . In this case, the final basis  $B_n$  is considered the same that  $B_1$ .

The great circle on the Bloch sphere has to be considered the circle that maximize the amount of extractable work from the entangled pairs. Defining  $\xi_\rho(A_i, B_j)$  the extractable work from two copies of the same bipartite state  $\rho$ , for a two bipartite system we define  $\xi$  as:

$$\xi_\rho = \frac{1}{2}[2 - H(A_i|B_j) - H(B_j|A_i)] = \frac{1}{2}[2 - 2H(A_i, B_j) + H(A_i) + H(B_j)] \quad (6.19)$$

which is a symmetric quantity with respect to  $A_i$  and  $B_j$ . For a state  $\rho$ , we define  $\Xi(\rho)$ :

$$\Xi(\rho) = \frac{1}{2\pi} \int_0^{2\pi} \xi_\rho(A(\theta), B(\theta)) d\theta \quad (6.20)$$

where  $\theta$  is the direction of measurement on the great circle on the Bloch-Poincaré sphere. This is a very important result in the context of quantum information theory considering that  $\Xi(\rho)$  represents the extractable work under local operation and classical communication (LOCC). This quantity permits to construct a Bell-like inequality to detect entanglement [126].

**Proposition 1 (Thermodynamical Separability Criterion)** *An inequality as:*

$$\Xi(\rho) \leq \Xi(|00\rangle) \quad (6.21)$$

*is a necessary condition for a two-dimensional bipartite state  $\rho$  to be separable. The state  $|00\rangle$  in the right hand side of (6.21) could be any pure product state and amounts to  $\Xi(|00\rangle) = 0.4427$  bits. This bound represents the Thermodynamical Separability Criterion (Thermodynamical Separability Criterion (TSC)).*

As the right hand side of (6.21) represents the maximum work that can be extracted by using classically correlated states, it is clear that any violation of TSC corresponds to the identification of entanglement. Violating TSC, Maxwell's demons could extract more work from entanglement than in the case of classically correlated states. There is the possibility to perform (6.20) by integrating not only on the great circle but on the entire Bloch sphere; this alternative version of (6.20) is:

$$\Xi(\rho) = \frac{1}{4\pi} \int_{BPS} \xi_\rho(A, B) d\Omega \leq \Xi_{BPS}(|00\rangle) \quad (6.22)$$

where BPS corresponds to the whole Bloch-sphere surface. In this situation  $\Xi_{BPS}(|00\rangle) = 0.2786$  bits numerically. Since these inequalities are derived by only thermodynamical considerations [126], without making any assumption on non-locality, they are physically different from Bell's inequalities but, at the same time their goal is similar as they can detect differences between classical and quantum correlations.

### 6.4.3 Exorcism of Maxwell's Demon in TSC

An alternative formulation of the second law of thermodynamics in the context of cyclic thermodynamic transformation is: there is no cycle of an heat engine that converts heat to work with no other changes made to the system or its environment. In the work extraction protocol, indeed, this is represented by the need to restore the initial state after extracting work.

The impossibility to violate the second law of thermodynamics follows from the consideration that the work investment is always non negative, regardless of the direction of the work extraction. As an example, let's suppose to invert the extraction work protocol shown on Sec. 6.5.2, considering that now Bob performs measurements and Alice extracts work on her side and that the state after the measurement is  $\sigma = \mathbb{I}/2 \otimes |0\rangle\langle 0|$ .

In the case in which Bob's outcome was 1, he can flip it by using a  $\sigma_x$  operation without an energy consumption (because a bitflip is a LOCC). In the case of only classical correlations, the simplest method to restore the initial state  $\rho_{cl}$ , after the measurement is by compression and decompression. To actively perform this procedure, both Alice and Bob need  $nS(\rho_{cl})$  copies of  $\mathbb{I}/2$  and  $n[1 - S(\rho_{cl})]$  copies of the standard pure state  $|0\rangle$ . Now:

- (1) Alice compresses  $n[1 - S(\rho_{cl})/2]$  copies of  $\mathbb{I}/2$  isothermally to  $|0\rangle$  consuming  $w_{cons}^A = [1 - S(\rho_{cl})/2]$  bits of work per qubit.
- (2) Bob acquires  $w_{ext}^B = S(\rho_{cl})/2$  bits of work per qubit transforming  $nS(\rho_{cl})/2$  copies of  $|0\rangle$  to  $\mathbb{I}/2$ .
- (3) Both can restore  $n$  copies of the initial classical state  $\rho_{cl}$  by decompressing the mixture  $\mathbb{I}/2 \otimes \mathbb{I}/2$  and  $|00\rangle$  without work consumption.

Starting from an entangled state, the restoration process and the exorcism itself becomes much easier:

- (1) Alice transforms her state  $\mathbb{I}/2$  into  $|0\rangle$  consuming a bit of energy to make  $|00\rangle$ .
- (2) Rotating Alice's state to  $(\alpha|0\rangle + \beta|1\rangle)|0\rangle$  continuously and with a unitary transformation, and applying a CNOT operation on the two qubits, it is possible to restore the starting entangled state.

For both the situations, it is necessary to delete the information of Bob's measurement and this procedure requires  $H(B(\theta))$  bits of work.

Finally the work investment  $W_{inv}$  can be computed for both the classical and the entangled cases.

- Classical:  $W_{inv}^{cl} = w_{cons}^A - w_{ext}^B + H(B(\theta)) - [1 - H(A(\theta)|B(\theta))] = H(A(\theta), B(\theta)) - S(\rho_{cl})$  bits of work
- Entangled:  $W_{inv}^{ent} = H(A(\theta), B(\theta))$  bits.

These work investments need to be bigger than zero in order for the second law to be not violated. This is easily demonstrated by considering the definitions of Shannon and Von Neumann entropies.

### 6.4.4 Protocol for tripartite systems

TSC constitutes a very important step in the comprehension of the connection between quantum thermodynamics and entanglement. Even without considering its centrality in quantum thermodynamics, TSC could result a very important tool to reveal the entanglement that is invisible to the Bell inequalities. Indeed it is important to remember that there are also entangled states that do not violate Bell inequalities.

This scenario completely changes in case of tripartite quantum systems. Svetlinchy and Mermin inequalities [105, 132, 133] are a natural generalization of Bell's inequalities and constitute the traditional starting point for the detection of tripartite entanglement. However it has been shown that both these inequalities cannot detect all the entangled states [134]: indeed Svetlinchy's and Mermin's inequalities are non-optimal entanglement witness criteria. The nature of this scenario becomes clear when one thinks that it has been impossible, until now, to control tripartite and multipartite entanglement for quantum information protocols.

On the other hand, it is possible to easily extend TSC for a tripartite system [131]. The previous protocol changes: each of three parties receives the outcomes of measurements from the other two. It is possible to take conditional entropies such as  $H(A(\theta)|B(\theta), C(\theta))$  instead of  $H(A(\theta)|B(\theta))$  in the definition of  $\xi$  and  $\Xi$ .

A simple extension such this in the case of a tripartite system tells little about the properties of multipartite entanglement. As the tripartite entanglement could be *weak* as a GHZ-like one or *strong* as a W-like one, as seen in Sec. 1.2.5, it could be very interesting to find a criterion that allows the detection of the fingerprint of these two states. In Fig. 6.4 we show the protocol to extract work from a tripartite system.

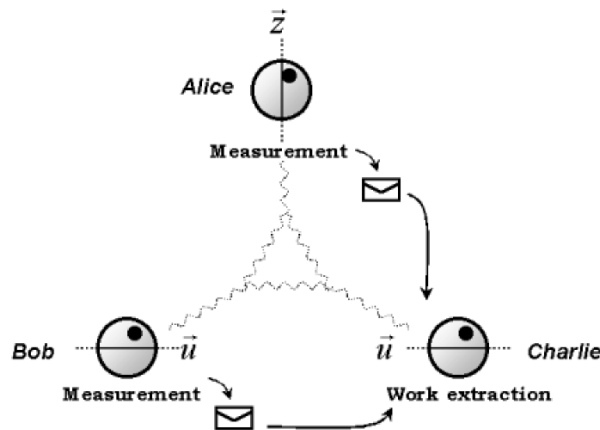


Figure 6.4: Work extraction protocol for a tripartite system. Alice and Bob realize a measure along the directions  $\hat{z}$  and  $\hat{u}$  respectively: Bob varies the direction of  $\hat{u}$  choosing one of the three orthogonal directions  $\{\hat{x}, \hat{y}, \hat{z}\}$  at each round. Charlie extracts work along  $\hat{u}$  only after receiving measurement results from the other two Maxwell's Demons, Alice and Bob. The three demons could exchange their role cyclically: in the protocol described here, the exchange of roles is not considered.

The three Maxwell's Demons considered here are Alice, Bob and Charlie: the protocol is based on the work extraction on the  $\hat{u}$  direction by Charlie after receiving information on the outcomes of the other two measurements made by Alice and Bob along  $\hat{z}$  and  $\hat{u}$  directions respectively. In the ensemble in which Alice and Bob measure while Charlie extracts work, the average amount of work obtainable is:

$$w_{\hat{z},\hat{u}}(\rho) = 1 - H(C(\hat{u})|A(\hat{z}), B(\hat{u})) \quad (6.23)$$

It will be possible to detect GHZ and W entanglement by varying the direction of  $\hat{u}$  while keeping  $\hat{z}$  fixed. A very important quantity,  $W(\rho)$ , allows to achieve this task. By defining  $\phi$  as the angle between  $\hat{x}$  and a certain predetermined direction in the space. Then, the averaged work can be written as:

$$W_\phi = \frac{1}{3} \sum_{\hat{u} \in \{\hat{x}, \hat{y}, \hat{z}\}} w_{\hat{z},\hat{u}}(\rho) \quad (6.24)$$

It is possible to take the maximum value of  $W_\phi(\rho)$  over  $\phi$  to remove the  $\phi$ -dependence:

$$W(\rho) = \max_\phi W_\phi(\rho) \quad (6.25)$$

The maximum amount of extractable work depends on the geometry of the tripartite quantum system: in the case of separable tripartite quantum states, the upper bound of extractable work is:

$$W(\rho) \leq \frac{1}{3} \quad (6.26)$$

This result is very similar to that of TSC for bipartite systems; however there is a deep difference between the two approaches: bipartite TSC requires an integral over a great circle on the Bloch-Poincaré sphere, tripartite TSC requires an average of work over just three directions.

### Detection of weak and strong tripartite entanglement

As stated in the previous sections, in tripartite system there are two classes of entangled states, either GHZ or W: the first one is also called *weak* because the entangled characteristic of the state vanishes after a reduced trace operation on one of the qubits. The behaviour is different for the *strong* entanglement of the W class that preserves a small degree of entanglement after a reduced trace operation on one qubit.

The tripartite thermodynamical work extraction criterion allows the detection of the fingerprint of the GHZ-like or W-like class becomes the maximum amount of extractable work. The max extractable work from a GHZ state, assessed from the TSC criterion, is 1 bit, while its minimum is 0.1619 bits (this value has been found numerically).

Regarding a W-state, the maximum amount of extractable work is 0.7778 bits, while the minimum is 0.1696 bits.

That means that whenever we find an extractable work greater than 0.778 bits we are witnessing a genuine GHZ state. While in Ref. [131] there is no discussion about the bounds that are obtainable in case of biseparable state, or cluster states, we present here an experimental demonstration of a working-extraction protocol which allows the characterization of the similarity of a tripartite quantum state to either a W or GHZ state.

## 6.5 Experimental work extraction protocol

In this section we present analytical and experimental result regarding the two- and three- qubit work extraction protocol described in Secs. 6.5.2,6.4.4. We will show that the nature of the correlations due to a strong or weak quantum state will lead to the extraction of different amount of work, thus permitting the distinction of these states. We will also show the difference between a Bell-like approach to the study of quantum correlations. The following sections refer to Ref. [135] which is one of the main works of this thesis.

### 6.5.1 Two-qubit separably criterion based on thermodynamics work-extraction protocol

Let us set the thermodynamic context that serves the basis for the interpretation of the thermodynamic criterion for separability. If we consider a single-particle gas in a Szilard machine-like device, i.e. a split chamber that is put in contact with a thermal reservoir at temperature  $T$ . By determining whether the particle occupies the left or right half-chamber, we can extract  $k_B T \ln 2$  of work out of the reservoir simply by letting the gas equilibrate with it (isothermally). Here,  $k_B$  is Boltzmann's constant.

Suppose now that only partial information about the position of the particle in the chamber is available. In this case, the work that could in principle be extracted is  $(k_B T \ln 2)[1 - H(X)]$ , where  $H(X)$  is the Shannon entropy of the binary position  $X$  of the particle. Clearly, here,  $k_B T \ln 2$  is a single scaling factor whose inclusion little adds to the physics of the problem.

From here on, we thus rescale work in units of  $k_B T \ln 2$ , and focus solely on the "information-theoretical" gain  $1 - H(X)$ , which encompasses the core of the work-extraction scheme illustrated here. In this sense, we can elevate the reservoir at the role of a virtual entity with limited physical relevance in the context here illustrated, besides the establishment of a "gauge" for the quantification of extractable work.

Let us now extend the scenario to the quantum domain and use projective operations to acquire information on the state of a two-level system that embodies the counterpart of the one-particle gas in the split chamber. In this case, we can store the measurement results in classical bits, so that the same process as above can be applied. Clearly, the entropy  $H(X)$  is associated to the outcomes of a measurement on a two-level state. Work extraction is then associated purely to the measurement and not to some dynamics of the state.

Moving from the single-particle to the bipartite case, we take inspiration from the fact that Maxwell had in mind Greek daimones and we introduce again Alice and Bob, each attempting at extracting work from a two-qubit system in a two-parties game. Thanks to the correlations present between their subsystems, a given daemon will implement her work extraction protocol based on the measurement strategy chosen by her competitor.

They share an ensemble of qubit pairs, each prepared in the same bipartite state  $\rho$ . Moreover, they agree on the choice of two sets of measurement operators (one per daemon), that densely cover a great circle on the Bloch sphere of a single qubit (see

Fig. 6.3).

For half of the ensemble, Alice should choose from the set  $\{\hat{A}_\theta\}$  the projection operator to use in order to measure her qubit. For the remaining half of the ensemble, Bob shall pick his measurement operator from the set  $\{\hat{B}_{\theta'}\}$ . In these sets,  $\theta$  and  $\theta'$  stand for the angular position, over a great circle of their respective single-qubit Bloch sphere, of the measurements performed by the daemons and  $\theta, \theta'=0$  correspond to the  $z$  axis.

In a given run of the game, Alice measures operator  $\hat{A}_\theta$  and communicates the corresponding outcome  $A_\theta$  to Bob, who attempts at “extracting work” owing to the information gathered, locally, by Alice’s measurement. In fact, the latter allows Bob to reduce the entropy associated to her measurement result from the value  $H(B_{\theta'})$  to  $H(B_{\theta'}|A_\theta)$  [9].

With such information, using a Szilard-like machine, Bob would be able to extract an amount of work  $1-H(B_{\theta'}|A_\theta)$  from a hypothetical heat reservoir. An analogous reasoning can be carried out when exchanging the role of the daemons, concluding that, for a given setting, the extractable work per run of the game is:

$$W_\rho(A_\theta, B_{\theta'}) = 1 - H(A_\theta, B_{\theta'}) + \frac{1}{2}[H(A_\theta) + H(B_{\theta'})], \quad (6.27)$$

where  $H(A_\theta, B_{\theta'})$  is the joint entropy of variables  $A_\theta$  and  $B_{\theta'}$ . For a sufficiently dense covering of the great circle, and for  $\theta' = \theta$ , the average extractable work achieved through the game, maximised over all the possible great circles, is  $\mathcal{W}(\rho) = \max_\phi \int_0^{2\pi} W_\rho(A_\theta, B_\theta) d\theta / 2\pi$ , where  $\phi$  is the azimuthal angle for the great circles being considered. In Ref. [article:viguie2005] it was shown that any separable state  $\rho$  is such that the value that  $\Xi$  can attain with separable states is bounded by

$$\mathcal{W}(\rho) \leq \mathcal{W}_f = 0.443 \text{ bits}. \quad (6.28)$$

where  $\mathcal{W}_f$  is the maximum average work evaluated for any pure factorized state. Therefore, any surplus of extractable work above  $\mathcal{W}_f$  arises in virtue of entanglement shared by the daemons. Eq. (6.28) can then be used as a thermodynamically rooted entropic witness for inseparability.

## 6.5.2 Two-qubit experiment

We employ the thermodynamic separability criterion in Eq. (6.28) for the characterisation of photonic entanglement. We point out that our aim is to use an information thermodynamic bound to assess entanglement, which makes our study distinct from the attempt at replicating the behaviour of a working medium in a photonic setup reported by Vidrighin et al. [136].

Polarization-entangled pairs of qubits, ideally prepared in  $|\Phi\rangle = \cos\varphi|HH\rangle + \sin\varphi|VV\rangle$ , are produced by using the double-pass source we described in Sec. 3.2 [see Fig. 6.5(a)]. Again,  $|H\rangle$  ( $|V\rangle$ ) stands for a photon in the horizontal (vertical) polarization state. By controlling the weight  $\cos\varphi$  between the two components of such a state, we tune the level of entanglement in our resource unbalancing the state.

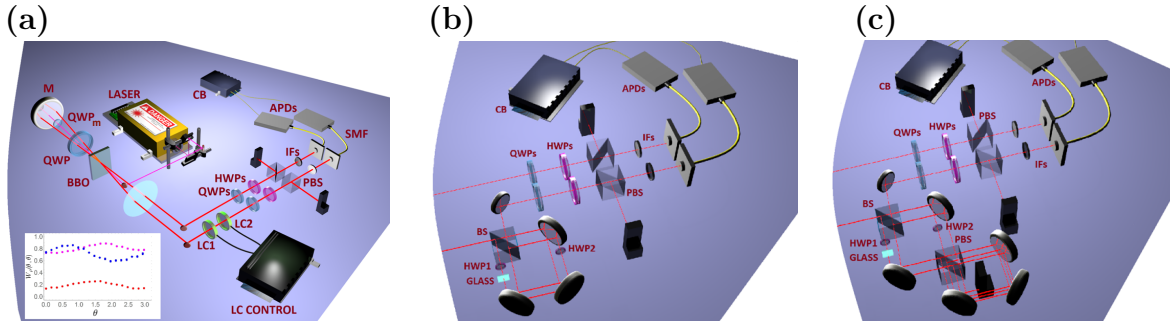


Figure 6.5: **(a)** Experimental setup for the extraction of work from inseparable bipartite state: The entangled photon source uses a 1.5mm thick  $\beta$  Barium-Borate (BBO) crystal pumped with 100 mW of laser at 355 nm, in conjunction with a spherical mirror (M), and delivers approximately 200 coincidences/s through 5 nm (FWHM) interference filters (IF). We encode the logical states of each qubit in the horizontal and vertical polarization states  $|H\rangle$  and  $|V\rangle$  of each photon. Using quantum state tomography, we estimate a fidelity  $F = 0.961 \pm 0.007$  of the entangled resource with the maximally entangled state  $\frac{1}{\sqrt{2}}(|HH\rangle + |VV\rangle)$ . The corresponding value of tangle is  $T = 0.911 \pm 0.008$ . The relative weight ( $\cos \varphi$ ) of the two polarization contributions in such state can be tuned by the quarter waveplate ( $\text{QWP}_m$ ) in the source. One of the photons passes through a depolarizing channel, consisting of two liquid crystals (LCs) and the associated control electronics, which selects the value of  $\mu$ . Finally, polarization measurements are performed at a polarisation-analysis module consisting of a QWP, a half waveplate (HWP), a polarising beam splitter (PBS), and an avalanche photodiode (APD) per mode. We also show the single-mode fibers (SMF) used to convey the photonics signal to the polarization analysis module. Inset: measured  $W_\rho(\theta, \theta)$  as a function of the measurement angle  $\theta$  for state  $|\rho\rangle$  with  $\cos \varphi = 0.85$ , and  $\mu = 0.98$  (blue);  $\cos \varphi = 0.62$ , and  $\mu = 0.98$  (purple);  $\cos \varphi = 0.62$ , and  $\mu = 0.51$  (red). **(b)** Experimental setup for the extraction of work from a GHZ-Cluster state. **(c)** Analogous setup for the extraction of work from a  $W$ -type resource.

Further, we explore how the thermodynamic bound evolves through a depolarising channel (of strength  $1 - \mu$ ) degrading the initial state to the mixture

$$\rho = \mu|\Phi\rangle\langle\Phi| + (1 - \mu)\mathbb{I}/4. \quad (6.29)$$

Here, the parameter  $1 - \mu$  quantifies the strength of the channel. This has been implemented by using two liquid crystals, with their axes at 0 and 45 degrees, onto the path of one photon. The two crystals are tuned in such a way that they perform a rapid succession of Pauli operators  $\hat{\sigma}_x$ ,  $\hat{\sigma}_y$ ,  $\hat{\sigma}_z$ , thus generating white noise on the state.

In the inset of Fig. 6.5 **(a)**, we show typical experimental curves for the work  $W_\rho(\theta, \theta)$  calculated according to Eq. (6.27), as we inspect the set of operator pairs used by Alice and Bob, labelled by the angle  $\theta$  on the great circle of the Bloch sphere corresponding to the linear polarizations (i.e. the equator of the single-qubit Bloch sphere). This is the set of directions allowing for optimal work extraction.

The observed oscillations are due to the polarization unbalance, while the average level is affected by the purity of the state. For each choice of  $\theta$ , we have calculated the Shannon entropy associated to single-particle operators, as well as the joint entropy associated to the joint operator. We have verified by numerical simulations that our covering with 19 different directions is sufficiently dense for the continuous approximation to hold. In addition, we have fully characterised our states with quantum state tomography, from which the maximal value of the Bell operator  $S$  has been extracted for a comparison with a standard entanglement witness.

In order to perform the average over the projections performed by the daemons, we removed the quarter waveplates (QWPs) from the polarization analysis-module shown in Fig. 6.5, and used the half waveplates (HWPs) to rotate the state along the correct big circle. The effect of the polarization beam splitter (PBS) is that of performing

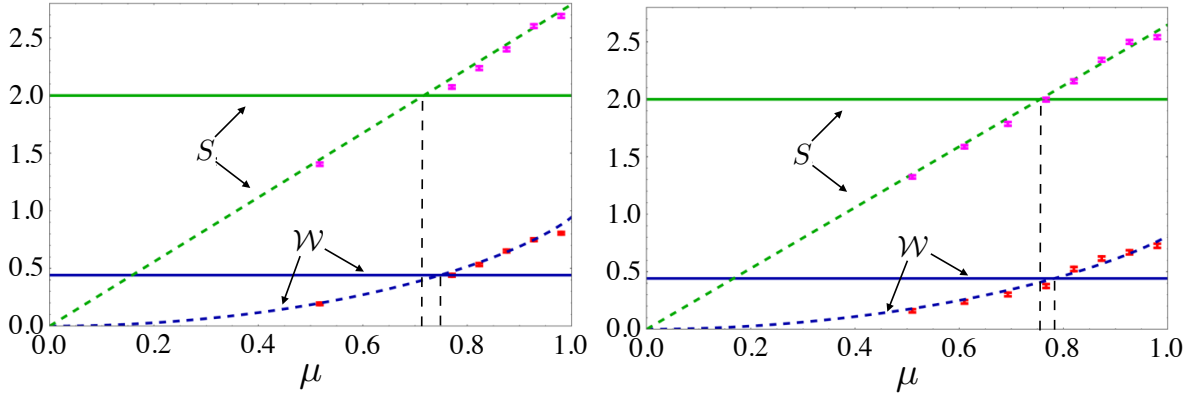


Figure 6.6: Experimental results for two different resource states corresponding to  $\cos \varphi = 0.62$  [panel (a)], and  $\cos \varphi = 0.85$  [panel (b)] for different strengths of the depolarising channels  $\mu$ . Red dots: experimental points for  $\mathcal{W}$  calculated from the experimental count rates measured in 30s. Magenta dots: experimental points corresponding to the values taken by the Bell parameter, evaluated from the fully reconstructed state tomographies of the resource  $\rho_{\text{exp}}$ . The value of  $\cos \varphi$  is evaluated by direct inspection of the coincidence rates, averaged over all the experimental states. The error bars take into account the Poissonian statistics of the measured rates and derived from direct error propagation for  $\mathcal{W}$  and Monte Carlo simulation for  $S$ . The green and blue dashed curves represent theoretical predictions based on state  $\rho$ , while the solid straight lines denote the entanglement thresholds for the work extraction and the Bell function. The dashed vertical lines identify the values of  $\mu$  for which  $\mathcal{W}$  and  $S$  cross their respective bounds.

the projection  $|H\rangle\langle H|$ . As we used just two avalanche photo-diodes (APDs) after the PBSs, we had to implement four different types of measurements for each of the 19 choices of angular direction on the equator of the single-qubit Bloch sphere.

In particular, we had to consider the four sets of directions  $(\theta_A, \theta'_B) = (\theta, \theta), (\theta, \theta + 45), (\theta + 45, \theta), (\theta + 45, \theta + 45)$ , where the first (second) angular direction is for Aletheia's (Bia's) measurements choice. The corresponding detected coincidences at the APDs are labelled as  $N_{\theta_A, \theta'_B}$ .

A full circulation of the Bloch-sphere equator is then achieved by rotating the HWPs from  $0\text{deg}$  to  $45\text{deg}$  in 19 steps. This implies that a total of 76 measurements were needed in order to acquire the necessary information to perform the evaluation of the work extraction performance. Upon suitable normalization of the detected coincidence counts, we have the following set of probabilities

$$p_{AB}(\theta) = N_{\theta, \theta+45}/D(\theta), \quad (6.30)$$

$$p_A(\theta) = (N_{\theta, \theta} + N_{\theta+45, \theta})/D(\theta), \quad (6.31)$$

$$p_B(\theta) = (N_{\theta, \theta} + N_{\theta, \theta+45})/D(\theta) \quad (6.32)$$

with  $D(\theta) = N_{\theta, \theta} + N_{\theta, \theta+45} + N_{\theta+45, \theta} + N_{\theta+45, \theta+45}$ . These are instrumental to the evaluation of the Shannon entropies needed to calculate  $W_\rho(\theta, \theta)$  and, in turn,  $\mathcal{W}$ .

We measured the extractable thermodynamic work for several sets of parameters  $\varphi$  and  $\mu$  in the resource state, which were estimated by reconstructing the density matrix of the experimentally engineered state  $\rho_{\text{exp}}$  via complete quantum state tomography for each position of the QWP in the source (setting  $\varphi$ ) and every configuration of the LCs (fixing  $\mu$ ). This has been performed by minimizing the Frobenius norm (see Sec. 1.3.3 for the definition)  $\min_{\mu, \xi} |\rho_{\text{out}} - \rho(\mu, \xi)_{AB}|_{\text{Frobenius}}$ .

Extractable work has been calculated by measuring Shannon entropy spanned over the whole big circle of the Bloch Sphere. Example of measured coincidence counts are  $N_{0,0} = 3578$ ,  $N_{0,45} = 58$ ,  $N_{45,0} = 173$ ,  $N_{45,45} = 4328$ , achieved in 30s of measurement.

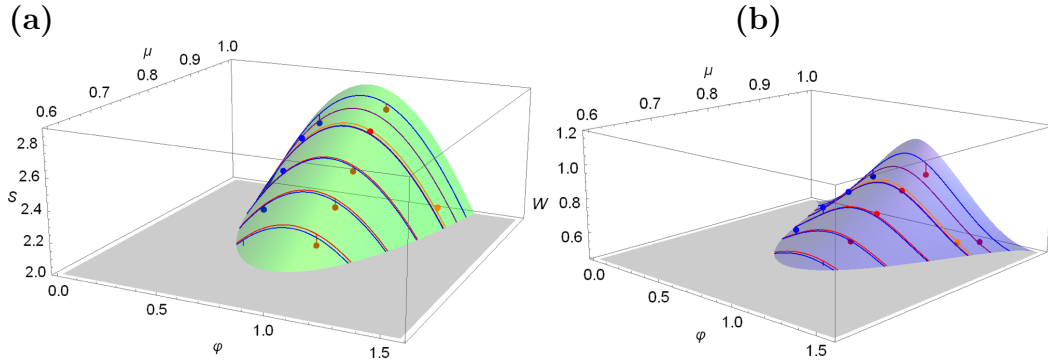


Figure 6.7: Comparison between theoretical predictions and experimental data for the Bell function [panel (a)] and the extractable work [panel (b)] against the strength  $\mu$  of the channel and the state unbalance  $\varphi$  (measured in degrees). The semi-transparent surfaces show the behavior of  $S$  and  $\mathcal{W}$ , while the dots represent the experimental points. Only the parts of the theoretical surfaces exceeding the local realistic bound [panel (a)] and the threshold  $\mathcal{W}_f$  [panel (b)] are displayed. Moreover, in order to highlight the relative position of the experimental points with respect to the theoretical surfaces, we show the curves on the latter associated with the same value of  $\mu$ .

In order to highlight the inherently different nature of the test implemented here and a standard Bell-CHSH test, we now consider the Bell function

$$S = \text{Tr}[\rho(\hat{O}_1 - \hat{O}_2 + \hat{O}_3 + \hat{O}_4)] \quad (6.33)$$

with  $\hat{O}_1 = \sigma_x \otimes \sigma_x(\alpha)$ ,  $\hat{O}_2 = \sigma_x \otimes \sigma_z(\alpha)$ ,  $\hat{O}_3 = \sigma_z \otimes \sigma_x(\alpha)$ , and  $\hat{O}_4 = \sigma_z \otimes \sigma_z(\alpha)$ . Here,  $\sigma_k(\alpha) = \hat{R}(\alpha)\sigma_k\hat{R}^\dagger(\alpha)$  with  $\hat{R}(\alpha) = \cos\alpha\mathbb{I} + i\sin\alpha\sigma_y$  and  $\sigma_k$  is the  $k = x, y, z$  Pauli matrix. Local realistic theories bound such function as  $|S| \leq 2$ , while quantum mechanically  $|S| \leq 2\sqrt{2}$ . Using state  $\rho$ , we find

$$S = \mu[1 + \sin(2\varphi)][\cos(2\alpha) + \sin(2\alpha)], \quad (6.34)$$

which we have used to estimate the value of the Bell function using  $\rho_{\text{exp}}$  for each set value of  $\mu$  and  $\varphi$ .

The results of our experiment are summarised in Fig. 6.6, where we show the measured extractable work and the Bell function for two resource states with different values of  $\varphi$ . The comparison with Bell's test reveals how both quantities capture the degradation resulting from the depolarisation channel, and that they are similarly robust against the bias between the  $|HH\rangle$  and  $|VV\rangle$  contributions. A complete analysis shows that the relation between the thermodynamic criterion and Bell's inequalities is not trivial.

In fact, we were able to find values of  $\mu$  and  $\varphi$  for which it is possible to violate just one of the two criteria, and vice versa. We have considered an experimental state with large bias ( $\cos\varphi = 0.25 \pm 0.03$ ) and purity ( $\mu = 0.97$ ) that offers no violation of the local realistic bound ( $S = 1.977 \pm 0.009$ ). However, the corresponding extractable work is  $\mathcal{W} = 0.491 \pm 0.021$ , which exceeds the separability threshold  $\mathcal{W}_f$  by 2 standard deviations.

This implies that the use of entanglement for powering a thermal machine is qualitatively different from that necessary for communication tasks, such as measurement-independent key distribution. Fig. 6.7 shows a comprehensive comparison between the theoretical predictions gathered by using Eq. (6.29) and the experimental data, revealing the great agreement between the latter and the former throughout the whole range of parameters assessed in our experimental investigation.

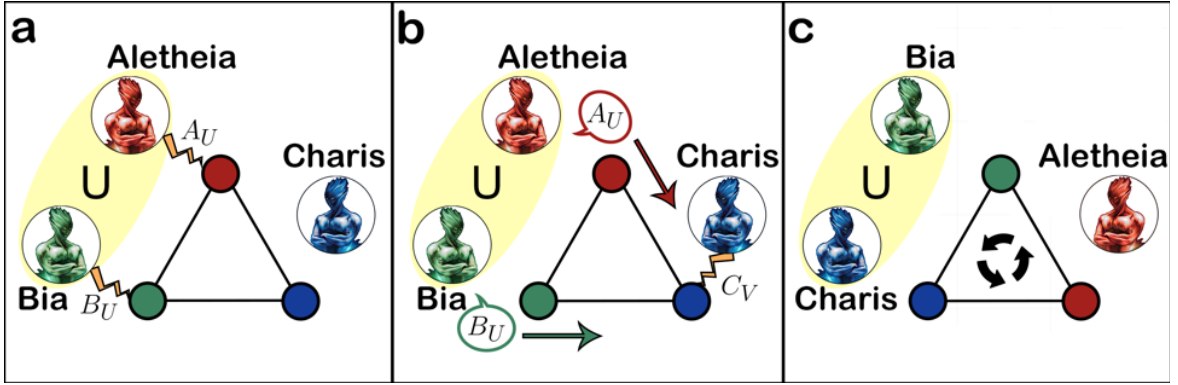


Figure 6.8: Diagrammatic representation of the scheme for work extraction from a tripartite system. Each panel illustrates one of the steps of the protocol described in the main text.

### 6.5.3 Three qubits experiment

We now extend our investigation to the case of a tripartite system, which naturally present a richer entanglement-sharing structure, and embody the first non trivial instance of systems exhibiting genuine multipartite entanglement [128]. In this scenario, both the figure of merit presented in Eq. (6.27) and the threshold for inseparability based on extractable work need to be adjusted to capture the above mentioned richness.

$\mu$	$\varphi$	$\mathcal{W}$	$S$	$T$
0.51	0.91(4)	0.193(5)	1.404(7)	0.04(1)
0.77	0.91(4)	0.441(6)	<b>2.073(7)</b>	0.34(4)
0.82	0.91(4)	<b>0.534(6)</b>	<b>2.237(8)</b>	0.48(5)
0.87	0.91(4)	<b>0.652(6)</b>	<b>2.400(8)</b>	0.60(5)
0.92	0.91(4)	<b>0.749(6)</b>	<b>2.602(8)</b>	0.81(6)
0.98	0.91(4)	<b>0.805(6)</b>	<b>2.690(8)</b>	0.91(4)
0.51	0.54(7)	0.160(7)	1.325(7)	0.03(1)
0.61	0.54(7)	0.238(8)	1.587(7)	0.13(2)
0.69	0.54(7)	0.302(8)	1.786(8)	0.20(2)
0.74	0.54(7)	0.376(8)	1.997(8)	0.34(3)
0.82	0.54(7)	<b>0.524(9)</b>	<b>2.157(8)</b>	0.45(2)
0.87	0.54(7)	<b>0.615(9)</b>	<b>2.343(8)</b>	0.62(3)
0.92	0.54(7)	<b>0.669(9)</b>	<b>2.499(8)</b>	0.78(3)
0.98	0.54(7)	<b>0.726(9)</b>	<b>2.541(8)</b>	0.82(3)
0.93	1.25(4)	<b>0.501(12)</b>	<b>2.131(9)</b>	0.34(4)
0.95	1.32(4)	<b>0.491(21)</b>	1.977(9)	0.24(4)

Table 6.1: Table of the experimental data. Here  $\mu$  is the strength of the channel, while  $\varphi$  determines the unbalance between the  $|HH\rangle$  and  $|VV\rangle$  components in the ideal resource state  $|\Phi\rangle$ . Both parameters have been estimated by performing state tomography of the experimental resource  $\rho_{\text{exp}}$ ;  $\mathcal{W}$  is the extractable work from the system. Its standard deviation  $\Delta\mathcal{W}$  has been obtained by considering Poissonian statistic on the coincidence counts.  $S$  is the Bell function, while  $T$  provides the value of tangle [128], which quantifies the degree of entanglement within the state of the system. Both these parameters (and associated uncertainties) have been estimated using state tomography. Values of  $\mathcal{W}$  and  $S$  reported in bold violate the separability and local realistic bound, respectively.

Here, we focus on the ability of distinguishing GHZ-type entanglement from W-type one using a criterion based on thermodynamics rather than state fidelity. The extractable work-based inseparability criterion should thus incorporate the possibility for the resource that we address to belong to either class.

The protocol now involves a further daemon, Charis, which is set to extract work from her subsystem, based on information provided by Alice and Bob. The strategy they agreed on consists of the following steps:

1. Alice and Bob perform a projective measurement along a common axis  $u$  in the single-qubit Bloch sphere chosen among the three Pauli settings;
2. Charlie receives information on the outcomes of such measurements. In light of such information, she can extract work from her system by performing a projective measurement along a suitably chosen direction  $v$  on the Bloch sphere;
3. In order to exclude bipartite entanglement and thus link the excess extractable work to the presence of genuine multipartite entanglement in our resource state, the protocol must be repeated by permuting the role of the three daemons.

Clearly, the amount of work that can be obtained in a single run of such a tripartite game is

$$W_\rho(A_u, B_u, C_v) = 1 - H(C_v|A_u, B_u) \quad (6.35)$$

with  $H(C_v|A_u, B_u)$  the Shannon entropy of variable  $C_v$  conditioned on the outcomes  $A_u$  and  $B_u$  performed by Alice and Bob. A bound for the average extractable work, obtained by maximizing over the choice of  $v$ , can be established for separable states as

$$\mathcal{W}(\rho) = \max_v \frac{1}{3} \sum_u W_\rho(A_u, B_u, C_v) \leq \mathcal{W}_f = \frac{1}{3}. \quad (6.36)$$

A violation of this bound signals the presence of entanglement in the state. Furthermore, it can be shown that W-type entanglement can only provide an extractable work of at most  $7/9 = 0.778$  [131]. Therefore, this thermodynamic criterion is well suited for identifying the entanglement class to which the state belongs: any extractable work in excess of 0.778 would signal GHZ character.

In order to achieve useful benchmarks for the performance of our experiments, we have performed a thorough theoretical analysis of the protocol for both pure and

$\mathcal{W}_1^{GHZc}$	$\mathcal{W}_2^{GHZc}$	$\mathcal{W}_3^{GHZc}$
$0.798 \pm 0.006$	$0.779 \pm 0.005$	$0.795 \pm 0.004$
$0.799 \pm 0.006$	$0.304 \pm 0.003$	$0.305 \pm 0.003$

Table 6.2: Extractable work in bits for the three permutations of roles in the protocol for work extraction-based inseparability evaluated using a GHZ-Cluster resource. The three columns are for the value of the extractable work achieved from the path-encoded qubit, the first polarization-encoded qubit, and the second polarization-encoded one, respectively. The first row refers to a tripartite entangled GHZ-Cluster state whose fidelity with the ideal resource  $(|HH0\rangle - |VV0\rangle + |HV1\rangle + |VH1\rangle)/2$  is found to be  $F = 0.851 \pm 0.008$ . The second row refers to the same resource where any coherence between path and polarization qubit is removed. Correspondingly,  $\mathcal{W}_2^{GHZ}$  and  $\mathcal{W}_3^{GHZ}$  are below the threshold for separability, showing that in the corresponding configuration we only have bipartite entanglement.

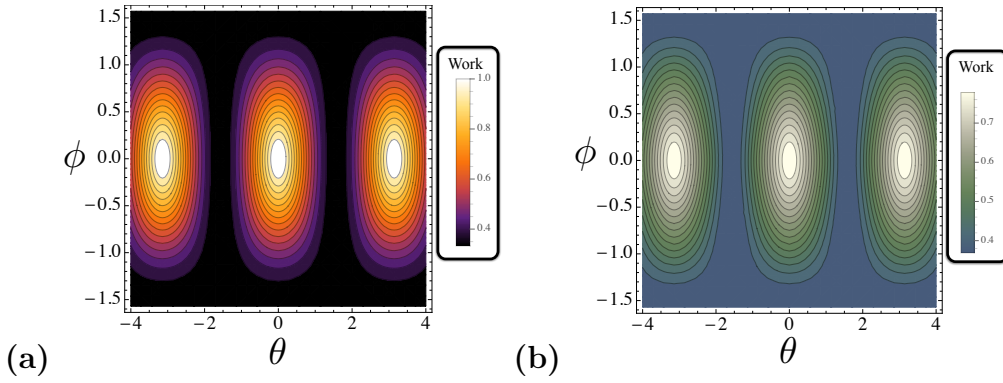


Figure 6.9: Density plot of the theoretical work that can be extracted from pure-state tripartite resources against the angles  $(\theta, \phi)$  that identify the angular direction of the Bloch sphere in which  $\mathcal{W}(\rho)$  can be optimized. Panel (a) is for a pure GHZ-Cluster state, while panel (b) shows the behavior for a  $W$  state. Evidently, the maximum work achievable in panel (a) can be larger than that resulting from using a  $W$  state.

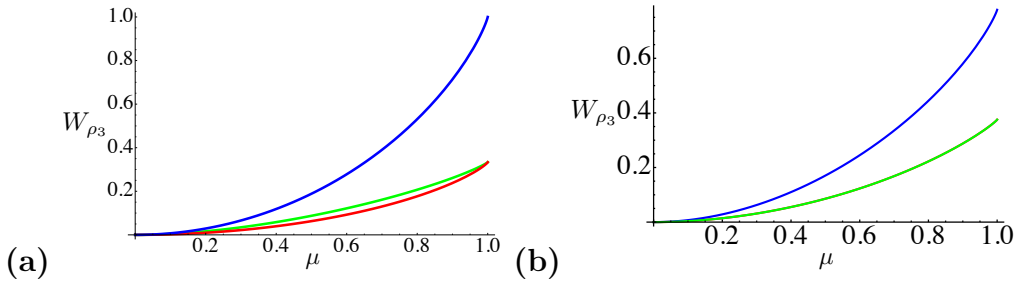


Figure 6.10: Theoretical work that can be extracted using a resource state embodied by  $\rho_3$  (Eq. in the main text) with  $|\Psi\rangle$  being a GHZ-Cluster state [panel (a)] or a  $W$  state [panel (b)], studied against  $\mu$  and for the three possible choices of  $U$  such as  $\hat{\sigma}_x, \hat{\sigma}_y, \hat{\sigma}_z$ . In both panels the red curve is for  $(\theta, \phi) = (90^\circ, 0^\circ)$ , the blue one is for  $(\theta, \phi) = (0^\circ, 0^\circ)$  and the green one for  $(\theta, \phi) = (0^\circ, 90^\circ)$ . In panel (b) the red and green curves are superimposed, implying that the work that can be extracted choosing these directions on the Bloch sphere is the same.

mixed-state resources. In particular, we have considered the achievable value of the extractable work  $\mathcal{W}$  when using the resource state

$$\rho_3 = \mu |\Psi\rangle \langle \Psi| + (1 - \mu)\mathbb{I}/8 \quad (6.37)$$

with  $|\Psi\rangle$  a tripartite pure state. We have first focused on the case of  $\mu = 1$  with  $|\Psi\rangle$  embodied by either a tripartite GHZ-Cluster state of the form

$$|GHZc\rangle = \frac{1}{2}(|000\rangle - |110\rangle + |011\rangle + |101\rangle)_{ABC} \quad (6.38)$$

where  $\{|0\rangle, |1\rangle\}$  are the logical states of the three qubits, labelled as  $A, B$ , and  $C$  and owned by Aletheia, Bia, and Charis respectively. This state can be shown to give rise to the same work extraction performance as a standard GHZ resource. The  $W$ -type resource is instead

$$|W\rangle = \frac{1}{\sqrt{3}}(|001\rangle + |010\rangle + |100\rangle)_{ABC}. \quad (6.39)$$

The results of our analysis are presented in Fig. 6.9, where the extra work-extraction possibilities offered by the use of a GHZ-Cluster are clearly showcased. The study can be extended to the case of mixed-state resources by addressing the effects that a non-unit value of  $\mu$  has on the performance of the work extraction protocol. This is

$\mathcal{W}_1^W$	$\mathcal{W}_2^W$	$\mathcal{W}_3^W$
$0.4715 \pm 0.0036$	$0.6625 \pm 0.0050$	$0.5966 \pm 0.0050$
$0.4715 \pm 0.0036$	$0.3205 \pm 0.0023$	$0.3282 \pm 0.0027$

Table 6.3: Extractable work in bits for the three permutations of roles in the protocol for work extraction-based inseparability evaluated using a  $W$  resource. The three columns are for the value of the extractable work achieved from the path-encoded qubit, the first polarization-encoded qubit, and the second polarization-encoded one, respectively. The first row refers to a tripartite entangled  $W$  state very close to an ideal  $|W\rangle$  state: The fidelity between the experimental resource and the ideal state  $(|HH1\rangle + |HV0\rangle + |VH0\rangle)/\sqrt{3}$  is  $F = 0.823 \pm 0.006$ . The second row refers to the same  $W$  configuration where, however, any coherence between path-encoded and polarization-encoded qubits is removed. Correspondingly,  $\mathcal{W}_2^W$  and  $\mathcal{W}_3^W$  are below the threshold for separability, showing that in the the corresponding configuration we only have bipartite entanglement.

done in Fig. 6.10, where we have investigated the behavior of work against  $\mu$  for the following sets of angles  $(\theta, \phi) = (90^\circ, 0^\circ)$ ,  $(0^\circ, 0^\circ)$  and  $(0^\circ, 90^\circ)$ , displaying the different performance of work extraction against different choices of great circle orientation.

Our two-photon implementation of three-qubit states relies on the addition of a third qubit, encoded in the two paths within a Sagnac interferometer (consisting of a 50:50 BS and three mirrors) on one of the two photons; the logical state  $|0\rangle$  correspond to the clockwise circulation of the photon inside the interferometer, and  $|1\rangle$  to the anticlockwise circulation. The phase  $\phi$  between such logical state can be tuned by tilting a thin glass plate, placed in one of the paths. This arrangement allowed us to engineer a GHZ-Cluster state of the form  $(|HH0\rangle - |VV0\rangle + |HV1\rangle + |VH1\rangle)_{ABC}/2$  by introducing a HWP at  $0deg$  on the clockwise path  $|0\rangle$  and a HWP at  $45deg$  on the anticlockwise one [cf. Fig. 6.5 (b)]. On the other hand, a  $W$ -type resource state of the form  $|W\rangle = (|HH1\rangle + |HV0\rangle + |VH0\rangle)/\sqrt{3}$  can be easily engineered by modifying the configuration for the GHZ-Cluster state. After changing the label of the two paths, a PBS can be added in the setup to perform a polarization-to-path mapping, and thus eliminate the contribution from state  $|VV1\rangle$  [cf. Fig. 6.5 (c)].

Path-qubit analysis was performed by either selecting one of the two paths, which implements a projection in the computational basis, or selecting the proper phase shift  $\phi$  between the two modes, thus enabling the projection on the diagonal basis ( $\phi = 0, \pi$ ) and the circular basis ( $\phi = \pi/2, -\pi/2$ ).

In all cases, there is a significant violation of the separability bound. Moreover, the symmetry among the results that we have achieved capture unambiguously the GHZ-Cluster character of the experimental resource. In order to show this feature more clearly, we have repeated the experiment when complete decoherence is introduced in one of the qubits of the system, in an attempt to render our resource state bi-separable and wash out its genuine tripartite entanglement. When full decoherence is introduced in the path-encoded qubit by inserting a thick glass plate on one of the paths, allowing to disrupt coherence between the two modes (independent of polarization), we get  $\mathcal{W}_1 = 0.799 \pm 0.006$ . However, decoherence lessens the values of the other two witnesses, to values that are very close to the separability threshold in Eq. (6.36), demonstrating the disappearance of tripartite entanglement.

A similar analysis has been conducted using the experimental  $W$ -type resource, whose corresponding experimental results are reported in Table 6.3. As done for the GHZ-Cluster state, we have assessed both the case of a close-to-ideal resource and

that of a strongly decohered one close to the separability threshold. The diversity (in terms of entanglement-sharing structure) of such resources is fully captured by the extractable work.

A comparison with non-locality-based criteria similar to the one reported for the study of bipartite entanglement can be made in this tripartite context. Here, rather than concentrating on two-qubit correlations, we shall investigate their genuinely multipartite nature, whose characterisation is clearly a much more demanding problem to tackle. A powerful tool in this respect is embodied by the genuinely tripartite versions of Bell's inequality, such as the inequality proposed by Svetlichny [132], whose violation witnesses the occurrence of multipartite non-local correlations.

In the Svetlichny game, the daemons locally rotate their respective qubit by an angle  $\alpha_j$  ( $j = A, B, C$ ) through the operator  $\hat{R}(\alpha_j) = \cos \alpha_j \sigma_z + \sin \alpha_j \sigma_x$  and project it over the basis of  $\sigma_z$ . If state  $|0\rangle$  ( $|1\rangle$ ) is found, they attach a dichotomic variable the value  $+1$  ( $-1$ ). This allows them to build the the statistical correlation function for local spin measurements  $E(\alpha_A, \alpha_B, \alpha_C)$  and, in turn, construct the Mermin-Ardehali-Belinskii-Klyshko function [105–107]

$$\begin{aligned} M_3 = & E(\alpha_A, \alpha_B, \alpha'_C) + E(\alpha_A, \alpha'_B, \alpha_C) \\ & + E(\alpha'_A, \alpha_B, \alpha_C) - E(\alpha'_A, \alpha'_B, \alpha'_C). \end{aligned} \quad (6.40)$$

The Svetlichny function is thus  $\mathcal{S}_3 = |M_3 + M'_3|$ , where  $M'_3$  is the same as  $M_3$  with  $\alpha_j \leftrightarrow \alpha'_j$ . Any biseparable state satisfies the inequality  $|\mathcal{S}_3| \leq 4$ . Tripartite entangled states violate the inequality up to the maximum value of  $4\sqrt{2} = 5.65685$ , which is obtained using GHZ-like states. In fact, state  $|GHZc\rangle$  allows to achieve such a maximum violation for  $(\alpha_A, \theta_B, \theta_C) = (3\pi/8, -\pi/4, 0)$  and  $(\alpha'_A, \theta'_B, \theta'_C) = (\pi/8, 0, \pi/4)$ .

We have used the experimental quantum state tomographies of the GHZ-Cluster and  $W$  resource states to evaluate the Svetlichny function. After a global optimisation over all the angles involved, we have found  $\mathcal{S}_3^{GHZc} = 4.83 \pm 0.07$  and  $\mathcal{S}_3^W = 3.39$ . This shows that the experimental GHZ-Cluster state is consistently found to be entangled in a genuinely tripartite sense by both the extractable work-based criterion and the Svetlichny one. On the other hand, the non locality-based entanglement criterion fails to detect the tripartite entangled nature of the experimental  $W$  resource, which is instead well captured by the sensitivity exhibited by the extractable work.

## 6.6 Discussion and perspective

We have demonstrated experimentally a fundamental result of information thermodynamics, showing that entangled working media are able to provide a significant surplus in the amount of work that can be extracted through a communication assisted game fundamentally based on Maxwell's daemon. Such protocols, in turn, represent viable tests for the inseparability of a given state resource that, as demonstrated in our experimental endeavors, are both practical and fundamentally interesting in light of their distinct nature from, say, non-locality based entanglement witnesses.

The contribution of the author to this work has been a theoretical investigation of the photonic-based quantum thermodynamics field, the experimental design and

realization of the two-qubits protocol, the experimental realization of the three-qubit protocol and the analysis of the data.

This work has implications for both technological and conceptual aspects. Concerning the technological advances that it entails, we contribute to the well sought-after and ongoing efforts aimed at setting up a photonics-based platform for information thermodynamics. Such platform has the capability of preparing, controlling and measuring, with high fidelity and a reduced experimental complexity, states of a multipartite working medium.

As for the fundamental aspects, the work highlights how non-classical correlations within the working medium should be interpreted as a resource for the performance of thermodynamic processes, not differently from quantities with a counterpart in classical thermodynamics. This points to an interesting direction for understanding the emergence of ordinary world from its quantum microscopic constituents.

# Conclusions and discussion

In this thesis work we tried to ask the following question: *what defines quantumness?* in the sense of defining what makes a quantum state something different compared to a classical state. We stated in the Introduction that quantum states allow to perform certain computational tasks more efficiently than classical states and in the thesis we gave few examples such as the performance of a Grover's algorithm and a thermodynamical work extraction protocol.

In Chapter 1 we started from the notion of information to build the basis of both Classical and Quantum Information Theory, while in Chapter 2 we described the photonic platform used to perform we conducted our experiments and we evaluated advantages and disadvantages of such platform, showing how qubits can be encoded and manipulated in both polarization and path of photons. We also discussed the advances into integrated photonics by describing femtosecond laser-writing technique, which allows to fabricate efficient, stable, cheap quantum devices in small glass chips.

In Chapter 3 we explained in details the functioning of a Hyperentangled Path-polarization source which generates a 2-photons, 4-qubits product tensor of two Bell states (one encoded in polarization, one in path). We showed how to manipulate qubits after their generation and we presentend an experiment in which we injected the generated state into an integrated device, adopted to manipulate the hyperentangled state.

In Chapter 4 we used the source to generate a 4-qubit linear cluster state on chip and we presented a protocol to analyze the strength of their internal correlations using multipartite non-locality inequalities. We used the cluster state to highlight a computational speedup via the application of a Grover's search algorithm.

In Chapter 5 we showed a protocol in which we used local noise to generate entanglement in a 2-qubit and 4-qubit uncorrelated state, which demonstrate that in particular conditions even noise can be a useful resource in the quantum world.

Finally in Chapter 6 we discussed in details work extraction in the sense of a Maxwell's Demon experiment, both in a classical and a quantum sense. We demonstrated both theoretically and experimentally that entanglement in a quantum state can be used to extract more work compared to a classical case. In addition we showed that work-extraction allowed the distinction of entanglement classes for higher dimensional states.

This brings us back to the beginning because we found a way to relate the presence of quantum correlations (that are the main feature distinguishing a quantum state from a classical one) to work, which is something easily comparable to the classical world. In addition, work is connected through Landauer's principle to information and that

closes the cycle.

In other worlds we showed two complementary and novel ways to assess the quantumness of a state. One is interpreting the state as qubits connected pairwise through non-local correlations, as we did for the cluster state and then assess correlations by testing multipartite non locality; the other is to evaluate the amount of information contained in the state by performing a work-extraction cycle and assessing the amount of the extractable work. This two approaches aren't perfectly equivalent, as we have shown in Sec.6.5.2, but they both give an estimate of *how much* a state is non-classical.

Here we believe that the answer lies in the fact that quantum states can be thought as *more dense* than their classical counterparts, e.g. they have the potential to support a greater amount of information which in turn can be used as *currency* to outperform classical resources in computational tasks.

The proof for this interpretation lies, in the opinion of the author, in the complete unification of Quantum Information Theory with Quantum Thermodynamics in the sense of giving an energy value for each step of a Quantum Information protocol, such as generation, manipulation and measurement of a system. For example giving this interpretation to a non unital transformation such as the noise in the experiment reported in Chap. 5 would mean that the noise itself is performing *work* in the system which in turn transforms this work into quantum correlation. On the other hand a measurement on a system in some way has a thermodynamical cost, as the system itself *loses* its quantumness after it.

In this section and in the discussion sections of each chapter we gave a brief overview of open problems and perspectives on the field that are deeply associated to the subject of the chapter itself. We think that those, altogether with what we presented in this thesis, are *interesting* and *useful* topics of discussion and research leading toward the common goal of finding how our World really works.

# Bibliography

- [1] A. Einstein, B. Podolsky, and N. Rosen. “Can Quantum-Mechanical Description of Physical Reality Be Considered Complete?” In: *Phys. Rev.* 47 (1935), p. 777. DOI: 10.1103/PhysRev.47.777 (cit. on pp. 5, 15, 23).
- [2] R. Feynman. “Simulating Physics with Computers”. In: *Int. J. Theor. Phys.* 21 (1982), p. 467 (cit. on pp. 5, 59).
- [3] G. Benenti, G. Casati, and G. Strini. *Principles of Quantum Computation and Information*. World Scientific Pub. Co. Inc., 2004 (cit. on pp. 5, 8, 13, 16, 108).
- [4] P. Shor. “Polynomial-Time Algorithms for Prime Factorization and Discrete Logarithms on a Quantum Computer”. In: *SIAM J. Comput.* 26 (1997), p. 1484 (cit. on pp. 5, 73).
- [5] L. K. Grover. “Quantum Mechanics Helps in Searching for a Needle in a Haystack”. In: *Phys. Rev. Lett* 79 (1997), p. 325 (cit. on pp. 5, 73, 87).
- [6] Vittorio Giovannetti, Seth Lloyd, and Lorenzo Maccone. “Quantum-Enhanced Measurements: Beating the Standard Quantum Limit”. In: *Science* 306 (2004), pp. 1330–1336. DOI: 10.1126/science.1104149 (cit. on p. 6).
- [7] Matteo Paris. “Quantum Estimation for Quantum Technology”. In: *International Journal of Quantum Information* 07 (2009), p. 125 (cit. on p. 6).
- [8] V. Vedral. “The role of relative entropy in quantum information theory”. In: *Rev. Mod. Phys.* 74 (2002), p. 197. DOI: 10.1103/RevModPhys.74.197 (cit. on pp. 6, 22, 30).
- [9] Koji Maruyama, Fumiaki Morikoshi, and Vlatko Vedral. “Thermodynamical detection of entanglement by Maxwell’s demons”. In: *Phys. Rev. A* 71 (1 2005), p. 012108. DOI: 10.1103/PhysRevA.71.012108 (cit. on pp. 6, 111, 118).
- [10] Robert Boyd. *Nonlinear Optics*. Academic Press, 2003 (cit. on pp. 8, 42, 44).
- [11] M. A. Nielsen and I. L. Chuang. *Quantum Computation and Quantum Information*. Cambridge University Press, Cambridge, 2000 (cit. on pp. 8, 26, 28, 38, 41, 52, 54, 77).
- [12] Micheal Keyl. “Fundamentals of Quantum Information Theory”. In: *Physics Reports* 369 (2002), pp. 5, 431–548 (cit. on p. 8).
- [13] J. A. Wheeler and W. H. Zurek. *Quantum Theory and Measurement*. Princeton University Press, New Jersey, 1983 (cit. on p. 13).

- [14] Erwin Schrodinger. “The present status of quantum Mechanics”. In: *Die Naturwissenschaften* 23 (1935), p. 807 (cit. on p. 15).
- [15] John Stewart Bell. *Speakable and Unspeakable in Quantum Mechanics*. Cambridge University Press, Cambridge, 2004 (cit. on p. 15).
- [16] Charles H. Bennett, Gilles Brassard, Claude Crepeau, Richard Jozsa, Asher Peres, and William K. Wootters. “Teleporting an unknown quantum state via dual classical and Einstein-Podolsky-Rosen channels”. In: *Phys. Rev. Lett.* 70 (1993), pp. 1895–1899. DOI: 10.1103/PhysRevLett.70.1895 (cit. on p. 15).
- [17] Dik Bouwmeester, J.-W. Pan, Klaus Mattle, Manfred Eibl, Harald Weinfurter, and Anton Zeilinger. “Experimental quantum teleportation”. In: *Nature* 390 (1997), p. 575 (cit. on pp. 15, 35).
- [18] D. Boschi, S. Branca, F. De Martini, L. Hardy, and S. Popescu. “Experimental Realization of Teleporting an Unknown Pure Quantum State via Dual Classical and Einstein-Podolsky-Rosen Channels”. In: *Phys. Rev. Lett.* 80 (6 1998), pp. 1121–1125. DOI: 10.1103/PhysRevLett.80.1121 (cit. on p. 15).
- [19] Artur Ekert. “Quantum cryptography based on Bell’s theorem”. In: *Physical Review Letters* 67 (1991), p. 661 (cit. on p. 15).
- [20] A. Acín, D. Bruß, M. Lewenstein, and A. Sanpera. “Classification of Mixed Three-Qubit States”. In: *Phys. Rev. Lett.* 87 (4 2001), p. 040401. DOI: 10.1103/PhysRevLett.87.040401 (cit. on pp. 15, 17, 19).
- [21] Marcus Revzen. “Universal maximally entangled states”. In: *Quantum Studies: Mathematics and Foundations* 2 (2015), pp. 1, 77–88 (cit. on p. 17).
- [22] C. Sabin and G. Garcia-Alcaine. “A classification of entanglement in three-qubit systems”. In: *G. Eur. Phys. J. D* 00112 (2008), p. 5 (cit. on p. 17).
- [23] Martin Plesch and Vladimír Buzek. “Entangled graphs: Bipartite entanglement in multiqubit systems”. In: *Phys. Rev. A* 67 (1 2003), p. 012322. DOI: 10.1103/PhysRevA.67.012322 (cit. on p. 19).
- [24] W. Dur, G. Vidal, and J. I. Cirac. “Three qubits can be entangled in two inequivalent ways”. In: *Phys. Rev. A* 62 (2000), p. 062314. DOI: 10.1103/PhysRevA.62.062314 (cit. on pp. 19, 92).
- [25] Dagmar Bruss. “Characterizing Entanglement”. In: *arXiv:0110078 [quant-ph]* (2001) (cit. on p. 21).
- [26] Asher Peres. “Separability Criterion for Density Matrices”. In: *Phys. Rev. Lett.* 77 (1996), pp. 1413–1415. DOI: 10.1103/PhysRevLett.77.1413 (cit. on p. 21).
- [27] Michail Horodecki, Pawel Horodecki, and Ryszard Horodecki. “Separability of Mixed States: Necessary and Sufficient Conditions”. In: *arXiv:9605038 [quant-ph]* (2001) (cit. on p. 21).
- [28] Ryszard Horodecki, Pawel Horodecki, Michal Horodecki, and Karol Horodecki. “Quantum entanglement”. In: *Rev. Mod. Phys.* 81 (2009), pp. 865–942. DOI: 10.1103/RevModPhys.81.865 (cit. on p. 21).

- [29] William K. Wootters. “Entanglement of Formation of an Arbitrary State of Two Qubits”. In: *Phys. Rev. Lett.* 80 (1998), pp. 2245–2248. DOI: 10.1103/PhysRevLett.80.2245 (cit. on p. 21).
- [30] Daniel F. V. James, Paul G. Kwiat, William J. Munro, and Andrew G. White. “Measurement of qubits”. In: *Phys. Rev. A* 64 (2001), p. 052312. DOI: 10.1103/PhysRevA.64.052312 (cit. on pp. 22, 52, 55).
- [31] R. Di Candia, B. Mejia, H. Castillo, J. S. Pedernales, J. Casanova, and E. Solano. “Embedding Quantum Simulators for Quantum Computation of Entanglement”. In: *Phys. Rev. Lett.* 111 (2013), p. 240502. DOI: 10.1103/PhysRevLett.111.240502 (cit. on p. 22).
- [32] J. S. Pedernales, R. Di Candia, P. Schindler, T. Monz, M. Hennrich, J. Casanova, and E. Solano. “Entanglement measures in ion-trap quantum simulators without full tomography”. In: *Phys. Rev. A* 90 (2014), p. 012327. DOI: 10.1103/PhysRevA.90.012327 (cit. on p. 22).
- [33] Juan C. Loredó, Marcelo P. Almeida, Roberto Di Candia, Julen S. Pedernales, Jorge Casanova, Enrique Solano, and Andrew G. White. “Measuring Entanglement in a Photonic Embedding Quantum Simulator”. In: *arXiv:1506.05108 [quant-ph]* (2015) (cit. on p. 22).
- [34] J. S. Bell. “On the Einstein-Podolsky-Rosen Paradox”. In: *Physics* 1 (1964), p. 195 (cit. on p. 23).
- [35] John F. Clauser, Michael A. Horne, Abner Shimony, and Richard A. Holt. “Proposed Experiment to Test Local Hidden-Variable Theories”. In: *Phys. Rev. Lett.* 23 (15 1969), pp. 880–884. DOI: 10.1103/PhysRevLett.23.880 (cit. on pp. 24, 82).
- [36] John F. Clauser, Michael A. Horne, Abner Shimony, and Richard A. Holt. “Proposed Experiment to Test Local Hidden Variable Theories.” In: *Phys. Rev. Lett.* 24 (10 1970), pp. 549–549. DOI: 10.1103/PhysRevLett.24.549 (cit. on p. 24).
- [37] B. S. Cirel’son. “Quantum generalizations of Bell’s inequality”. In: *Letters in Mathematical Physics* 4 (1980), pp. 2, 93–100 (cit. on p. 24).
- [38] Alain Aspect, Philippe Grangier, and Gerard Roger. “Experimental Tests of Realistic Local Theories via Bell’s Theorem”. In: *Phys. Rev. Lett.* 47 (1981), p. 460. DOI: 10.1103/PhysRevLett.47.460 (cit. on pp. 24, 35).
- [39] Philipp Hyllus, Otfried Gühne, Dagmar Bruß, and Maciej Lewenstein. “Relations between entanglement witnesses and Bell inequalities”. In: *Phys. Rev. A* 72 (1 2005), p. 012321. DOI: 10.1103/PhysRevA.72.012321 (cit. on p. 24).
- [40] Carl W. Helstrom. *Quantum Detection and Estimation Theory*. Academic Press, Inc., 1976 (cit. on p. 29).
- [41] Harold Ollivier and Wojciech H. Zurek. “Quantum Discord: A Measure of the Quantumness of Correlations”. In: *Phys. Rev. Lett.* 88 (2001), p. 017901. DOI: 10.1103/PhysRevLett.88.017901 (cit. on p. 31).

- [42] L. Henderson and V. Vedral. “Classical, quantum and total correlations”. In: *Journal of Physics A: Mathematical and General* 34.35 (2001), p. 6899 (cit. on p. 31).
- [43] Animesh Datta, Anil Shaji, and Carlton M. Caves. “Quantum Discord and the Power of One Qubit”. In: *Phys. Rev. Lett.* 100 (2008), p. 050502. DOI: 10.1103/PhysRevLett.100.050502 (cit. on p. 32).
- [44] B. P. Lanyon, M. Barbieri, M. P. Almeida, and A. G. White. “Experimental Quantum Computing without Entanglement”. In: *Phys. Rev. Lett.* 101 (2008), p. 200501. DOI: 10.1103/PhysRevLett.101.200501 (cit. on p. 32).
- [45] Davide Girolami, Alexandre M. Souza, Vittorio Giovannetti, Tommaso Tufarelli, Jefferson G. Filgueiras, Roberto S. Sarthour, Diogo O. Soares-Pinto, Ivan S. Oliveira, and Gerardo Adesso. “Quantum Discord Determines the Interferometric Power of Quantum States”. In: *Phys. Rev. Lett.* 112 (2014), p. 210401. DOI: 10.1103/PhysRevLett.112.210401 (cit. on p. 32).
- [46] Vaibhav Madhok and Animesh Datta. “Quantum discord as a resource in quantum communication”. In: *arXiv:1204.6042 [quant-ph]* (2012) (cit. on p. 32).
- [47] Borivoje Dak, Vlatko Vedral, and x Brukner. “Necessary and Sufficient Condition for Nonzero Quantum Discord”. In: *Phys. Rev. Lett.* 105 (2010), p. 190502. DOI: 10.1103/PhysRevLett.105.190502 (cit. on p. 32).
- [48] Animesh Datta. “A Condition for the Nullity of Quantum Discord”. In: *arXiv:1003.5256 [quant-ph]* (2011) (cit. on p. 32).
- [49] Borivoje Dak, Yannick Ole Lipp, Xiaosong Ma, Sebastian Ringbauer Martin Kropatschek, Stefanie Barz, Tomasz Paterek, Vlatko Vedral, Anton Zeilinger, Caslav Brukner, and Philip Walther. “Quantum discord as resource for remote state preparation”. In: *Nature Phys.* 8 (2012), p. 666 (cit. on p. 32).
- [50] Kavan Modi, Aharon Brodutch, Hugo Cable, Tomasz Paterek, and Vlatko Vedral. “The classical-quantum boundary for correlations: Discord and related measures”. In: *Rev. Mod. Phys.* 84 (2012), pp. 1655–1707. DOI: 10.1103/RevModPhys.84.1655 (cit. on p. 32).
- [51] E. Knill, R. Laflamme, and G. J. Milburn. “A scheme for efficient quantum computation with linear optics”. In: *Nature* 409 (2001), p. 46 (cit. on pp. 33, 50).
- [52] Robert Raussendorf and Hans J. Briegel. “A One-Way Quantum Computer”. In: *Phys. Rev. Lett.* 86 (2001), pp. 5188–5191. DOI: 10.1103/PhysRevLett.86.5188 (cit. on pp. 33, 73–75, 77, 87).
- [53] J. L. O’Brien. “Optical Quantum Computing”. In: *Science* 318 (2007), p. 1567 (cit. on pp. 33, 36).
- [54] J. Carolan, C. Harrold, C. Sparrow, E. Martin Amsn-Lopez, N. J. Russell, J. W. Silverstone, P. J. Shadbolt, and Mikitaka Itoh Graham D. Marshall Mark G. Thompson Jonathan C. F. Matthews Toshikazu Hashimoto Jeremy L. O’Brien Anthony Laing Nobuyuki Matsuda Manabu Oguma. “Universal Linear Optics”. In: *Science* 320 (2008), p. 646 (cit. on pp. 33, 51, 52, 73).

- [55] Giuseppe Vallone, Davide Bacco, Daniele Dequal, Simone Gaiarin, Vincenza Luceri, Giuseppe Bianco, and Paolo Villoresi. “Experimental Satellite Quantum Communications”. In: *Phys. Rev. Lett.* 115 (2015), p. 040502. DOI: 10.1103/PhysRevLett.115.040502 (cit. on p. 34).
- [56] Robert H. Hadfield. “Single-photon detectors for optical quantum information applications”. In: *Nature Phot.* 3 (2009), p. 696 (cit. on pp. 34, 40).
- [57] J. L. O’Brien, G. J. Pryde, A. G. White, T. C. Ralph, and D. Branning. “Demonstration of an all-optical quantum controlled-NOT gate”. In: *Nature* 426 (2003), p. 263 (cit. on pp. 35, 51).
- [58] C. K. Hong, Z. Y. Ou, and L. Mandel. “Measurement of subpicosecond time intervals between two photons by interference”. In: *Phys. Rev. Lett.* 59 (1987), pp. 2044–2046. DOI: 10.1103/PhysRevLett.59.2044 (cit. on p. 35).
- [59] Michael E. Reimer, Gabriele Bulgarini, Nika Akopian, Moara Hocevar, Maaike Bouwes Bavinck, Marcel A. Verheijen, Erik P.A.M. Bakkers, Leo P. Kouwenhoven, and Val Zwiller. “Bright single-photon sources in bottom-up tailored nanowires”. In: *Nature Comm.* 3 (2012), p. 737 (cit. on p. 35).
- [60] Marijn A. M. Versteegh, Michael E. Reimer, Klaus D. Jns, Dan Dalacu, Philip J. Poole, Angelo Gulinatti, Andrea Giudice, and Val Zwiller. “Observation of strongly entangled photon pairs from a nanowire quantum dot”. In: *Nature Comm.* 5 (2014), p. 5298 (cit. on p. 35).
- [61] Xinlun Cai, Jianwei Wang, Michael J. Strain, Benjamin Johnson-Morris, Jiangbo Zhu, Marc Sorel, Mark G. O’Brien Jeremy L. an Thompson, and Siyuan Yu. “Integrated Compact Optical Vortex Beam Emitters”. In: *Science* 338 (2012), p. 363 (cit. on pp. 35, 52).
- [62] J. W. Silverstone, D. Bonneau, K. Ohira, N. Suzuki, H. Yoshida, N. Iizuka, M. Ezaki, C. M. Natarajan, M. G. Tanner, R. H. Hadfield, V. Zwiller, G. D. Marshall, J. G. Rarity, J. L. O’Brien, and M. G. Thompson. “On-chip quantum interference between silicon photon-pair sources”. In: *Nature Phot.* 8 (2013), p. 104 (cit. on pp. 35, 52).
- [63] William K. Wootters and Wojciech H. Zurek. “Complementarity in the double-slit experiment: Quantum nonseparability and a quantitative statement of Bohr’s principle”. In: *Phys. Rev. D* 19 (1979), pp. 473–484. DOI: 10.1103/PhysRevD.19.473 (cit. on p. 37).
- [64] Michael Reck, Anton Zeilinger, Herbert J. Bernstein, and Philip Bertani. “Experimental realization of any discrete unitary operator”. In: *Phys. Rev. Lett.* 73 (1994), pp. 58–61. DOI: 10.1103/PhysRevLett.73.58 (cit. on p. 38).
- [65] Rodney Loudon. *The Quantum Theory of Light*. Oxford University Press, Oxford, 1992 (cit. on pp. 42, 43).
- [66] M. Barbieri, F. De Martini, G. Di Nepi, and P. Mataloni. “Generation and Characterization of Werner States and Maximally Entangled Mixed States by a Universal Source of Entanglement”. In: *Phys. Rev. Lett.* 92 (2004), p. 177901. DOI: 10.1103/PhysRevLett.92.177901 (cit. on p. 48).

- [67] M. Barbieri, C. Cinelli, P. Mataloni, and F. De Martini. “Polarization-momentum hyperentangled states: Realization and characterization”. In: *Phys. Rev. A* 72 (2005), p. 052110. DOI: 10.1103/PhysRevA.72.052110 (cit. on pp. 48, 59–61, 65, 70).
- [68] Paul G. Kwiat, Klaus Mattle, Harald Weinfurter, Anton Zeilinger, Alexander V. Sergienko, and Yanhua Shih. “New High-Intensity Source of Polarization-Entangled Photon Pairs”. In: *Phys. Rev. Lett.* 75 (1995), pp. 4337–4341. DOI: 10.1103/PhysRevLett.75.4337 (cit. on p. 50).
- [69] Taehyun Kim, Marco Fiorentino, and Franco N. C. Wong. “Phase-stable source of polarization-entangled photons using a polarization Sagnac interferometer”. In: *Phys. Rev. A* 73 (2006), p. 012316. DOI: 10.1103/PhysRevA.73.012316 (cit. on p. 50).
- [70] Alessandro Fedrizzi, Thomas Herbst, Andreas Poppe, Thomas Jennewein, and Anton Zeilinger. “A wavelength-tunable fiber-coupled source of narrowband entangled photons”. In: *Opt. Express* 15.23 (2007), pp. 15377–15386. DOI: 10.1364/OE.15.015377 (cit. on p. 50).
- [71] Alberto Politi, Jonathan C. F. Matthews, and Jeremy L. O’Brien. “Shor’s Quantum Factoring Algorithm on a Photonic Chip”. In: *Science* 325 (2009), p. 1221 (cit. on pp. 51, 59, 73).
- [72] J. L. O’Brien, G. J. Pryde, A. G. White, and T. C. Ralph. “High-fidelity Z-measurement error encoding of optical qubits”. In: *Phys. Rev. A* 71 (2005), p. 060303. DOI: 10.1103/PhysRevA.71.060303 (cit. on p. 51).
- [73] Sebastien Tanzilli, Anthony Martin, Florian Kaiser, Marc De Micheli, Olivier Alibart, and Daniel Barry Ostrowsky. “On the genesis and evolution of Integrated Quantum Optics”. In: *arXiv:1108.3162 [quant-ph]* (2011) (cit. on p. 51).
- [74] Regina Kruse, Linda Sansoni, Sebastian Brauner, Raimund Ricken, Craig S. Hamilton, Igor Jex, and Christine Silberhorn. “On-chip dual-path entangled photon pair sources by coupled non-linear waveguides”. In: *arXiv:1108.3162 [quant-ph]* (2015) (cit. on p. 52).
- [75] Harald Herrmann, Xu Yang, Abu Thomas, Andreas Poppe, Wolfgang Sohler, and Christine Silberhorn. “Post-selection free, integrated optical source of non-degenerate, polarization entangled photon pairs”. In: *Opt. Express* 21.23 (2013), pp. 27981–27991. DOI: 10.1364/OE.21.027981 (cit. on p. 52).
- [76] Oliver Kahl, Simone Ferrari, Vadim Kovalyuk, Gregory N. Goltsman, Alexander Korneev, and Wolfram H. P. Pernice. “Waveguide integrated superconducting single-photon detectors with high internal quantum efficiency at telecom wavelengths”. In: *Scientific Reports* 5 (2015), p. 10941 (cit. on p. 52).
- [77] J. P. Sprengers, D. Sahin, S. Jahanmirinejad, G. Frucci, R. Leoni F. Mattioli, J. Beetz, M. Lerner, M. Kamp, S. Hofling, R. Sanjines, A. Gaggero, and A. Fiore. “Waveguide superconducting single-photon detectors for integrated quantum photonic circuits”. In: *Appl. Phys. Lett.* 99 (2011), p. 181110 (cit. on p. 52).

- [78] Grant R. Fowles. *Introduction to Modern Optics*. Dover Publication Inc., New York, 1975 (cit. on p. 53).
- [79] P. Walther, K. J. Resch, T. Rudolph, E. Schenck, H. Weinfurter, V. Vedral, M. Aspelmeyer, and A. Zeilinger. “Experimental one-way quantum computing”. In: *Nature* 434 (2005), p. 169 (cit. on pp. 54, 77, 87, 88).
- [80] Wei-Bo Gao, Chao-Yang Lu, Xing-Can Yao, Ping Xu, Otfried Gühne, Alexander Goebel, Yu-Ao Chen, Cheng-Zhi Peng, Zeng-Bing Chen, and Jian-Wei Pan. “Experimental demonstration of a hyper-entangled ten qubit Schrödinger cat state”. In: *Nature Physics* 6 (2010), pp. 331–335 (cit. on pp. 58, 59).
- [81] Xi-Lin Wang, Xin-Dong Cai, Zu-En Su, Ming-Cheng Chen, Dian Wu, Li Li, Nai-Le Liu, Chao-Yang Lu, and Jian-Wei Pan. “Quantum teleportation of multiple degrees of freedom of a single photon”. In: *Nature* 518.7540 (2015), pp. 516–519 (cit. on p. 59).
- [82] A. Politi, M.J. Cryan, J. G. Rarity, S. Yu, and J. L. O’Brien. “Silica-on-Silicon Waveguide Quantum Circuits”. In: *Science* 320 (2008), p. 646 (cit. on p. 59).
- [83] J. T. Barreiro, T-C Wei, and P. G. Kwiat. “Beating the channel capacity limit for linear photonic superdense coding”. In: *Nature Physics* 4 (2008), pp. 282–286 (cit. on p. 59).
- [84] Seth Lloyd. “Universal quantum simulators”. In: *Science* 273 (1996), pp. 1073–1078 (cit. on p. 59).
- [85] Marco Bentivegna, Nicolás Spagnolo, Chiara Vitelli, Fulvio Flamini, and Niko et al. Viggianiello. “Experimental scattershot boson sampling”. In: *Science Advances* 1 (2015), e1400255 (cit. on p. 59).
- [86] Andrea Crespi, Roberta Ramponi, Roberto Osellame, Linda Sansoni, Irene Bongioanni, Fabio Sciarrino, Giuseppe Vallone, and Paolo Mataloni. “Integrated photonic quantum gates for polarization qubits”. In: *Nature Comm.* 2 (2011), p. 566 (cit. on p. 59).
- [87] Eleonora Nagali, Fabio Sciarrino, Francesco De Martini, Lorenzo Marrucci, Bruno Piccirillo, Ebrahim Karimi, and Enrico Santamato. “Quantum Information Transfer from Spin to Orbital Angular Momentum of Photons”. In: *Phys. Rev. Lett.* 103 (1 2009), p. 013601. DOI: 10.1103/PhysRevLett.103.013601 (cit. on p. 59).
- [88] I. Marcikic, H. de Riedmatten, W. Tittel, V. Scarani, H. Zbinden, and N. Gisin. “Time-bin entangled qubits for quantum communication created by femtosecond pulses”. In: *Phys. Rev. A* 66 (6 2002), p. 062308. DOI: 10.1103/PhysRevA.66.062308 (cit. on p. 59).
- [89] Raino Ceccarelli, Giuseppe Vallone, Francesco De Martini, Paolo Mataloni, and Adán Cabello. “Experimental Entanglement and Nonlocality of a Two-Photon Six-Qubit Cluster State”. In: *Phys. Rev. Lett.* 103 (16 2009), p. 160401. DOI: 10.1103/PhysRevLett.103.160401 (cit. on p. 61).

- [90] Mario Arnolfo Ciampini, Adeline Orieux, Stefano Paesani, Fabio Sciarrino, Giacomo Corrielli, Andrea Crespi, Roberta Ramponi, Roberto Osellame, and Paolo Mataloni. “Path-polarization hyperentangled and cluster states of photons on a chip”. In: *Light: Science & Applications* 5 (2016). To be published., e16064 (cit. on pp. 65, 83).
- [91] Linda Sansoni, Fabio Sciarrino, Giuseppe Vallone, Paolo Mataloni, Andrea Crespi, Roberta Ramponi, and Roberto Osellame. “Polarization Entangled State Measurement on a Chip”. In: *Phys. Rev. Lett.* 105 (2010), p. 200503. DOI: 10.1103/PhysRevLett.105.200503 (cit. on pp. 65, 70).
- [92] Linda Sansoni, Fabio Sciarrino, Giuseppe Vallone, Paolo Mataloni, Andrea Crespi, Roberta Ramponi, and Roberto Osellame. “Two-Particle Bosonic-Fermionic Quantum Walk via Integrated Photonics”. In: *Phys. Rev. Lett.* 108 (2012), p. 010502. DOI: 10.1103/PhysRevLett.108.010502 (cit. on pp. 65, 66).
- [93] G Della Valle, R Osellame, and P Laporta. “Micromachining of photonic devices by femtosecond laser pulses”. In: *Journal of Optics A: Pure and Applied Optics* 11.1 (2009), p. 013001 (cit. on p. 66).
- [94] Fred Heismann, Steven Korotky, and John Veselka. *Optical Fiber Telecommunications IIIB*. Ed. by Academic Press. Academic Press, 2012 (cit. on p. 68).
- [95] Stefanie Barz, Ivan Kassal, Martin Ringbauer, Yannick Ole Lipp, Borivoje Dakic, Alan Aspuru-Guzik, and Philip Walther. “A two-qubit photonic quantum processor and its application to solving systems of linear equations”. In: *Scientific Reports* 4 (2014), p. 6115 (cit. on p. 73).
- [96] Giuseppe Vallone, Enrico Pomarico, Paolo Mataloni, Francesco De Martini, and Vincenzo Berardi. “Realization and Characterization of a Two-Photon Four-Qubit Linear Cluster State”. In: *Phys. Rev. Lett.* 98 (2007), p. 180502. DOI: 10.1103/PhysRevLett.98.180502 (cit. on pp. 77, 80, 83).
- [97] Giuseppe Vallone, Enrico Pomarico, Francesco De Martini, and Paolo Mataloni. “Active One-Way Quantum Computation with Two-Photon Four-Qubit Cluster States”. In: *Phys. Rev. Lett.* 100 (2008), p. 160502. DOI: 10.1103/PhysRevLett.100.160502 (cit. on pp. 77, 88).
- [98] Giuseppe Vallone, Enrico Pomarico, Francesco De Martini, and Paolo Mataloni. “One-way quantum computation with two-photon multiqubit cluster states”. In: *Phys. Rev. A* 78 (2008), p. 042335. DOI: 10.1103/PhysRevA.78.042335 (cit. on pp. 77, 87, 88).
- [99] Chao-Yang Lu, Xiao-Qi Zhou, Otfried Gühne, Wei-Bo Gao, Jin Zhang, Zhen-Sheng Yuan, Alexander Goebel, Tao Yang, and Jian-Wei Pan. “Experimental entanglement of six photons in graph states”. In: *Nature Phys.* 3 (2007), p. 91 (cit. on p. 77).
- [100] Giuseppe Vallone, Gaia Donati, Raino Ceccarelli, and Paolo Mataloni. “Six-qubit two-photon hyperentangled cluster states: Characterization and application to quantum computation”. In: *Phys. Rev. A* 81 (2010), p. 052301. DOI: 10.1103/PhysRevA.81.052301 (cit. on p. 77).

- [101] Xing-Can Yao, Tian-Xiong Wang, Ping Xu, He Lu, Ge-Sheng Pan, Xiao-Hui Bao, Cheng-Zhi Peng, Chao-Yang Lu, Yu-Ao Chen, and Jian-Wei Pan. “Observation of eight-photon entanglement”. In: *Scientific Reports* 6 (2012), p. 225 (cit. on p. 77).
- [102] Géza Tóth and Otfried Gühne. “Entanglement detection in the stabilizer formalism”. In: *Phys. Rev. A* 72 (2 2005), p. 022340. DOI: 10.1103/PhysRevA.72.022340 (cit. on pp. 79, 80).
- [103] R. F. Werner and M. M. Wolf. “All-multipartite Bell-correlation inequalities for two dichotomic observables per site”. In: *Phys. Rev. A* 64 (3 2001), p. 032112. DOI: 10.1103/PhysRevA.64.032112 (cit. on p. 81).
- [104] Marek Zukowski and Caslav Brukner. “Bell’s Theorem for General  $N$ -Qubit States”. In: *Phys. Rev. Lett.* 88 (21 2002), p. 210401. DOI: 10.1103/PhysRevLett.88.210401 (cit. on pp. 81, 82).
- [105] N. David Mermin. “Extreme quantum entanglement in a superposition of macroscopically distinct states”. In: *Phys. Rev. Lett.* 65 (15 1990), pp. 1838–1840. DOI: 10.1103/PhysRevLett.65.1838 (cit. on pp. 82, 115, 126).
- [106] M. Ardehali. “Bell inequalities with a magnitude of violation that grows exponentially with the number of particles”. In: *Phys. Rev. A* 46 (9 1992), pp. 5375–5378. DOI: 10.1103/PhysRevA.46.5375 (cit. on pp. 82, 126).
- [107] A. V. Belinskii and D. N. Klyshko. “Bell’s theorem for trichotomic observables”. In: *Phys. Usp.* 36 (1993), p. 653 (cit. on pp. 82, 126).
- [108] Daniel E. Browne and Terry Rudolph. “Resource-Efficient Linear Optical Quantum Computation”. In: *Phys. Rev. Lett.* 95 (2005), p. 010501. DOI: 10.1103/PhysRevLett.95.010501 (cit. on p. 87).
- [109] P. G. Kwiat, J. R. Mitchell, P. D. D. Schwindt, and A. G. White. “Grover’s search algorithm: An optical approach”. In: *Journal of Modern Optics* 47.2-3 (2000), pp. 257–266. DOI: 10.1080/09500340008244040. eprint: <http://www.tandfonline.com/doi/pdf/10.1080/09500340008244040> (cit. on p. 88).
- [110] Adeline Orioux, Mario A. Ciampini, Paolo Mataloni, Dagmar Bruß, Matteo Rossi, and Chiara Macchiavello. “Experimental Generation of Robust Entanglement from Classical Correlations via Local Dissipation”. In: *Phys. Rev. Lett.* 115 (16 2015), p. 160503. DOI: 10.1103/PhysRevLett.115.160503 (cit. on p. 90).
- [111] Alexander Streltsov, Hermann Kampermann, and Dagmar Bruß. “Behavior of Quantum Correlations under Local Noise”. In: *Phys. Rev. Lett.* 107 (17 2011), p. 170502. DOI: 10.1103/PhysRevLett.107.170502 (cit. on p. 91).
- [112] Francesco Ciccarello and Vittorio Giovannetti. “Creating quantum correlations through local nonunitary memoryless channels”. In: *Phys. Rev. A* 85 (1 2012), p. 010102. DOI: 10.1103/PhysRevA.85.010102 (cit. on p. 91).
- [113] Xueyuan Hu, Heng Fan, D. L. Zhou, and Wu-Ming Liu. “Necessary and sufficient conditions for local creation of quantum correlation”. In: *Phys. Rev. A* 85 (3 2012), p. 032102. DOI: 10.1103/PhysRevA.85.032102 (cit. on p. 91).

- [114] B. P. Lanyon, P. Jurcevic, C. Hempel, M. Gessner, V. Vedral, R. Blatt, and C. F. Roos. “Experimental Generation of Quantum Discord via Noisy Processes”. In: *Phys. Rev. Lett.* 111 (10 2013), p. 100504. DOI: 10.1103/PhysRevLett.111.100504 (cit. on p. 91).
- [115] Marco Piani, Sevag Gharibian, Gerardo Adesso, John Calsamiglia, Paweł Horodecki, and Andreas Winter. “All Nonclassical Correlations Can Be Activated into Distillable Entanglement”. In: *Phys. Rev. Lett.* 106 (22 2011), p. 220403. DOI: 10.1103/PhysRevLett.106.220403 (cit. on pp. 91, 97).
- [116] Gerardo Adesso, Vincenzo D’Ambrosio, Eleonora Nagali, Marco Piani, and Fabio Sciarrino. “Experimental Entanglement Activation from Discord in a Programmable Quantum Measurement”. In: *Phys. Rev. Lett.* 112 (14 2014), p. 140501. DOI: 10.1103/PhysRevLett.112.140501 (cit. on p. 91).
- [117] Takafumi Nakano, Marco Piani, and Gerardo Adesso. “Negativity of quantumness and its interpretations”. In: *Phys. Rev. A* 88 (1 2013), p. 012117. DOI: 10.1103/PhysRevA.88.012117 (cit. on pp. 96, 97, 102).
- [118] Linda del Rio, Johan Aberg, Renato Renner, Oscar Dahlsten, and Vlatko Vedral. “The thermodynamic meaning of negative entropy”. In: *Nature* 474 (2011), pp. 61–63 (cit. on p. 103).
- [119] Jochen Gemmer, M. Michel, and Gunter Mahler. *Quantum Thermodynamics, Emergence of Thermodynamic Behavior Within Composite Quantum Systems*. Ed. by Springer. Springer-Verlag Berlin Heidelberg, 2009 (cit. on p. 103).
- [120] Harvey Leff and Andrew Rex, eds. *Maxwell’s Demon: Entropy, Information, Computing*. Princeton Legacy Library, 1990 (cit. on p. 104).
- [121] R. Landauer. “Irreversibility and Heat Generation in the Computing Process”. In: *IBM Journal of Research and Development* 5.5 (1961), pp. 183–191 (cit. on pp. 105, 106).
- [122] Leo Szilard. “On the decrease of entropy in a thermodynamic system by the intervention of intelligent beings”. In: *Zeitschrift fur Physik* 53 (1929), pp. 840–856 (cit. on p. 105).
- [123] M. B. Plenio and V. Vitelli. “The physics of forgetting: Landauer’s erasure principle and information theory”. In: *Contemporary Physics* 42.1 (2001), pp. 25–60 (cit. on p. 105).
- [124] Janet Anders and Vittorio Giovannetti. “Thermodynamics of discrete quantum processes”. In: *New Journal of Physics* 15.3 (2013), p. 033022 (cit. on p. 107).
- [125] J. Machta. “Entropy, Information, and Computation”. In: *American Journal of Physics* 67 (1999), p. 1074 (cit. on p. 108).
- [126] Koji Maruyama, Franco Nori, and Vlatko Vedral. “Colloquium : The physics of Maxwell’s demon and information”. In: *Rev. Mod. Phys.* 81 (1 2009), pp. 1–23. DOI: 10.1103/RevModPhys.81.1 (cit. on pp. 109, 113).

- [127] Jonathan Oppenheim, Michał Horodecki, Paweł Horodecki, and Ryszard Horodecki. “Thermodynamical Approach to Quantifying Quantum Correlations”. In: *Phys. Rev. Lett.* 89 (18 2002), p. 180402. DOI: 10.1103/PhysRevLett.89.180402 (cit. on pp. 109, 111).
- [128] Michail Horodecki, P. Horodecki, and R. Horodecki. “Separability of mixed states: necessary and sufficient conditions”. In: *Physics Letters* 223.1-2 (1996), pp. 1–8 (cit. on pp. 111, 122).
- [129] Michał Horodecki, Karol Horodecki, Paweł Horodecki, Ryszard Horodecki, Jonathan Oppenheim, Aditi Sen(De), and Ujjwal Sen. “Local Information as a Resource in Distributed Quantum Systems”. In: *Phys. Rev. Lett.* 90 (10 2003), p. 100402. DOI: 10.1103/PhysRevLett.90.100402 (cit. on p. 111).
- [130] Harold Ollivier and Wojciech H. Zurek. “Quantum Discord: A Measure of the Quantumness of Correlations”. In: *Phys. Rev. Lett.* 88 (1 2001), p. 017901. DOI: 10.1103/PhysRevLett.88.017901 (cit. on p. 111).
- [131] Vincent Viguie, Koji Maruyama, and Vlatko Vedral. “Work extraction from tripartite entanglement”. In: *New Journal of Physics* 7 (2005), pp. 1–10 (cit. on pp. 111, 115, 116, 123).
- [132] George Svetlichny. “Distinguishing three-body from two-body nonseparability by a Bell-type inequality”. In: *Phys. Rev. D* 35 (10 1987), pp. 3066–3069. DOI: 10.1103/PhysRevD.35.3066 (cit. on pp. 115, 126).
- [133] Ashok Ajoy and Pranaw Rungta. “Svetlichny’s inequality and genuine tripartite nonlocality in three-qubit pure states”. In: *Phys. Rev. A* 81 (5 2010), p. 052334. DOI: 10.1103/PhysRevA.81.052334 (cit. on p. 115).
- [134] S. Ghose, N. Sinclair, S. Debnath, P. Rungta, and R. Stock. “Tripartite Entanglement versus Tripartite Nonlocality in Three-Qubit Greenberger-Horne-Zeilinger-Class States”. In: *Phys. Rev. Lett.* 102 (25 2009), p. 250404. DOI: 10.1103/PhysRevLett.102.250404 (cit. on p. 115).
- [135] Mario Arnolfo Ciampini, Luca Mancino, Adeline Orioux, Caterina Vigliar, Paolo Mataloni, Mauro Paternostro, and Marco Barbieri. “Experimental entanglement-enhanced work extraction based on a Maxwell’s demon”. In: *arXiv:1601.06796* (2016). arXiv:1601.06796 (cit. on p. 117).
- [136] Mihai D. Vidrighin, Oscar Dahlsten, Marco Barbieri, M. S. Kim, Vlatko Vedral, and Ian A. Walmsley. “Photonic Maxwell’s Demon”. In: *Phys. Rev. Lett.* 116 (5 2016), p. 050401. DOI: 10.1103/PhysRevLett.116.050401 (cit. on p. 118).

# List of publications

1. A. Orioux, M.A. Ciampini, P. Mataloni, D. Bruss, M. Rossi, and C. Macchiavello, “Experimental Generation of Robust Entanglement from Classical Correlations via Local Dissipation”, *Physical Review Letters*, **115**, 160503 (2015)
2. M.A. Ciampini, A. Orioux, S. Paesani, F. Sciarrino, G. Corrielli, A. Crespi, R. Ramponi, R. Osellame and P. Mataloni, “Path-polarization hyperentangled and cluster states of photons on a chip”, *Light: Science & Applications* **5**, e16064; (2016) doi:10.1038/lsa.2016.64
3. M.A. Ciampini, N. Spagnolo, C. Vitelli, L. Pezzé, A. Smerzi, F. Sciarrino, “Quantum-enhanced multiparameter estimation in multiarm interferometers”, *Scientific Reports* **6**, 28881; (2016) doi:10.1038/srep28881
4. M.A. Ciampini, L. Mancino, A. Orioux, C. Vighiar, P. Mataloni, M. Paternostro and M. Barbieri, “Experimental entanglement-enhanced work extraction based on a Maxwell’s demon”, **submitted**, arXiv Preprint arXiv:1601.06796, (2016)
5. M.A. Ciampini, C. Vighiar, V. Cimini, S. Paesani, F. Sciarrino, A. Crespi, G. Corrielli, R. Osellame, P. Mataloni, M. Paternostro and M. Barbieri, “Experimental nonlocality-based network diagnostics of multipartite entangled states”, **submitted**, arXiv Preprint arXiv:1609.09731, (2016)
6. A. Cuevas, M. Proietti, M.A. Ciampini, S. Duranti, P. Mataloni, M. Sacchi, C. Macchiavello, “Experimental detection of quantum channel capacities”, **submitted**, arXiv Preprint arXiv:1612.07754, (2016)